Study of thermal aging effect on fatigue behaviors of a short glass fiber reinforced Polyphenylene Sulfide (PPS/GF) composite

Peiyuan Zuo

2018-ENAM-0063

École doctorale n° 432 : Sciences des Métiers de l'ingénieur

Doctorat ParisTech

T H È S E

pour obtenir le grade de docteur délivré par

l'École Nationale Supérieure d'Arts et Métiers

Spécialité " Mécanique et Matériaux "

présentée et soutenue publiquement par

Peiyuan ZUO

Le 18 Décembre 2018

Etude de l'effet du vieillissement thermique sur le comportement en fatigue du composite de poly (sulfure de phénylène) renforcé par des fibres de verre (PPS/FV)

Directeur de thèse : **Abbas TCHARKHTCHI**
Co-encadrement de la thèse : **Joseph FITOUSSI**

Jury

M.	**Jean-Pierre HABAS**, Professeur, Institut Charles Gerhardt Montpellier,	Président
Mme.	**Jocelyne GALY**, Professeur, INSA Lyon,	Rapporteur
M.	**Kalappa PRASHANTHA**, Professeur, École des Mines de Douai,	Rapporteur
M.	**Mario Domingo MONZÓN VERONA**, Professeur, ULPGC-Espagne,	Examinateur
M.	**Joseph FITOUSSI**, Docteur, Arts et Métiers Paristech,	Examinateur
M.	**Abbas TCHARKHTCHI**, Professeur, Arts et Métiers Paristech,	Examinateur
M.	**Rodrigo Carvalho BENEVIDES**, Docteur, Valeo Powertrain Thermal Systems,	Invité

T H È S E

Arts et Métiers ParisTech - Campus de Paris
PIMM - Procédés et Ingénierie en Mécanique et Matériaux

Acknowledgments

This thesis is done for and in collaboration with the Valeo Research Center with duration of 36 months. It was conducted in the PIMM laboratory (Processes and Engineering in Mechanics and Materials) of the ENSAM Paris Campus. I spent the fantastic 3 years with my dear colleagues in PIMM to accomplish this work.

First of all, I would like to thank all the members in Jury to accept participating for my PhD defense. They come from different countries and universities: The President of Jury is Prof. Jean-Pierre HABAS (Institut Charles Gerhardt Montpellier); The Jury members are as follows: Prof. Jocelyne GALY (INSA Lyon), Prof. Kalappa PRASHANTHA (Ecole des Mines de Douai), and Prof. Mario Domingo MONZON VERONA (ULGPC-Spain), Dr. Rodrigo BENEVIDES (Valeo Powertrain Thermal Systems) as well as my 2 directors.

Also, I would like to give my best thanks to Prof. Abbas TCHARKHTCHI, who is one of the most important person during my PhD time. I still remember much detail for numerous mornings' academic discussions with this lovely professor and Prof. Abbas TCHARKHTCHI will definitely become my role model for my future's academic career.

At the same time, it is my honor to mention my co-director Dr. Joseph FITOUSSI, who is very professional and strict to the academic issues. This quality helps me to achieve much progress during my research and makes contribution in a good way to my academic future.

Dr.Mohammadali SHIRINBAYAN is very kind to me during the PhD time, I really appreciate his help and his support for every moment.

Prof. Michel .BOCQUET is very kind to correct my thesis which makes an obvious improvement for my thesis's quality. I appreciate it.

I would like to thank all the organizers for the fantastic "POT" after my defense.

Of course, I cannot forget all the happy moments with all of you, my colleagues in ENSAM (Arts et Métiers Paristech). I cannot give a very detailed list (my colleagues in my office: Amine, Houssem, Abir as well as other good and close friends: Vajihe, Hamidreza, Yan, Jing, Justine, Clement, Sarah, Maximum, Camille, Nyhal, Shuanglin, Shaobo, Xixi, Xiaoxin, Anne, Amine. L,

Eeva, Quentin, Mohamed, Moisis, Farid, Tiphane, Abderazek, Xavier, Bruno, Abir.B, Paulo, Anne.G, Alain.G, Albert, Gaelle, Emmanuel, Lauriane,Navideh, Kherieddin, Abderrahmane, Hassen, Tang, … all of you in PIMM and Dynfuild), and I would like to say "I love all of you guys from PIMM and Dynfluid laboratories. I will cherish these memories regarding the past three years with you for my whole life".

I wish all of you enjoy your daily life and I hope someday we can see each other in CHINA.

Also, it is very important to thank my parents, my sister, my brother and my girlfriend as well as my big family members. I really love all of you.

I would like also to thank my classmates, teachers, professors and friends in China.

It is a good journey for the three years in Paris, FRANCE. I love the culture here and I appreciate the French Spirit. Hopefully, someday I can come back again to meet all of you again.

Thank you all and all my best wishes to you!

Peiyuan
January 11, 2019
Arts et Métiers Paristech (ENSAM), Paris, FRANCE

Table des matières

Liste des Figures :

Liste des Tableaux :

Résumé étendu (En Français)

I. Introduction générale

La réduction des coûts et de la consommation d'énergie sont des facteurs clés dans de nombreux secteurs industriels comme l'aéronautique et l'automobile. De même, dans la société moderne, le poids de la pièce est devenu un critère important sur le choix des matériaux pour la fabrication des produits industriels. Il existe donc une tendance selon laquelle les matériaux légers tels que les composites polymères et en particulier les composites renforcés à matrice thermoplastique, remplaceront progressivement certains matériaux métalliques traditionnels au cours des prochaines décennies. Les composites renforcés à matrice thermoplastique sont maintenant envisagés pour des applications dans des environnements thermiques sévères tels que les zones proches de sources de chaleur (par exemple les environnements techniques automobiles) [1-3].

En outre, parmi les divers polymères à hautes performances, ceux contenant des unités aromatiques, tels que le PEEK de poly (éther éther cétone) [4-10], le poly (éther sulfone) PES [11-13] et le poly (sulfure de Phénylène) (PPS) [14-20], ont beaucoup attiré l'attention au cours de ces dernières décennies. Le poly (sulfure de Phénylène) (PPS) est donc un de ces types de polymères qui, chargés de fibres organiques, allient à la fois une haute résistance mécanique à une très bonne tenue à la température. Il présente ainsi une combinaison unique d'excellentes propriétés environnementales. Il est utilisé dans de nombreux secteurs comme l'électronique et les appareils électriques, les instruments de précision, les domaines de la chimie et de l'aérospatiale [21-24]. En particulier, le poly (sulfure de Phénylène) (PPS) renforcé par des fibres de verre courtes, mis en œuvre par le procédé d'injection, est utilisé fréquemment dans l'industrie automobile (cas des refroidisseurs d'air). D'une façon générale, ce matériau présente des

propriétés mécaniques (rigidité, résistance mécanique, …) intéressantes. Les PPS présentent également un comportement en fatigue très intéressant, une bonne performance thermomécanique ($T_g \approx 110$ °C et $T_f \approx 285$ °C) ainsi qu'une grande résistance chimique.

Cependant, tous les polymères et les composites à matrice polymère, se heurtent aux mêmes problèmes de stabilité thermique et de résistance à la dégradation [18, 25-28]. Ceci est une des préoccupations majeures des utilisateurs de ces matériaux dans des conditions ou certains éléments environnementaux comme l'oxygène de l'air peut agresser le matériau ; en particulier lorsque la température est relativement élevée. Cette préoccupation exige des chercheurs de s'investir et de réaliser des activités de recherche dans ce domaine. L'objectif est de mieux comprendre les processus et les mécanismes de vieillissement thermique afin de permettre d'offrir plus de solutions pour une meilleure utilisation. Dans la présente étude, les aspects multi-échelles doivent être pris en compte car l'oxydation des polymères est un phénomène complexe touchant le matériau à différentes échelles : moléculaire, macromoléculaire, morphologique, micro-méso et macroscopique [29-32]. En conséquence, il convient de prendre en compte diverses conditions au cours du vieillissement. Ceci, peut non seulement permettre davantage de protections lors de l'utilisation, mais également de mieux comprendre le processus de dégradation détaillé des polymères et de leurs parties renforcées.

Par ailleurs, aujourd'hui l'industrie a grand besoin de données sur le comportement mécanique (propriétés d'utilisation) des matériaux dans les conditions de sollicitation diverses. Un des modes de sollicitation très courant est la sollicitation en fatigue où la pièce est soumise à une contrainte cyclique d'amplitude modérée qui contribue à la dégradation mécanique du matériau dans le temps [9, 33-38]. Dans ces conditions, les pièces à base de polymère ou composites doivent avoir une bonne résistance à la fatigue pour garantir une longue durée de vie [39, 40].

Dans le cas d'une utilisation pratique réelle, le problème est souvent plus compliqué. La pièce industrielle est souvent sollicitée mécaniquement (par exemple en fatigue) dans un milieu chaud en contact avec les éléments environnants comme l'air sous le capot moteur. Par conséquent, la pièce est soumise à l'influence combinée de l'oxydation et de la fatigue. Par conséquent, il est nécessaire de réaliser des recherches en prenant en compte les deux types de dégradation (mécanique et thermique) ainsi que leur interaction.

C'est avec cet esprit que nous avons organisé notre travail objet de cette thèse. Nous avons essayé de suivre ce fil rouge au cours de ces trois dernières années. Ce fil rouge relie les différents volets suivants : caractérisation du PPS/FV, étude de l'oxydation du matériau, étude du comportement en fatigue du matériau, étude de l'influence du vieillissement sur le comportement en fatigue.

Le matériau composite PPS/FV est fourni par notre partenaire industriel Valeo. Ce travail est réalisé pour et en collaboration avec le centre de recherche Valeo. Il a été mené au sein du laboratoire PIMM (Procédés et Ingénierie en Mécanique et Matériaux) du Campus ENSAM de Paris.

Le présent document se scinde en deux parties : le résumé étendu en français et en anglais (Partie I) ; puis les articles publiés ou en cours de publication dans des revues internationales de rang A en anglais (Partie II). L'organisation des différentes parties du résumé étendu respecte la démarche suivante :

- Une description des matériaux composites PPS et leur comportement physico-chimique et mécanique ;
- Une modélisation des propriétés sous vieillissement thermique du matériau PPS ;
- L'analyse expérimentale du comportement en fatigue de ces matériaux ;

- L’étude de l’effet de l’oxydation thermique sur le comportement mécanique des composites PPS étudiés.

Ci-après est présentée la liste des articles publiés lors de cette étude ou en cours de publication. Ils sont cités dans le texte sous la forme : « Article N°-- ».

Article N°1: P. Zuo, A. Tcharkhtchi, M. Shirinbayan, J. Fitoussi, F. Bakir, “Overall investigation of PolyPhenylene Sulfide (PPS) / from synthesis, process to applications – A review”. Macromolecular Materials & Engineering. **Accepted.**

Article N°2: P. Zuo, R. C. Benevides, M. A. Laribi, J. Fitoussi, M. Shirinbayan, F. Bakir, A. Tcharkhtchi, "Multi-scale analysis of the effect of loading conditions on monotonic and fatigue behavior of a glass fiber reinforced polyphenylene sulfide (PPS) composite", Composites Part B: Engineering, 2018, 145: 173-181. **Published.**

Article N°3: P. Zuo, A. Tcharkhtchi, M. Shirinbayan, J. Fitoussi, F. Bakir, "Multi-scale physicochemical characterization of a short glass fiber reinforced Polyphenylene Sulfide composite under aging and its thermo-oxidative mechanism", Polymers for advanced technologies, 2018. **In press.**

Article N°4: P. Zuo, J. Fitoussi, M. Shirinbayan, F. Bakir, A. Tcharkhtchi, "Thermal aging effects on overall mechanical behavior of short glass fiber reinforced PolyPhenylene Sulfide composites ", Polymer Engineering & Science, 2018. **In press.**

II. Matériaux et méthodes expérimentales

II-1 Matériaux

Les composites PPS/FV, objet de la présente étude, sont utilisés pour diverses applications dans l'industrie automobile, en particulier pour des pièces de refroidisseur d'air (pièce spécifique à Valeo). Le poly (sulfure de Phénylène) (PPS) est un polymère constitué de noyaux aromatiques liés aux sulfures. Sa formule chimique est illustrée à la Figure 1.

Le matériau composite utilisé pour cette étude est constitué de trois phases : la matrice, les charges minérales (si elles existent) et les fibres de verre. La matrice est le poly (sulfure de Phénylène) (PPS); il s'agit d'un polymère thermoplastique semi-cristallin à haute performance.

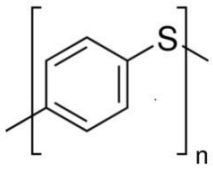

Figure 1 : Structure chimique du PPS.

Les renforts sont des fibres de verre ayant un diamètre 15 µm et une longueur de 200 µm en moyenne.

II-2 Echantillonnage

Deux types d'échantillon sont utilisés. Ils sont tirés de plaques de 3mm d'épaisseur de PPS/FV obtenues par injection et fournies par la société Valéo.

Des éprouvettes haltères découpées par jet d'eau ont une longueur totale de 72 mm et donc une épaisseur de 3 mm. La zone utile présente une longueur de 20 mm et une largeur de 10 mm.

Des films : ces mêmes plaques sont aussi utilisées pour préparer des films. Tout d'abord, une partie d'une plaque d'origine a été découpée et collée sur un support de base. Ensuite, cet échantillon complet avec un support de base a été fixé sur un microtome de marque LEICA. Le LEICA RM2255 est un microtome rotatif, entièrement automatique et motorisé avec un panneau de commande séparé pour l'élaboration de minces sections d'échantillons de dureté variable. Cet appareil peut afficher différentes vitesses d'avancement et aussi permettre d'obtenir les diverses épaisseurs de coupe nécessaires en contrôlant automatiquement une distance et une localisation précise de la lame. Pour cette étude, l'épaisseur des films est de 20 µm et chaque film est placé dans un sac pour être stocké et utilisé pour les besoins de l'étude du vieillissement thermique du matériau.

II-3 Méthodes de caractérisation physico-chimiques et mécaniques des échantillons vierges et vieillis

Les films d'une épaisseur de 20 µm et les éprouvettes haltères ont été placés dans des fours à circulation d'air sous des températures de vieillissement fixées à 100 °C, 140 °C, 160 °C, 180 °C et 200 °C. Les échantillons sont analysés par les méthodes suivantes :

Thermogravimétrie : Les éprouvettes haltères découpés dans les plaques de PPS/FV ont été suspendues dans l'enceinte d'un four, en contact avec l'air, à différentes températures. Le poids de l'échantillon a été mesuré à des intervalles de temps différents pour déterminer le pourcentage de perte de masse : W%, en utilisant l'équation suivante :

$$W\% = \frac{W_0 - W_t}{W_0} * 100\% \qquad \text{(e.q. 1)}$$

où w_t est le poids après un laps de temps t et w_0 est le poids de l'échantillon vierge.

Pour l'essai en perte de masse, quatre températures de vieillissement (100, 140, 180 et 200 °C) ont été imposées durant des périodes de 5256 heures au maximum.

Des essais de thermogravimétrie non-isotherme sont réalisés entre la température ambiante et 800°C avec une vitesse de chauffe de 10°C/min dans une atmosphère d'azote (40 ml/min), à l'aide d'un TGA Q500. La masse de l'échantillon initial est comprise entre 10 et 20 mg et est placée dans un creuset en Al_2O_3.

La spectrométrie IRTF a été utilisée pour caractériser les produits et déterminer l'ampleur de l'oxydation du polymère. L'appareil utilisé est un spectrophotomètre Nicolet Impact 410 configuré en mode transmission. Les mesures ont été effectuées sur des spectres résultant de l'accumulation de 32 analyses, la résolution étant de 4 cm^{-1}. Les films d'une épaisseur de 20 µm ont été utilisés. La concentration en C=O, correspondant au pic à 1780 cm^{-1}[41], est calculée selon la loi de Beer-Lambert suivante:

$$C = \frac{A}{\varepsilon \cdot e} \qquad \text{(e.q. 2)}$$

où A est l'absorbance du spectre IRTF, e est l'épaisseur des échantillons (ici 20 µm) et ε est le coefficient d'extinction (300 L. mol^{-1}. cm^{-1} pour le groupe C=O[41]). De même, les concentrations en [C-S] (1075 cm^{-1}) et [C-H] (2923 cm^{-1}) sont calculées de la même manière et les coefficients d'extinction de [C-S] et de [C-H] sont 114 [42]et 42 [43] L. mol^{-1}. cm^{-1}, respectivement.

Pour le test IRTF, les échantillons ont été prélevés à une durée de vieillissement allant de 0 h à 5256 h au maximum, avec quatre températures de vieillissement (140, 160, 180 et 200 °C).

L'absence ou la présence de stabilisants dans le matériau est vérifiée à l'aide d'un spectrophotomètre UV-visible PERKINELMER (modèle Lambda 5), équipé d'une sphère intégrée. Les spectres sont enregistrés en mode d'absorbance 66 sur une plage spectrale allant de 200 à 400 nm. L'analyse des données est effectuée en appliquant la concentration en espèces déterminée par la même méthode de spectrométrie IRTF et toujours selon la loi de Beer-Lambert.

Pour le test UV, un échantillon de film vierge (20 µm) a été utilisé.

Pour l'analyse en microscopie optique, des échantillons vierges et vieillis à 180 et 200 °C ont été utilisés. Le temps de vieillissement a été choisi entre 0 h et 5256 h au maximum.

La caractérisation de la microstructure des différents composites élaborés a été réalisée à l'aide d'un microscope électronique à balayage (HITACHI 4800 SEM).

L'épaisseur de la couche oxydée pour une éprouvette de PPS est mesurée par microscopie optique (microscope ZEISS- modèle Axio Imager 2). Une platine chauffante y a aussi été adaptée afin d'étudier la cristallisation de la matrice.

Des essais de calorimétrie différentielle ont été menés à l'aide de l'appareil DSC de NETZSCH Q10, dans le but de déterminer la température de transition vitreuse (T_g), la température de fusion (T_f) et la variation d'enthalpie de fusion (ΔH_f) qui permet de calculer le taux de cristallinité (X_c). Une rampe en température entre 20°C et 350°C avec une vitesse de 5 à 25°C/min est appliquée pour les échantillons de PPS. Le taux de cristallinité, X_C, est calculé à partir de relation suivante :

$$X_C = \frac{\Delta H_f}{\Delta H_f^0 * \varphi} * 100\% \qquad \text{(e.q. 3)}$$

avec X_C =taux de cristallinité, ΔH_f =enthalpie de fusion, ΔH_f^0 = enthalpie de phase cristalline pure, φ = pourcentage de la matrice.

Des tests d'analyse mécanique dynamique (DMA) ont été effectués sur des échantillons PPS/FV à l'aide de l'instrument DMA Q800 afin d'évaluer les principales températures de transition et le comportement viscoélastique. Ces tests ont été réalisés dans les conditions suivantes: une configuration de flexion alternée (nécessaire dans notre cas) et les températures de test retenues ont été choisies entre 25 °C et 200 °C, la fréquence est comprise entre 0,1 et 50 Hz et la vitesse d'évolution de la température de 0,5 °C/min. L'échantillon à section rectangulaire présentait des dimensions de 35 × 12 × 3 mm^3. De même, pour le test DMA, quatre températures de vieillissement (100, 140, 180 et 200 °C) ont été enregistrées de 0 h à 5688 h au maximum.

Des mesures de viscosité ont été effectuées avec le rhéomètre MCR 502 de chez Anton Paar. 2 types d'essais sont réalisés :

- Essais isotherme (à 290 °C), à déformation (0,2%) et à fréquence angulaire de 1 rad/s.
- Essais isotherme (à 300 °C), à déformation (0,2%) et à fréquence angulaire entre 0,1 et 100 rad / s.

Ces essais (isothermes) ont été réalisés sur des échantillons de film à différentes températures sous azote ainsi que dans une configuration plan-plan avec un intervalle de 1 mm entre les deux plateaux.

Pour les tests rhéologiques, des échantillons vierges et des échantillons vieillis à 180 et 200 °C ont été utilisés. Le temps de vieillissement a été choisi entre 0 heure et 606 heures.

Les essais de traction à basse vitesse de déformation (quasi-statique) ont été réalisés sur une machine hydraulique MTS 830 avec les éprouvettes de PPS/FV selon deux directions 0 et

90° par rapport à la direction de fluage. Un tableau récapitulatif (Tableau 1) regroupe les principales caractéristiques de notre matériau. Les articles N°2 et N°3 présentent des informations détaillées sur les caractéristiques physico-chimiques de ce matériau.

	E (MPa)	σ_r (MPa)	ε_r (%)	T_g	T_m	T_c	Densité (g/cm^3)
Pure PPS [44]	3697	82	2.7				
PPS-90°	4300±41	84±4.3	3±0.14	105	283	244	1.58
PPS-0°	6000±45	104±4.4	2.85±0.24	109	-	-	-

Tableau 1: Certains paramètres caractéristiques physicochimiques et mécaniques du PPS

Pour l'essai de traction, quatre températures de vieillissement (100, 140, 180, 200 °C) ont été choisies et la durée de vieillissement allait de 0 h à 5256 h au maximum.

Les essais de fatigue en traction-traction ont été réalisés sous différentes contraintes maximales appliquées sur la machine de fatigue hydraulique MTS 830. La contrainte minimale appliquée est toujours choisie égale à 10% de la contrainte maximale appliquée (R = 0,1). Dans cette étude, nous présentons les résultats des essais effectués à deux fréquences : 10 Hz et 50 Hz. Afin de mesurer avec précision l'évolution de la rigidité lors de la première étape de chargement (endommagement initial), chaque essai de fatigue est précédé d'une étape de charge-décharge-recharge en traction quasi-statique. Pendant le chargement cyclique, l'évolution de la température (due à l'auto-échauffement) a été mesurée à la surface des échantillons à l'aide d'une caméra infrarouge (Raynger-MX4). L'effet des dommages a été évalué par la mesure de l'évolution du module de Young.

III. Stratégie de recherche

Fondamentalement, le vieillissement conduit à un phénomène impliquant un changement lent et irréversible des propriétés des matériaux. Ce changement peut être la conséquence d'une action chimique ou physique. En général, on peut classer les différents types de vieillissement en deux grandes catégories:

1) Vieillissement physique sans changement de structure.

2) Vieillissement chimique avec changement de structure.

Dans le cas de l'oxydation ou thermo-oxydation des thermoplastiques, le vieillissement est un phénomène chimique pouvant entrainer une réaction de réticulation ou couper les chaînes macromoléculaires. La réticulation apporte une résistance à la traction, une dureté et un module de Young accrus, ainsi qu'une diminution de l'allongement à la rupture tandis que la coupure des chaînes est la cause de la fragilisation, l'affaiblissement et l'endommagement du matériau. En conséquence, l'oxydation est un phénomène multi-physique très complexe. A cette complexité, il faut rajouter les difficultés liées à la forme et à la structure 3D de la pièce. De plus, le mécanisme d'oxydation du PPS est moins connu dans la littérature et il n'y a pas beaucoup d'étude dans ce domaine. Pour nous confronter à l'ensemble de ces problèmes, notre stratégie de recherche est basée sur les points suivants :

- Présenter les phénomènes de façon simplifiée et accessible en étant vigilant à ce que cette simplification n'aboutisse pas à des interprétations et des conclusions erronées.
- Utiliser les résultats expérimentaux convergents obtenus par différentes méthodes complémentaires.

- Prendre en compte l'aspect multi-physique de ce sujet.

En effet, pour étudier l'influence de la thermo-oxydation sur les propriétés mécaniques et en particulier sur le comportement en fatigue du composite PPS/FV, nous utilisons :

1) La méthode directe en réalisant des essais de fatigue sur les échantillons vieillis au cours du temps.
2) Les méthodes indirectes qui permettent d'étudier cette influence à l'aide de l'effet d'oxydation sur les autres propriétés en lien avec les propriétés mécaniques.

Il est important de rappeler que le PPS est un polymère semi-cristallin constitué de deux phases : l'une amorphe et l'autre cristalline.

- D'une part, les deux phases ne s'oxydent pas de la même façon. La phase amorphe est moins compacte et l'oxygène peut pénétrer dans cette phase et réagir avec la structure chimique plus facilement. La phase cristalline est une phase compacte plus stable et elle ne se modifie pas facilement lors de l'oxydation du polymère. L'oxydation de la phase amorphe se produit souvent surtout à haute température et à long terme et aboutit à la coupure des chaînes macromoléculaires, au réarrangement et la modification de la phase amorphe. Dans certains cas, ce réarrangement augmente le taux de cristallinité du polymère.
- D'autre part, la phase cristalline est plus résistante, plus rigide et plus fragile que la phase amorphe ; donc la modification de la morphologie de la phase cristalline, à cause du vieillissement, impacte plus facilement le comportement mécanique (fatigue dans cette étude) du polymère.

Pour cette raison, nous avons mis un accent sur la phase cristalline et son évolution au cours de l'oxydation du polymère.

Il faut également rappeler que le polymère ne s'oxyde pas de la même façon à différents états physiques. A l'état vitreux, la phase amorphe est relativement figée et la mobilité des chaînes est faible. De même, la réaction du polymère avec l'oxygène qui est plus difficile et plus lente. En revanche, à l'état caoutchoutique l'oxydation se réalise plus facilement et plus rapidement. Dans le cas du PPS, le résultat de l'essai de DMA (Figure 2) nous indique que, au cours d'oxydation à 140°C, 160°C, 180°C et 200°C, la phase amorphe est à l'état caoutchoutique. A 100°C, cette phase se trouve dans la zone de transition vitreuse avec une mobilité moléculaire et une réactivité plus faible.

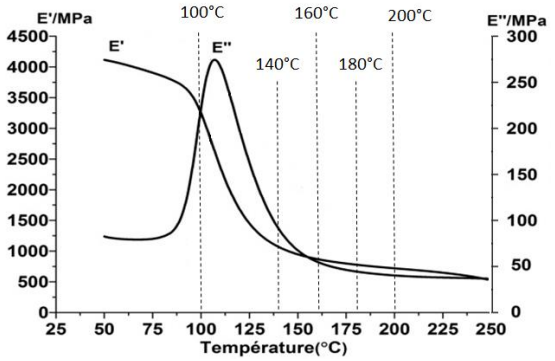

Figure 2 : Résultats de DMA : les différents états physiques (vitreux et caoutchoutique) et les températures du vieillissement.

En conséquence, pour bien comprendre l'effet de la thermo-oxydation sur le comportement en fatigue du PPS, il est nécessaire d'étudier, d'une part, l'interaction entre la morphologie, l'état physique et les propriétés mécaniques de ce polymère et d'autre part leur évolution au cours du vieillissement. Cet aspect est bien illustré sur le Schéma.1.

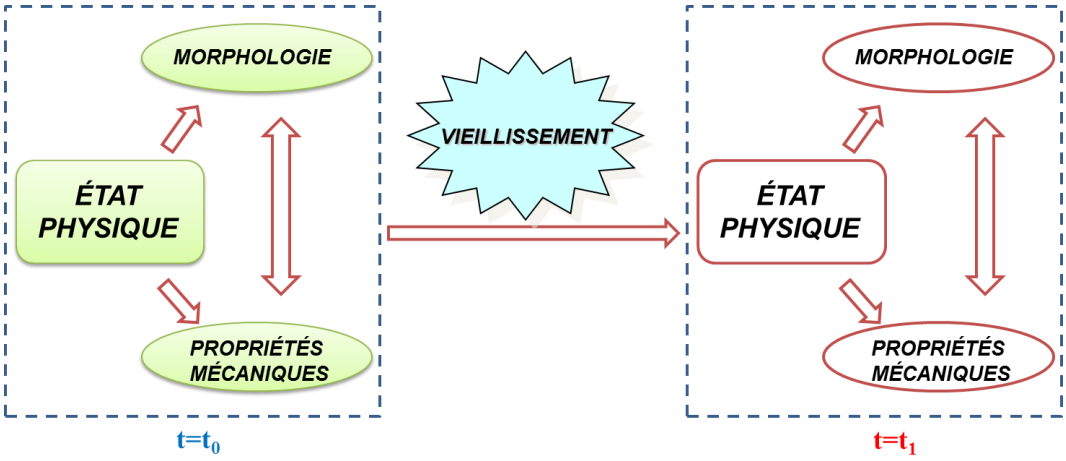

Schéma.1 : Stratégie de recherche des effets du vieillissement thermique sur l'état physique des composites PPS.

Avant de montrer de façon synthétique les résultats obtenus, il est également nécessaire d'évoquer les points suivants :

Dans cette étude, le polymère n'est pas seul ; il est dans un milieu comprenant d'autres constituants qui pourrait intervenir dans les processus de vieillissement :

1) Les fibres de verre

Les questions sont les suivantes :

- Est-ce que les fibres sont ensimées ? L'ensimage permet d'avoir une bonne adhésion entre les fibres et la matrice. La présence d'un ensimage a pour effet une diminution de l'espace vide dans la zone interfaciale ce qui rend plus difficile la diffusion de l'oxygène dans cette zone.
- Est-ce que la présence des fibres favorise l'oxydation du polymère ?

- Il est clair que la fragilisation du composite est due à l'oxydation de la matrice et à la dégradation de l'interface. Parmi ces deux causes, laquelle est prédominante lors du vieillissement ?

2) Les stabilisants thermiques dans la matrice

Les stabilisants thermiques sont souvent utilisés pour ralentir le processus d'oxydation et retarder le vieillissement du polymère. On emploie assez souvent au moins deux stabilisants ayant chacun une nature et un rôle différents. Ces stabilisants peuvent protéger le polymère dans les différentes conditions de mise en œuvre et au cours de son utilisation. Dans certaines conditions la présence de plusieurs stabilisants peut créer une sorte de synergie qui permet d'augmenter leur efficacité.

Dans notre étude, en raison de l'absence d'informations du fournisseur sur les antioxydants ou stabilisants thermiques, une analyse par spectrométrie UV est nécessaire pour détecter la possibilité d'existence d'antioxydants traditionnels, notamment des polyphénols, des polymères phénoliques, etc.

3) Les charges minérales

De façon générale, à cause de la faible masse molaire, le PPS est relativement fluide lors du moulage par injection ou de l'extrusion. Ceci peut mettre en difficulté la mise en œuvre du polymère. Pour optimiser la condition de cette mise en œuvre du matériau, une des méthodes consiste à rajouter des charges minérales. On peut ainsi augmenter la viscosité du polymère à l'état fondu. Pour vérifier l'absence et la présence des charges, on peut utiliser plusieurs méthodes. Une des méthodes simples consiste à utiliser la pyrolyse. Chauffer le composite à une

température élevée (800°C) pendant un certain temps permet d'éliminer la matrice et de récupérer les fibres et les charges minérales si elles existent.

IV. Etude de la morphologie de la phase cristalline

IV-1 Cristallisation et sa cinétique

Pour pouvoir comprendre l'influence du vieillissement du PPS sur ses propriétés mécaniques, comme il a été déjà expliqué précédemment au paragraphe III, il est nécessaire d'étudier l'évolution de la morphologie au cours temps. Pour ceci, nous avons effectué une étude exhaustive dans ce domaine. Les résultats de cette étude font l'objet d'un article en phase de rédaction. Pour rester cohérent avec ce résumé étendu, nous ne présentons pas la totalité de ces résultats. Nous ne présenterons de façon synthétique, une partie de ces résultats qui montre l'influence du vieillissement sur la phase cristalline.

Comme nous avons déjà indiqué, le PPS est un polymère thermoplastique semi-cristallin avec un taux de cristallinité compris entre 40 et 45%. La phase cristalline de ce polymère comme beaucoup d'autres polymères semi-cristallins présente une texture sphérolitique. Les études dans la littérature [45] (voir la Figure 3), ont bien montré que la formation de la phase cristalline est sensible à la vitesse de refroidissement. Ces résultats montrent que la taille (le diamètre moyen) des sphérolites à la fin de la cristallisation diminue avec l'augmentation de la vitesse de refroidissement.

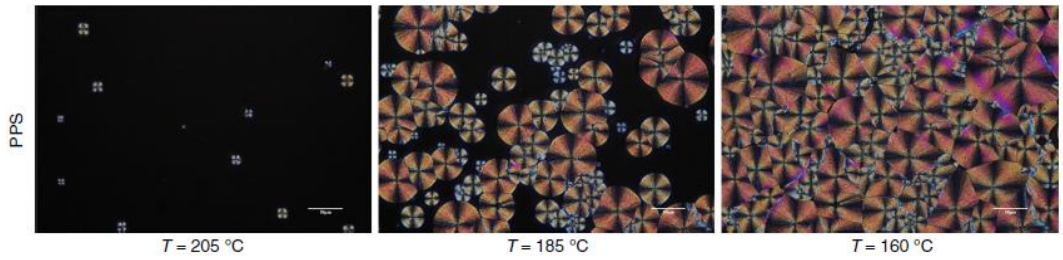

(a)

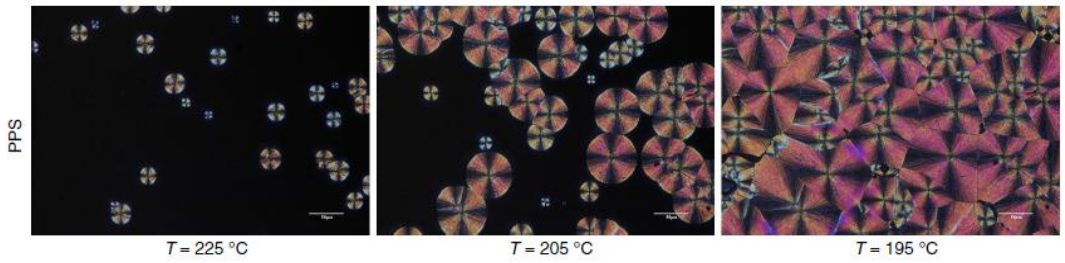

(b)

Figure 3 : Images de microscopie optique polarisées du PPS pur lors de la cristallisation non isotherme à deux vitesses de refroidissement différentes : (a) 20°C/min et (b) 5°C/min.

Nous avons réalisé des essais de DSC à vitesse de refroidissement allant de 5 à 25 °C sur les échantillons de PPS/FV. Les résultats sont montrés sur la Figure 4 (a). On peut noter que la vitesse de refroidissement a un effet significatif sur le processus de cristallisation du PPS. La température de cristallisation (T_c) diminue avec l'augmentation de la vitesse de refroidissement. La T_c diminue de 243°C à 230°C, quand la vitesse de refroidissement augmente respectivement de 5°C/min à 25°C/min.

A partir des résultats de DSC nous avons suivi l'évolution du taux d'avancement de cristallisation en fonction du temps à différentes vitesses de refroidissement; Figure 4 (b). On

constate, chaque fois, 3 étapes lors de la cristallisation. La première étape correspond à la nucléation et à la formation de cristallites (l'unité structurale de la phase cristalline). Lors de cette étape, le taux d'avancement de cristallisation n'évolue pas. Cette période est plus importante quand la vitesse de refroidissement est plus faible. La deuxième étape correspond à la phase de formation des sphérolites et à leur croissance. La vitesse de croissance (la pente de la courbe) est directement liée à la vitesse de refroidissement. Elle est plus importante pour la vitesse de refroidissement la plus grande. La troisième étape correspond à la phase finale de la formation des sphérolites. Lors de cette étape, les sphérolites interagissent entre eux pour former des polygones solides à la fin de cristallisation. On constate que la durée globale de cristallisation diminue avec l'augmentation de la vitesse de refroidissement.

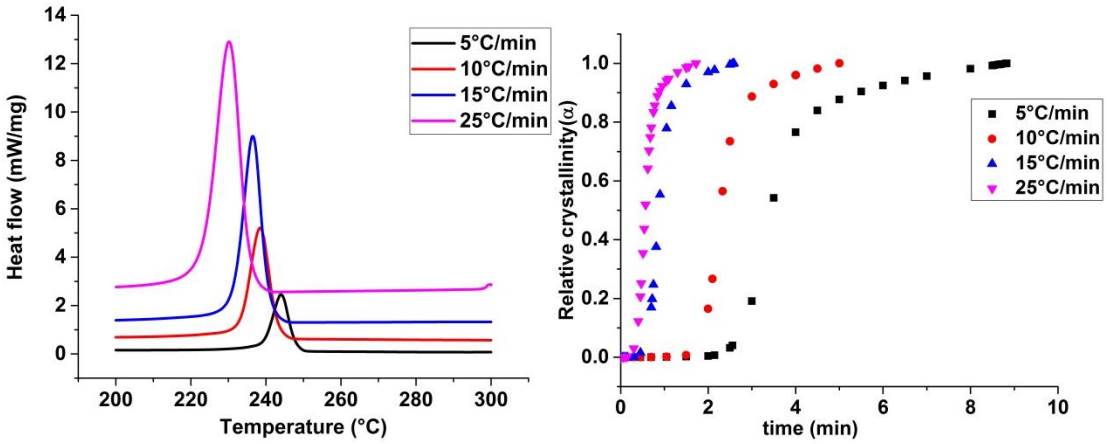

(a) (b)

Figure 4 : Courbes de flux de chaleur (a) et de cristallinité relative (b) des composites PPS à différentes vitesses de refroidissement (5 ~ 25 °C /min).

Basé sur le modèle d'Avrami, le modèle de Jeziorny [46] est couramment utilisé pour modéliser le processus de cristallisation non-isotherme. On peut présenter ce modèle par l'équation suivante [47-50]:

$$\alpha = \ln[-\ln(1-\chi(t))] = \ln K + n \ln t \qquad \text{(e.q. 4)}$$

$$\ln Kc = \frac{\ln K}{\beta} \qquad \text{(e.q. 5)}$$

où α est taux de cristallinité relative, χ(t) est le taux d'avancement de cristallisation, K (une constante) est la vitesse de cristallisation, K_c est la vitesse de cristallisation corrigée, n est la constante d'Avrami et β est la vitesse de refroidissement.

La Figure 5 montre que l'évolution de $\ln(-\ln(1-\chi(t)))$ en fonction de ln(t) est linéaire avec un coefficient de corrélation linéaire, R^2 proche de 1 ($1>R^2>0{,}99$) pour toutes les vitesses de refroidissement. Cela signifie que le modèle de Jeziorny peut parfaitement décrire et vérifier le processus de cristallisation non-isotherme de ce matériau PPS/ FV.

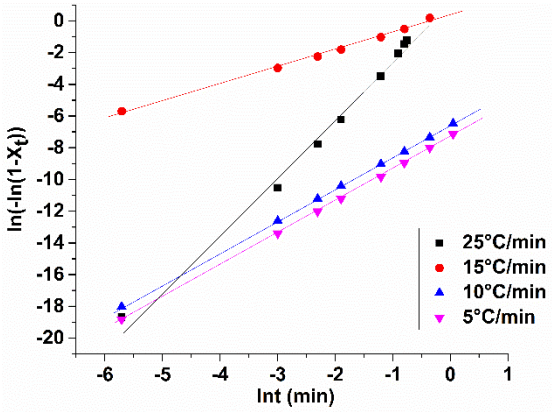

Figure 5: Courbe du ln (-ln (1-*X*(t))) par rapport au ln(t) à différentes vitesses de refroidissement (5 à 25 °C/ min).

Le Tableau 2 récapitule les valeurs des constantes de cette loi obtenues après identification pour les différentes vitesses de refroidissement. On constate que les valeurs de K et K_c augmentent avec la vitesse de refroidissement.

	R^2	n	Ln K	K_c
5 °C/min	0,99	2,02	-7,33	0,23
10 °C/min	1	2,00	-6,61	0,52
15 °C/min	0,99	1,08	0,34	1,02
25 °C/min	0,99	3,55	0,91	1,04

Tableau 2 : Paramètres cinétiques de cristallisation non isothermes obtenus à l'aide du modèle de Jeziorny.

Pour calculer l'énergie d'activation relative à la cristallisation non-isotherme, Kissinger et ses collaborateurs [51] ont proposé une équation basée sur le modèle cinétique d'ordre n, comme suit:

$$\ln\frac{\beta}{T_p^2} = \ln\frac{AR}{E} - \ln[G(\alpha)] - \frac{E}{RT_p} \qquad \text{(e.q. 6)}$$

où β est la vitesse de refroidissement, T_p est la température du pic de cristallisation. A est le facteur pré-exponentiel et R est la constante universelle des gaz parfaits. E est l'énergie d'activation et G (α) est la fonction de conversion. Pour déterminer l'énergie d'activation nous avons utilisé l'équation de Kissinger, et nous avons tracé $\ln\frac{\beta}{T_p^2}$ en fonction de $\frac{1}{Tp}$. On obtient une droite avec un coefficient de corrélation linéaire proche à 1. A partir de la pente de cette droite nous avons déterminé l'énergie d'activation de la cristallisation non-isotherme (-58,78 kJ / mol).

IV-2 L'effet de vieillissement sur le phénomène de cristallisation

Le PPS est un polymère semi-cristallin, possédant une phase amorphe et une phase cristalline. La phase amorphe est beaucoup moins compacte. Par conséquent, il constitue le point faible vis-à-vis des phénomènes d'oxydation. Par contre, l'oxygène ne peut pas diffuer dans la phase cristalline. En conséquence le vieillissement thermo-oxydatif du PPS est en réalité attribué

essentiellement à la modification chimique de la phase amorphe. Cette modification peut se manifester de différentes façons : la réticulation (dans certains cas et pour certaines périodes du vieillissement), la scission des chaînes macromoléculaire, la diminution de la masse molaire, la fragilisation, la rigidification, la réorientation des macromolécules,… Tous ces phénomènes se déroulent dans la phase amorphe tandis que la phase cristalline reste relativement inchangée. Pour pouvoir comprendre l'effet du vieillissement sur les propriétés mécaniques, il est nécessaire d'étudier cette modification morphologique. A travers de cette modification microstructurale, la compréhension de l'origine des changements de propriétés mécaniques devient possible. Dans le cas du PPS/FV, nous avons déterminé les caractéristiques morphologiques à partir des résultats d'essais sur les échantillons de PPS/FV vierge et vieillis (à 200 °C) en utilisant les techniques de la DSC et de la DMA. Nous avons ensuite déterminé la T_g, la T_f, le taux de cristallinité ainsi que les constantes du modèle cinétique de cristallisation précédemment présenté (paragraphe précédent). Le tableau 3 récapitule l'ensemble de ces résultats.

Echantillons	Phase amorphe	Phase cristalline		
	T_g (*) (°C)	X_c (**) (%)	n (**)	K_c (**)
Vierge	106	44,2	2,00	0.5
200°C-20h	108	45,0	2,10	0,88
200°C-96h	108	55,8	2,19	0,82
200°C-144h	-	52,9	2,27	0,97
200°C-1080h	121	36,6	0,8	0,6

(*) T_g, obtenue par l'essai de DMA au pic de E'', (f=1 Hz) ; (**)X_c, n, K_c, obtenus à part des résultats de DSC avec une vitesse à 10 °C/min.

Tableau 3 : Les paramètres identifiés grâce aux analyses de DMA et DSC sur les échantillons vieillis et vierge.

On constate d'abord qu'à l'issue d'une exposition de 1080 h à 200°C, la T_g passe de 106 °C (échantillon vierge) à 121 °C. Cette augmentation peut être attribuée aux deux phénomènes suivants : la réticulation (à court terme), à la réorientation et la rigidification des macromolécules à la suite de la rupture des chaînes par l'oxydation. Les macromolécules deviennent moins mobiles dans la zone amorphe.

On constate également que le taux de cristallinité augmente de 44% (échantillon vierge) à 56% après 96 h de vieillissement à 200°C. Après une plus longue période d'oxydation (1080 h), le taux de cristallinité diminue à 36,6%. Il est difficile d'interpréter cette baisse conséquente du taux cristallinité. En revanche, ce qui est évident c'est qu'à ce stade de dégradation (1080 h) à 200°C, la phase amorphe est bien endommagée et la texture du matériau est fortement modifiée.

Contrairement à notre hypothèse de départ, on peut donc se poser la question suivante : est-ce que la phase cristalline est aussi dégradée et de quelle façon ?

Concernant la modification de la phase cristalline au cours du vieillissement, l'analyse du changement des valeurs des constantes du modèle ((e.q. 4) et (e.q. 5)) nous permet d'avancer les idées suivantes :

- La constante n dépend de la nature de la nucléation, de la géométrie des cristallites et de la densité des sphérolites. On constate que la valeur de n est plus ou moins égale à 2 pour les échantillons vierges et vieillis à 200°C jusqu'à 144 h. On peut supposer que pendant cette période la phase cristalline n'est pas modifiée de façon significative. Cependant, pour les échantillons vieillis après 1080 h à 200 °C, n diminue à 0,8. Cela peut impliquer que le PPS par rapport à son état initial a presque perdu sa capacité de nucléation et de cristallisation en raison du vieillissement thermique bien avancé.
- De même, K_c dépend de la vitesse de cristallisation et l'augmentation de K_c correspond à l'augmentation de la capacité de cristallisation. Au début du vieillissement thermique, une augmentation de K_c de 0,5 (échantillon vierge) à 0,97 (échantillon 200 °C - 144 h) a été observée. Cela indique que le vieillissement peut accélérer le processus de cristallisation. Toutefois, à long terme (comme 200 °C -1080 h), quand le vieillissement est bien avancé, le polymère est complétement dégradé ce qui produit une diminution de la cinétique de cristallisation. En effet, à ce stade, la valeur de K_c redescend à 0,6.

V. Comportement à long terme du PPS composite

Cette partie est dédiée dans un premier temps à l'étude du vieillissement thermo-oxydatif du composite à matrice PPS. Il s'agit d'une étude de vieillissement accéléré à températures

élevées (de 100 à 200 °C). Pour ce faire, nous effectuerons des analyses par spectrométrie IR afin de détecter et suivre l'évolution des produits d'oxydation dans les matériaux. Ceci permettra de proposer une interprétation des mécanismes de dégradation qui seront utilisés dans un second temps pour la construction d'un modèle cinétique capable de décrire l'évolution des produits d'oxydation.

Pour cette partie de l'étude, la méthodologie consiste d'une part à réaliser des essais de vieillissement accéléré avec suivi l'évolution de certains groupements chimiques (tel que C=O) (indicateur d'avancement du vieillissement), et d'autre part de proposer un mécanisme d'oxydation du PPS. Ce mécanisme permet de proposer un modèle cinétique pour l'évolution de C=O. L'étape suivante est donc de confronter les résultats expérimentaux avec le modèle théorique. Le schéma 2 présente cette démarche.

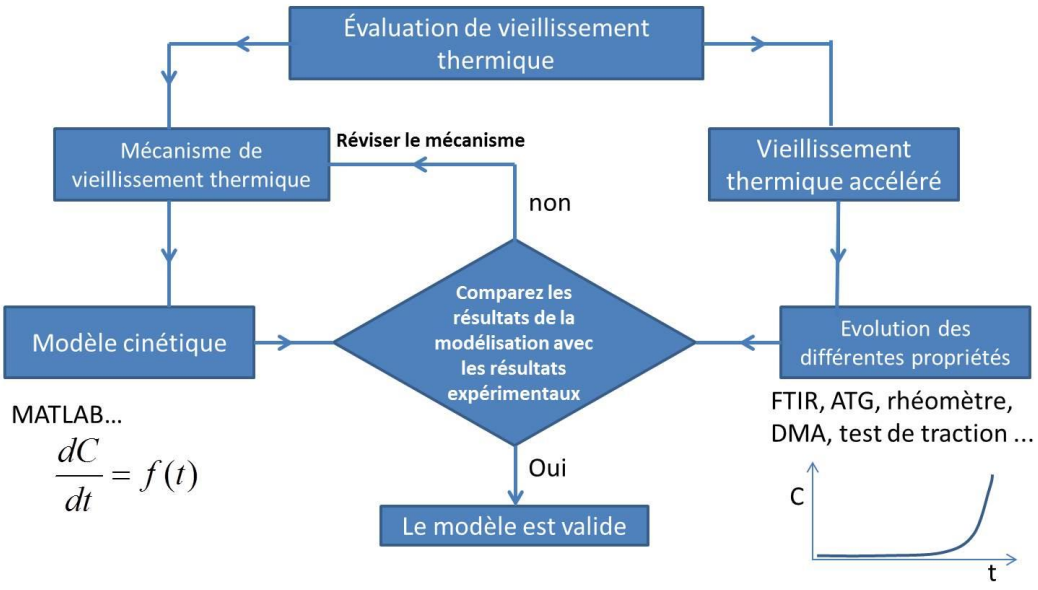

Schéma.2: Approche de la modélisation par oxydation thermique.

A la suite de cette introduction, nous présentons la mise en œuvre de notre étude et notamment la modélisation de la thermo-oxydation du PPS/FV. Les résultats détaillés de cette étude font l'objet de l'Article N°3.

V-1 Analyse préliminaire

En raison du manque d'informations précises sur la composition de ce matériau fourni par le fournisseur, les pics pour les matériaux d'origine compris entre 1700 et 1800 cm^{-1} peuvent s'expliquer par le fait qu'il existe des groupes phényle ou un ester vinylique. Ces pics pourraient apparaître dans la position des groupes terminaux. Pour simplifier la recherche, il est nécessaire de prendre en compte uniquement l'oxydation thermique du matériau PPS lui-même.

Pour étudier l'évolution des produits d'oxydation, on a utilisé une approche classique qui consiste à suivre la concentration totale des produits carbonyles à partir des absorbances des pics IR grâce à la loi de Beer-Lambert. La concentration de [C=O] donne une indication claire sur l'avancée de l'oxydation. La Figure 6 montre les résultats FTIR des pics C=O, qui sont situés aux positions d'onde de 1780 cm^{-1}, 1735 cm^{-1} et 1710 cm^{-1}, respectivement. Plus précisément, ils peuvent être divisés en trois types différents de doubles liaisons C=O. Ainsi, on peut noter qu'il existe une tendance à l'augmentation évidente de l'absorbance des doubles liaisons C=O, ce qui indique que les composites PPS/FV sont sérieusement oxydés à 200 °C.

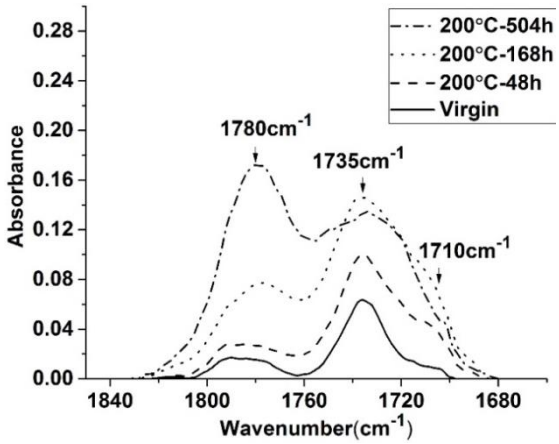

Figure 6 : Evolution des produits d'oxydation du PPS à 200°C.

La Figure 7 représente les différentes évolutions des produits d'oxydation du PPS pour les 4 températures d'exposition. Les courbes d'accumulation des produits d'oxydation (C=O) au cours du vieillissement mettent en évidence les trois étapes caractéristiques de la cinétique d'oxydation :

- Une période d'induction précédant l'apparition des premiers produits carbonyles.
- Une accélération rapide (auto-accélération) de l'oxydation à la fin de la période d'induction.
- Un régime stationnaire à vitesse d'oxydation globale apparente quasi-constante.

On peut constater que les taux d'accumulation des produits oxydants augmentent avec l'augmentation de la température d'exposition.

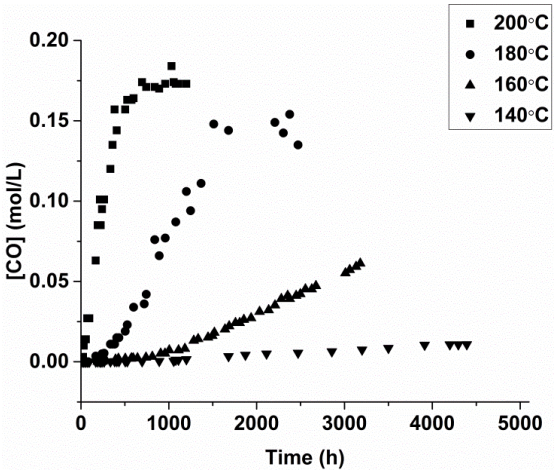

Figure 7 : Evolution des produits d'oxydation du PPS à 140 °C, 160 °C, 180 °C et 200 °C.

Classiquement, l'oxydation peut être divisée en trois périodes: induction, propagation et terminaison. On peut voir que le temps d'induction est très court (environ 24 h) pour les échantillons vieillis à 200 °C ; alors que cette valeur augmente significativement pour les températures de 180 °C et 160 °C (240 h et au-delà de 1100 h, respectivement). A la température de 140 °C, le temps d'induction est très long (plus de 2000 h). On peut donc noter que les temps d'induction aux températures de 180 °C et 160 °C sont respectivement environ 10 et 45 fois plus élevés qu'à 200 °C. En outre, la cinétique est très rapide pour les températures d'oxydation de 200 °C et 180 °C. Après environ 1000 h d'oxydation à 200 °C, la propagation a tendance à être saturée lorsque la quantité de produits d'oxydation atteint un maximum. A 180 °C, la saturation semble être atteinte après 2000 h d'exposition. Comparativement, il n'y a pas d'évolution comparable et aucune tendance de plateau stable observable pour l'oxydation à 140 °C même après plus de 4000 h d'exposition. Ainsi, on peut conclure que, pour ce composite, les rapports d'oxydation à 200 °C et 180 °C sont considérablement plus sévères et plus rapides qu'aux températures de 160 °C et 140 °C.

V-2 Modélisation de la cinétique du vieillissement

- **La théorie d'oxydation**

Dans cette partie de l'étude du vieillissement thermique, une modélisation de la cinétique d'oxydation a pu être réalisée à partir des résultats expérimentaux.

Les polymères hydrocarbonés soumis au vieillissement thermique dans l'air se dégradent généralement par oxydation en chaîne radicalaire [52, 53]. Le modèle du mécanisme standard sous air ou oxygène, considérant la décomposition simultanée d'hydroperoxyde uni- et bi-moléculaire, est rapporté dans plusieurs travaux de recherche [54-56] (voir Schéma 3):

$$POOH \rightarrow 2P^{\circ} + \Upsilon co\ PC = O \qquad (k1u)$$

$$POOH + POOH \rightarrow P^{\circ} + POO^{\circ} + \Upsilon co\ PC = O \qquad (k1b)$$

$$P^{\circ} + O2 \rightarrow POO^{\circ} \qquad (k2)$$

$$POO^{\circ} + PH \rightarrow POOH + P^{\circ} \qquad (k3)$$

$$P^{\circ} + P^{\circ} \rightarrow \text{inactive products} \qquad (k4)$$

$$P^{\circ} + POO^{\circ} \rightarrow \text{inactive products} \qquad (k5)$$

$$POO^{\circ} + POO^{\circ} \rightarrow \text{inactive products} + O2 \qquad (k6)$$

Schéma.3 : Schéma proposé de la dégradation du polymère.

Ici, [P °], [POO °], [POOH], [PH] représentent la concentration des radicaux alkyles, des radicaux peroxyde, des hydro-peroxydes et du substrat, respectivement ; les nombres k1u à k6 représentent les constantes cinétiques de chaque réaction.

Plusieurs recherches antérieures ont étudié le mécanisme de dégradation des polymères PPS [57-62]. En dessous de 200 °C, le diagramme schématique possible de la dégradation des composites PPS / FV est donné dans le schéma 4. Selon la littérature [61] et selon la théorie de l'énergie des liaisons, les liaisons carbone-soufre (C-S) et carbone-hydrogène (C-H) sont plus faibles que la double liaison carbone-carbone (C=C). Ainsi, la première scission principale se produit dans les liaisons C-S ou C-H. Dans des conditions de vieillissement thermique, il se produit une dégradation par abstraction radicalaire, recombinaison, cyclisation et/ou d'autres réactions plus complexes, avec un processus de production de différents composés tels que le sulfure d'hydrogène, le benzènethiol, le diphénylsulfure, le dibenzothiophène, etc [63].

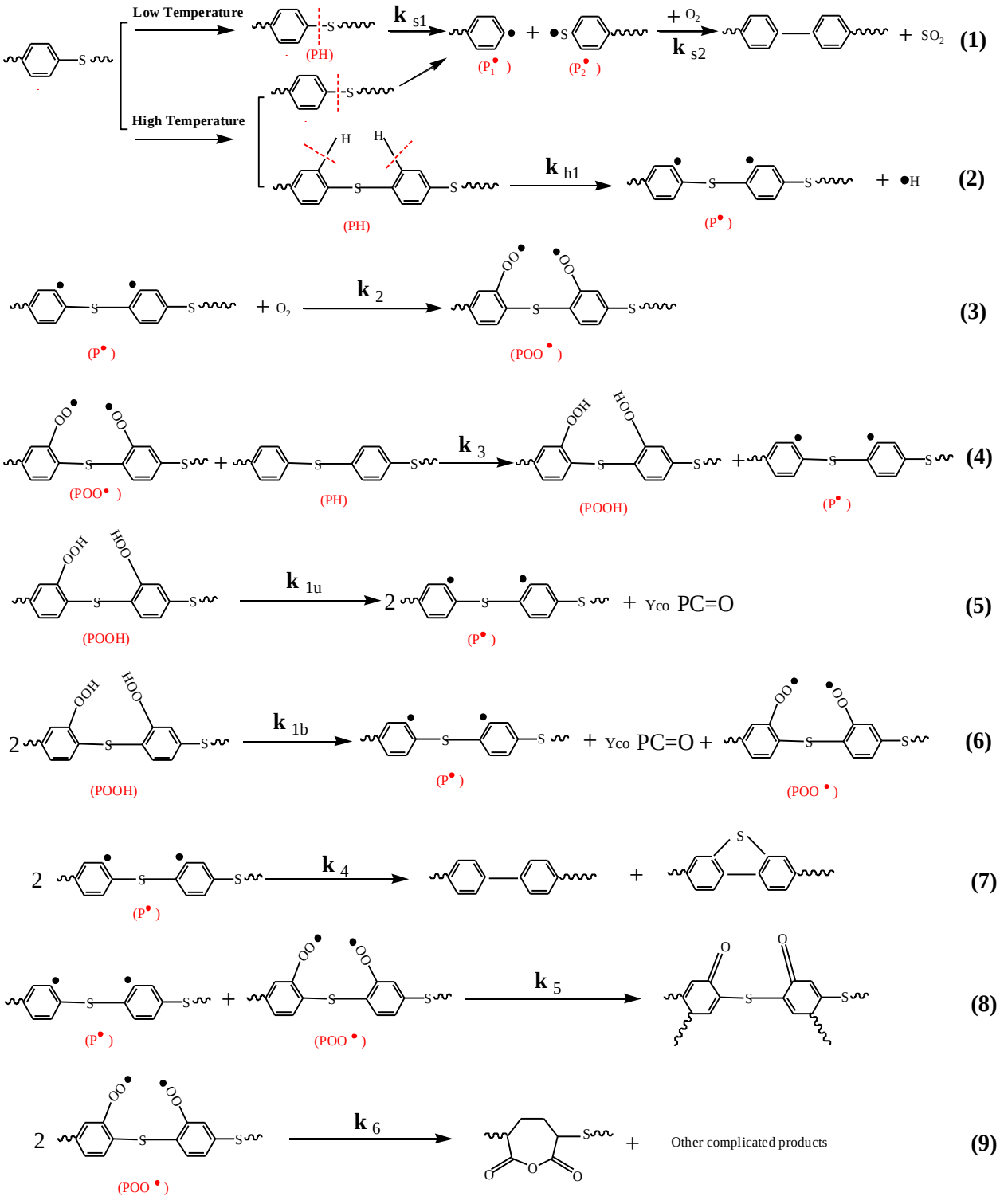

Schéma.4 : Schéma proposé de dégradation du PPS au sein du composite PPS/FV.

Selon ce schéma, on peut clairement noter que le processus de dégradation oxydative contient des voies principales qui peuvent se produire au niveau des liaisons C-S ou C-H. Il est remarquable que, comme dans les recherches antérieures [52] [54], le mécanisme de dégradation oxydative du PPS peut être présenté par des équations différentielles. En utilisant ces équations différentielles, il est alors possible de calculer quantitativement l'évolution de la concentration en liaison [C=O] en fonction du temps sous différentes températures de vieillissement oxydatif comme suit :

$$\frac{d[P^\circ]}{dt} = 2 * k_{1u} * [POOH] + k_{1b} * [POOH]^2 - k_2 * [P^\circ] * [O]$$

$$+k_3 * [POO^\circ] * [PH] - 2 * k_4 * [P^\circ]^2 - k_5 * [P^\circ] * [POO^\circ] + k_{h1} * [PH] \quad (e.q.7)$$

$$\frac{d[POO^\circ]}{dt} = k_{1b} * [POOH]^2 + k_2 * [P^\circ] * [O] - k_3 * [POO^\circ]^2 * [PH]$$

$$-k_5 * [P^\circ] * [POO^\circ] - 2 * k_6 * [POO^\circ]^2 \quad (e.q.8)$$

$$\frac{d[POOH]}{dt} = -k_{1u} * [POOH] - 2 * k_{1b} * [POOH]^2 + k_3 * [POO^\circ] * [PH] \quad (e.q.9)$$

$$\frac{d[PH]}{dt} = -k_3 * [POO^\circ] * [PH] - k_{s1} * [PH] \quad (e.q.10)$$

$$\frac{d[CO]}{dt} = k_{1u} * [POOH] + k_{1b} * [POOH]^2 \quad (e.q.11)$$

$$\frac{d[P_1^\circ]}{dt} = k_{s1} * [PH] - k_{s2} * [P_1^\circ][P_2^\circ] * [O] \quad (e.q.12)$$

$$\frac{d[P_2^\circ]}{dt} = k_{s1} * [PH] - k_{s2} * [P_1^\circ][P_2^\circ] * [O] \quad (e.q.13)$$

Ici, [P °], [POO °], [POOH], [PH] représentent la concentration des radicaux alkyles, des radicaux peroxy, des hydro-peroxydes et du substrat, respectivement ; les nombres k1u à k6 sont les constantes cinétiques de chaque réaction.

- **Validation du modèle cinétique**

L'identification et la validation du modèle cinétique proposé ont étés effectuées. La corrélation avec les évolutions des données expérimentales obtenues entre 160° et 200 °C est montrée en Figure 8. Les valeurs des paramètres du modèle ayant permis d'obtenir les meilleures simulations des résultats expérimentaux correspondant aux températures d'exposition de 160 °C, 180 °C et 200 °C sont récapitulées dans le Tableau 4. On peut voir que les résultats expérimentaux sont très cohérents avec la modélisation. Cela signifie que notre modèle mécanistique de dégradation oxydative semble approprié. On peut donc conclure que cette modélisation nous permet de traduire correctement l'effet des mécanismes de dégradation d'une manière quantitative.

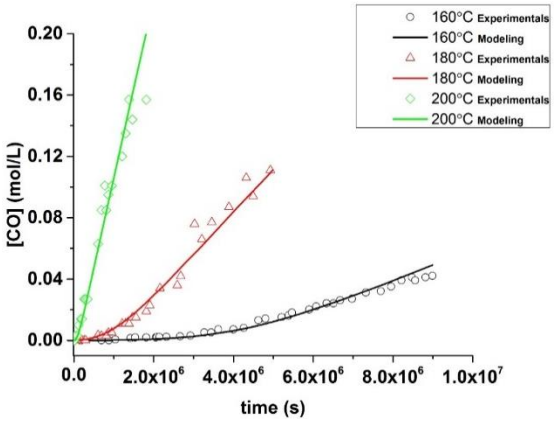

Figure 8 : Comparaison expérience-simulations de l'évolution des produits d'oxydation à 160 °C, 180 °C et 200 °C.

	k1u (s^{-1})	k1b ($l\ mol^{-1}s^{-1}$)	k2 ($l\ mol^{-1}s^{-1}$)	k3 ($l\ mol^{-1}s^{-1}$)	k4 ($l\ mol^{-1}s^{-1}$)	k5 ($l\ mol^{-1}s^{-1}$)	k6 ($l\ mol^{-1}s^{-1}$)
T=160 °C	$1.3x10^{-7}$	$1.1x10^{-5}$	$1.3x10^{6}$	$1.1x10^{-3}$	$1.0x10^{12}$	$2.0x10^{9}$	$3.0x10^{3}$
T=180 °C	$1.6x10^{-6}$	$1.8x10^{-5}$	$1.5x10^{6}$	$1.8x10^{-3}$	$1.0x10^{12}$	$2.0x10^{9}$	$3.4x10^{3}$
T=200 °C	$2.0x10^{-5}$	$2.0x10^{-5}$	$1.6x10^{6}$	$6.0x10^{-3}$	$1.0x10^{12}$	$2.0x10^{9}$	$4.0x10^{3}$

Tableau 4 : Constantes cinétiques et paramètres d'Arrhenius des réactions

VI. Comportement du matériau en fatigue

La fatigue est l'application de contraintes ou de déformations cycliques (répétées) dans le temps qui peuvent modifier les propriétés locales et globales d'un matériau. La fatigue peut entraîner d'une part des déformations irréversibles (plasticité) et/ou la formation de microfissures aboutissant à la rupture de la pièce. La progression de l'endommagement en fatigue peut suivre différentes étapes :

- La création de sites de nucléations
- La formation de microfissures
- La croissance et la coalescence de fissures microscopiques dominantes
- La propagation et la coalescence des microfissures donnant lieu à l'apparition de macro-fissures dominantes
- La rupture

Les principales caractéristiques et propriétés régissant le comportement en fatigue d'un composite à matrice polymère, sont les suivantes :

- La nature de la matrice : sa composition chimique, sa morphologie, l'état physique…
- Les additifs et les charges : billes de verre, particules minérales,…
- La nature des renforts : matière, architecture et dimensions
- L'état de l'interface : l'ensimage, l'adhésion chimique, physique ou mécanique entre matrice et fibres
- Le type et les conditions de sollicitation (température, amplitude des contraintes ou des déformations, fréquence, rapport de charge …)

Dans le cadre de ce travail, des essais de fatigue en traction-traction ont été réalisés sur une machine hydraulique MTS 830 (Elastomère Test System) avec application d'une force maximale constante à une fréquence de 10 Hz. Les échantillons ont été découpés par jet d'eau en utilisant la géométrie représentée sur la Figure 9-(a).

L'amplitude de sollicitation affecte directement et de façon conséquente la durée de vie du matériau. Dans le but de comprendre l'effet de la microstructure sur le comportement en fatigue des matériaux, nous avons effectué une étude préliminaire en fatigue sur deux matériaux renforcés en fibres orientées à 90° et 0°. Les courbes de Wöhler à 10 Hz correspondantes sont représentées dans la Figure 9-(b) [64].

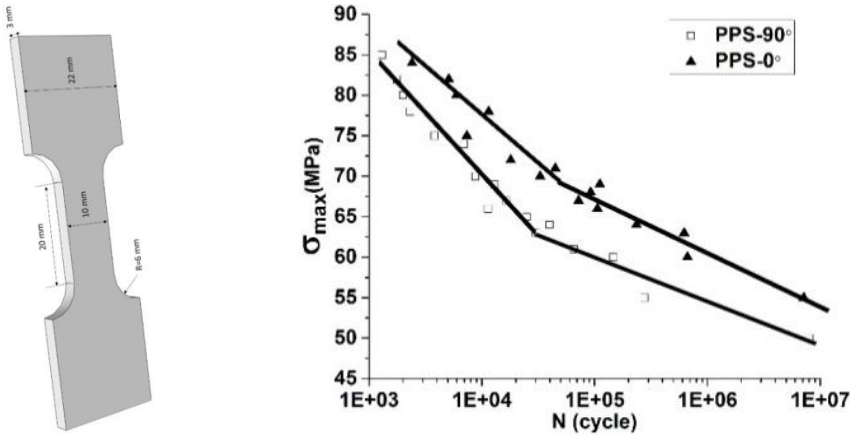

(a) (b)

Figure 9 : (a) Géométrie d'éprouvette (b) Courbes de Wöhler pour les éprouvettes PPS-0° et PPS-90° à 10 Hz.

On peut faire les remarques suivantes :

- Pour les échantillons PPS-0° et PPS-90°, les courbes de Wöhler ne présentent pas de valeur asymptotique notable représentative d'une limite d'endurance. Contrairement aux matériaux métalliques, ceci est souvent observé dans le cas des composites thermoplastiques [65].
- Pour une amplitude de contrainte de 60 MPa, le PPS-90° rompt après 10^5 cycles de fatigue. Alors que pour la même amplitude, le PPS-0° se rompt après plus de 10^6 cycles. Ce constat démontre clairement que la durée de vie est fortement influencée par l'orientation des fibres.
- Pour les deux configurations, les courbes de Wöhler montrent deux domaines différents; haute et basse amplitudes. Dans chaque domaine, la courbe S-N peut être modélisée par une équation linéaire-logarithmique:

$$\sigma_{max} = A.\log N + B \qquad \text{(e.q. 14)}$$

Dans cette équation, A et B sont des paramètres matériels identifiés par la pente de la droite et l'ordonnée à l'origine, respectivement. La pente montre la sensibilité de la résistance à la fatigue et l'ordonnée à l'origine B est lié à la résistance à la traction apparente.

Le Tableau 5 montre les valeurs de A et B pour le PPS-0° et le PPS-90° liées aux domaines de contraintes élevées et faibles.

Échantillons	A (MPa)		B (MPa)	
	Domaine à forte contrainte	Domaine à faible contrainte	Domaine à forte contrainte	Domaine à faible contrainte
PPS-0°	-12,0	- 6,7	125,7	108
PPS-90°	-15,2	- 5,5	131	87,5

Tableau 5 : Les valeurs de A et B pour PPS-0° et PPS-90° dans chaque domaine

VII. Effets du vieillissement thermique sur le comportement mécanique

Dans cette partie nous présentons de façon synthétique l'effet du vieillissement thermique sur le comportement mécanique du PPS/FV. Des informations détaillées sur le comportement à long terme sont présentées dans l'Article N°4.

La revue de la littérature fournit beaucoup d'informations sur les propriétés générales des composites PPS. Cependant, il existe un manque d'informations sur la réponse à la fatigue lorsqu'ils ont été exposés au vieillissement thermique. Il est donc impératif de proposer des travaux innovants pour mieux comprendre les effets du vieillissement thermique sur les propriétés mécaniques, notamment en ce qui concerne le comportement en fatigue. Ce type de

recherche concerne et intéresse directement des applications industrielles et est indispensable notamment pour les calculs de structure en particulier dans le secteur automobile.

Un point clé de notre approche est de suivre la concentration [C=O] au cours du vieillissement thermique en tant qu'indicateur du processus d'oxydation et de degré de dégradation dans la matrice. De plus, une relation entre l'oxydation thermique et le comportement mécanique est établie afin de fournir un outil d'aide au choix de la structure matériau et au dimensionnement pour le bureau d'études.

La première partie du document concerne l'analyse des effets du vieillissement thermique. Les réponses en chargement quasi-statique et les essais charge-décharge avec augmentation progressive de la contrainte maximale des échantillons vierges et vieillis sont analysés. L'effet du vieillissement thermique sur les propriétés de fatigue du composite PPS est ensuite également étudié.

Ci-après, trois types d'essais mécaniques ont donc été considérés :

- **Essai de traction :** Les effets du vieillissement sur les courbes contrainte-déformation obtenues par des essais de traction sont présentés. Les évolutions du module de Young, de la contrainte à la rupture et de la déformation à la rupture sont tracées pour différentes conditions de vieillissement. La réponse en traction est analysée pour une température d'oxydation de 200 °C après différents temps de vieillissement : 0 h, 30 h, 50 h, 100 h et 200 h.

- **Essai de charge-décharge :** Il est nécessaire d'analyser la perte de rigidité et l'évolution de la déformation plastique pour comprendre l'effet des conditions de vieillissement sur

les mécanismes d'endommagement et la déformation. Les essais de traction charge-décharge sont effectués à une température de vieillissement de 200 °C pour différents temps d'oxydation à savoir : 0 h, 30 h, 50 h, 100 h et 200 h.

- **Essai de fatigue en traction-traction :** Les essais de fatigue ont été effectués à 10 Hz pour comparer la durée de vie du composite PPS soumis à diverses températures et temps de vieillissement. De plus, les analyses de la perte de rigidité et de la fractographie sont présentées. Les comportements en fatigue sur quatre types d'échantillons oxydés à 140 °C, 160 °C, 180 °C et 200 °C aux différents temps de vieillissement ont été analysés. On peut noter que les amplitudes de chargement de 40 MPa et de 70 MPa ont été sélectionnées après l'analyse de la courbe de Wöhler obtenue sur des échantillons vierges.

VII-1 Résultats des essais de traction

Les résultats des essais de traction sur les échantillons non vieillis et les échantillons vieillis à la température de 200 °C pour différents temps de vieillissement sont présentés sur la Figure 10.

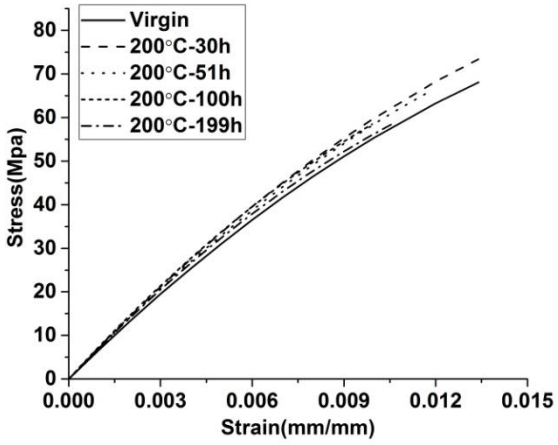

Figure 10 : Courbes de contrainte-déformation à différents stades de vieillissement à 200 °C.

On peut noter qu'au début de l'exposition à 200 °C, de 0 h à 30 h, la contrainte à la rupture augmente. Ceci est principalement dû à la post-réticulation, qui conduit à l'extension des chaînes moléculaires. Après cette étape préliminaire, la contrainte à la rupture diminue de 25% pendant 200 h. Ceci montre que l'oxydation thermique à 200 °C favorise la mobilité des chaînes moléculaires en raison de la scission de celles-ci.

On peut noter que le module de Young relatif augmente lentement au début de l'exposition à 200°C (en raison de la post-réticulation). De plus, tous les échantillons vieillis possèdent un module d'Young supérieur à celui des échantillons vierges, ce qui indique que la réticulation peut affecter le comportement mécanique des composites PPS. La déformation à la rupture présente une diminution constante d'environ 1,4% à 1% durant l'oxydation. Cela indique une fragilisation due à l'oxydation.

Les résultats des essais de traction montrent bien l'influence du vieillissement sur les propriétés mécaniques du composite PPS (Tableau 6 et Figure 11). Il a été montré une augmentation du module d'élasticité et de la contrainte à la rupture au cours de la première phase d'exposition. Pour être plus précis, au cours du processus de vieillissement, la scission des chaînes moléculaires et la post-réticulation peuvent se produire simultanément dans le matériau polymère PPS. De plus, il convient de noter qu'au début de l'oxydation thermique, la post-réticulation est plus prononcée tandis que l'oxydation thermique à long terme correspond principalement à une scission des chaînes et à une dégradation importante du polymère PPS.

De ce fait, après la première étape d'exposition, une deuxième étape de vieillissement montrant que l'effet de scission des chaînes devient prédominant à la surface de l'échantillon, ce qui finit par entraîner une perte des propriétés du composite de PPS, notamment en termes de ductilité du fait de la fissuration en surface facilitée par l'oxydation. En effet, les

thermoplastiques ont une structure moléculaire linéaire ou ramifiée et par conséquent ils deviennent plus fragiles en raison de la scission de la chaîne moléculaire ou de la réticulation dans la structure chimique du polymère PPS en surface.

Vieillissement	n°	t(h)	σ_r (MPa)	ε_r (%)	E (MPa)
Vierge	1	-	75,4	1,3	5900
	2	-	74,4	1,2	5890
200 °C-30h	1	30	79,4	1,35	6100
	2	30	78,9	1,4	6200
200 °C-51h	1	51	70,5	1,2	6000
	2	51	70,8	1,2	6150
200 °C-100h	1	100	63,4	1	6600
	2	100	58,4	1	6300
200 °C-199h	1	199	66,5	1,1	6500
	2	199	61,1	1	6400

Tableau 6: Résultats de traction aux différents stades de vieillissement à 200 °C

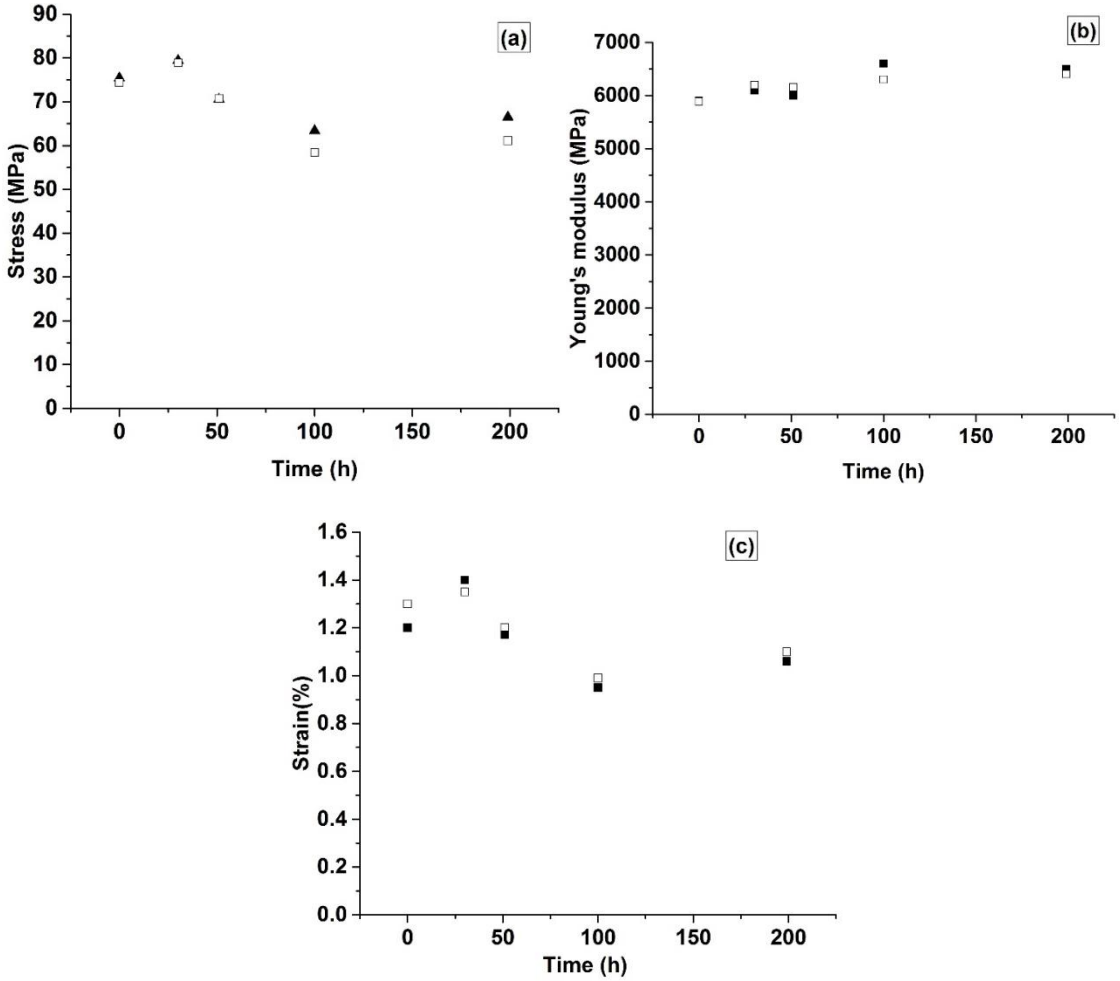

Figure 11 : Évolution de (a) la contrainte à la rupture, (b) le module de Young et (c) la déformation à la rupture au cours du vieillissement à 200 °C.

L'analyse de la microstructure des échantillons vierges (Figure 12-(a)) montre que l'adhérence fibre-matrice semble être de très bonne qualité, probablement en raison de la présence de l'agent de couplage. En effet, les fibres ont été arrachées de manière fragile mais restent encore recouvertes d'une fine couche de matrice PPS.

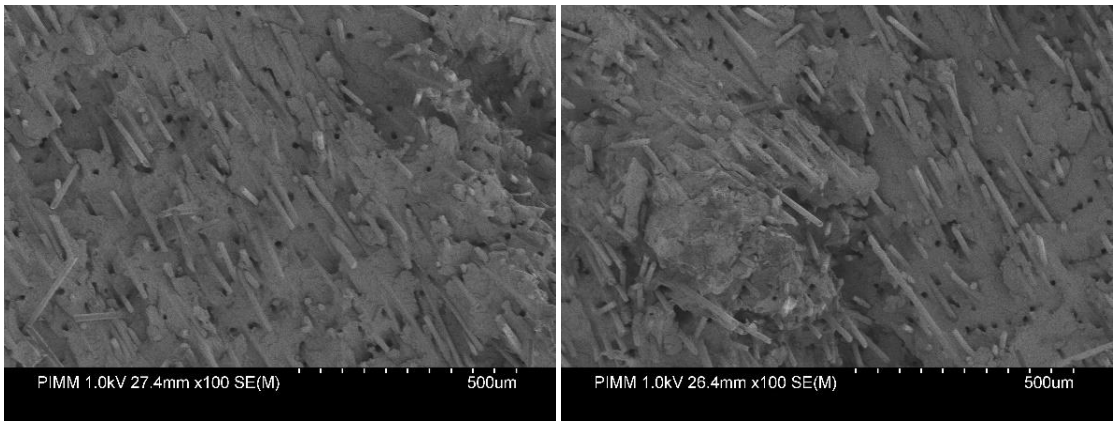

(a) Essai de traction-échantillon vierge

(b) Essai de traction-échantillon vieilli à 200 °C - 199h

Figure 12 : Faciès de rupture : (a) échantillon vierge et (b) échantillon vieilli à 200 °C - 199 h

Comparativement, dans le cas d'un échantillon vieilli à 200 °C - 199 h, Figure 12-(b), on peut noter que la matrice se dégrade très sérieusement. Le vieillissement thermique a dégradé la matrice et conduit à la séparation de la matrice des fibres, ce qui réduit les propriétés mécaniques du matériau d'origine PPS.

VII-2 Essai de charge-décharge

Afin de quantifier la possibilité de déformation plastique et d'endommagement, un essai de traction charge-décharge avec augmentation progressive de la contrainte maximale a été réalisé dans deux configurations : échantillons vierges et éprouvettes vieillies à 200 °C pendant 199 h (Figure 13 - (a)). La Figure 13 - (b) montre les évolutions de la déformation plastique (ε_p) et du paramètre d'endommagement (E/E_0) en fonction de la contrainte maximale pour les éprouvettes vierges et vieillies. Comme il a été montré ci-dessus, la contrainte à la rupture et la déformation à la rupture diminuent avec le vieillissement. On peut remarquer la stabilité relative du module de Young qui indique un faible niveau d'endommagement lors d'un chargement

quasi-statique (diminution de moins de 1%). Par contre, la plasticité augmente progressivement à partir de 5% de la contrainte à la rupture ce qui nous pousse à dire que la déformation du composite est essentiellement due à la non-linéarité du PPS.

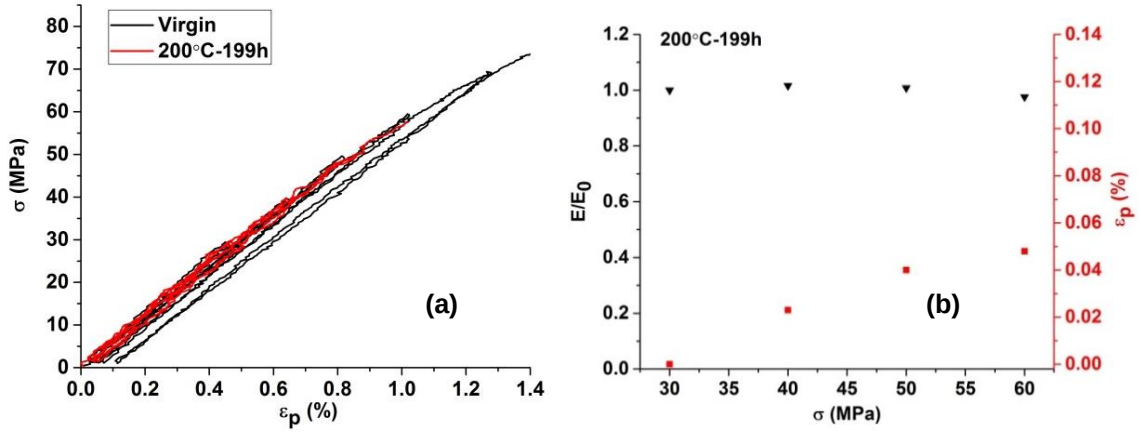

Figure 13 : (a) Essai de charge-décharge, et (b) évolution de la déformation plastique (ε_p) et du paramètre de perte de raideur (E/E_0) en fonction de la contrainte appliquée

VII-3 Comportement en fatigue

- Effet de l'amplitude

La Figure 14 montre la courbe de Wöhler obtenue lors d'essais de fatigue traction-traction à une fréquence de 10 Hz pour des échantillons PPS-90° à la température ambiante. La rupture finale et la durée de vie en fatigue du composite PPS dépendent fortement des conditions de chargement et de la microstructure locale. Les courbes de Wöhler bilinéaires soulignent l'influence de l'amplitude de chargement.

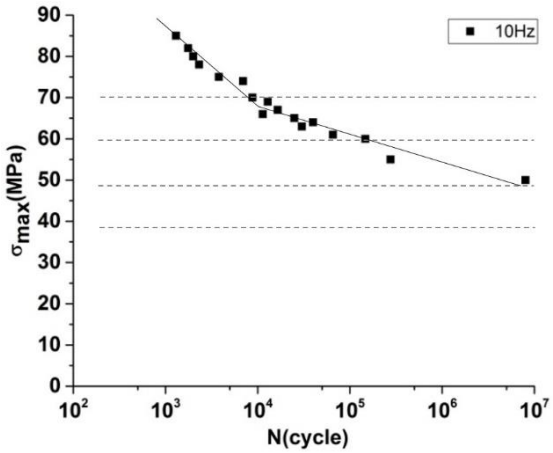

Figure 14 : Courbe de Wöhler du composite PPS réalisée sur des échantillons PPS-90°.

Essai de fatigue traction-traction à la fréquence de 10 Hz et à la température ambiante, R = 0,1.

Afin d'étudier la durée de vie en fatigue du composite PPS vieilli à 180 °C et à différents temps de vieillissement, des essais de fatigue traction-traction ont été effectués aux amplitudes de chargement de 40 MPa et 70 MPa (voir Figure 15). On peut remarquer que le nombre de cycles à la rupture diminue avec l'augmentation des amplitudes de chargement. On peut également remarquer une réduction considérable du nombre de cycles pour une amplitude de 70 MPa, de 1,4 $\times 10^4$ à 1,2 $\times 10^3$ et pour un temps d'oxydation d'environ 250 h. Les résultats montrent que la durée de vie en fatigue diminue fortement avec le temps de vieillissement en particulier dans le cas des hautes amplitudes de chargement.

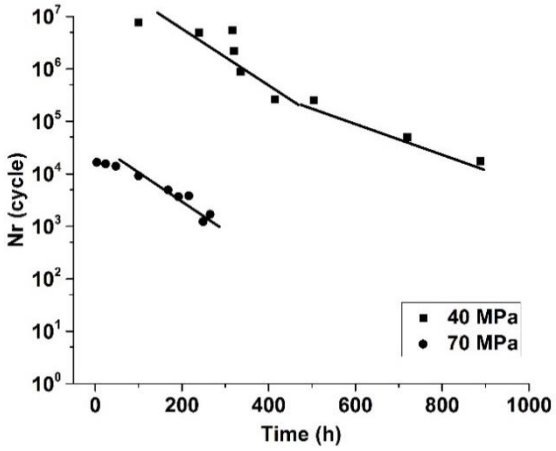

Figure 15 : Effet du vieillissement et de l'amplitude de charge sur la durée de vie en fatigue des échantillons, vieillis à 180 °C (f = 10 Hz).

- Effet de la température de vieillissement thermique

La Figure 16 montre l'évolution de la durée de vie en fatigue en fonction du temps d'oxydation aux différentes températures d'oxydation de 140 °C, 180 °C et 200 °C. On peut noter que la vitesse de réduction de la durée de vie en fatigue augmente avec la température de vieillissement thermique. En effet, à 200 °C, la durée de vie en fatigue est soumise à une très forte diminution.

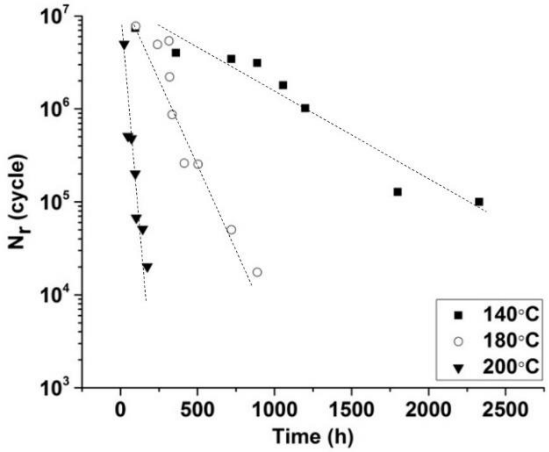

Figure 16 : Effet de la température de vieillissement sur la durée de vie en fatigue.

Essais de fatigue à 10 Hz et une amplitude maximale de chargement de 40 MPa (R=0,1).

Ceci indique que l'application d'une température de 200 °C affecte très fortement les propriétés mécaniques des matériaux PPS. La durée de vie en fatigue est donc très sensible à la température d'oxydation.

- Analyse des faciès de rupture

Une analyse des faciès de rupture en fatigue a été réalisée sur les échantillons vierges et vieillis afin de comprendre l'influence de la température et du temps d'exposition.

Différents temps de vieillissement pour une température d'oxydation de 200 °C:

La Figure 17 montre l'évolution globale des faciès de rupture des éprouvettes vieillies à 200 °C, depuis le début de l'oxydation jusqu'à 5256 h. La Figure 17 - (a) montre l'échantillon vierge pour lequel on peut noter que la surface est assez lisse, sans fissures apparentes, indiquant que les fibres adhèrent étroitement à la matrice. L'augmentation du temps d'oxydation (96 h, 1056 h et 5256 h : Figure 17 - (b), (c) et (d), respectivement), conduit à une rupture de la matrice plus accidentée en raison de l'instabilité à la rupture provenant de la surface oxydée plus élevée.

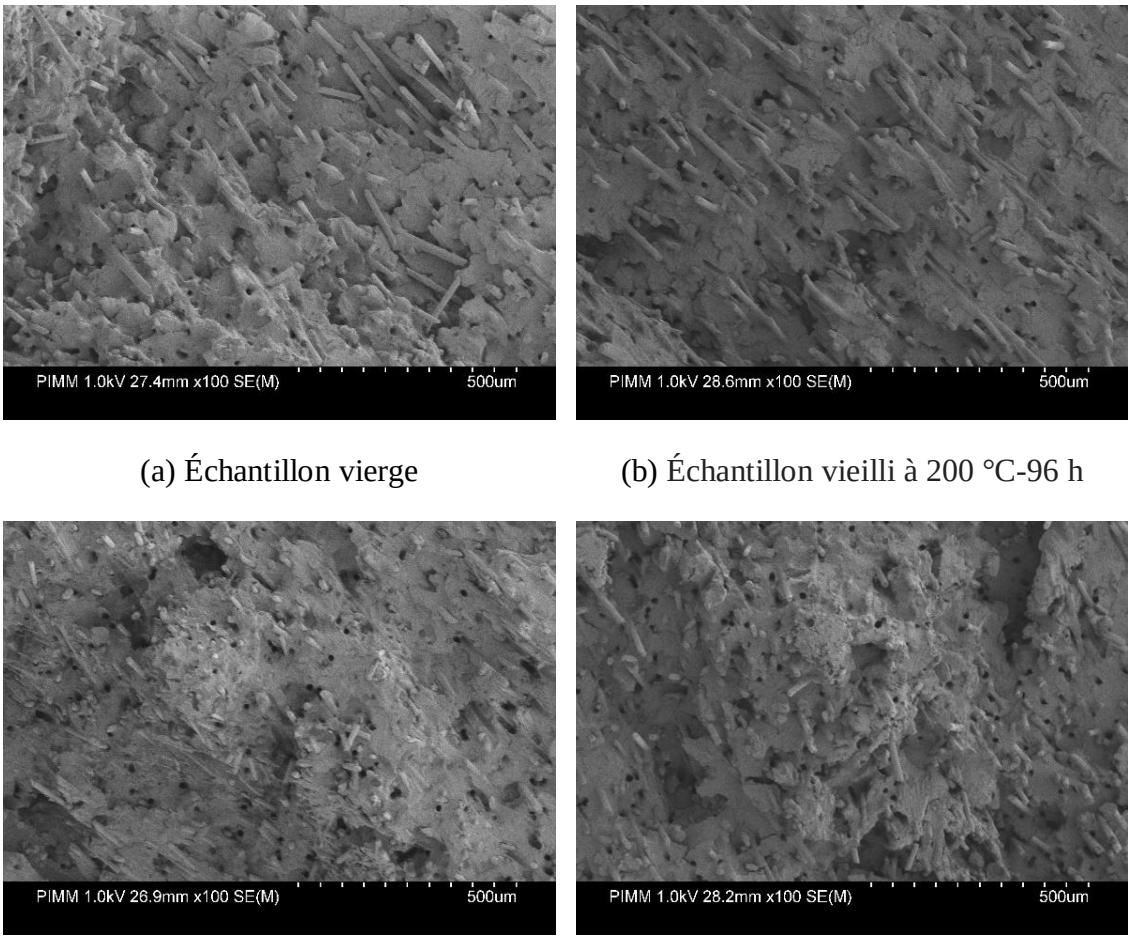

(a) Échantillon vierge (b) Échantillon vieilli à 200 °C-96 h

(c) Échantillon vieilli à 200 °C-1056 h (d) Échantillon vieilli à 200 °C-5256 h

Figure 17 : Faciès de rupture: a) échantillon vierge, b) échantillon vieilli à 200 °C-96 h, c) échantillon vieilli à 200 °C-1056 h et d) échantillon vieilli à 200 °C 5256 h (σ_{max} = 40 MPa).

Différentes températures de vieillissement après 1056 h d'oxydation:

La Figure 18 présente les faciès de rupture du composite PPS vieilli à 140 °C et 200 °C après 1056 h de vieillissement. Comparativement, à 200 °C, on peut voir de la matrice résiduelle sur la surface exposée des fibres et aussi que certaines surfaces de fibre sont lisses. On peut

également observer que la matrice se dégrade plus sérieusement à 200 °C. De plus, les micrographies montrent que de nombreuses particules se sont agrégées à cause de l'oxydation.

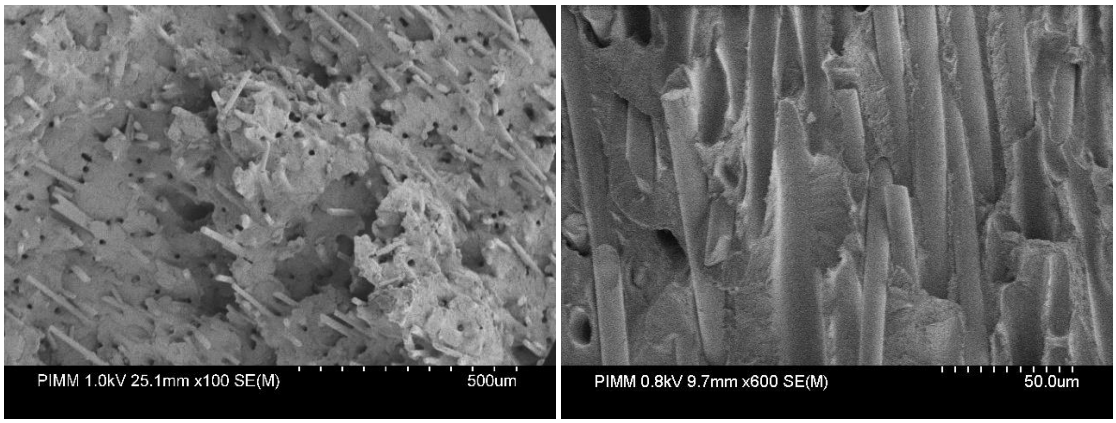

(a) Échantillon vieilli à 140 °C-1056 h

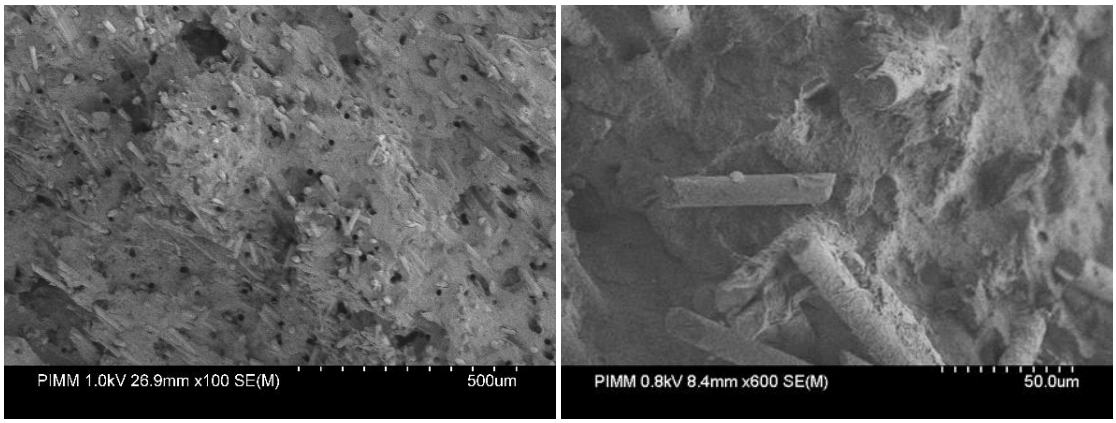

(b) Échantillon vieilli à 200 °C-1056 h

Figure 18 : Faciès de rupture: a) d'un échantillon vieilli à 140 °C-1056 h et b) échantillon vieilli à 200 °C-1056 h (σ_{max} = 40 MPa).

VII-4 Couplage vieillissement - fatigue

La Figure 19 montre la relation entre le nombre de cycles à la rupture (Nr) et [C=O] à différentes températures d'oxydation.

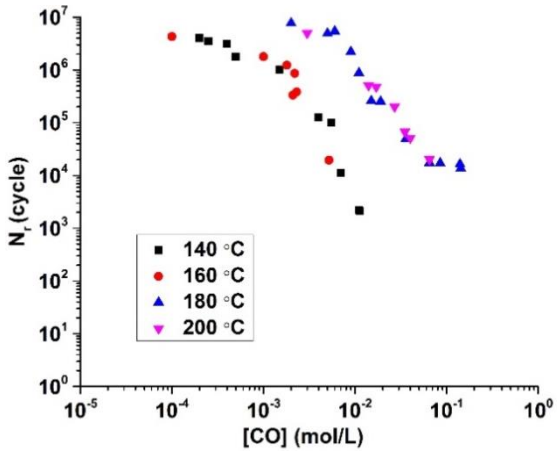

Figure 19 : Relation entre N_r et [C=O] aux différentes températures d'oxydation.

On peut noter qu'en général, cette courbe peut être divisée en deux zones, des températures d'oxydation élevées (par exemple 200 °C et 180 °C) et des températures modérées (160 °C et 140 °C). Pour le même nombre de cycles à la rupture (N_r), nous pouvons signaler que les températures modérées produisent moins de liaisons [C = O] tandis que les températures élevées correspondent à plus de liaisons [C = O].

Pour un matériau polymère PPS soumis à une charge cyclique, les échantillons vieillis à haute température ne nécessiteront que peu de temps pour atteindre la dégradation tandis qu'à basse température un temps plus important sera nécessaire pour obtenir le même degré de dégradation. De même la concentration [C=O] peut aussi représenter le degré de dégradation. Lorsque le même nombre de cycles a été appliqué jusqu'à la rupture, la température élevée entraîne une dégradation plus importante, ce qui équivaut à une concentration [C=O] plus élevée alors qu'elle sera plus faible pour une température basse. De plus, on peut voir que Nr diminue fortement avec l'augmentation de [C=O], non seulement dans le cas des températures élevées (180 °C et 200 °C), mais aussi dans le cas des basses températures (160 °C et 140 °C).

VIII. Conclusions et perspectives

Dans le travail de cette thèse, l'effet du vieillissement thermique sur le comportement en fatigue du composite de poly (sulfure de phénylène) renforcé par fibres de verre (PPS/FV) a été étudié.

Tout d'abord, deux types d'échantillons PPS/FV (PPS-0°, PPS-90°) ont été préparés par moulage et par injection (Article N°2). On a constaté que l'orientation des fibres dans le sens du chargement améliore la résistance monotone et la résistance à la fatigue. Une caractérisation complète a été réalisée à l'aide de plusieurs méthodes expérimentales. La microstructure, les propriétés physico-chimiques et mécaniques ont été explorées, notamment le comportement à la fatigue et les différents paramètres affectant la durée de vie. Il a été montré que même avec une amplitude de contrainte appliquée élevée et une fréquence élevée, le phénomène d'auto-échauffement observé en fatigue n'est pas suffisamment prononcé pour avoir une incidence sur la durée de vie en fatigue du composite PPS/FV.

Ensuite l'étude du phénomène de cristallisation du PPS/FV, a montré que la vitesse de refroidissement a une influence relativement importante sur ce phénomène ; la température de cristallisation, du PPS diminue sensiblement avec l'augmentation de la vitesse de refroidissement. Les résultats montrent que le modèle de Jeziorny (basé sur le modèle d'Avrami) peut très bien décrire et vérifier le processus de cristallisation non isotherme de ce matériau PPS/FV. Les échantillons vieillis jusqu'à 144 h à 200 °C conservent une bonne capacité de nucléation et de croissance géométrique du cristal tandis que pour l'échantillon vieilli après 1080 h à 200 °C, n diminue à 0,8 en raison de l'effet néfaste du vieillissement thermique.

Troisièmement, sur la base de l'étude de vieillissement à différentes températures et le suivi du matériau au cours du temps par différentes méthodes d'analyse, notamment par IRTF et

thermogravimétrie, un mécanisme d'oxydation est proposé et un modèle cinétique de prédiction de durée de vie, est construit et sa validité est vérifiée. Cette modélisation a permis de déterminer les constantes de vitesse des différentes réactions d'oxydation.

Enfin, les effets du vieillissement thermo-oxydatif sur les propriétés mécaniques sont étudiés par plusieurs types de sollicitation mécanique (de traction, de charge/décharge et de fatigue). Nous avons montré que du à la réticulation et à l'augmentation du taux de cristallinité au cours du vieillissement (à 200 °C), pour une période, la résistance (en traction) et le module d'Young s'améliorent. Les essais de fatigue sur les éprouvettes de PPS/FV avec une amplitude maximale (σ_{max}=40 MPa) et un rapport de chargement (R=0,1) ont également montré que le nombre de cycles à la rupture diminue sensiblement au cours du vieillissement.

Pour la suite et en perspective :

- Le PPS/FV est un système complexe. Il est nécessaire d'étudier de façon approfondie le rôle de la matrice, des fibres de verre et leur interface. Pour cela il est nécessaire d'étudier en parallèle le vieillissement du PPS pur et l'influence de ce vieillissement sur ses propriétés mécaniques.
- Pour des considérations de confidentialité, l'accès à certaines informations était limité. La nature de l'adhésion fibre/matrice n'était pas connue. Est-ce que les fibres étaient ensimées ? La réponse à cette question est très importante pour l'étude de l'interface fibre/matrice en particulier quand l'étude s'intéresse aux propriétés mécaniques du PPS/FV. Pour bien mener cette étude le choix de méthodes expérimentales adaptées est crucial.
- Pour la même raison, il est très important de mettre en évidence de façon directe ou indirecte l'effet de l'oxydation sur l'interface fibre/matrice. Il est bien de noter que

l’oxygène peut facilement pénétrer dans cette zone inter-faciale et réagir avec le produit d’ensimage (s’il existe) et avec la matrice autour des fibres.

- Pour pouvoir réaliser une vraie étude de couplage oxydation/fatigue, il est nécessaire de réaliser une recherche approfondie (avec tous les éléments nécessaires y compris ceux confidentiels) pour montrer la relation entre la microstructure (physico-chimique et morphologique) et les propriétés mécaniques (comportement en fatigue par exemple).

Références

[1] Yao S-S, Jin F-L, Rhee KY, Hui D, Park S-J. Recent advances in carbon-fiber-reinforced thermoplastic composites: A review. Composites Part B. 2017.
[2] Karger-Kocsis J, Mahmood H, Pegoretti A. Recent advances in fiber/matrix interphase engineering for polymer composites. Prog Mater Sci. 2015;73:1-43.
[3] Gao C, Yu L, Liu H, Chen L. Development of self-reinforced polymer composites. Prog Polym Sci. 2012;37:767-80.
[4] Sandler J, Werner P, Shaffer MS, Demchuk V, Altstädt V, Windle AH. Carbon-nanofibre-reinforced poly (ether ether ketone) composites. Compos Part A Appl Sci Manuf. 2002;33:1033-9.
[5] Jones D, Leach D, Moore D. Mechanical properties of poly (ether-ether-ketone) for engineering applications. Polymer. 1985;26:1385-93.
[6] Werner P, Altstädt V, Jaskulka R, Jacobs O, Sandler JK, Shaffer MS, et al. Tribological behaviour of carbon-nanofibre-reinforced poly (ether ether ketone). Wear. 2004;257:1006-14.
[7] Rae P, Brown E, Orler E. The mechanical properties of poly (ether-ether-ketone)(PEEK) with emphasis on the large compressive strain response. Polymer. 2007;48:598-615.
[8] Bangarusampath D, Ruckdäschel H, Altstädt V, Sandler JK, Garray D, Shaffer MS. Rheology and properties of melt-processed poly (ether ether ketone)/multi-wall carbon nanotube composites. Polymer. 2009;50:5803-11.
[9] Berer M, Tscharnuter D, Pinter G. Dynamic mechanical response of polyetheretherketone (PEEK) exposed to cyclic loads in the high stress tensile regime. Int J Fatigue. 2015;80:397-405.
[10] Hou T, Chen H. Isothermal physical aging of PEEK and PPS investigated by fractional Maxwell model. Polymer. 2012;53:2509-18.
[11] Vatanpour V, Madaeni SS, Moradian R, Zinadini S, Astinchap B. Novel antibifouling nanofiltration polyethersulfone membrane fabricated from embedding TiO2 coated multiwalled carbon nanotubes. Separation and purification technology. 2012;90:69-82.
[12] Susanto H, Ulbricht M. Characteristics, performance and stability of polyethersulfone ultrafiltration membranes prepared by phase separation method using different macromolecular additives. J Membr Sci. 2009;327:125-35.
[13] Raghava R. Role of matrix‐particle interface adhesion on fracture toughness of dual phase epoxy‐polyethersulfone blend. J Polym Sci, Part B: Polym Phys. 1987;25:1017-31.
[14] Albouy W, Vieille B, Taleb L. Experimental and numerical investigations on the time-dependent behavior of woven-ply PPS thermoplastic laminates at temperatures higher than glass transition temperature. Compos Part A Appl Sci Manuf. 2013;49:165-78.
[15] Anagreh N, Dorn L, Bilke-Krause C. Low-pressure plasma pretreatment of polyphenylene sulfide (PPS) surfaces for adhesive bonding. Int J Adhes Adhes. 2008;28:16-22.
[16] André NM, Goushegir SM, dos Santos JF, Canto LB, Amancio-Filho ST. Friction Spot Joining of aluminum alloy 2024-T3 and carbon-fiber-reinforced poly (phenylene sulfide) laminate with additional PPS film interlayer: Microstructure, mechanical strength and failure mechanisms. Composites Part B. 2016;94:197-208.
[17] Auer C, Kalinka G, Krause T, Hinrichsen G. Crystallization Kinetics of Pure and Fiber-Reinforced Poly (Phenylene Sulfide). J Appl Polym Sci. 1994;51:407-13.
[18] Batista NL, Rezende MC, Botelho EC. Effect of crystallinity on CF/PPS performance under weather exposure: Moisture, salt fog and UV radiation. Polym Degrad Stab. 2018;153:255-61.

[19] Bhardwaj I, Kumar V, Das A. Studies of the thermal and crystallization behaviour of polyphenylene sulphide/polycarbonate blends. Thermochim Acta. 1989;144:165-72.
[20] Chen Z, Li T, Yang Y, Liu X, Lv R. Mechanical and tribological properties of PA/PPS blends. Wear. 2004;257:696-707.
[21] Hill HW, Brady D. Properties, environmental stability, and molding characteristics of polyphenylene sulfide. Polym Eng Sci. 1976;16:831-5.
[22] López LC, Wilkes GL. Non-isothermal crystallization kinetics of poly (p-phenylene sulphide). Polymer. 1989;30:882-7.
[23] Caramaro L, Chabert B, Chauchard J, Vu-Khanh T. Morphology and mechanical performance of polyphenylenesulfide carbon fiber composite. Polym Eng Sci. 1991;31:1279-85.
[24] Favaloro M. Properties and Processes of Linear Polyphenylene Sulfide (PPS) for Continuous Fiber Composites Aerospace Applications. SAE International2009.
[25] Celina M, Gillen KT, Assink RA. Accelerated aging and lifetime prediction: Review of non-Arrhenius behaviour due to two competing processes. Polym Degrad Stab. 2005;90:395-404.
[26] Damian C, Espuche E, Escoubes M. Influence of three ageing types (thermal oxidation, radiochemical and hydrolytic ageing) on the structure and gas transport properties of epoxy–amine networks. Polym Degrad Stab. 2001;72:447-58.
[27] Pei Y-m, Wang K, Zhan M-s, Xu W, Ding X-j. Thermal-oxidative aging of DGEBA/EPN/LMPA epoxy system: Chemical structure and thermal–mechanical properties. Polym Degrad Stab. 2011;96:1179-86.
[28] Kiliaris P, Papaspyrides CD, Pfaendner R. Influence of accelerated aging on clay-reinforced polyamide 6. Polym Degrad Stab. 2009;94:389-96.
[29] Rose N, Le Bras M, Bourbigot S, Delobel R. Thermal oxidative degradation of epoxy resins: evaluation of their heat resistance using invariant kinetic parameters. Polymer Degradation and Stability. 1994;45:387-97.
[30] Rivaton A, Mailhot B, Soulestin J, Varghese H, Gardette JL. Comparison of the photochemical and thermal degradation of bisphenol-A polycarbonate and trimethylcyclohexane–polycarbonate. Polymer Degradation and Stability. 2002;75:17-33.
[31] Forsström D, Terselius B. Thermo oxidative stability of polyamide 6 films I. Mechanical and chemical characterisation. Polymer Degradation and Stability. 2000;67:69-78.
[32] Buch X, Shanahan MER. Thermal and thermo-oxidative ageing of an epoxy adhesive. Polymer Degradation and Stability. 2000;68:403-11.
[33] Bellenger V, Tcharkhtchi A, Castaing P. Thermal and mechanical fatigue of a PA66/glass fibers composite material. Int J Fatigue. 2006;28:1348-52.
[34] Vieille B, Albouy W. Fatigue damage accumulation in notched woven-ply thermoplastic and thermoset laminates at high-temperature: Influence of matrix ductility and fatigue life prediction. Int J Fatigue. 2015;80:1-9.
[35] Tanaka K, Oharada K, Yamada D, Shimizu K. Fatigue crack propagation in short-carbon-fiber reinforced plastics evaluated based on anisotropic fracture mechanics. Int J Fatigue. 2016.
[36] Růžek R, Kadlec M, Petrusová L. Effect of fatigue loading rate on lifespan and temperature of tailored blank C/PPS thermoplastic composite. Int J Fatigue. 2018;113:253-63.
[37] Chambers A, Earl J, Squires C, Suhot M. The effect of voids on the flexural fatigue performance of unidirectional carbon fibre composites developed for wind turbine applications. Int J Fatigue. 2006;28:1389-98.

[38] Albouy W, Vieille B, Taleb L. Influence of matrix ductility on the high-temperature fatigue behavior of off-axis woven-ply thermoplastic and thermoset laminates. Int J Fatigue. 2014;63:85-96.
[39] Skelton RP. Hysteresis, yield, and energy dissipation during thermo-mechanical fatigue of a ferritic steel. Int J Fatigue. 2004;26:253-64.
[40] Gosar A, Nagode M. Energy dissipation under thermomechanical fatigue loading. Int J Fatigue. 2012;43:160-7.
[41] Lisa G, Hamciuc C, Hamciuc E, Tudorachi N. Thermal and thermo-oxidative stability and probable degradation mechanism of some polyetherimides. J Anal Appl Pyrolysis. 2016;118:144-54.
[42] Jing C, Lei Y, Jieping Z, Sidong L, Yongjun C, Kui X. Drying kinetics and cross-linking of sulfur prevulcanized thick natural rubber latex film. Rubber Chem Technol. 2013;86:57-67.
[43] Matyshak V, Krylov O. Problems of quantitative spectroscopic measurements in heterogeneous catalysis: molar absorption coefficients of vibrations in adsorbed substances. Kinet Catal. 2002;43:391-407.
[44] SEPPÄLÄ J, HEINO M, KAPANEN C. Injection-moulded blends of a thermotropic liquid crystalline polymer with polyethylene terephthalate, polypropylene, and polyphenylene sulfide. J Appl Polym Sci. 1992;44:1051-60.
[45] Ye L, Scheuring T, Friedrich K. Matrix morphology and fibre pull-out strength of T700/PPS and T700/PET thermoplastic composites. J Mater Sci. 1995;30:4761-9.
[46] Jeziorny A. Parameters characterizing the kinetics of the non-isothermal crystallization of poly (ethylene terephthalate) determined by DSC. Polymer. 1978;19:1142-4.
[47] Weng W, Chen G, Wu D. Crystallization kinetics and melting behaviors of nylon 6/foliated graphite nanocomposites. Polymer. 2003;44:8119-32.
[48] Zhang Y, Jiang X, Guan Y, Zheng A. Crystallization kinetics of ATPU grafted polypropylene. Mater Lett. 2005;59:3626-34.
[49] Botines E, Puiggalí J. Crystallization kinetics of poly (glycolic acid-alt-6-aminohexanoic acid). Eur Polym J. 2006;42:1595-608.
[50] Kuo M, Huang J, Chen M. Non-isothermal crystallization kinetic behavior of alumina nanoparticle filled poly (ether ether ketone). Mater Chem Phys. 2006;99:258-68.
[51] Kissinger HE. Reaction kinetics in differential thermal analysis. Anal Chem. 1957;29:1702-6.
[52] Tobolsky AV, Metz DJ, Mesrobian RB. Low Temperature Autoxidation of Hydrocarbons: the Phenomenon of Maximum Rates1, 2. J Am Chem Soc. 1950;72:1942-52.
[53] Audouin L, Gueguen V, Tcharkhtchi A, Verdu J. “Close loop” mechanistic schemes for hydrocarbon polymer oxidation. J Polym Sci, Part A: Polym Chem. 1995;33:921-7.
[54] Richaud E, Farcas F, Fayolle B, Audouin L, Verdu J. Hydroperoxide build-up in the thermal oxidation of polypropylene–a kinetic study. Polym Degrad Stab. 2007;92:118-24.
[55] Rychly J, Matisova-Rychla L, Csmorova K, Achimsky L, Audouin L, Tcharkhtchi A, et al. Kinetics of mass changes in oxidation of polypropylene. Polym Degrad Stab. 1997;58:269-74.
[56] Tcharkhtchi A, Farzaneh S, Abdallah-Elhirtsi S, Esmaeillou B, Nony F, Baron A. Thermal aging effect on mechanical properties of polyurethane. Int J Polym Anal Charact. 2014;19:571-84.
[57] Yamashita T, Tomitaka H, Kudo T, Horie K, Mita I. Degradation of sulfur-containing aromatic polymers: Photodegradation of polyethersulfone and polysulfone. Polym Degrad Stab. 1993;39:47-54.

[58] Landel RF, Nielsen LE. Mechanical properties of polymers and composites: CRC Press; 1993.
[59] Kim K, Lee C, Kim P, Ryu B. Dielectric properties on the radiation and thermal aged PEEK. Solid Dielectrics, 2004 ICSD 2004 Proceedings of the 2004 IEEE International Conference on: IEEE; 2004. p. 332-5.
[60] Kang PH, Lee C, Kim KY. Radiation and thermal effects on the dielectric relaxation properties of PEEK. Journal of industrial and engineering chemistry-seoul-. 2007;13:250.
[61] George K, Komalan C, Kumar P, Varughese K, Thomas S. Dynamic mechanical analysis of binary and ternary polymer blends based on nylon copolymer/EPDM rubber and EPM grafted maleic anhydride compatibilizer. 2007.
[62] Ibarra L, Macias A, Palma E. Viscoelastic properties of short carbon fiber thermoplastic (SBS) elastomer composites. J Appl Polym Sci. 1995;57:831-42.
[63] Ernault E, Richaud E, Fayolle B. Thermal-oxidation of epoxy/amine followed by glass transition temperature changes. Polym Degrad Stab. 2017;138:82-90.
[64] Zuo P, Benevides RC, Laribi MA, Fitoussi J, Shirinbayan M, Bakir F, et al. Multi-scale analysis of the effect of loading conditions on monotonic and fatigue behavior of a glass fiber reinforced polyphenylene sulfide (PPS) composite. Composites Part B. 2018;145:173-81.
[65] Fatemi A, Socie DF. A critical plane approach to multiaxial fatigue damage including out‐of‐phase loading. Fatigue Fract Eng Mater Struct. 1988;11:149-65.

Contents

List of Figures :

List of Tables :

Extended Summary (In English)

I. General introduction

Reducing costs and energy consumption is the key factor in many industries such as aerospace and automobile. Similarly, in modern society, the weight of the piece has become an important criterion in the choice of materials for the manufacturing industrial products. There is also a trend that lightweight materials such as polymer composites, in particular reinforced thermoplastic matrix composites, will gradually replace some traditional metallic materials over the next few decades. Reinforced thermoplastic composites are now being considered for applications in severe thermal environments such as areas near heat sources (e.g., automotive technical environments) [1-3].

In addition, among the various high performance polymers, those containing aromatic units, such as PEEK (polyether ether ketone) [4-10], poly (ether sulfone) PES [11-13] and poly (phenylene Sulfide) (PPS) [14-20], have attracted a great deal of interests and attentions in recent decades. Poly (phenylene Sulfide) (PPS) is one of these types of polymers and it has a unique combination of excellent environmental properties when reinforced with fibers. In detail, it is applied in many sectors such as electronics and electrical appliances, precision instruments, the fields of chemistry and aerospace [21-24]. In addition, PPS polymer, reinforced with short glass fibers and implemented by the injection process, is used frequently in the automotive industry (case of air coolers). In general, this material has interesting mechanical properties (rigidity, mechanical strength, etc.). PPS also has a very interesting fatigue behavior, a good thermo-mechanical performance ($T_g \approx 110$ °C and $T_f \approx 285$ °C) and a high chemical resistance.

However, all polymers and polymer matrix composites face the same problems of thermal stability and degradation resistance [18, 25-28]. This is one of the major concerns to the

applications of these materials in conditions where certain environmental elements such as oxygen in the air could attack the material; especially when the temperature is relatively high. These concerns require researchers to investigate and carry out research activities in this area. The goal is to better understand the processes and mechanism of thermal aging that can provide more solutions for better utilization. In the present study, the multi-scale aspects must be taken into account because the oxidation of polymers is a complex phenomenon affecting the material at different scales: molecular, macromolecular, morphological, micro-meso and macroscopic aspects, etc [29-32]. As a result, various aging conditions should be taken into account, which may not only allow more protection during use, but also enhance our understanding with regard to the detailed degradation process of polymer and their reinforced parts.

Moreover, today the industry is in great need of data on the mechanical behavior (properties of utilization) of materials under various stress conditions. Actually, one of the most common modes of solicitation is fatigue stress where the part is under a cyclic stress of moderate amplitude which contributes to the mechanical degradation of the material over time [9, 33-38]. In this condition, the polymer-based or composite parts must have good fatigue strength to ensure a long service life.

In the case of real practical use, the problem is often more complicated. The industrial part is often mechanically stressed (for example in fatigue) in a hot environment in contact with the surrounding elements such as the air under the bonnet. Then, in this configuration, the piece will be under the combined influence of oxidation and fatigue. Therefore, it is necessary to carry out research considering the two types of degradation (mechanical and thermal) as well as their interaction [39, 40].

It is with this spirit that we have organized our work which is the subject of this thesis. We have tried to follow this red route in the past three years. This red route connects the following components: characterization of the PPS/GF, study of the oxidation of the material, study of the fatigue behavior of the material, study of the influence of aging on the fatigue behavior.

The PPS/GF composite material is supplied by our industrial partner Valeo. This work is done for and in collaboration with the Valeo Research Center. It was conducted in the PIMM laboratory (Processes and Engineering in Mechanics and Materials) of the ENSAM Paris Campus.

This document is divided into two parts: the Extended Summary in French and English (Part I); then the articles published or being published in international journals of rank A in English (Part II). The organization of the different parts of the extended summary respects the following approach:

- A description of PPS composite materials and their physicochemical and mechanical behavior;
- A modeling of the properties under thermal aging of the material PPS;
- The experimental analysis of the fatigue behavior of these materials;
- The study of the effect of thermal oxidation on the mechanical behavior of PPS composites.

The following is a list of articles published during this study or being published. They are quoted in the text as: « Article N°-- ».

Article N°1: P. Zuo, A. Tcharkhtchi, M. Shirinbayan, J. Fitoussi, F. Bakir, "Overall investigation of PolyPhenylene Sulfide (PPS) / from synthesis, process to applications – A review". Macromolecular Materials & Engineering. **Accepted.**

Article N°2: P. Zuo, R. C. Benevides, M. A. Laribi, J. Fitoussi, M. Shirinbayan, F. Bakir, A. Tcharkhtchi, "Multi-scale analysis of the effect of loading conditions on monotonic and fatigue behavior of a glass fiber reinforced polyphenylene sulfide (PPS) composite", Composites Part B: Engineering, 2018, 145: 173-181. **Published.**

Article N°3: P. Zuo, A. Tcharkhtchi, M. Shirinbayan, J. Fitoussi, F. Bakir, "Multi-scale physicochemical characterization of a short glass fiber reinforced Polyphenylene Sulfide composite under aging and its thermo-oxidative mechanism", Polymers for advanced technologies, 2018. **In press.**

Article N°4: P. Zuo, J. Fitoussi, M. Shirinbayan, F. Bakir, A. Tcharkhtchi, "Thermal aging effects on overall mechanical behavior of short glass fiber reinforced PolyPhenylene Sulfide composites ", Polymer Engineering & Science, 2018. **In press.**

II. Materials and experimental methods

II-1 Materials

The PPS/GF composites, which are the subject of the present study, are used for various applications in the automotive industry, in particular for air cooler parts (Valeo specific part). Polyphenylene sulfide (PPS) is a polymer consisting of sulfur-bonded aromatic rings and its chemical formula is illustrated in Figure 1.

The composite material used for this study consists of different phases: the matrix, the mineral fillers (if they exist) and the glass fibers. The matrix is Polyphenylene Sulfide and it is a semi-crystalline thermoplastic polymer with a high performance.

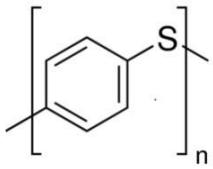

Figure 1: Chemical structure of PPS.

The reinforcements are glass fibers having a diameter of 15 µm and an average length of 200 µm.

II-2 Sampling

Two types of sample are used.

They are derived from plates of PPS/GF with a 3 mm thickness which were obtained by injection and supplied by Valéo.

Dog-bone shape samples made by water jet have a total length of 72 mm and a thickness of 3 mm. The useful area has a length of 20 mm and a width of 10 mm.

Films: these same plates are also used to prepare films. Firstly, a portion of an original plate was cut and glued onto a base support. Then this complete sample with a base support was fixed on a LEICA microtome. The LEICA RM2255 is a fully automatic and motorized rotary microtome with a separate control panel for the elaboration of thin sections of samples of varying hardness. This device can display different speeds of advancement and also allow obtaining the various cutting thicknesses required by automatically controlling a distance and a precise

location. For this study, the thicknesses of the films are 20 µm and each film is placed in a bag to be stored and used during research of thermal aging.

II-3 Physicochemical and mechanical characterization methods for virgin and aged samples

Films with a thickness of 20 µm and the dog bone-shape test samples were placed in the ovens (with circulation of air) and the temperatures of aging were fixed at 100 °C, 140 °C, 160 °C, 180 °C and 200 °C, respectively. Samples are analyzed by the following methods:

Thermogravimetry: The dog bone-shape specimens cut from the PPS/GF plates were suspended in ovens, in contact with the air, at different temperatures. The weight of the sample was measured at different time intervals to determine the percentage of mass loss: W%, using the following equation:

$$W\% = \frac{W_0 - W_t}{W_0} * 100\% \qquad \text{(e.q. 1)}$$

Where w_t is the weight at time t and w_0 is the weight of the virgin sample.

For the mass loss test, four aging temperatures (100, 140, 180 and 200 °C) were recorded from 0 hours to maximum 5256 hours.

The non-isothermal thermogravimetry tests are carried out between room temperature and 800 °C with a heating rate of 10 °C/min in the nitrogen atmosphere (40 ml/min), using TGA Q500. The mass of the initial sample is 10 to 20 mg, which is placed in the Al_2O_3 crucible.

FTIR spectrometry was used to characterize the products and determine the extent of polymer oxidation. The apparatus used is a Nicolet Impact 410 spectrophotometer configured in transmission mode. The measurements were made on spectra resulting from the accumulation of 32 analyzes, the resolution being 4 cm^{-1}. The films with a thickness of 20 µm were used. The

concentration of C=O corresponding to peak at 1780 cm^{-1}[41], is calculated according to the law of Beer-Lambert, which is as following:

$$C = \frac{A}{\varepsilon . e} \quad \text{(e.q. 2)}$$

Where A is the absorbance of the FTIR spectrum, e is the thickness of the samples (20 μm) and ε is the extinction coefficient (300 L. mol^{-1} cm^{-1} for the C=O group [41]). Similarly, the concentrations of [C-S] (1075 cm^{-1}) and [C-H] (2923 cm^{-1}) are calculated in the same way and the extinction coefficients of [C-S] and [C-H] are 114 [42]et 42 [43] L. mol^{-1}. cm^{-1}, respectively.

For the FTIR test, the samples were taken at an aging time ranging from 0 h to maximum 5256 h, with four aging temperatures (140, 160, 180 and 200 °C).

The absence or the presence of stabilizers in the material is verified using a PERKINELMER UV-visible spectrophotometer (model Lambda 5), equipped with an integrated sphere. The spectra are recorded in absorbance mode 66 over a spectral range of 200 to 400 nm. The analysis of the data is performed by applying the species concentration which is determined by the same method of FTIR spectrometry using the Beer-Lambert law.

For the UV test, a virgin film sample (20 μm) was used.

For optical microscopy analysis, virgin and aged samples at 180 and 200 °C were used. The aging time was chosen between 0 hours and 5256 hours.

The characterization of the microstructure of the various composites was carried out using a scanning electron microscope (HITACHI 4800 SEM).

The thickness of the oxidized layer for each PPS test sample was measured by Optic Microscopy in ZEISS (Axio Imager 2 model). We also used the OM (platinum heating) to study the crystallization of the matrix.

The differential calorimetry tests were conducted by the NETZSCH DSC Q10, with the aim of determining the glass transition temperature (T_g) and the melting temperature (T_f) as well as the melting enthalpy variation (ΔH_f) which allow to calculate the degree of crystallinity (X_c). A temperature ramp between 20 °C and 350 °C with a speed of 5 to 25 °C/min is applied for the PPS samples. The degree of crystallinity X_C is calculated from the following relationship:

$$X_C = \frac{\Delta H_f}{\Delta H_f^0 * \varphi} * 100\% \quad \text{(e.q. 3)}$$

With X_C =crystallinity degree, ΔH_f =enthalpy of fusion, ΔH_f^0 = pure crystalline phase enthalpy of fusion, φ = percent of matrix.

Dynamic Mechanical Analysis (DMA) tests were performed on PPS/GF samples using the Q800 DMA instrument to measure major transition temperatures and viscoelastic behavior. These tests were carried out under the following conditions: an alternating bending configuration was necessary in our case and the selected test temperatures were chosen between 25 °C and 200 °C. The frequency is between 0.1 and 50 Hz with the temperature rate of 0.5 °C/min. The sample had a rectangular shape with dimensions of 35 × 12 × 3 mm^3.

For the DMA test, four aging temperatures (100, 140, 180 and 200 °C) were recorded from 0 to maximum 5688 hours.

Viscosity measurements were performed with the MCR 502 rheometer at Anton Paar. 2 types of tests are carried out:

- Isothermal tests (at 290 °C), strain (0.2%) and constant angular frequency of 1 rad/s.
- Isothermal tests (at 300 °C), strain (0.2%) with variable angular frequency between 0.1 and 100 rad/s.

These (isothermal) tests were carried out on film samples at different temperatures under nitrogen as well as in a plane-plane configuration with an interval of 1 mm between the two plates.

For the rheological tests, virgin samples and samples aged at 180 and 200 °C were used. The aging time was chosen between 0 hours and 606 hours.

Tensile tests with low test velocity (quasi-static) were performed by the MTS 830 hydraulic machine on the PPS/GF specimens in two 0° and 90° directions (depending on the direction of the fibers). A summary table (see Table 1) shows the main characteristics of our material. Articles N°2 and N°3 present detailed information on the physicochemical characteristics of this material.

	E (MPa)	σ_r (MPa)	ε_r (%)	T_g	T_m	T_c	Density (g/cm^3)
Pure PPS [44]	3697	82	2.7				
PPS-90°	4300±41	84±4.3	3±0.14	111	283	244	1.58
PPS-0°	6000±45	104±4.4	2.85±0.24	109	-	-	-

Table 1 : Some physicochemical and mechanical parameters of the PPS

For the tensile test, four aging temperatures (100, 140, 180, 200 °C) were selected and the aging time ranged from 0 hours to maximum 5256 hours.

The tension-tension fatigue tests were carried out under different maximum stresses applied on the MTS 830 hydraulic fatigue machine. The minimum stress applied is always chosen equal to 10% of the maximum applied stress (R = 0.1). In this study, we present the results of tests carried out at two frequencies, 10 Hz and 50 Hz. In order to accurately measure the evolution of the rigidity during the first loading step (initial damage), each fatigue test is preceded by a loading-unloading-loading step in quasi-static tensile test. During cyclic loading, the temperature evolution (due to self-heating) was measured on the surface of the samples using an infrared camera (Raynger-MX4). The effect of the damage was evaluated by measuring the evolution of Young's modulus.

III. Research framework of our Project

Basically, aging leads to a phenomenon involving a slow and irreversible change in the properties of materials. This change may be the consequence of a chemical or physical reaction. In general, we can classify the different types of aging into two broad categories:

1) Physical aging without structural change.

2) Chemical aging with change of structure.

In the case of oxidation or thermo-oxidation of thermoplastics, aging is a chemical phenomenon that can cause a crosslinking reaction or cut the macromolecular chains. Crosslinking provides increased tensile strength, toughness and Young's modulus, as well as a decrease in elongation at break while chain cutting is the cause of embrittlement, weakening and

damage of the material. As a result, oxidation is a very complex multi-physics phenomenon. To this complexity, we must add the difficulties related to the shape and 3D structure of the pieces. In addition, the mechanism of oxidation of PPS is less known in the literature and there is not much study in this field. To confront all these problems, our search strategy is based on the following points:

- Presenting the phenomena in a simplified way, being careful that this simplification not leading to erroneous interpretations and conclusions.
- Using the experimental results obtained by different complementary methods.
- Taking the multi-physical aspects of this subject into account.

Indeed, to study the influence of thermo-oxidation on the mechanical properties and in particular on the fatigue behavior of the composite PPS/GF, we use:

1) The direct method by performing fatigue tests on samples aged over time.
2) Indirect methods that make it possible to study this influence by means of the oxidation effect on the other properties related to the mechanical properties.

It is important to remember that the PPS is a semi-crystalline polymer consisting of two phases: one amorphous and the other crystalline.

- On the one hand, the two phases do not oxidize in the same way. The amorphous phase is less compact and oxygen can penetrate into this phase and react with the chemical structure more easily. The crystalline phase is a compact phase and it does not change easily during the oxidation of the polymer. The oxidation of the amorphous phase often and especially happens at high temperature and in the long term leads to the scission of the macromolecular chains, the rearrangement and the modification of this phase. In some cases, this rearrangement increases the degree of crystallinity of the polymer.

- On the other hand, the crystalline phase is more resistant, more rigid and more fragile than the amorphous phase; therefore the modification of the morphology of the crystalline phase, because of aging, can influence the mechanical behavior (fatigue in this study) of the polymer.

For this reason, we have focused on the crystalline phase and its evolution during the oxidation of the polymer.

It should also be remembered that the polymer does not oxidize in the same way at different physical states. In the vitreous state, the amorphous phase is relatively fixed and the mobility of the chains is weak as well as the reaction of the polymer with oxygen is more difficult and slower. On the other hand, in the rubbery state, the oxidation is carried out more easily and more rapidly. In the case of PPS, the result of the DMA test (Figure 2) indicates that during oxidation at 140 °C, 160 °C, 180 °C and 200 °C, the amorphous phase is rubbery state. At 100 °C, this phase is in the glass transition zone with a lower molecular mobility and reactivity.

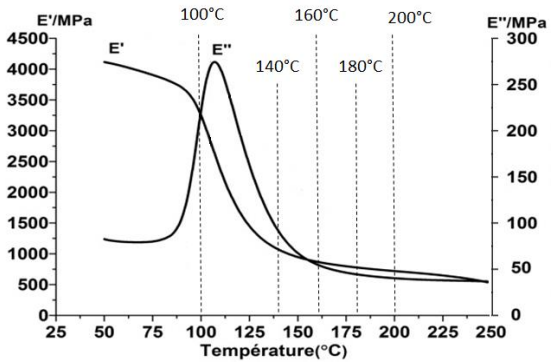

Figure 2: DMA results: different physical states (glassy and rubbery) and the thermal aging temperatures.

Consequently, in order to understand the effect of thermo-oxidation on the fatigue behavior of PPS, it is necessary to study, on the one hand, the interaction between the

morphology, the physical state and the mechanical properties of this polymer material and secondly their evolution during aging. This aspect is well illustrated in Schema.1.

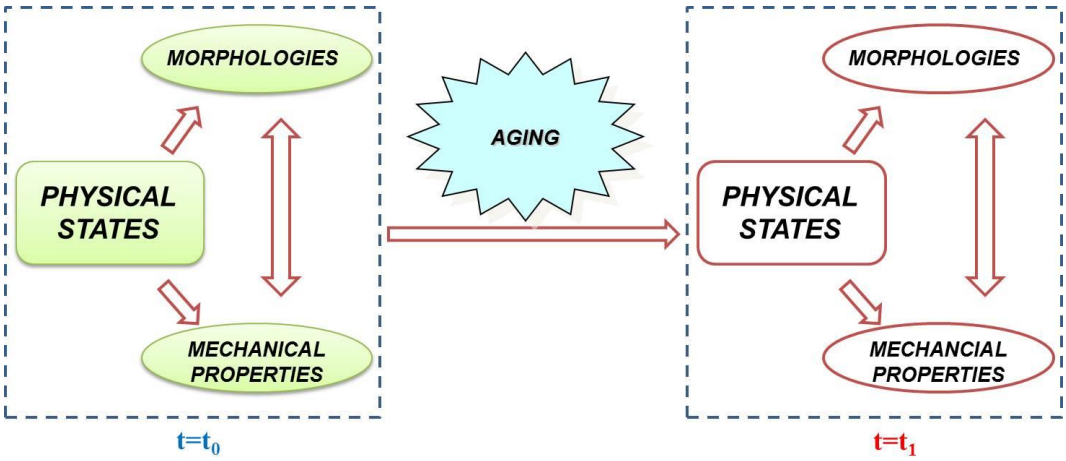

Schema.1: Strategy to investigate the effects of thermal aging on the physical state of PPS composites.

Before showing in a synthetic way the results obtained, it is also necessary to evoke the following points:

In this study, the polymer is not alone; it is in an environment comprising:

1) Glass fibers

The questions are as follows:

- Are the fibers sized? The size allows a good adhesion between the fibers and the matrix. In this condition, there will be less empty space in the inter-facial area and oxygen diffusion in this area is more difficult.
- Does the presence of fibers promote the oxidation of the polymer?
- It is clear that the embrittlement of the composite is due to the oxidation of the matrix and the degradation of the interface. Which of these two causes is predominant in aging?

2) Thermal stabilizers in the matrix

Thermal stabilizers are often used to slow down the oxidation process and delay polymer aging. At least two stabilizers of different natures and capacities are often used. These stabilizers can protect the polymer under the various conditions of utilizations. Under certain conditions the presence of several stabilizers can create a kind of synergy which makes it possible to increase the effectiveness of these stabilizers.

In our study, due to the lack of information from the supplier on antioxidants or thermal stabilizers, a UV spectrometric analysis is necessary to detect the possibility of existence of traditional antioxidants, including polyphenols and phenolic polymers, etc.

3) Mineral fillers

In general, because of the low molecular weight, the PPS is relatively fluid during injection molding or extrusion. This can put in difficulty for the implementation of the polymer. To optimize the condition of this implementation of the material, one of the methods consists of adding mineral fillers. It is thus possible to increase the viscosity of the polymer in the molten state. To check the absence and the presence of the mineral fillers, one can use several methods. One of the simple methods is to use pyrolysis. Heating the composite to a high temperature for a certain time allows the matrix to be removed and the fibers and the mineral fillers (if they exist) to be recovered.

IV. Morphological study of PPS/GF

IV-1 Crystallization and its kinetic aspect

To be able to understand the influence of the aging on its mechanical properties of the PPS, as already explained in the paragraph of the research strategy, it is necessary to study the

evolution of morphology over time. For this, we conducted a comprehensive study in this area. The results of this study are the subject of an article in the progress. To stay consistent with this extended summary, we do not present all of these results. We present in a synthetic way and some part of these results shows the influence of aging on the crystalline phase.

As already indicated, PPS is a semi-crystalline thermoplastic polymer with a crystallinity level between 40 and 45%. The crystalline phase of this polymer, like many other semi-crystalline polymers, has a spherulitic texture. Studies in literature, [45] (see la Figure 3), have clearly shown that the formation of the crystalline phase is sensitive to the cooling rate. These results show that the size (diameter) of spherulites at the end of crystallization decreases with increasing cooling rate.

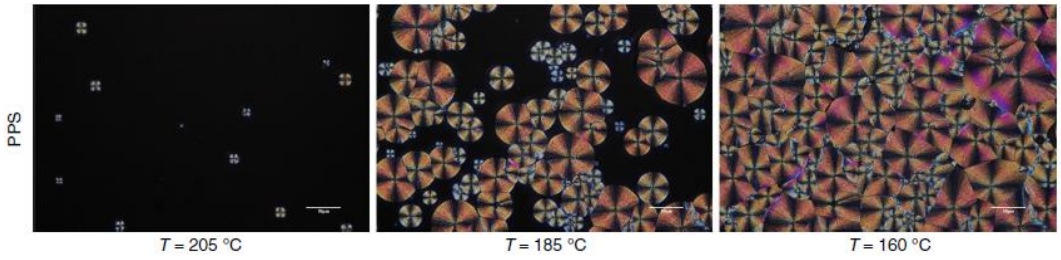

(a)

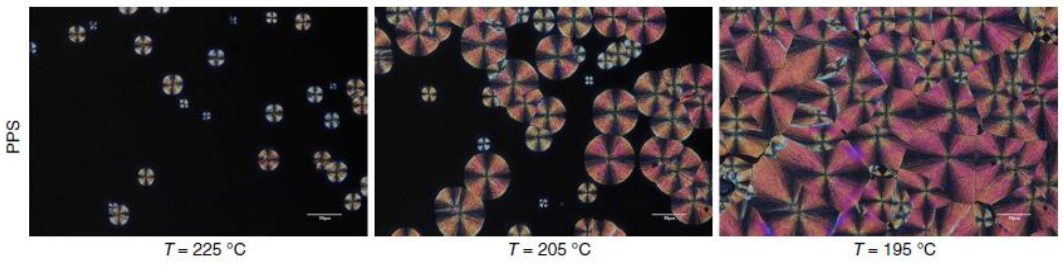

(b)

Figure 3 : POM photos of pure PPS during non-isothermal crystallization with different cooling rates: (a) 20 °C/min and (b) 5 °C/min.

We performed DSC tests with a cooling rate of 5 to 25 °C on the PPS/GF samples. The results are shown in Figure 4 (a). From these results, it can be noted that the cooling rate has a significant effect on the PPS crystallization process. The crystallization temperature (T_c) decreases with increasing cooling rate. T_c decreases from 243 °C to 230 °C as the cooling rate increases from 5 °C/min to 25 °C/min, respectively.

From the DSC results we have followed the evolution of the relative crystallization as a function of time at different cooling rates; Figure 4 (b). Each time, 3 steps are observed during crystallization. The first stage corresponds to nucleation and crystallite formation (the structural unit of the crystalline phase). In this step the rate of advancement of crystallization does not evolve. This period is more important when the cooling rate is lower. The second stage corresponds to the formation phase of spherulites and their growth. The growth rate (the slope of the curve) is directly related to the cooling rate. It is more important for the faster cooling rate. The third step corresponds to the final phase of spherulites. During this step, the spherulites interact to form solid polygons at the end of crystallization. It can be seen that the overall crystallization time decreases with the increase of the cooling rate.

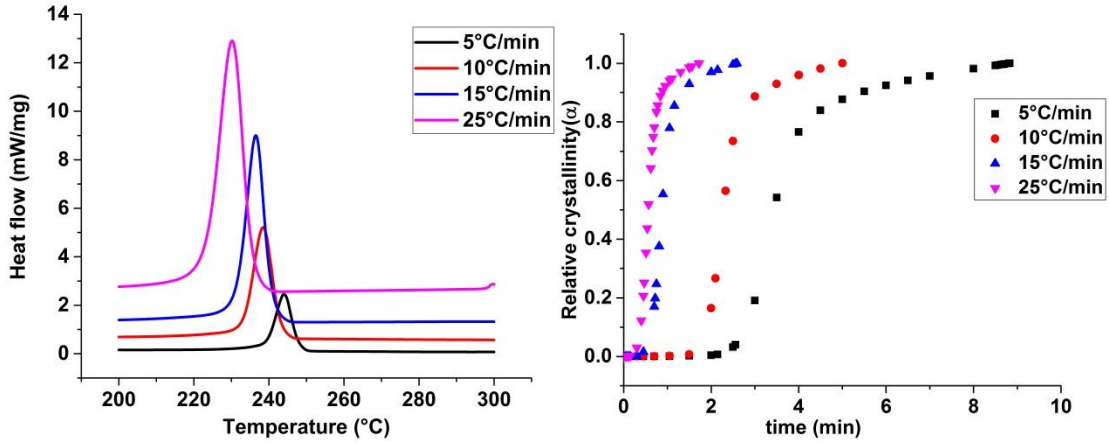

(a) (b)

Figure 4: The heat flow (a) and relative crystallinity (b) curves of PPS composites at various cooling rates (5~25 °C/min).

Based on the model of Avrami, the model of Jeziorny [46] is commonly used to model the non-isothermal crystallization process. This model can be presented by the following equation [47-50]:

$$\alpha = \ln[-\ln(1-\chi(t))] = \ln K + n \ln t \qquad \text{(e.q. 4)}$$

$$\ln Kc = \frac{\ln K}{\beta} \qquad \text{(e.q. 5)}$$

Where α is the fraction of relative crystallinity and χ(t) is relative crystallization fraction at time t; K is crystallization rate constant; n is the Avrami constant and K_c is corrected crystallization rate constant, β is cooling rate.

Figure 5 shows that $\ln(-\ln(1-\chi(t)))$ vs ln t gives a straight line with a linear correlation coefficient, R^2 close to 1 ($1>R^2>0.99$) for all cooling speeds. This means that the Jeziorny model can perfectly describe and verify the non-isothermal crystallization process of this PPS/GF material.

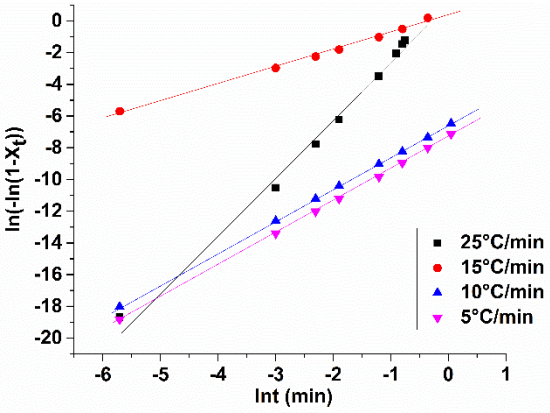

Figure 5: Plot of ln (-ln (1-*X* (t))) versus ln (t) at various cooling rates (5~25 °C / min).

Table 2 summarizes the values of the constants of this law obtained after the modeling for the different cooling rates. It is found that the values of K and K_c increase with the increase of the cooling rate.

	R^2	n	Ln K	K_c
5 °C/min	0.99	2.02	-7.33	0.23
10 °C/min	1	2.00	-6.61	0.52
15 °C/min	0.99	1.08	0.34	1.02
25 °C/min	0.99	3.55	0.91	1.04

Table 2: Non-isothermal crystallization kinetic parameters from Jeziorny model

To calculate the activation energy related to non-isothermal crystallization, Kissinger et al. [51] have proposed an equation based on the kinetic model of n-order, as follows:

$$ln\frac{\beta}{T_p^2} = ln\frac{AR}{E} - ln[G(\alpha)] - \frac{E}{RT_p} \quad \text{(e.q. 6)}$$

Where β is the cooling rate, T_p is the temperature of the crystallization peak. A is the pre-exponential factor and R is the universal constant of perfect gases. E is the activation energy and G (α) is the conversion function. To determine the activation energy we used the Kissinger

equation, and we plotted $\ln \frac{\beta}{T_p^2}$ as a function of $\frac{1}{Tp}$. We obtain a line with a linear correlation coefficient close to 1. From the slope of this line we have determined the activation energy of the non-isothermal crystallization (-58.78 kJ / mol).

IV-2 Aging effect on crystallization behavior

PPS is a semi-crystalline polymer, having an amorphous phase and a crystalline phase. The amorphous phase is much less compact. The oxygen attacking sites are in the amorphous phase. Oxygen cannot diffuse in the crystalline phase. As a result, the thermo-oxidative aging of the PPS has in fact led to the chemical modification of the amorphous phase. This modification can be manifested in different ways: the crosslinking (in certain cases and for certain period of aging), the session of the macromolecular chains, the reduction of the molar mass, the embrittlement, the stiffening, the reorientation of the macromolecules, ... All these phenomenon will occur in the amorphous phase and the crystalline phase during this period remains relatively intact. To be able to understand the effect of aging on the mechanical properties, it is necessary to study this morphological modification. Through this microstructural modification, the change in mechanical properties is more comprehensive. In the case of PPS/GF, we determined the morphological characteristics from the results of tests on virgin and aged PPS/GF samples (at 200 °C), with DSC and DMA. We then determined the T_g, the T_f, the crystallinity degree and the constants of the kinetic model of crystallization previously presented (previous paragraph). Table 3 summarizes all these results.

It is first noted that the T_g increases from 106 °C (virgin sample) to 121 °C (after 1080 h aging at 200 ° C). This increase can be attributed to two phenomena: (short-term) crosslinking and the reorientation and stiffening of macromolecules as a result of the chains breaking through oxidation. Macromolecules become less mobile in the amorphous zone.

It is also shown that the degree of crystallinity increases from 44% (virgin sample) to 56% after 96 hours of aging at 200°C. After a long period of oxidation up to 1080 h at 200 °C, the crystallinity degree decreases to 36.6%. It is difficult to interpret this consequent drop in the crystallinity rate. On the other hand what is obvious is that at this stage of degradation (1080 h) at 200 °C, the amorphous phase is well damaged and the texture of the morphology is completely modified. The question can also be asked: is the crystalline phase degraded and in what way?

Concerning the modification of the crystalline phase during aging, the analysis of the change of the values concerning the constants of the model ((e.q. 4) and (e.q. 5)) enables us to obtain the following ideas:

- The constant n depends on the nature of nucleation, the geometry of the crystallites and the density of the spherulites. The value of n is about 2 for virgin samples and aged at 200 °C up to 144 h. It can be assumed that during this period the crystalline phase is not very modified. However, for the samples aged after 1080 h at 200 °C, n decreases to 0.8. This may imply that the PPS compared to its initial state has almost lost its ability to nucleate and crystallize due to well excessive thermal aging.
- Similarly, K_c depends on the crystallization rate and the increase in K_c corresponds to the increase in the crystallization capacity. At the beginning of thermal aging, the increase in K_c was observed from 0.5 (virgin sample) to 0.97 (sample of 200 °C - 144 h). This indicates that aging can enhance the rate of crystallization. But in the long term (as 200 °C - 1080 h), when aging is well excessive and the polymer is completely degraded and the value of K_c (0.6) shows that the polymer crystallizes more slowly during crystallization.

Samples	Amorphous phase	Crystalline Phase		
	T_g (*) (°C)	X_c (**)	n (**)	K_c (**)
Virgin	106	44,2	2,00	0.5
200°C-20h	108	45,0	2,10	0,88
200°C-96h	108	55,8	2,19	0,82
200°C-144h	-	52,9	2,27	0,97
200°C-1080h	121	36,6	0,8	0,6

(*) T_g, obtained by DMA test at peak of E'', (f=1 Hz); (**) X_c, n, K_c, obtained by DSC with a cooling speeding of 10 °C/min.

Table 3 : The parameters obtained from DMA and DSC.

V. Long-term behavior of PPS composite

This part is dedicated initially to the study of the thermal aging of the composite PPS. It is an accelerated aging study at high temperatures (from 100 to 200 °C). To do this, we will perform IR spectrometric analysis to detect and monitor the evolution of oxidation products in materials. This will allow a good understanding of the degradation mechanisms that will be used in the second period for the construction of a kinetic model capable of describing the evolution of the oxidation products.

For this part of the study, the methodology includes:

1) On the one hand, carrying out accelerated aging tests and monitoring the evolution of certain chemical groups (such as C=O) (indicator of progress in aging);

2) On the other hand, proposing a mechanism of oxidation of the PPS. This mechanism makes it possible to propose a kinetic model for the evolution of C=O. The next step is therefore to compare the experimental results with the theoretical model. Schema 2 presents this approach and methodology.

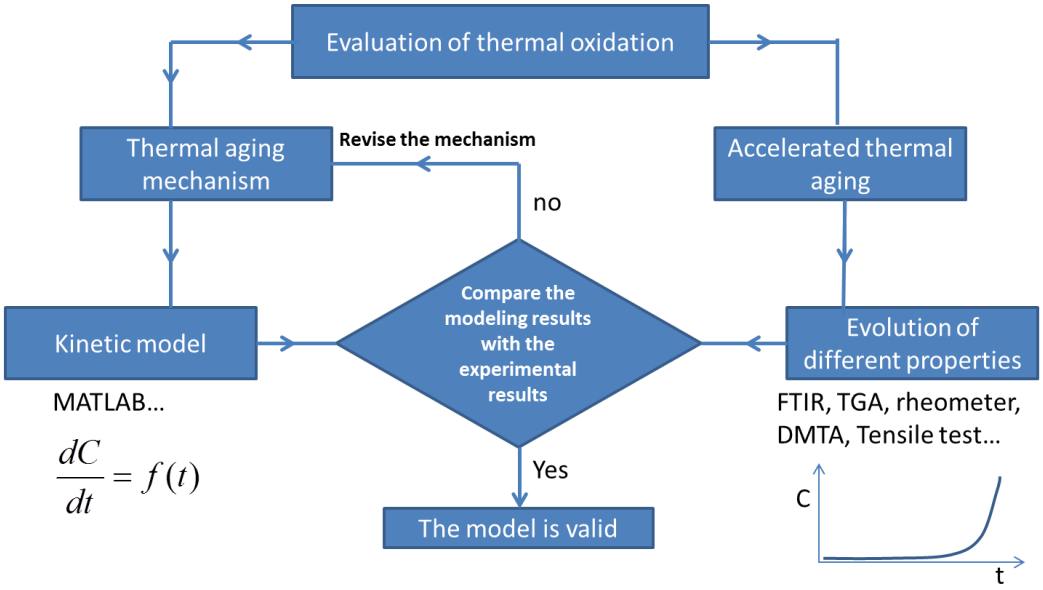

Schema.2: Pathway for validating thermal oxidation modeling.

Following this introduction, we present our study and modeling of the thermo-oxidation of PPS/GF. The detailed results of this study are the subject of Article N°3.

V-1 Preliminary analysis

Due to the lack of precise information on the composition of this material provided by the supplier, the peaks for original materials between 1700 and 1800 cm^{-1} can be explained by the fact that there are phenyl groups or vinyl esters. These peaks could appear in the position of the end groups. To simplify the research, it is necessary to take only the thermal oxidation of PPS material itself into account.

To study the evolution of the oxidation products, a conventional approach has been used which consists of following the total concentration of the carbonyl products from the absorbance of the IR peaks by means of the Beer-Lambert law. The concentration of [C=O] gives a clear indication of the oxidation. Figure 6 shows the FTIR results of the C=O peaks, which are at the wave positions of 1780 cm^{-1}, 1735 cm^{-1} and 1710 cm^{-1}, respectively. More precisely, they can be divided into three different types of C=O double bonds. Thus, it can be noted that there is a trend towards an obvious increase in the C=O double bond absorbance, indicating that the PPS/GF composites are seriously oxidized at 200 °C.

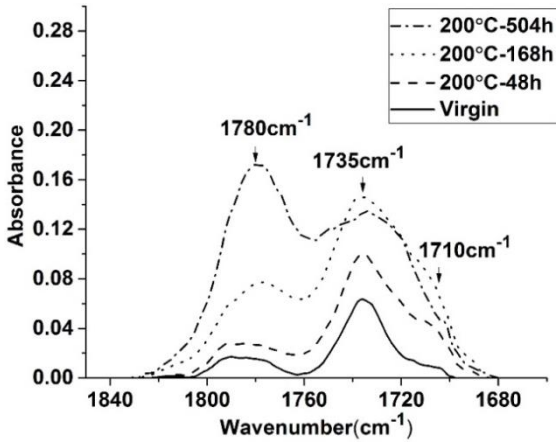

Figure 6: Evolution of oxidation products of PPS at 200°C.

Figure 7 shows the different evolutions of the oxidation products of the PPS for 4 aging temperatures. The accumulation curves of the oxidation products (C=O) during aging highlight the three characteristic stages of the oxidation kinetics:

- A period of induction preceding the appearance of the first carbonyl products.
- Fast acceleration (self-acceleration) of the oxidation at the end of the induction period.
- A stationary regime with apparent overall rate of constant oxidation.

It can be seen that the rates of accumulation of the oxidant products increases with the increase of the exposure temperature.

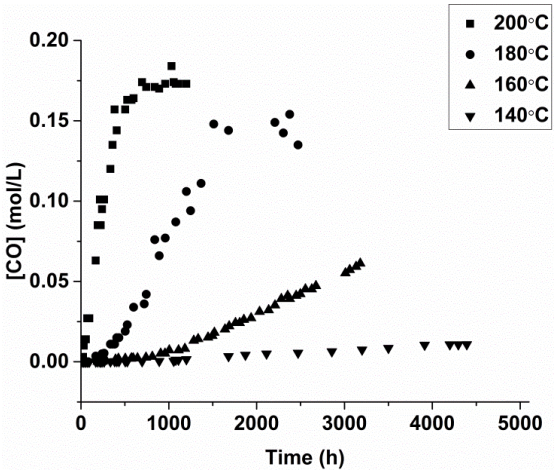

Figure 7: Evolution of the oxidation products of PPS at 140 °C, 160 °C, 180 °C and 200 °C.

Conventionally, oxidation can be divided into three periods: induction, propagation and termination. It can be seen that the induction time is very short (approximately 24 h) for the specimens aged at 200 °C whereas this value increases significantly for the temperatures of 180 °C and 160 °C (approximately 240 h and above 1100 hours, respectively). At the temperature of 140 °C, the induction time is very long (more than 2000 h). It can thus be noted that the induction time at temperatures of 180 °C and 160 °C is about 10 and 45 times higher than in the case of 200 °C, respectively. In addition, the propagation speed is very high for the oxidation temperature at 200 °C and 180 °C. After about 1000 hours of oxidation at 200 °C, the propagation tends to be saturated when the amount of oxidation products reaches a maximum. At 180 °C saturation appears to be reached after 2000 hours of exposure. Comparatively, there is no comparable trend and no stable plateau trend observable for oxidation at 140 °C even after more than 4000 h of exposure. Thus, it can be concluded that for this composite, the oxidation ratios at 200 °C and 180 °C are considerably more severe and faster than at temperatures of 160 °C and 140 °C.

V-2 Modeling the kinetics of aging

- **The oxidation theory**

In this part of the study of thermal aging, a modeling of the kinetics of the oxidation could be realized from the experimental results.

Hydrocarbon polymers subjected to thermal aging in the air generally degrade by radical chain oxidation [52, 53]. The model of the standard mechanism under air or oxygen, considering the simultaneous decomposition of uni- and bi-molecular hydro-peroxide, is reported in several research works [54-56] (see Schema 3):

$$POOH \rightarrow 2P^{\circ} + \Upsilon co\ PC = O \qquad (k1u)$$

$$POOH + POOH \rightarrow P^{\circ} + POO^{\circ} + \Upsilon co\ PC = O \qquad (k1b)$$

$$P^{\circ} + O2 \rightarrow POO^{\circ} \qquad (k2)$$

$$POO^{\circ} + PH \rightarrow POOH + P^{\circ} \qquad (k3)$$

$$P^{\circ} + P^{\circ} \rightarrow \text{inactive products} \qquad (k4)$$

$$P^{\circ} + POO^{\circ} \rightarrow \text{inactive products} \qquad (k5)$$

$$POO^{\circ} + POO^{\circ} \rightarrow \text{inactive products} + O2 \qquad (k6)$$

Schema.3: Possible scheme of the degradation of the polymer.

Here, [P°], [POO°], [POOH], [PH] represent the concentration of alkyl radicals, peroxy radicals, hydro-peroxides and substrate, respectively; the numbers k1u to k6 represent the kinetic constants of each equation.

Several previous studies have investigated the degradation mechanism of PPS polymers [57-62]. Below 200 °C, the possible schematic diagram of the degradation of PPS/GF composites is given in Schema 4. According to the literature [61] and the theory of bond energy, the carbon-sulfur (C-S) and carbon-hydrogen (C-H) bonds are weaker than the carbon-carbon double bond (C = C). Thus, the first major scission occurs in the C-S bond or the C-H bond. Under aging conditions, degradation, radical abstraction, recombination, cyclization and/or other more complex reactions occur, with a process of producing different compounds such as hydrogen sulfide, benzenethiol, diphenylsulfide, dibenzothiophene, etc [63].

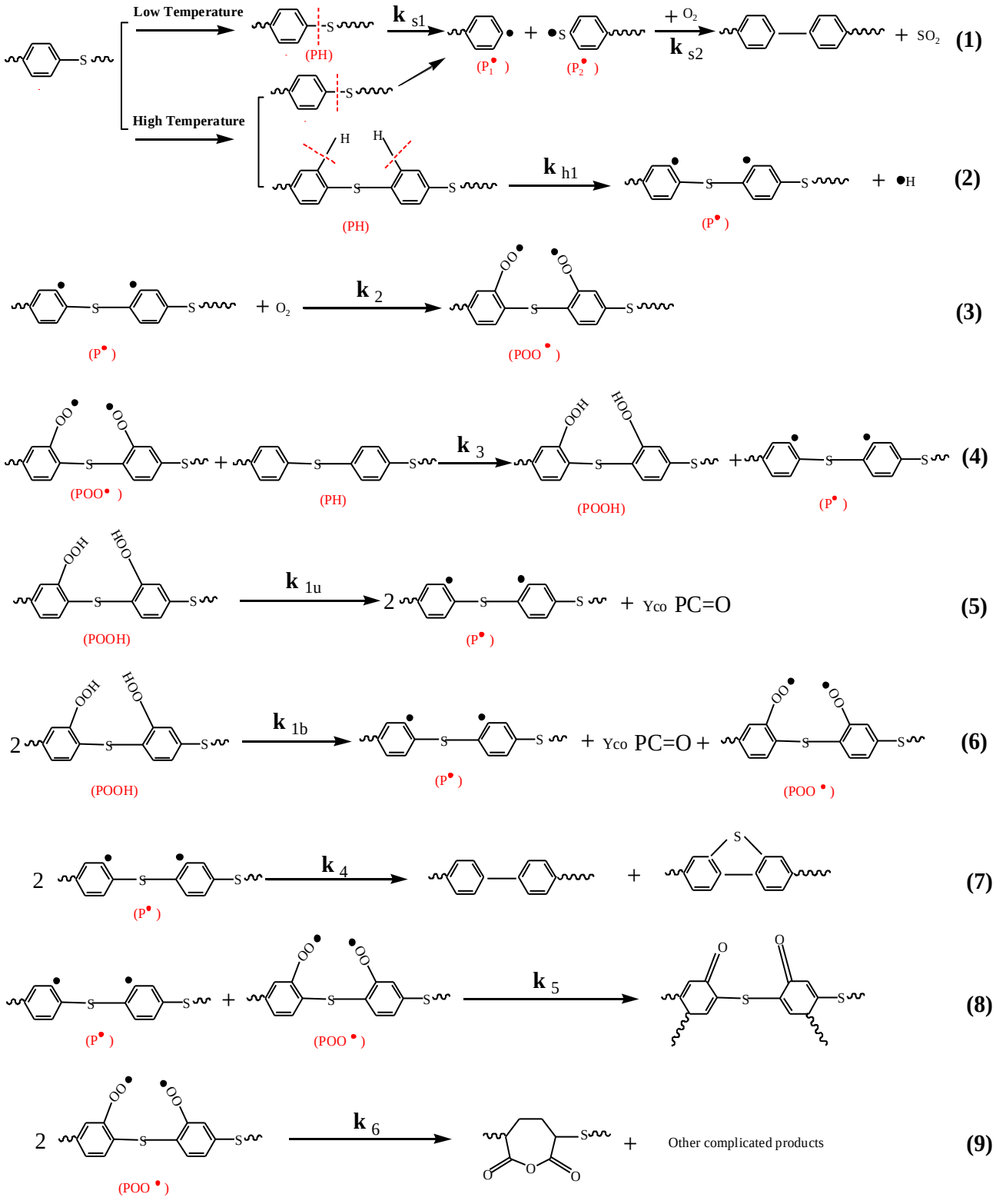

Schema.4: Possible schema of degradation of the PPS/GF composite.

According to this scheme, it can clearly be noted that the oxidative degradation process contains major pathways that may occur in the C-S or C-H bond positions. It is remarkable that, as shown in previous research [52, 54], the mechanism of oxidative degradation of PPS can be presented by differential equations. By using these differential equations, it is then possible to quantitatively calculate the evolution of [C=O] as a function of time under different oxidative aging temperatures as follows:

$$\frac{d[P^{\circ}]}{dt} = 2 * k_{1u} * [POOH] + k_{1b} * [POOH]^2 - k_2 * [P^{\circ}] * [O] + k_3 * [POO^{\circ}] * [PH] - 2 * k_4 * [P^{\circ}]^2 - k_5 * [P^{\circ}] * [POO^{\circ}] + k_{h1} * [PH] \quad (e.q.7)$$

$$\frac{d[POO^{\circ}]}{dt} = k_{1b} * [POOH]^2 + k_2 * [P^{\circ}] * [O] - k_3 * [POO^{\circ}]^2 * [PH] - k_5 * [P^{\circ}] * [POO^{\circ}] - 2 * k_6 * [POO^{\circ}]^2 \quad (e.q.8)$$

$$\frac{d[POOH]}{dt} = -k_{1u} * [POOH] - 2 * k_{1b} * [POOH]^2 + k_3 * [POO^{\circ}] * [PH] \quad (e.q.9)$$

$$\frac{d[PH]}{dt} = -k_3 * [POO^{\circ}] * [PH] - k_{s1} * [PH] \quad (e.q.10)$$

$$\frac{d[CO]}{dt} = k_{1u} * [POOH] + k_{1b} * [POOH]^2 \quad (e.q.11)$$

$$\frac{d[P_1^{\circ}]}{dt} = k_{s1} * [PH] - k_{s2} * [P_1^{\circ}][P_2^{\circ}] * [O] \quad (e.q.12)$$

$$\frac{d[P_2^{\circ}]}{dt} = k_{s1} * [PH] - k_{s2} * [P_1^{\circ}][P_2^{\circ}] * [O] \quad (e.q.13)$$

Here, [P°], [POO°], [POOH], [PH] represent the concentration of alkyl radicals, peroxy radicals, hydro-peroxides and substrate, respectively; the numbers k1u to k6 represent the kinetic constants of each equation.

- **Validation of the kinetic model**

The validation of the proposed kinetic model has been done. It was able to better simulate the experimental data obtained between 160 °C and 200 °C (see Figure 8). The values of the model parameters are summarized in Table 4, which provide the best simulations of the experimental results corresponding to exposure temperatures of 160 °C, 180 °C and 200 °C. It can be seen that the experimental results are very consistent with the modeling. This means that our model of oxidative degradation mechanism is appropriate. Based on this analysis, it can be concluded that with this modeling, we can translate the oxidative degradation mechanism in a quantitative way.

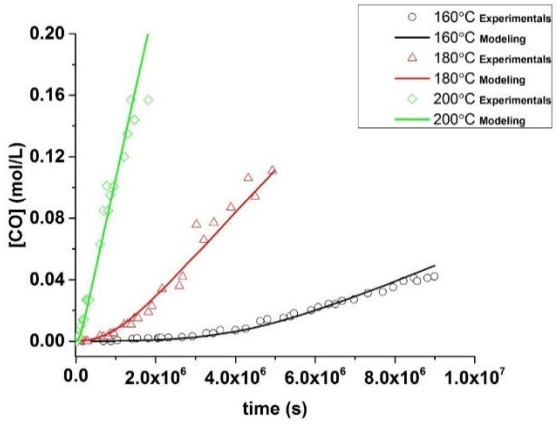

Figure 8: Numerical simulations of oxidation products at 160 °C, 180 °C and 200 °C.

	k1u (s^{-1})	k1b ($l\ mol^{-1}s^{-1}$)	k2 ($l\ mol^{-1}s^{-1}$)	k3 ($l\ mol^{-1}s^{-1}$)	k4 ($l\ mol^{-1}s^{-1}$)	k5 ($l\ mol^{-1}s^{-1}$)	k6 ($l\ mol^{-1}s^{-1}$)
T=160 °C	$1.3x10^{-7}$	$1.1x10^{-5}$	$1.3x10^{6}$	$1.1x10^{-3}$	$1.0x10^{12}$	$2.0x10^{9}$	$3.0x10^{3}$
T=180 °C	$1.6x10^{-6}$	$1.8x10^{-5}$	$1.5x10^{6}$	$1.8x10^{-3}$	$1.0x10^{12}$	$2.0x10^{9}$	$3.4x10^{3}$
T=200 °C	$2.0x10^{-5}$	$2.0x10^{-5}$	$1.6x10^{6}$	$6.0x10^{-3}$	$1.0x10^{12}$	$2.0x10^{9}$	$4.0x10^{3}$

Table 4 : Kinetic constants and Arrhenius parameters of the reactions

VI. Fatigue behavior of PPS material

Fatigue is an action of time-varying stresses or deformations that can modify the local properties of a material. Fatigue can lead to crack formation leading to breakage of the workpiece. The progression of the fatigue damage can follow different stages:

- The creation of nucleation sites
- The formation of micro cracks
- Growth and coalescence of dominant microscopic cracks
- The propagation and percolation of dominant macro cracks
- Breaking

The main characteristics and properties governing the fatigue behavior of a polymer matrix composite are as follows:

- The nature of the matrix: its chemical composition, morphology, physical state…
- Additives and fillers: glass marbles, mineral particles...
- The nature of the reinforcements: material, architecture and dimensions
- The state of the interface: the size, the chemical, physical or mechanical adhesion between matrix and fibers
- The type and condition of stress (temperature, amplitude of stresses or deformations, frequency, load ratio ...)

As a part of this work, tension-tension fatigue tests were carried out on the MTS 830 (Elastomer Test System) hydraulic machine with application of a force at 10 Hz. The samples were cut by water jet in using the geometry shown in Figure 9 (a).

The amount of stress directly and substantially affects the life of the material. In order to understand the effect of the microstructure on the fatigue behavior of materials, we carried out a preliminary fatigue study on two fiber reinforced materials oriented at 90° and 0°. The Wöhler curve at 10 Hz is shown in Figure 9 (b)[64].

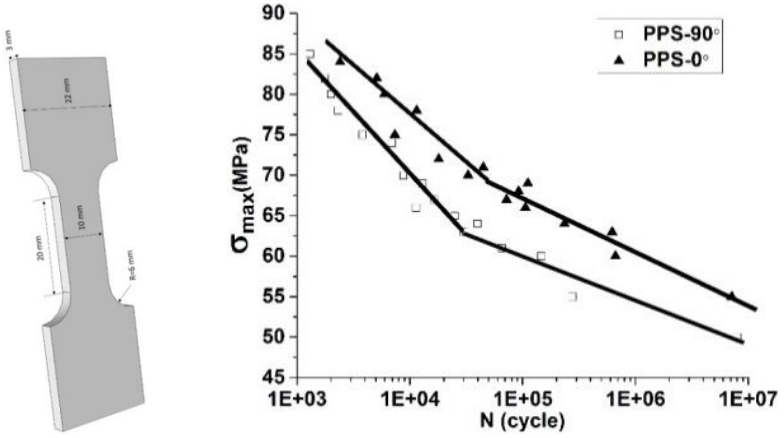

(a) (b)

Figure 9: Specimen geometry (a) and Wöhler curves for PPS-0° and PPS-90° samples at 10 Hz (b).

We can give the following comments:

- For the PPS-0° and PPS-90° samples, the Wöhler curves do not have a significant asymptotic value representing an endurance limit. Unlike metal materials, this is often observed in the case of thermoplastic composites [65].
- For stress amplitude of 60 MPa, the PPS-90° is broken after $1x10^5$ fatigue cycles. While for the same amplitude, the PPS-0° breaks after more than 10^6. This observation clearly demonstrates that the service life is strongly influenced by the orientation of the fibers.
- For both configurations, the Wöhler curves show two different domains; high and low amplitudes. In each domain, the S-N curve can be modeled by a linear-logarithmic equation:

$$\sigma_{max} = A. \log N + B \qquad \text{(e.q. 14)}$$

In this equation, A and B are the material parameters corresponding to the slope of the curve and the intercept, respectively. The slope A shows the sensitivity of the fatigue strength and the intercept B represents the apparent tensile strength.

Table 5 shows the values of A and B for the PPS-0° and the PPS-90° related to the high and low stress domains.

Samples	A (MPa)		B (MPa)	
	High stress domain	Low stress domain	High stress domain	Low stress domain
PPS-0°	-12.0	- 6.7	125.7	108
PPS-90°	-15.2	- 5.5	131	87.5

Table 5 : The values of A and B for PPS-0° and PPS-90° in each domain

VII. Effects of thermal aging on mechanical behavior

In this part we summarize the effect of thermal aging on the mechanical behavior of PPS/GF. Detailed information on long-term behavior is presented in the Article N°4.

The literature review provides much information on the general properties of PPS composites. However, there is a lack of information on the response to fatigue when exposed to thermal aging. It is therefore imperative to propose innovative work to better understand the effects of thermal aging coupling with mechanical properties, particularly with regard to fatigue behavior. This type of research is very interested to very practical and useful industrial aspects, particularly for structural calculations in automotive sector.

A key point in our approach is to track the [C=O] concentration during thermal aging as an indicator of the oxidation process and degree of degradation in the matrix. In addition, a relationship between thermal oxidation and mechanical behavior is established to provide a tool to help the choice of material structure and its design.

The first part deals with the analysis of the effects of thermal aging. Quasi-static loading responses and loading-unloading tests with gradual increase to the maximum stress of virgin and aged samples are analyzed. Also, the effect of thermal aging on the fatigue properties of PPS is subsequently studied.

Hereinafter, three types of mechanical tests were considered:

- **Tensile test:** The effects of aging on stress-strain curves obtained by tensile tests are presented. Changes in Young's modulus, tensile stress, and ultimate strain are plotted for different aging conditions. The tensile response is analyzed for an oxidation temperature of 200 °C after various aging times of 0 h, 30 h, 50 h, 100 h and 200 h.
- **Loading-unloading test:** It is necessary to analyze the loss of stiffness and the evolution of plastic deformation to understand the effect of aging conditions on the mechanisms of damage and deformation. The tensile and loading-unloading tests are carried out at an aging temperature of 200 °C. for different oxidation times, namely 0 h, 30 h, 50 h, 100 h and 200 h.

- **Tension-Tension fatigue test:** The fatigue tests were performed at 10 Hz to compare the life of the PPS composite at various temperatures and aging times. In addition, the analysis of stiffness loss and fractography is presented. The fatigue behaviors on four types of samples oxidized at 140 °C, 160 °C, 180 °C and 200 °C at different aging times

were analyzed. It can be noted that the loading amplitudes of 40 MPa and 70 MPa were selected after the analysis of the Wöhler curve obtained on the virgin samples.

VII-1 Results of tensile tests

The results of tensile tests on virgin samples and samples aged at 200 °C for different aging times are shown in Figure 10.

It can be noted that at the beginning of the exposure at 200 °C from 0 h to 30 h, the breaking stress increases. This is mainly due to post-crosslinking, which leads to the extension of the molecular chains. After this preliminary step, the breaking stress decreases by 25% for 200 hours. This shows that thermal oxidation at 200 °C promotes the mobility of the molecular chains due to the cleavage of chemical bonds.

It can be noted that the relative Young's modulus increases slowly at the beginning of thermal aging at 200 °C (due to post-crosslinking). In addition, all aged samples have a higher Young's modulus than virgin samples, indicating that crosslinking can affect the mechanical behavior of PPS composites. The breaking strain exhibits a constant decrease from about 1.4% to 1% during oxidation. This indicates embrittlement phenomenon due to oxidation.

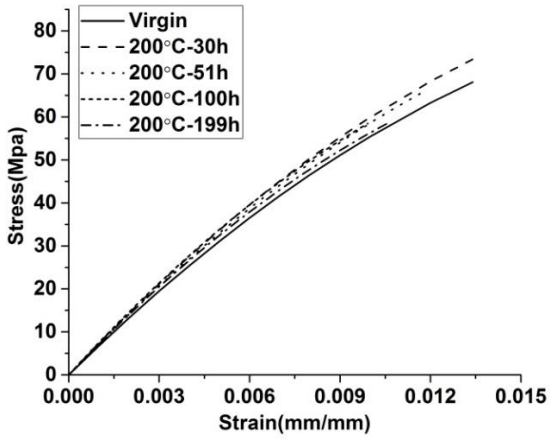

Figure 10: Stress-strain curves at different stages of aging at 200 °C.

The tensile test results clearly show the influence of aging on the mechanical properties of the PPS composite (Table 6 and Figure 11). An increase in modulus of elasticity and stress at break was shown during the first period of thermal aging. To be more precise, during the aging process, cleavage of the molecular chains and post-crosslinking can occur simultaneously in the PPS polymer material. In addition, it should be noted that at the beginning of the thermal oxidation, the post-crosslinking is more pronounced while the long-term thermal oxidation mainly corresponds to a chain cleavage and a significant degradation of the PPS polymer.

As a result, after the first exposure step, a second aging step showing chain scission effect becomes predominant at the surface of the sample, ultimately leading to a loss of properties of the PPS composite, especially in terms of ductility. This can be explained by the fact that the thermoplastics have a linear or branched molecular structure and that therefore they become more fragile due to the cleavage of the molecular chain or the crosslinking in the chemical structure of the PPS polymer.

Aging	n°	t(h)	σ_r (MPa)	ε_r (%)	E (MPa)
Virgin	1	-	75,4	1,3	5900
	2	-	74,4	1,2	5890
200 °C-30h	1	30	79,4	1,35	6100
	2	30	78,9	1,4	6200
200 °C-51h	1	51	70,5	1,2	6000
	2	51	70,8	1,2	6150
200 °C-100h	1	100	63,4	1	6600
	2	100	58,4	1	6300
200 °C-199h	1	199	66,5	1,1	6500
	2	199	61,1	1	6400

Table 6 : Tensile results at different stages of aging at 200 °C

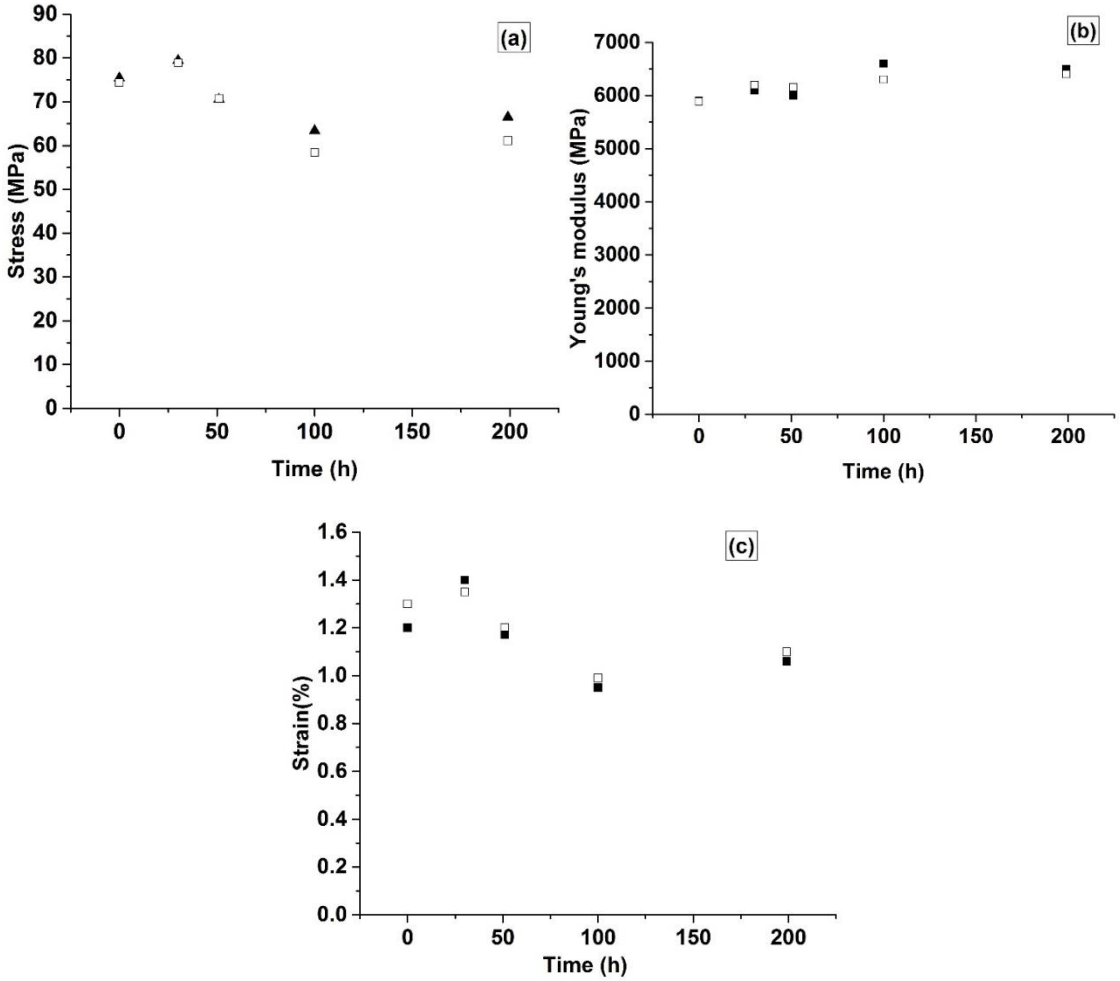

Figure 11: Evolution of (a) the stress at break, (b) Young's modulus and (c) Strain at break during aging at 200 °C.

From the microstructure analysis of the virgin sample (Figure 12-(a)), it is evident that the fiber-matrix adhesion appears to be of very good quality, probably due to the presence of the coupling agent. Indeed, the fibers were torn off in a fragile manner but still remain covered with a thin layer of PPS matrix.

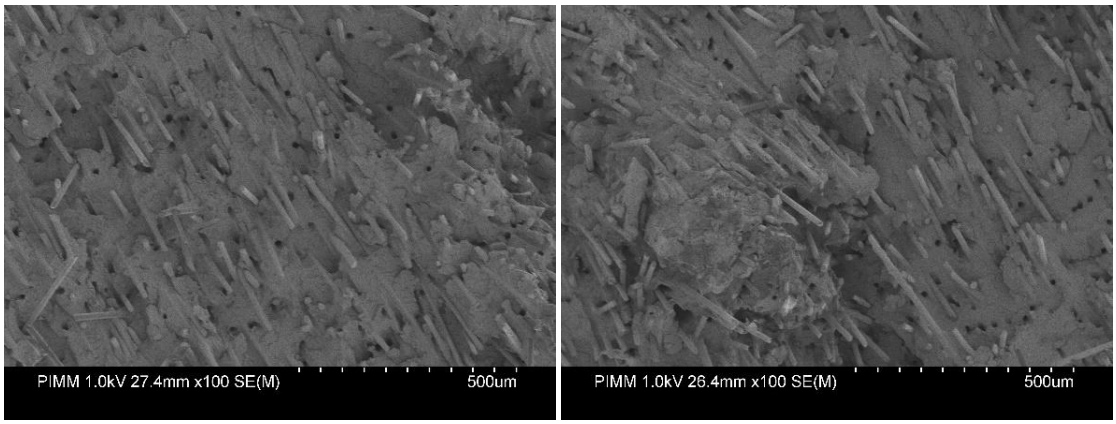

(a) Tensile test-virgin sample

(b) Tensile test-aged sample at 200 °C-199h

Figure 12: Fracture surface: (a) virgin sample and (b) sample aged at 200 °C -199 h.

Comparatively, in the case of a sample aged at 200 °C during 199h (see Figure 12 - (b)), it can be noted that the matrix degrades very seriously. Thermal aging has destroyed the matrix and led to the separation of the fiber and matrix, which reduces the mechanical property of the original PPS material.

VII-2 Loading-unloading test

In order to quantify the possibility of plastic deformation and damage, a loading-unloading test with progressive increase of the maximum stress was carried out in two configurations: virgin samples and specimens aged at 200 °C for 199 h (Figure 13 (a)). Figure 13 (b) shows the evolutions of the plastic deformation (ε_p) and the damage parameter (E/E_0) as a function of the maximum stress for aged specimens. As shown above, the breaking stress and the breaking strain decrease with aging. One can notice the relative stability of the Young's modulus which indicates a low level of damage during a quasi-static loading (decrease of less than 1%). On the other hand, the plasticity increases progressively from 5% of the stress to the rupture

which pushes us to say that the deformation of the composite is essentially due to the non-linearity of the PPS.

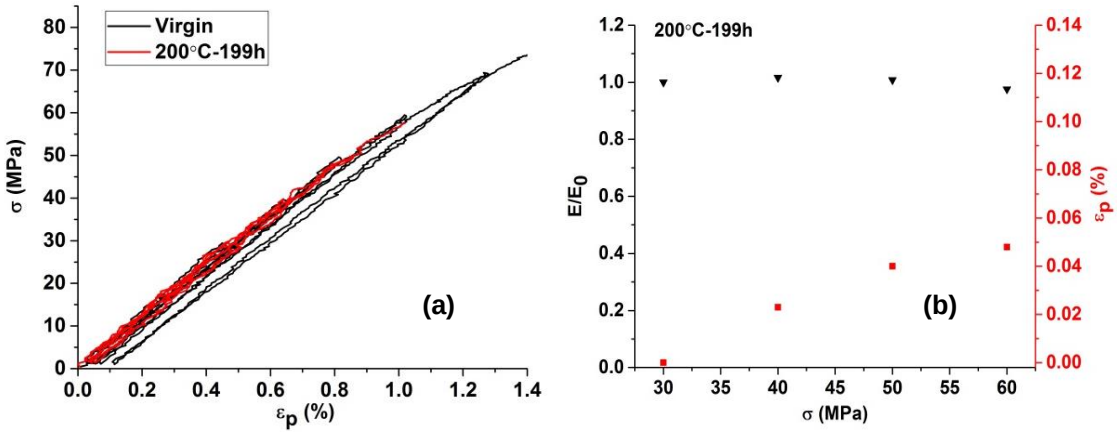

Figure 13: (a) Loading-unloading test, and (b) evolution of plastic strain (ε_p) and stiffness loss parameter (E/E_0) as a function of applied stress.

VII-3 Fatigue behaviors

- Amplitude effect

Figure 14 shows the Wöhler curve obtained in tension-tension fatigue tests at a frequency of 10 Hz for PPS-90° samples at room temperature. The final fracture and fatigue life of the PPS composite strongly depend on the loading conditions and the local microstructure. The bilinear Wöhler curves emphasize the influence of loading amplitude.

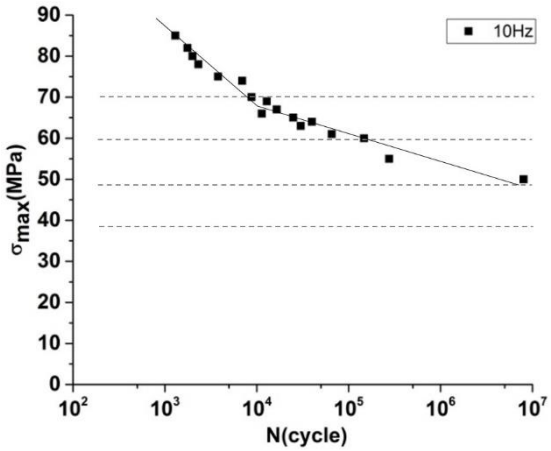

Figure 14: Wöhler curve of the PPS composite made on PPS-90° samples.

Tension-Tension fatigue test at a frequency of 10 Hz and at room temperature, R = 0.1.

In order to study the fatigue life of the PPS composite aged at 180 °C and at different aging times, tension- tension fatigue tests were carried out at loading amplitudes of 40 MPa and 70 MPa (see Figure 15). It can be noted that the number of cycles at break decreases with increasing loading amplitudes. One can also notice a considerable reduction in the number of cycles with the amplitude of 70 MPa, from 1.4×10^4 to 1.2×10^3 with an oxidation time of about 250 h. The results show that the fatigue life decreases sharply with aging time in the event of an increase in loading amplitude.

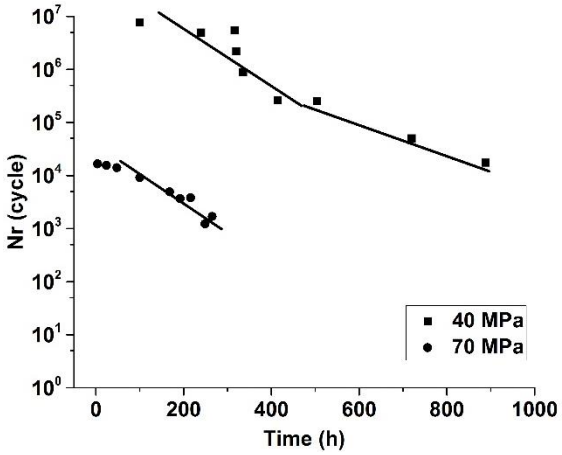

Figure 15: Effect of aging and load amplitude on fatigue life

samples, aged at 180 °C (f = 10 Hz).

- Effect of the thermal aging temperature

Figure 16 shows the evolution of the fatigue life as a function of the oxidation time at different oxidation temperatures of 140 °C, 180 °C and 200 °C. It can be noted that the speed of reduction of the fatigue life increases with the temperature of thermal aging. Indeed, at 200 °C, the fatigue life is subjected to a very sharp decrease.

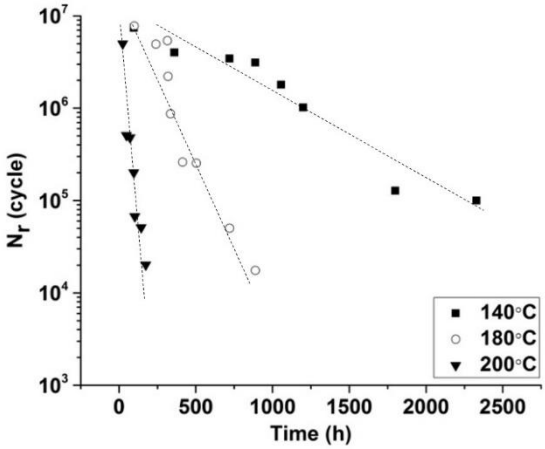

Figure 16: Effect of aging temperature on fatigue life.

Fatigue tests at 10 Hz with a maximum load amplitude of 40 Mpa (R=0.1).

This indicates that the temperature of 200 °C is very favorable to destroy the mechanical properties of PPS materials. The fatigue life is therefore very sensitive to the oxidation temperature.

- Analysis of fracture surface

A fracture surface analysis was performed on virgin and aged samples to understand the influence of temperature and fatigue exposure time.

Different aging times for an oxidation temperature of 200 °C:

Figure 17 shows the global evolution of fracture surface of test samples aged at 200 °C, from the beginning of oxidation to 5256 h. Figure 17 - (a) shows the virgin sample from which it can be noted that the surface is quite smooth, with no obvious cracks, indicating that the fibers adhere tightly with the matrix. The increase in oxidation time (96 h, 1056 h and 5256 h; Figure 17 - (b), (c) and (d), respectively), leads to more aggregated particles due to the higher instability surface energy.

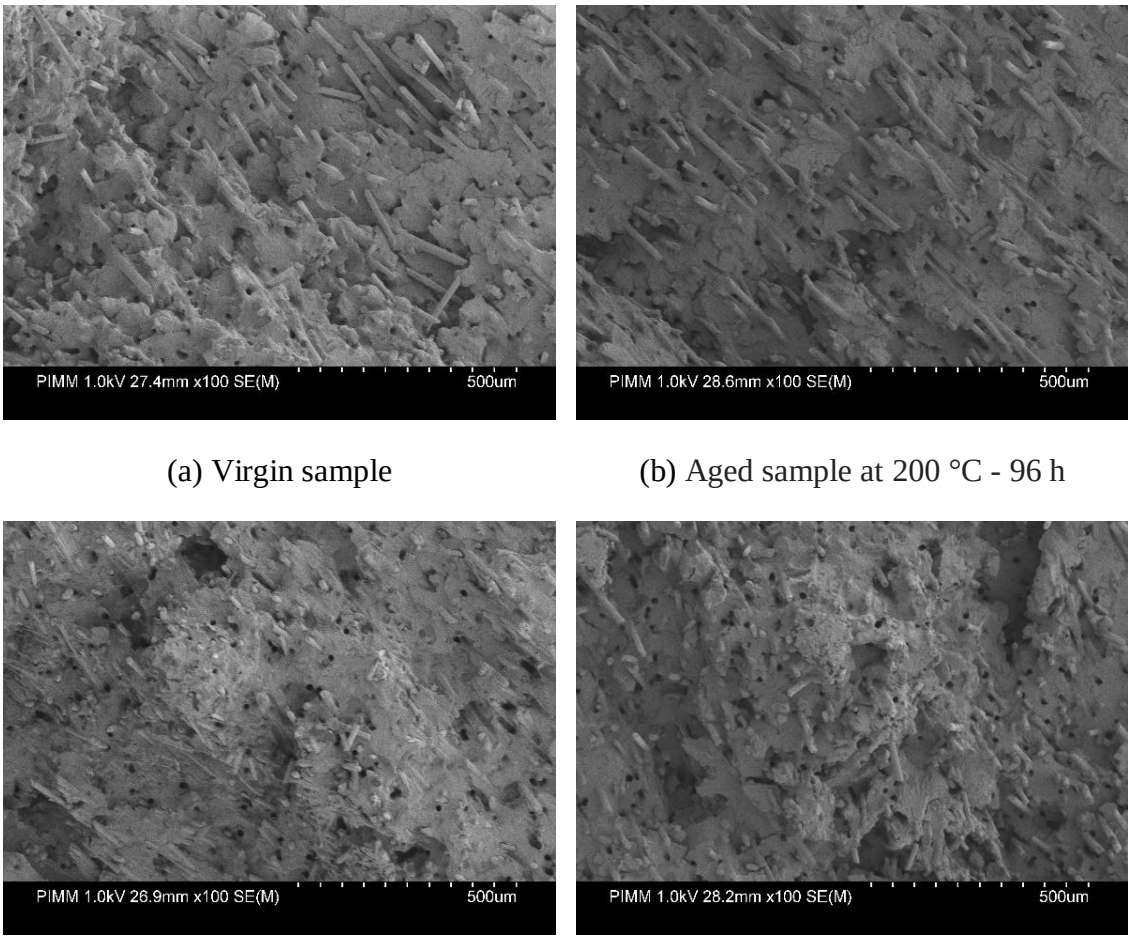

(a) Virgin sample (b) Aged sample at 200 °C - 96 h

(c) Aged sample at 200 °C-1056 h (d) Aged sample at 200 °C-5256 h

Figure 17: Fracture surface: a) virgin sample, b) sample aged at 200 °C-96 h, c) sample aged at 200 °C -1056 h and d) sample aged at 200 °C - 5256 h (σ_{max} = 40 MPa) .

Different aging temperatures after 1056 h of oxidation:

Figure 18 shows the fracture surface of the PPS composite aged at 140 °C and 200 °C after 1056 h of aging. Comparatively, at 200 °C, residual matrix can be seen on the exposed surface of the fibers and also some fiber surfaces are smooth. It can also be observed that the matrix degrades more seriously at 200 °C. In addition, the micrographs show that many particles have aggregated due to oxidation.

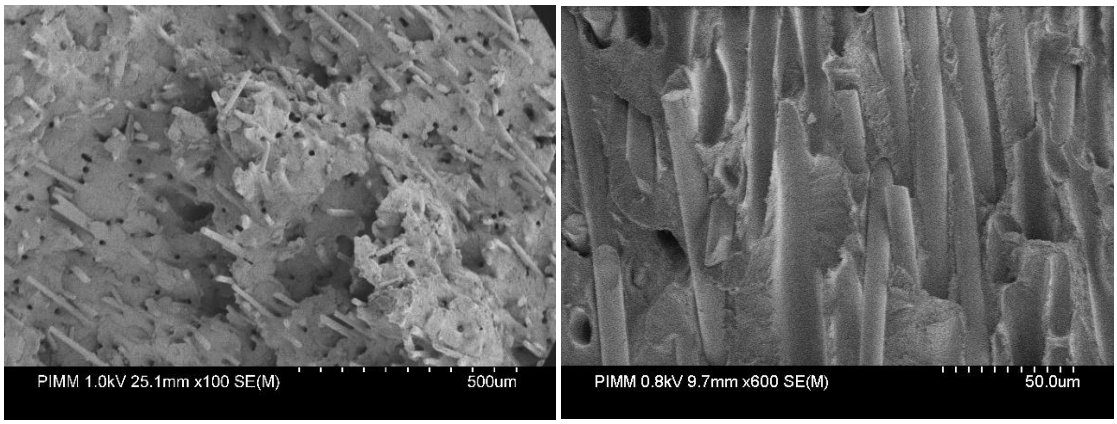

(a) sample aged at 140 °C-1056 h

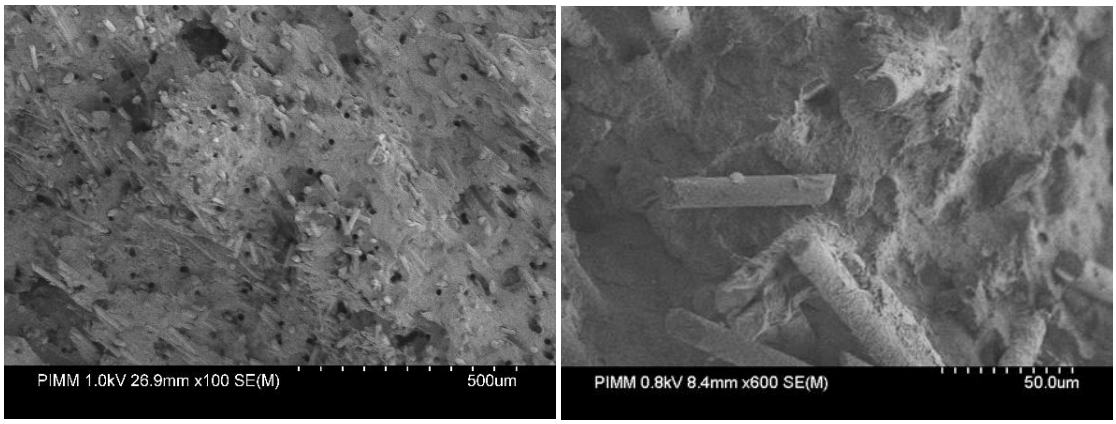

(b) sample aged at 200 °C-1056 h

Figure 18: Fracture surface: a) a sample aged at 140 °C - 1056 h and (b) sample aged at 200 °C - 1056 h (σ_{max} = 40 MPa).

VII-4 Coupling aging - fatigue

Figure 19 shows the relationship between number of cycles at failure (N_r) and [C=O] at different oxidation temperatures. It can be noted that, in general, this curve can be divided into two zones, high oxidation temperatures (for example 200 °C and 180 °C) and moderate temperatures (160 °C and 140 °C). For the same number of cycles at break (N_r), we can see that moderate temperatures produce less [C=O] while high temperatures correspond to more [C=O].

For a PPS polymer material subjected to a cyclic loading, samples aged at high temperature will require only a short time to achieve degradation while at a lower temperature a longer time will be required to achieve the same degree of degradation. Similarly, the concentration [C=O] can also represent the degree of degradation. When the same number of cycles has been applied until breaking, the high temperature causes a greater degradation, which is equivalent to a high [C=O] concentration while it will be lower for a moderate temperature. In addition, it can be seen that N_r decreases sharply with increasing [C=O], not only in the case of high temperatures (180 °C and 200 °C), but also in the case of low temperatures (160 °C and 140 °C).

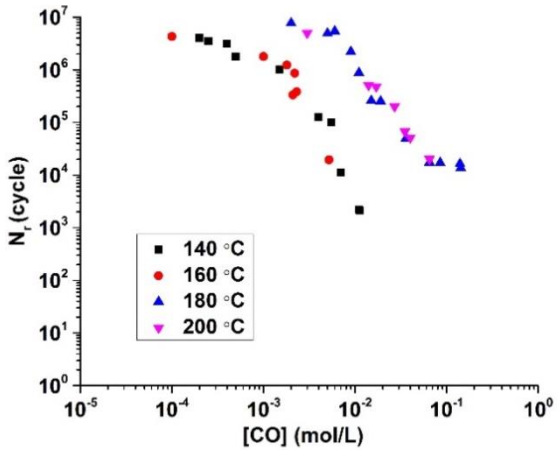

Figure 19: Relationship between N_r and [C=O] at different oxidation temperatures.

VIII. Conclusions and perspectives

In the work of this thesis, the effect of thermal aging on the fatigue behavior of the glass fiber reinforced poly (phenylene sulfide) composite (PPS/GF) has been studied.

First two types of PPS/GF samples (PPS-0°, PPS-90°) were prepared by injection molding (Article N°2). Fiber orientation in the loading direction has been found to improve monotonic strength and fatigue resistance. A complete characterization was carried out using several experimental methods. The microstructure, the physicochemical and mechanical properties have been explored, notably the fatigue behavior and the various parameters affecting the service life. It has been shown that even with high applied stress amplitude and a high frequency, the self-heating phenomenon observed in fatigue is not sufficiently pronounced to affect the fatigue life of the PPS/GF composite.

Then the study of the PPS/GF crystallization phenomenon showed that the crystallization cooling rate has a relatively large influence on this phenomenon, the crystallization temperature of the PPS decreases substantially with the increase of the cooling rate. The results show that the Jeziorny model (based on the Avrami model) can very well describe and verify the non-isothermal crystallization process of this PPS/GF material. Samples aged up to 144 h at 200 °C retain a good nucleation and crystal geometric growth capacity, whereas for the sample aged after 1080 h at 200 °C, n decreases to 0.8 due to harmful effect of thermal aging.

Thirdly, based on the study of aging at different temperatures and the follow-up of the material with the aging time by the different methods, notably FTIR and thermogravimetry, an oxidation mechanism is proposed and a kinetic model of the duration prediction of life is built and its validity is verified. This modeling has made it possible to determine the rate constants of different oxidation reactions.

Finally, the effect of thermo-oxidative aging on mechanical properties is studied by several types of mechanical stress (tension, loading-unloading and fatigue). We have shown that due to the crosslinking and the increase of the crystallinity degree during aging (at 200 °C), for a period, the resistance (tensile test) and the Young's modulus improve. Fatigue tests on PPS/GF specimens with a maximum amplitude (σ_{max} = 40 MPa) and a loading ratio (R = 0.1) have also shown that the number of cycles at fracture decreases substantially with the aging time increasing.

For the future and in perspective:

- PPS/GF is a complex system. It is necessary to study in depth the role of the matrix, the glass fibers and their interface. For this it is necessary to study in parallel the aging of pure PPS and the influence of this aging on its mechanics.
- For the problem of confidentiality, the access to certain information was limited. The nature of fiber/matrix adhesion was not known. Were the fibers sized? The answer to this question is very important for the study of the fiber/matrix interface especially when the study is interested in the mechanical properties of PPS/GF. To properly conduct this study, the choice of suitable experimental methods is crucial.
- For the same reason, it is very important to highlight directly or indirectly the effect of oxidation on the fiber/matrix interface. It should be noted that oxygen can easily penetrate this inter-facial area and react with the sizing product (if it exists) and with the matrix around the fibers.
- To be able to carry out a true oxidation/fatigue coupling study, it is necessary to carry out a detailed study to show the relation between the microstructures (physicochemical and morphological aspects) and the mechanical properties (for example fatigue behavior).

References

[1] Yao S-S, Jin F-L, Rhee KY, Hui D, Park S-J. Recent advances in carbon-fiber-reinforced thermoplastic composites: A review. Composites Part B. 2017.
[2] Karger-Kocsis J, Mahmood H, Pegoretti A. Recent advances in fiber/matrix interphase engineering for polymer composites. Prog Mater Sci. 2015;73:1-43.
[3] Gao C, Yu L, Liu H, Chen L. Development of self-reinforced polymer composites. Prog Polym Sci. 2012;37:767-80.
[4] Sandler J, Werner P, Shaffer MS, Demchuk V, Altstädt V, Windle AH. Carbon-nanofibre-reinforced poly (ether ether ketone) composites. Compos Part A Appl Sci Manuf. 2002;33:1033-9.
[5] Jones D, Leach D, Moore D. Mechanical properties of poly (ether-ether-ketone) for engineering applications. Polymer. 1985;26:1385-93.
[6] Werner P, Altstädt V, Jaskulka R, Jacobs O, Sandler JK, Shaffer MS, et al. Tribological behaviour of carbon-nanofibre-reinforced poly (ether ether ketone). Wear. 2004;257:1006-14.
[7] Rae P, Brown E, Orler E. The mechanical properties of poly (ether-ether-ketone)(PEEK) with emphasis on the large compressive strain response. Polymer. 2007;48:598-615.
[8] Bangarusampath D, Ruckdäschel H, Altstädt V, Sandler JK, Garray D, Shaffer MS. Rheology and properties of melt-processed poly (ether ether ketone)/multi-wall carbon nanotube composites. Polymer. 2009;50:5803-11.
[9] Berer M, Tscharnuter D, Pinter G. Dynamic mechanical response of polyetheretherketone (PEEK) exposed to cyclic loads in the high stress tensile regime. Int J Fatigue. 2015;80:397-405.
[10] Hou T, Chen H. Isothermal physical aging of PEEK and PPS investigated by fractional Maxwell model. Polymer. 2012;53:2509-18.
[11] Vatanpour V, Madaeni SS, Moradian R, Zinadini S, Astinchap B. Novel antibifouling nanofiltration polyethersulfone membrane fabricated from embedding TiO2 coated multiwalled carbon nanotubes. Separation and purification technology. 2012;90:69-82.
[12] Susanto H, Ulbricht M. Characteristics, performance and stability of polyethersulfone ultrafiltration membranes prepared by phase separation method using different macromolecular additives. J Membr Sci. 2009;327:125-35.
[13] Raghava R. Role of matrix-particle interface adhesion on fracture toughness of dual phase epoxy-polyethersulfone blend. J Polym Sci, Part B: Polym Phys. 1987;25:1017-31.
[14] Albouy W, Vieille B, Taleb L. Experimental and numerical investigations on the time-dependent behavior of woven-ply PPS thermoplastic laminates at temperatures higher than glass transition temperature. Compos Part A Appl Sci Manuf. 2013;49:165-78.
[15] Anagreh N, Dorn L, Bilke-Krause C. Low-pressure plasma pretreatment of polyphenylene sulfide (PPS) surfaces for adhesive bonding. Int J Adhes Adhes. 2008;28:16-22.
[16] André NM, Goushegir SM, dos Santos JF, Canto LB, Amancio-Filho ST. Friction Spot Joining of aluminum alloy 2024-T3 and carbon-fiber-reinforced poly (phenylene sulfide) laminate with additional PPS film interlayer: Microstructure, mechanical strength and failure mechanisms. Composites Part B. 2016;94:197-208.
[17] Auer C, Kalinka G, Krause T, Hinrichsen G. Crystallization Kinetics of Pure and Fiber-Reinforced Poly (Phenylene Sulfide). J Appl Polym Sci. 1994;51:407-13.
[18] Batista NL, Rezende MC, Botelho EC. Effect of crystallinity on CF/PPS performance under weather exposure: Moisture, salt fog and UV radiation. Polym Degrad Stab. 2018;153:255-61.
[19] Bhardwaj I, Kumar V, Das A. Studies of the thermal and crystallization behaviour of polyphenylene sulphide/polycarbonate blends. Thermochim Acta. 1989;144:165-72.

[20] Chen Z, Li T, Yang Y, Liu X, Lv R. Mechanical and tribological properties of PA/PPS blends. Wear. 2004;257:696-707.
[21] Hill HW, Brady D. Properties, environmental stability, and molding characteristics of polyphenylene sulfide. Polym Eng Sci. 1976;16:831-5.
[22] López LC, Wilkes GL. Non-isothermal crystallization kinetics of poly (p-phenylene sulphide). Polymer. 1989;30:882-7.
[23] Caramaro L, Chabert B, Chauchard J, Vu-Khanh T. Morphology and mechanical performance of polyphenylenesulfide carbon fiber composite. Polym Eng Sci. 1991;31:1279-85.
[24] Favaloro M. Properties and Processes of Linear Polyphenylene Sulfide (PPS) for Continuous Fiber Composites Aerospace Applications. SAE International2009.
[25] Celina M, Gillen KT, Assink RA. Accelerated aging and lifetime prediction: Review of non-Arrhenius behaviour due to two competing processes. Polym Degrad Stab. 2005;90:395-404.
[26] Damian C, Espuche E, Escoubes M. Influence of three ageing types (thermal oxidation, radiochemical and hydrolytic ageing) on the structure and gas transport properties of epoxy–amine networks. Polym Degrad Stab. 2001;72:447-58.
[27] Pei Y-m, Wang K, Zhan M-s, Xu W, Ding X-j. Thermal-oxidative aging of DGEBA/EPN/LMPA epoxy system: Chemical structure and thermal–mechanical properties. Polym Degrad Stab. 2011;96:1179-86.
[28] Kiliaris P, Papaspyrides CD, Pfaendner R. Influence of accelerated aging on clay-reinforced polyamide 6. Polym Degrad Stab. 2009;94:389-96.
[29] Rose N, Le Bras M, Bourbigot S, Delobel R. Thermal oxidative degradation of epoxy resins: evaluation of their heat resistance using invariant kinetic parameters. Polymer Degradation and Stability. 1994;45:387-97.
[30] Rivaton A, Mailhot B, Soulestin J, Varghese H, Gardette JL. Comparison of the photochemical and thermal degradation of bisphenol-A polycarbonate and trimethylcyclohexane–polycarbonate. Polymer Degradation and Stability. 2002;75:17-33.
[31] Forsström D, Terselius B. Thermo oxidative stability of polyamide 6 films I. Mechanical and chemical characterisation. Polymer Degradation and Stability. 2000;67:69-78.
[32] Buch X, Shanahan MER. Thermal and thermo-oxidative ageing of an epoxy adhesive. Polymer Degradation and Stability. 2000;68:403-11.
[33] Bellenger V, Tcharkhtchi A, Castaing P. Thermal and mechanical fatigue of a PA66/glass fibers composite material. Int J Fatigue. 2006;28:1348-52.
[34] Vieille B, Albouy W. Fatigue damage accumulation in notched woven-ply thermoplastic and thermoset laminates at high-temperature: Influence of matrix ductility and fatigue life prediction. Int J Fatigue. 2015;80:1-9.
[35] Tanaka K, Oharada K, Yamada D, Shimizu K. Fatigue crack propagation in short-carbon-fiber reinforced plastics evaluated based on anisotropic fracture mechanics. Int J Fatigue. 2016.
[36] Růžek R, Kadlec M, Petrusová L. Effect of fatigue loading rate on lifespan and temperature of tailored blank C/PPS thermoplastic composite. Int J Fatigue. 2018;113:253-63.
[37] Chambers A, Earl J, Squires C, Suhot M. The effect of voids on the flexural fatigue performance of unidirectional carbon fibre composites developed for wind turbine applications. Int J Fatigue. 2006;28:1389-98.
[38] Albouy W, Vieille B, Taleb L. Influence of matrix ductility on the high-temperature fatigue behavior of off-axis woven-ply thermoplastic and thermoset laminates. Int J Fatigue. 2014;63:85-96.
[39] Skelton RP. Hysteresis, yield, and energy dissipation during thermo-mechanical fatigue of a ferritic steel. Int J Fatigue. 2004;26:253-64.

[40] Gosar A, Nagode M. Energy dissipation under thermomechanical fatigue loading. Int J Fatigue. 2012;43:160-7.
[41] Lisa G, Hamciuc C, Hamciuc E, Tudorachi N. Thermal and thermo-oxidative stability and probable degradation mechanism of some polyetherimides. J Anal Appl Pyrolysis. 2016;118:144-54.
[42] Jing C, Lei Y, Jieping Z, Sidong L, Yongjun C, Kui X. Drying kinetics and cross-linking of sulfur prevulcanized thick natural rubber latex film. Rubber Chem Technol. 2013;86:57-67.
[43] Matyshak V, Krylov O. Problems of quantitative spectroscopic measurements in heterogeneous catalysis: molar absorption coefficients of vibrations in adsorbed substances. Kinet Catal. 2002;43:391-407.
[44] SEPPÄLÄ J, HEINO M, KAPANEN C. Injection-moulded blends of a thermotropic liquid crystalline polymer with polyethylene terephthalate, polypropylene, and polyphenylene sulfide. J Appl Polym Sci. 1992;44:1051-60.
[45] Ye L, Scheuring T, Friedrich K. Matrix morphology and fibre pull-out strength of T700/PPS and T700/PET thermoplastic composites. J Mater Sci. 1995;30:4761-9.
[46] Jeziorny A. Parameters characterizing the kinetics of the non-isothermal crystallization of poly (ethylene terephthalate) determined by DSC. Polymer. 1978;19:1142-4.
[47] Weng W, Chen G, Wu D. Crystallization kinetics and melting behaviors of nylon 6/foliated graphite nanocomposites. Polymer. 2003;44:8119-32.
[48] Zhang Y, Jiang X, Guan Y, Zheng A. Crystallization kinetics of ATPU grafted polypropylene. Mater Lett. 2005;59:3626-34.
[49] Botines E, Puiggalí J. Crystallization kinetics of poly (glycolic acid-alt-6-aminohexanoic acid). Eur Polym J. 2006;42:1595-608.
[50] Kuo M, Huang J, Chen M. Non-isothermal crystallization kinetic behavior of alumina nanoparticle filled poly (ether ether ketone). Mater Chem Phys. 2006;99:258-68.
[51] Kissinger HE. Reaction kinetics in differential thermal analysis. Anal Chem. 1957;29:1702-6.
[52] Tobolsky AV, Metz DJ, Mesrobian RB. Low Temperature Autoxidation of Hydrocarbons: the Phenomenon of Maximum Rates1, 2. J Am Chem Soc. 1950;72:1942-52.
[53] Audouin L, Gueguen V, Tcharkhtchi A, Verdu J. “Close loop” mechanistic schemes for hydrocarbon polymer oxidation. J Polym Sci, Part A: Polym Chem. 1995;33:921-7.
[54] Richaud E, Farcas F, Fayolle B, Audouin L, Verdu J. Hydroperoxide build-up in the thermal oxidation of polypropylene–a kinetic study. Polym Degrad Stab. 2007;92:118-24.
[55] Rychly J, Matisova-Rychla L, Csmorova K, Achimsky L, Audouin L, Tcharkhtchi A, et al. Kinetics of mass changes in oxidation of polypropylene. Polym Degrad Stab. 1997;58:269-74.
[56] Tcharkhtchi A, Farzaneh S, Abdallah-Elhirtsi S, Esmaeillou B, Nony F, Baron A. Thermal aging effect on mechanical properties of polyurethane. Int J Polym Anal Charact. 2014;19:571-84.
[57] Yamashita T, Tomitaka H, Kudo T, Horie K, Mita I. Degradation of sulfur-containing aromatic polymers: Photodegradation of polyethersulfone and polysulfone. Polym Degrad Stab. 1993;39:47-54.
[58] Landel RF, Nielsen LE. Mechanical properties of polymers and composites: CRC Press; 1993.
[59] Kim K, Lee C, Kim P, Ryu B. Dielectric properties on the radiation and thermal aged PEEK. Solid Dielectrics, 2004 ICSD 2004 Proceedings of the 2004 IEEE International Conference on: IEEE; 2004. p. 332-5.

[60] Kang PH, Lee C, Kim KY. Radiation and thermal effects on the dielectric relaxation properties of PEEK. Journal of industrial and engineering chemistry-seoul-. 2007;13:250.
[61] George K, Komalan C, Kumar P, Varughese K, Thomas S. Dynamic mechanical analysis of binary and ternary polymer blends based on nylon copolymer/EPDM rubber and EPM grafted maleic anhydride compatibilizer. 2007.
[62] Ibarra L, Macias A, Palma E. Viscoelastic properties of short carbon fiber thermoplastic (SBS) elastomer composites. J Appl Polym Sci. 1995;57:831-42.
[63] Ernault E, Richaud E, Fayolle B. Thermal-oxidation of epoxy/amine followed by glass transition temperature changes. Polym Degrad Stab. 2017;138:82-90.
[64] Zuo P, Benevides RC, Laribi MA, Fitoussi J, Shirinbayan M, Bakir F, et al. Multi-scale analysis of the effect of loading conditions on monotonic and fatigue behavior of a glass fiber reinforced polyphenylene sulfide (PPS) composite. Composites Part B. 2018;145:173-81.
[65] Fatemi A, Socie DF. A critical plane approach to multiaxial fatigue damage including out-of-phase loading. Fatigue Fract Eng Mater Struct. 1988;11:149-65.

Article N°1:

P. Zuo, A. Tcharkhtchi, M. Shirinbayan, J. Fitoussi, F. Bakir, "Overall investigation of PolyPhenylene Sulfide (PPS) from synthesis and process to applications – A review". Macromolecular Materials & Engineering. **Accepted.**

Overall investigation of Poly (Phenylene Sulfide) (PPS) from synthesis and process to applications – A review

Peiyuan Zuo[1]*, Abbas Tcharkhtchi[1], Mohammadi Shirinbayan[1], Joseph Fitoussi[1]

[1] Arts et Métiers ParisTech, PIMM – UMR CNRS 8006, 151 Boulevard de l'Hôpital, 75013 Paris, France

E-mails: abbas.tcharkhtchi@ensam.eu, joseph.fitoussi@ensam.eu, mohammadali.shirinbayan@ensam.eu;

*Corresponding author: Peiyuan ZUO, 2015-1027@ensam.eu;

Farid Bakir[2]

[2] Arts et Métiers ParisTech, Dynfluid, 151 Boulevard de l'Hôpital, 75013 Paris, France

E-mails: farid.bakir@ ensam.eu

Keywords: Polyphenylene sulfide materials; synthesis; process; applications.

Abstract

Poly (phenylene sulfide) (PPS) is one kind of high-performance polymer with high thermal stability that can be used widely in different industrial domains. However, according to an investigation of the literature, few reviews have comprehensively focused on the continuous development of PPS applications in the past decade. To meet this demand, this paper provides an overall investigation of PPS polymer and PPS-based composites from synthesis and process to applications. Briefly, this paper introduces PPS materials according to the following topics. First, the molecular weight distribution and morphology of PPS, as well as their reinforced parts, are introduced. Afterwards, the topic is focused on the synthesis, process and blending of PPS. In the next part, this paper investigates the key points regarding PPS as a high-performance polymer, focusing on the aspect of thermal behavior and mechanical properties. Finally, PPS composite applications are emphasized and overviewed from a wide range of aspects.

1 Introduction

Generally, polymers can be divided into three categories: thermoplastics, elastomers and thermosets according to their chemical structure and physical behaviors. The thermoplastics, with linear or branched macromolecules, can be re-melted back into a liquid, whereas elastomers and thermoset always remain in a permanent solid-state due to the molecular structure of their crosslinked network. Moreover, thermosets have a structure with very high crosslinking densities, and their molecular networks will only break at high temperatures[1]. As a matter of fact, many researchers pay much more attention to thermoplastic polymers, especially high-performance polymers with excellent thermal and mechanical properties. Figure 1 shows the schematic pyramid distribution of low- to high-performance amorphous and semicrystalline polymers corresponding to their cost. This pyramid provides the information of common thermoplastic materials consisting of 3 categories (common, mid-range and high-performance polymers) according to thermal and chemical as well as mechanical properties. Additionally, Table 1 exhibits some parameters of certain high-performance polymers with high resistant-temperatures.

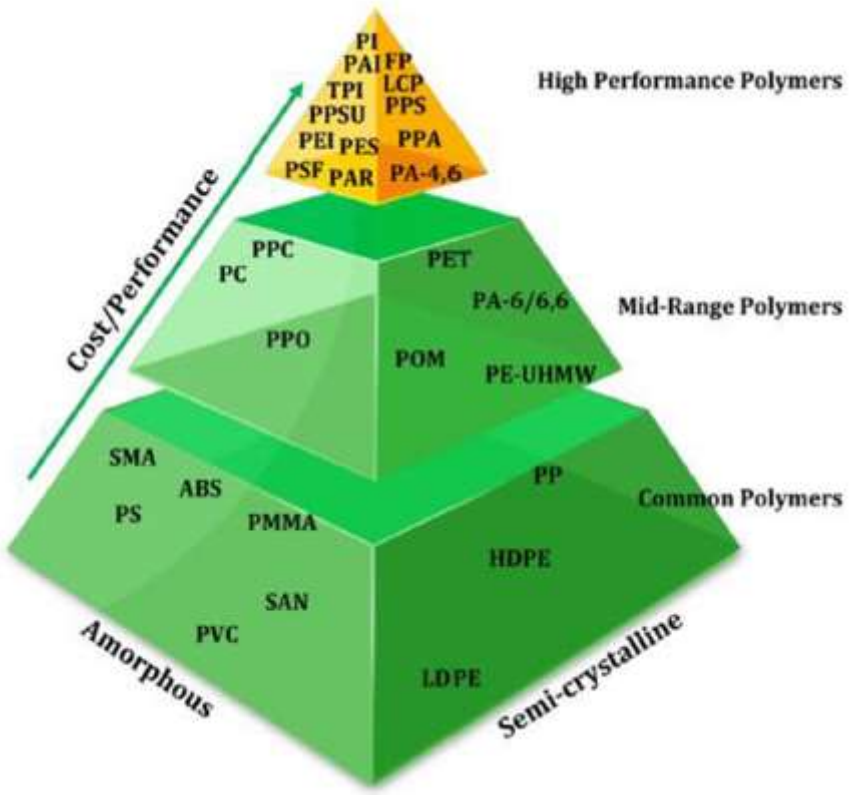

Figure 1: The pyramid graphic of common thermoplastic materials. Note: polyamide (PA), polyamide Imide (PAI), thermoplastic polyimide (TPI), polyphenylene sulfone (PPSU), polyether-imide (PEI), polyethersulfone (PES), polysulfone (PSF), polyaromatic (PAR), fluoropolymers (FP), liquid crystal polymers (LCP), polyphenylene sulfide (PPS), polyphthalamide (PPA), polyamide-4.6 (PA-4.6), polyphthalate carbonate (PPC), polycarbonate (PC), polyphenylene oxide (PPO), polyethylene terephthalate (PET), polyamide-6/6.6 (PA-6/6.6), polyoxymethylene (POM), ultrahigh molecular weight polyethylene (PE-UHMW), styrene maleic anhydride (SMA), acrylonitrile butadiene styrene (ABS), polystyrene (PS), polymethyl methacrylate (PMMA), styrene acrylonitrile (SAN), polyvinyl chloride (PVC), polypropylene (PP), high density polyethylene (HDPE), low density polyethylene (LDPE). [244] Copyright 2018, Elsevier Sci. Ltd.

Table 1: Some high temperature resistant thermoplastic polymers [244]

Abbreviation	Polymer	T_g (℃)	Continuous temperature of usage (℃)	Heat deflection temperature (℃)
PAI	Polyamide-Imide	275	250	279
PI	Polyimide	250	288	246
PES	Polyethersulfone	224	177-204	204-238
PEI	Polyetherimide	213	177-204	199-216
PSF	Polysulfone	190	149-171	171-182
PEEK	Polyetheretherketone	143	204-232	177-321
PPA	Polyphthalamide	134	204-232	277-285
PPS	Polyphenylene Sulfide	92	204-232	149-288

It is widely acknowledged that among a wide range of high-performance polymers, those containing aromatic units, such as poly (ether ether ketone) (PEEK), poly (ether sulfone) (PES) and poly (phenylene sulfide) (PPS), have attracted much attention in the past several decades. In particular, PPS, as one of these polymers, is widely used as a high strength/high temperature engineering thermoplastic for applications such as molding resins, organic fibers, and matrices for thermoplastic composites. Additionally, PPS is commonly and widely used as an engineering polymer with a unique combination of excellent environmental and mechanical as well as thermal properties. In addition, it is applied in a wide range including electronics and electrical appliances, automobiles, precision instruments, chemical sectors and aerospace fields [2-15]. More intensively, glass fiber or carbon fiber reinforced PPS composites are also popularly used in the automobile, aerospace and other widespread industrial sectors [16][17][18][19][20][21][22-27][28-35]. In particular, PPS and their reinforced parts are capable of enduring high temperatures and resisting well under mechanical loading in some special environmental conditions.

PPS, a semicrystalline polymer with repeated thiophenyl units, has high thermal oxidation and chemical resistance. It has advantages of good toughness, low density, high abrasion resistance and high chemical as well as thermal stability comparable to other high-performance engineering resins, such as polyimide, polyarylester and polyetheretherketone [36-38]. Furthermore, PPS, as a high-performance polymer, has better comprehensive mechanical properties than common or middle range polymers such as polypropylene, polyamide, and UHMWPE according to the cost/performance characteristics [39-41].

Comparatively, PEEK is also one of the most promising alternative materials, but it still has some drawbacks such as weak adhesive properties [42]. Moreover, PEEK has a

relatively high price when compared with most other polymers and it is insoluble in industrial solvents [43-45]. It also has some disadvantages such as difficulties regarding synthesis and complex processing conditions [46-49].

Furthermore, considering an epoxy thermoset, it can be widely used as coating, adhesives as well as electric encapsulates, etc. However, epoxy materials have obvious disadvantages such as brittleness due to an intrinsically high degree of crosslinking [50]. Additionally, it has some shortcomings, such as the inherently low fracture toughness and poor resistance to fracture as well as relatively low mechanical properties [51, 52].

Moreover, polyimide (PI) is widely used in microelectronics and aerospace fields due to its comprehensively excellent properties [53, 54]. However, PI polymer materials still encounter problems such as difficult processing and high cost.

In addition, UHMWPE is a good choice in applications that require wear resistance and low friction as well as toughness. However, as we know, it is very difficult to directly process UHMWPE due to its very high viscosity [55, 56].

In addition to these resins, there are also thermosetting bismaleimide (BMI) resins, which can be applied for advanced polymer composites [57, 58]. However, BMI resin also suffers from inherent brittleness because of its highly crosslinked structures, and some microcracks are easily generated and propagated under friction stress. This is an obvious drawback which needs to be overcome when these resins used [59].

PF (phenol-formaldehyde) resins and their reinforced materials can also resist harsh thermal conditions, they can be used as carbon-mineral materials by blending with other

substances and they also have other applications [60-62]; however, researchers should also consider their adhesive and toughness properties during applications.

Additionally, the study of Cyanate resin (CE) should be focused on improvement of its fracture toughness and the applied temperatures as well as its comprehensive properties, especially in terms of mechanics [63-65].

All of the polymers are widely used in various industrial sectors. However, it should be mentioned that, considering the performance and cost of these mentioned materials, it seems very necessary to develop the PPS materials in different ways because PPS materials have excellent comprehensive properties and their price is appropriate when their performance is taken into account.

2 PPS materials

2.1 Overview of PPS

Poly-Phenylene Sulfide (PPS) is a polymer consisting of aromatic rings linked with sulfides, and its chemical formula is shown in Figure 2. Additionally, FTIR results of PPS in Figure 3 give detailed information concerning the chemical bonds of the PPS polymer chain.

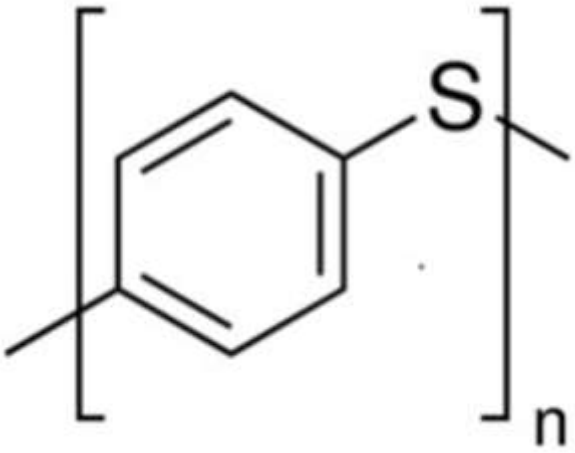

Figure 2: Chemical structure of PPS.

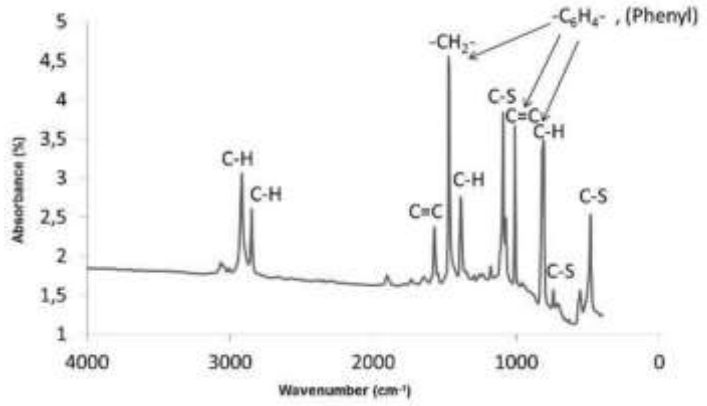

Figure 3: FTIR spectrum results from transmission mode of PPS.

According to previous reports, PPS was obtained by the polycondensation polymerization method. Macallum synthesized phenylene sulfide polymers from the melt reaction of p-dichlorobenzene with alkali and alkaline earth metal sulfides catalyzed by sulfur[66]. The reaction occurred at approximately 300 ℃ under a certain pressure together

with the solid-liquid phases. Furthermore, the main work was based on the condensation of p-dichlorobenzene with sodium carbonate and sulfur. It is shown in Figure 4.

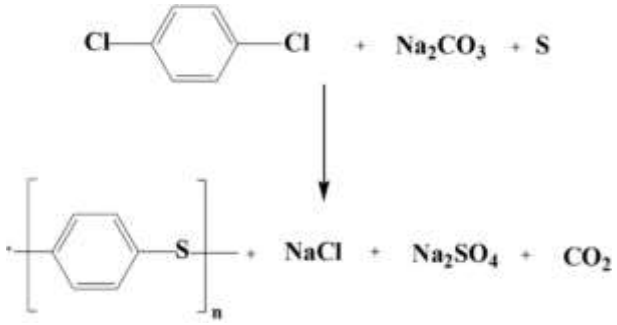

Figure 4: Synthesis of PPS. [66] Copyright 1948, American Chemical Society.

The detailed mechanism of the Macallum polymerization reaction was proposed by Lenz and other coworkers [67-69]. They proposed several steps concerning this mechanism as follows:

The reaction can be resumed as the following equations:

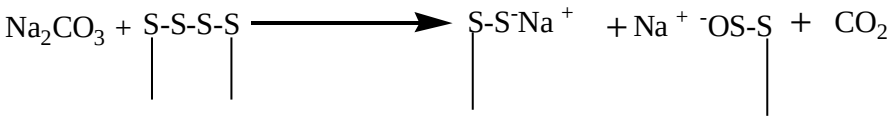

Equation (1)

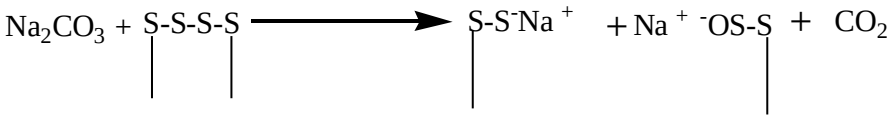

Equation (2)

Equation (3)

As a conclusion, the following comments are outlined:

- The reaction would start by the formation of polysulfide through a series of nucleophilic substitution types of oxidation-reduction reactions between Na_2CO_3 and sulfur.
- Initiation of the polymerization would occur through radical attack by sulfur on the aromatic ring to form a polysulfide side chain.
- Propagation of the reaction would result from successive nucleophilic substitutions by sulfide and thiophenoxide anions on the haloaryl sulfides.

Moreover, the commercial grades of PPS were first introduced by Phillips Petroleum Company in the 1960s under the trade name "Ryton". In detail, they produced two types: one kind is called a thermoplastic branched polymer with a very high viscosity, which was processed by PTFE-type processes, while the other one is an initial linear polymer, which could be processed by compressing molding that is laminated with glass fiber[70].

2.2 Molecular weight of thermoplastic PPS

There are two types of PPS: thermoplastic branched PPS with high viscosity and linear PPS polymer. Due to the high melting point (T_m=285 ℃) and high dissolution temperature (>200 ℃) of PPS in 1-chloronaphthalene (solvent), it is difficult to characterize the molecular distribution and rheological properties in the molten state. However, it tends to be facilitated with the development of high temperature gel

permeation chromatography technology. Stacy et al. [71] measured the molecular weight distribution of PPS by high-temperature gel permeation chromatography (GPC). In their research, they used the Mark-Houwink-Sakurada (MHS) equation (see Equation (4)) to explain the relation of [η] (intrinsic viscosity) and M (molecular weight) and gave the values of the constants K (8.91x10^5) and a (0.747) for PPS.

$$[\eta] = KM^{a} \qquad \text{Equation (4)}$$

From other research reports, they listed the weight average molecular weight ($\bar{M}_w$) and the number-average ($\bar{M}_n$) of PPS from different commercial suppliers (see Table 2)[72].

Table 2: Molecular weight parameters of PPS samples [72]

Sample	Supplier	$\bar{M}_w$ $*10^{3\,b}$ g/mol	$\bar{M}_n$ $*10^{3\,b}$ g/mol	$\bar{M}_w/\bar{M}_n^a$	$\bar{M}_w$ $*10^{3\,c}$ g/mol	$\bar{M}_n$ $*10^{3\,c}$ g/mol	$\bar{M}_w/\bar{M}_n^c$
A	Phillips	18.1	2.8	6.4	22.0	15.8	1.39
B	Kureha	35.7	2.2	16.2	39.8	20.6	1.94
C	Kureha	46.7	2.5	18.5	50.7	26.6	1.91

a: Determined in 1-chloronaphthalene at 210 ℃; b: Obtained by the modified UV/Vis absorption detector method; c: Obtained by the Stacy viscometric detector method.

In addition, the report in [73] provided an interesting solution to determine the molecular weight distribution of PPS by the following equations:

$$a_T = \frac{\eta_0}{\eta_{inf}}\left(\frac{T_0}{T}\right)\left(\frac{L_0}{L}\right) \quad \text{Equation (5)}$$

$$\eta_0 = 2.06\bar{M}_w^{4.68} \times 10^{-20} \quad \text{Equation (6)}$$

where η_0 is the zero-shear viscosity at T (temperature), η_{inf} is the zero-shear viscosity at the reference temperature (315 ℃, the processing temperature of PPS),L is the density, a_T is the shifted factor, T_0 is the reference temperature (315 ℃) and L_0 is the density at the reference temperature (315 ℃). The molecular distribution for thermal-aged PPS is shown in Figure 5. From this Figure, one can note the evolution of the molecular weight distribution of thermal-aged PPS with the time of aging increasing after 30 minutes and 60 minutes of heating temperature at 315 ℃.

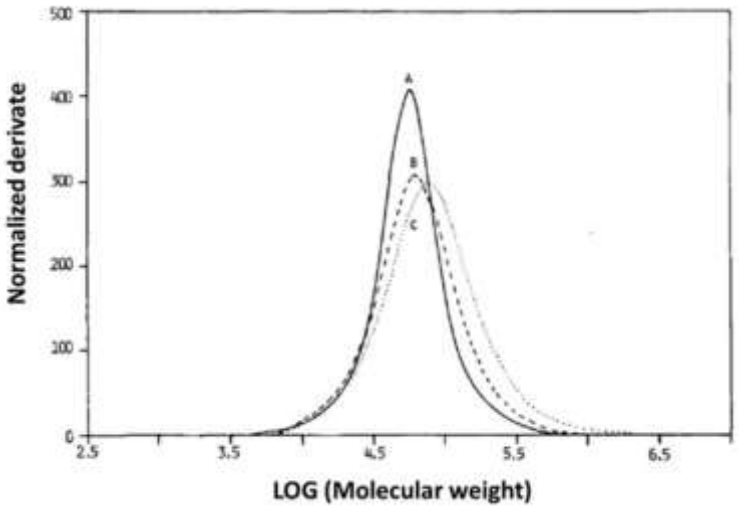

Figure 5: Differential molecular weight distribution curves obtained from dynamic melt viscosity using exact for PPS resin: (A,─) virgin; (B, --) preheated in air for 30 min; (C, ⋯) preheated in air for 60 min. [73] Copyright 1990, Wiley-VCH.

2.3 Morphology of PPS

PPS is a semicrystalline thermoplastic polymer and similar to all semicrystalline polymers, its morphology consists of amorphous and crystalline phases [74]. In this section, we discuss the morphology of PPS from the following 7 parts: 1) formation of the crystalline phase and spherulites, 2) kinetics of crystallization and kinetic models, 3) effect of the nucleating agent and thermal history (e.g., curing or annealing), 4) effect of fibers in the case of composites, 5) trans-crystallization and 6) the relation between the crystalline phase and mechanical properties as well as 7) thermal treatment effect on crystallization.

2.3.1 Formation of crystalline phase and spherulites

For the study in this section, the cooling process can be divided into two types: isothermal crystallization and nonisothermal crystallization.

From the aspect of isothermal crystallization, Figure 6 represents the formation of the spherulites under an optical microscope equipped with a heating device. The photo presented in this figure was taken in the stage of the isothermal growth of spherulites with spherical morphology at 221 ℃; one can note the typical homogeneous spherulites with a diameter of approximately 2 μm at 221 ℃ [75].

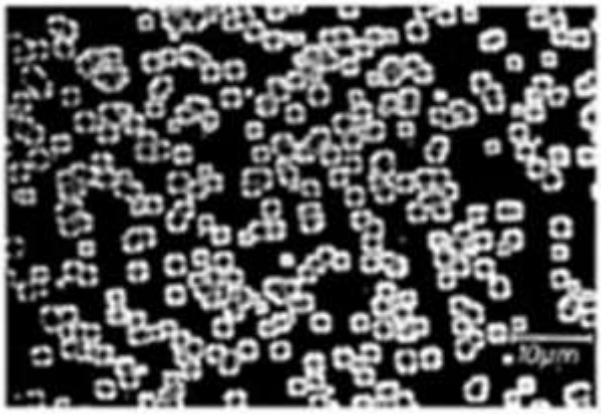

Figure 6: Optical microscopy photo of pure PPS at T_c=221 ℃. [75] Copyright 1994, Wiley-VCH.

Furthermore, DSC and PLM (polarized light microscopy) techniques are popularly used to characterize the isothermal crystallization process, not only in the domains of metals but also in polymers and composites domains. Liliana et al. [76] studied the isothermal crystallization behavior of PPS by DSC and PLM techniques. The highest crystallization rate was obtained with isothermal treatment at 268 ℃.

From the aspect of nonisothermal crystallization, Lian et al. [77] studied the morphology of the nonisothermal crystallization process for pure PPS which has been shown by the polarized optical microscopy (POM) photos. These photos show (see Figure 7) that the pure PPS presented well developed spherulites with distinct boundaries. In this work, the authors also studied the effect of the cooling rate on crystallization phenomena. They have performed three different tests at different cooling rates (5, 20 and 30 ℃/min). One can see different crystallization stages and nucleation as well as growth at different rates of cooling. When the cooling rate was low (5 ℃/min), the beginning and final stages of crystallization can be observed at the high temperature range (225 ℃ – 195 ℃), but at

the high cooling rate (30 ℃/min), crystallization would be seen at the lower temperature range (195 ℃ – 140 ℃) under microscopy. In addition, the final spherulites were larger when the cooling rate was lower.

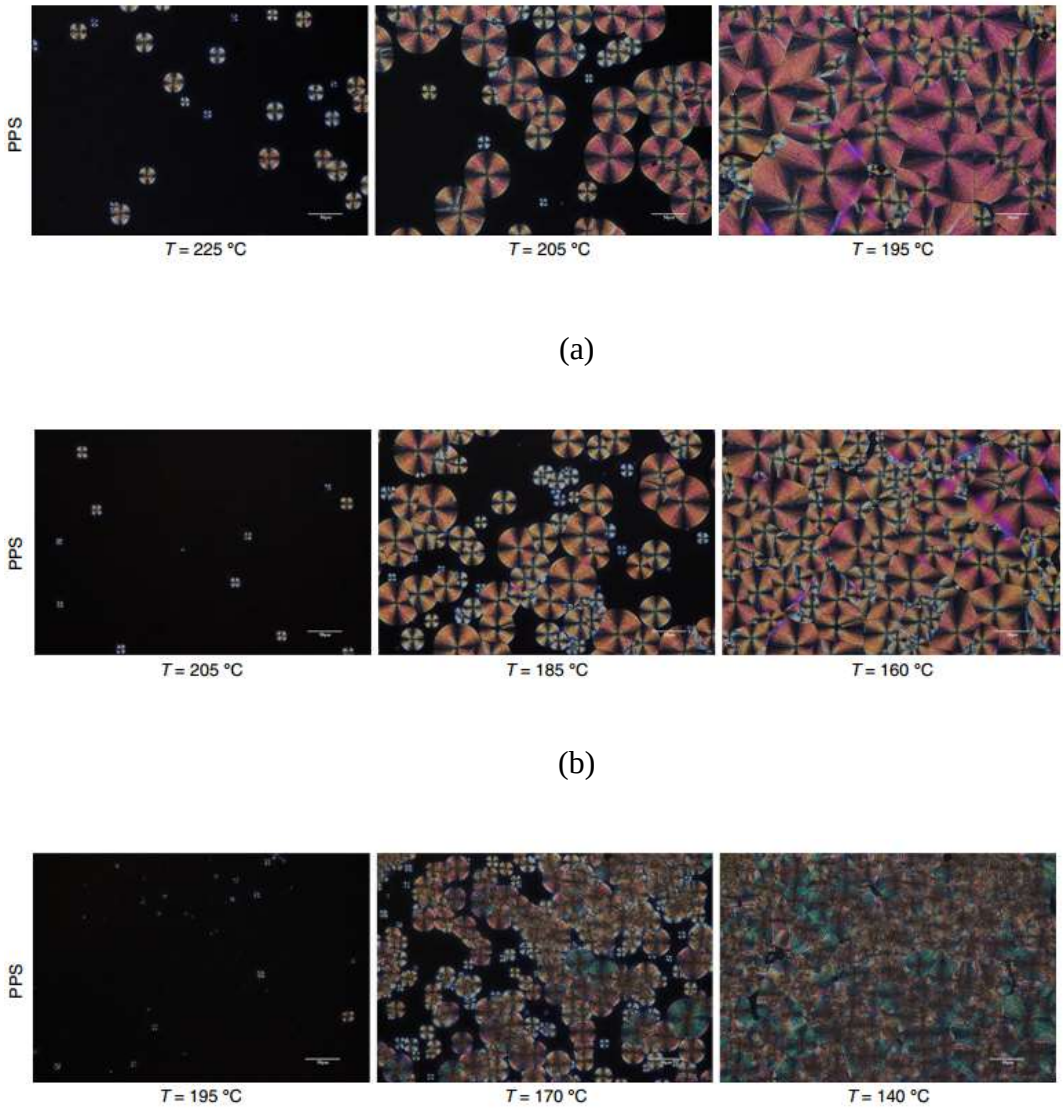

Figure 7: POM images of virgin PPS during nonisothermal crystallization process at (a) 5 ℃/min; (b) 20 ℃/min; (c) 30 ℃/min. [77] Copyright 2017, Springer.

2.3.2 Kinetics of crystallization and kinetic models

Some researchers in ref [78] compared the crystallization kinetics of virgin and solvent treated PPS. The overall crystallization rates were found to be much faster for the solvent-treated PPS than for the virgin neat PPS. Some other investigators compared different polymers: For example, Song et al. [79] studied the crystallization kinetics and nucleating agents for enhancing the crystallization of PPS. The comparison of PPS crystallization rates with those of other polymers indicates that it crystallizes much more slowly than polyethylene or isotactic polypropylene.

Moreover, some kinetic models (e.g., Avrami model) were applied to investigate the crystallization kinetics of PPS. The Avrami model can be used as follows:

$$X_t = X_{vcr} = 1 - \exp(-kt^n) \qquad \text{Equation (7)}$$

$$Log[-Log(1 - X_{vcr})] = Log\ k + n\ Log\ t \qquad \text{Equation (8)}$$

where $X_t = X_{vcr} = {X_{vc}}/{X_{vcmax}}$ at time t is the relative volume fraction of crystallinity, X_{vc} is the volume fraction of crystallinity, n is the Avrami exponent and k is a temperature-dependent rate constant.

As seen in Figure 8, a good linear regression implies the Avrami model can be well applied to perform modeling concerning the isothermal crystallization for PPS materials with reinforcement.

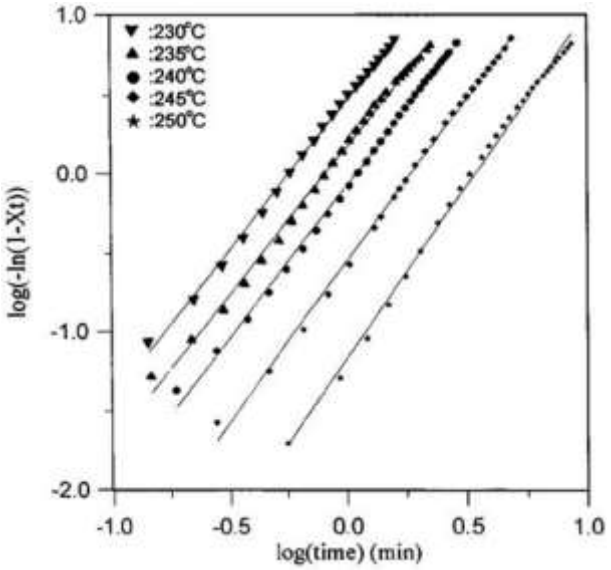

Figure 8: Avrami plots of carbon (10%)-filled PPS samples crystallized at 230, 235, 240, 245 and 250 ℃. [245] Copyright 1995, Wiley-VCH.

2.3.3 Effect of the nucleating agent and thermal history (e.g., curing or annealing)

-Nucleating agent

In practice, the nucleation may begin on the surface with the nucleation sites such as fillers or additives (e.g., fibers, nanotubes). For example, Jiang et al. [80] prepared a series of composites by mixing PPS with multiwalled carbon nanotubes at 1, 2 and 3 wt % to investigate the nucleation effect of hydroxyl-purified multiwalled carbon nanotubes in PPS composites. They revealed that the enthalpy ΔH_c of the composites increased with increasing the amounts of multiwalled carbon nanotubes, whereas the crystallization temperature decreased dramatically in parallel.

Moreover, with the addition of carbon nanofiber in PPS, there was a slight decrease in the crystallization temperature but no significant change in the melting point or the glass transition temperature [81]. From the results of Figure 9 and Table 3, one can conclude that the higher the proportion of CNF, the lower was the crystallinity. This is mainly due to the propensity of CNF in hindering the orderly arrangement of PPS molecules.

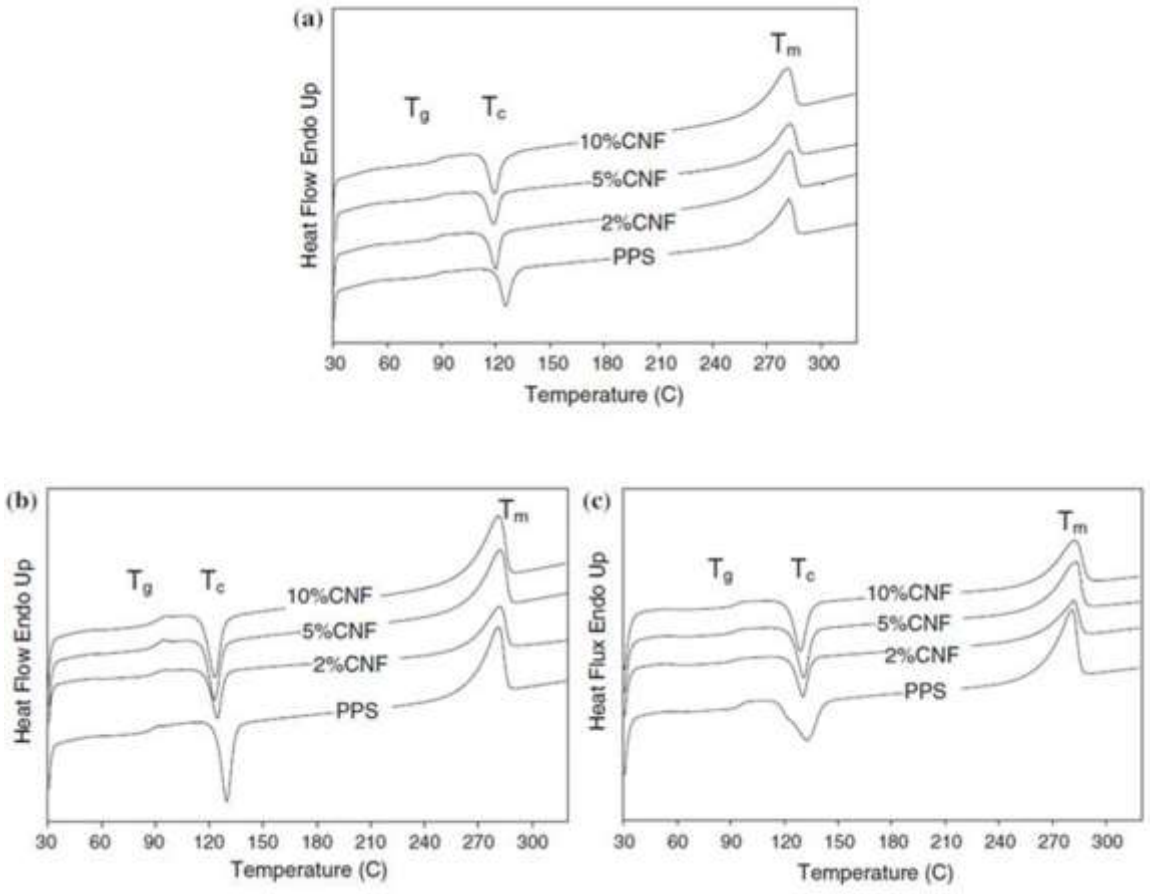

Figure 9: Differential Scanning Calorimetry (DSC) analysis of PPS-CNF composites as a function of heating rate: (a) 5 ℃/ min, (b) 10 ℃/min, and (c) 20 ℃/min. CNF proportions corresponding to volume. [81] Copyright 2017, Springer.

Table 3: Effect of CNF on the thermal properties from DSC analysis [81]

Sample	Heating rate (℃/min)	T_g (℃)	T_c (℃)	T_m (℃)	ΔH_c (J/g)	ΔH_m (J/g)	X_c (%)
PPS	5	83.9	125.1	281.9	39.5	59.2	16.3
PPS-2% CNF		83.5	119.9	282.3	16.9	34.1	14.6
PPS-5% CNF		84.5	118.3	282.1	18.6	34.0	13.6
PPS-10% CNF		84.7	120.3	281.9	17.0	29.6	11.9
PPS	10	84.8	129.5	281.0	38.8	60.0	16.7
PPS-2% CNF		85.4	124.2	281.5	23.8	42.0	15.4
PPS-5% CNF		86.5	123.0	281.8	20.2	35.0	13.1
PPS-10% CNF		85.9	123.8	281.5	16.5	30.0	12.7
PPS	20	86.6	132.6	281.0	29.3	45.6	13.5
PPS-2% CNF		86.4	130.6	281.8	27.8	41.9	12.0
PPS-5% CNF		86.2	130.9	282.5	19.6	33.4	12.2
PPS-10% CNF		87.1	129.0	282.2	17.0	27.1	9.6

Other additives can also be regarded as a nucleating agent for PPS. For example, Ref [82] reported nanodiamond (ND) as an efficient nucleating agent for PPS, and they clarified that the Avrami equation and Mo method provided a fairly satisfactory description for the nonisothermal crystallization of PPS in both pure and composite forms. Nanodiamond particles can supply a heterogeneous nucleation point for PPS by dramatically improving the crystallization temperature and crystallization rate. In particular, it can be seen the ND particles morphology is spherical or nearly spherical in Figure 10. Moreover, the micrographs show that many particles are aggregated together due to the high instability resulting from the high surface energy and the large surface area of the particle quantity. Comparatively, the morphology of the composite surface tends to be meticulous and smooth after mixing with ND particles.

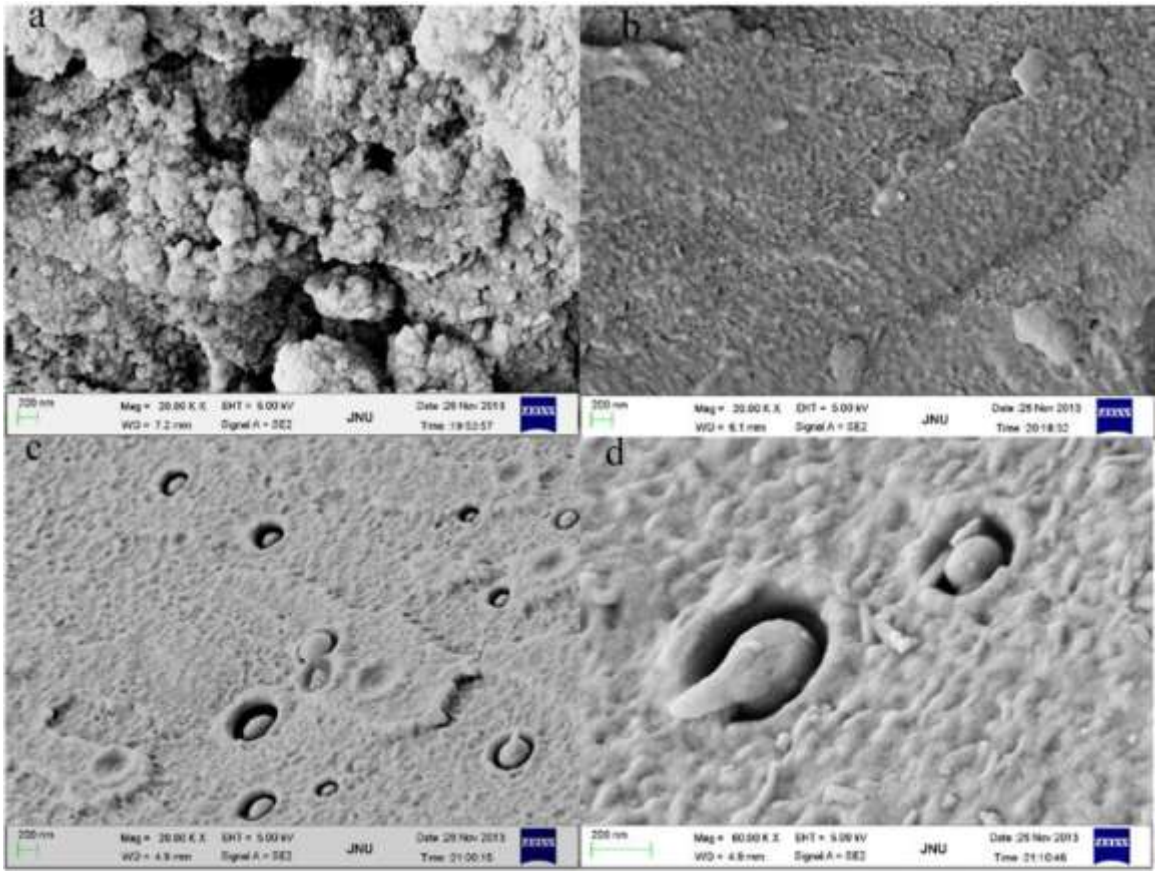

Figure 10: SEM images of: (a) nanodiamond; (b) PPS; and (c and d) PPS/ND. [82]

-Thermal history

Thermal history (e.g., curing or annealing) plays an important role during the crystallization process because the thermal history can not only affect the crystallization behavior but can also change the crystal structure. Some commercial PPS treated by thermal curing was studied by Lee et al.[83], and they found an increase of molecular weight due to crosslinking. The reasons can be explained as follows: PPS is a thermoplastic polymer with generally low molecular weight. Some phenomena such as oxidation (or thermal treatment) may create a crosslinked junction between molecular chains; however, the density of crosslinking is not high and the structure is not truly a 3D network. It is

indeed the branched macromolecules with a higher molecular weight. They concluded the crosslinking of PPS can significantly affect crystallization behaviors. Lu et al.[84] studied the effects of annealing on the relaxation behavior and charge trapping in film-processed PPS. DSC results suggested that annealing increased the crystallinity of PPS film. Brady et al.[85] examined the crystallinity of PPS, and they concluded that curing (crosslinking and chain extending) the resin by heating in air affected the crystallization ability of the resin. As previously mentioned, because of the thermal treatment, the formation of some crosslinking points in the structure of PPS occurs. The chains around these crosslinking points are less mobile. They may act as nucleating agents which increase the degree of crystallinity. However, high crosslinking density hinders the crystallization. Moreover, the observation of crystalline morphologies by optical microscopy suggests that thermal curing for as little as 1 day contributes to the formation of smaller size crystallinity of spherulites in regard to nontreated pure PPS.

Moreover, Ref [86] studied the effect of thermal history on the crystal structure of PPS. The results showed the dimensions of the crystal lattice were strongly dependent on previous thermal conditions. With the annealing time improving at the fixed temperature, the decrease of lattice a, b led to an increase in lattice density. In this study, the plots of unit cell parameters and the lattice density versus the cold-crystallization temperature are shown in Figure 11. The unit cell parameters a and b first showed a decrease with the cold-crystallization temperature increasing, but when the crystallization temperature increased above 245 ℃, the unit cell parameters a and b varied. The unit cell parameter c first increased until reaching the cold-crystallization temperature of 245 ℃, and then fluctuated. However, the density of PPS crystal increased with crystallization temperature up to 255

℃ and decreased when the temperature was 265 ℃. This implies that thermal history can significantly affect the crystal structure.

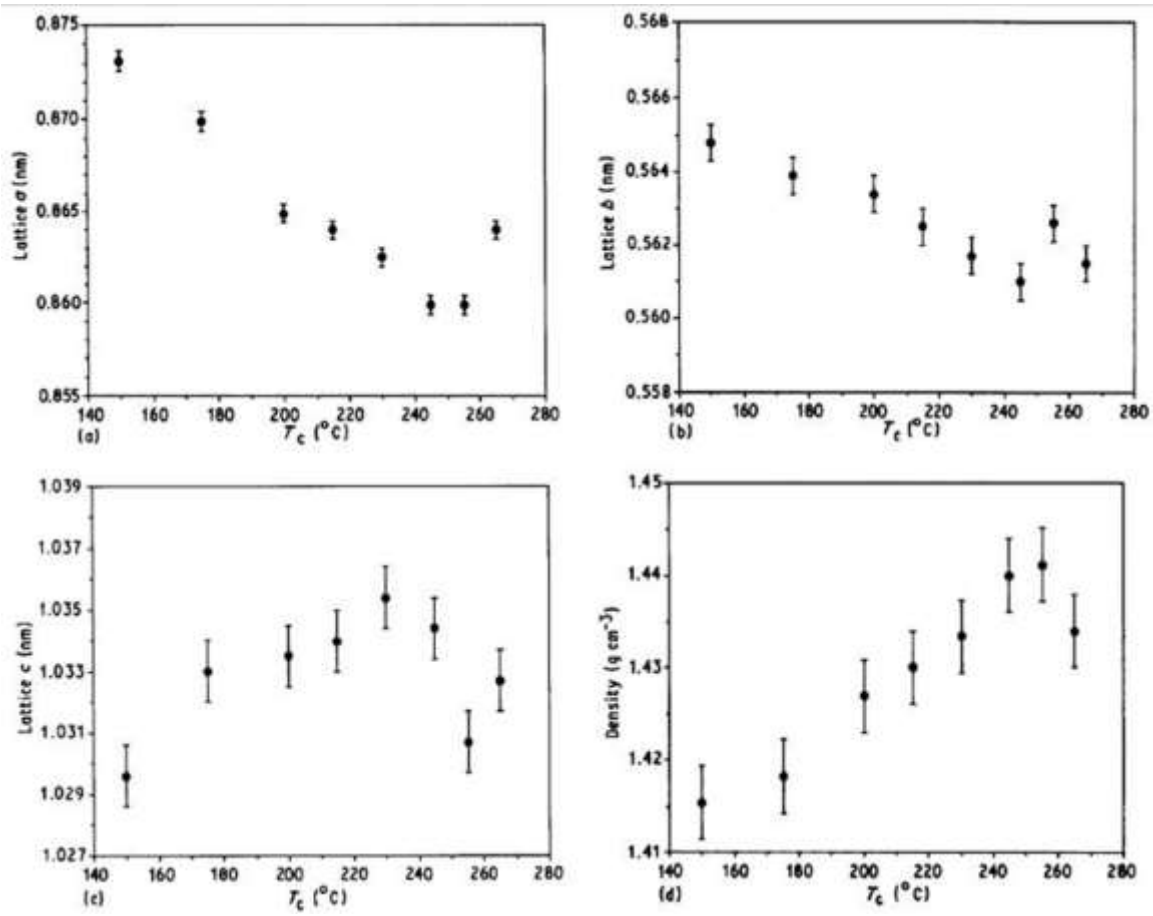

Figure 11: Lattice parameters versus cold-crystallization temperature: (a) unit cell parameter; (b) unit cell parameter; (c) unit cell parameter; (d) lattice density. [86]

2.3.4 Effect of fibers in the case of composites

Generally, the thermal history can modify the extent and nature of crystallization for any thermoplastic polymers. However, in the case of composites that are reinforced

with fibers, the morphology can also be affected by the fibers. For example, the report of [87] studied the isothermal crystallization from the melt of unreinforced PPS and of model carbon and aramid as well as glass fiber reinforced PPS composites. The result indicated that the influence of fibers on PPS crystallization was decided not only by surface treatment but also by fibers themselves. Additionally, as we discussed above, the fibers can provide the nucleation site for crystallization and this may have some effect on crystallization process.

2.3.5 Trans-crystallization

Interestingly, some trans-crystallization phenomena can be observed in some composites during cooling and formation of crystalline morphology. First, it should be noted that the black line is the fiber, and trans-crystallization starts from this place situated around the fiber. In detail, it can be concluded as follows: the surface of the fibers provides the nucleation sites, which could form the spherulites around these nucleation sites (see Figure 12). One can note the trans-crystalline layer grew over the whole embedded fiber length and subsequently the layer thickness increased [88].

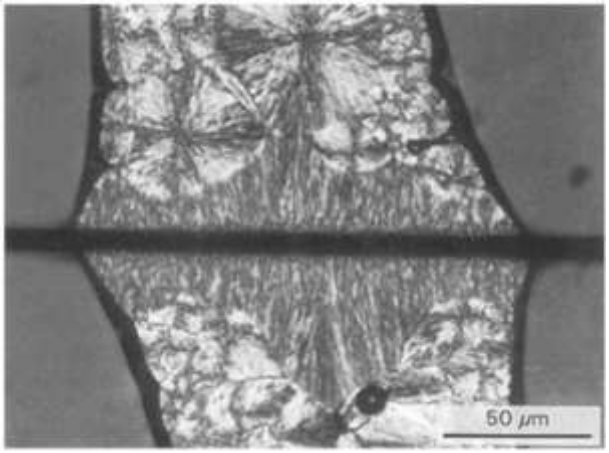

Figure 12: Typical PPS trans-crystallization morphology around T700S fiber in fiber pull-out samples. [88] Copyright 1995, Springer.

2.3.6 The relation between the crystalline phase and mechanical properties

As we know, the crystallization behaviors can also directly affect mechanical properties. For example, Lu et al. [89] studied the effect of the crystallinity on impact properties and they found the relationship as follows: the impact strength of PPS blends increased with the decrease in crystallinity. Moreover, fracture toughness was studied by Nishihata et al. [90]. They used the linear PPS, heat-treated PPS and branched PPS as specimens. The results showed that the fracture toughness of linear PPS was superior to that of heat-treated PPS and branched PPS, and the fracture toughness was affected by the crystallinity. Nevertheless, we should mention that in this reference, they used different kinds of PPS (for example several types of linear PPS), and the effect of crystallinity on fracture toughness cannot be concluded by a monotonic tendency.

2.3.7 Thermal treatment effect on crystallization

Wide angle X-ray diffraction (WXRD) methodology was used by Liu et al.[91], and they evaluated the crystallization behavior of PPS during processing and thermal treatment. One can see that major diffraction peaks at 18.7, 20.7, 25.6 and 27.7 °can refer to the index of reflections on the (110), (200), (112), and (211) lattices' planes of the orthorhombic structure (see Figure 13 (a)). Additionally, from Figure 13 (b), one can conclude that the thermal treatment can lead to an increase in the intensity peaks. This mainly indicates that an improvement of crystal perfection occurs due to the molecular chain rearrangement arising from the annealing or thermal treatment process.

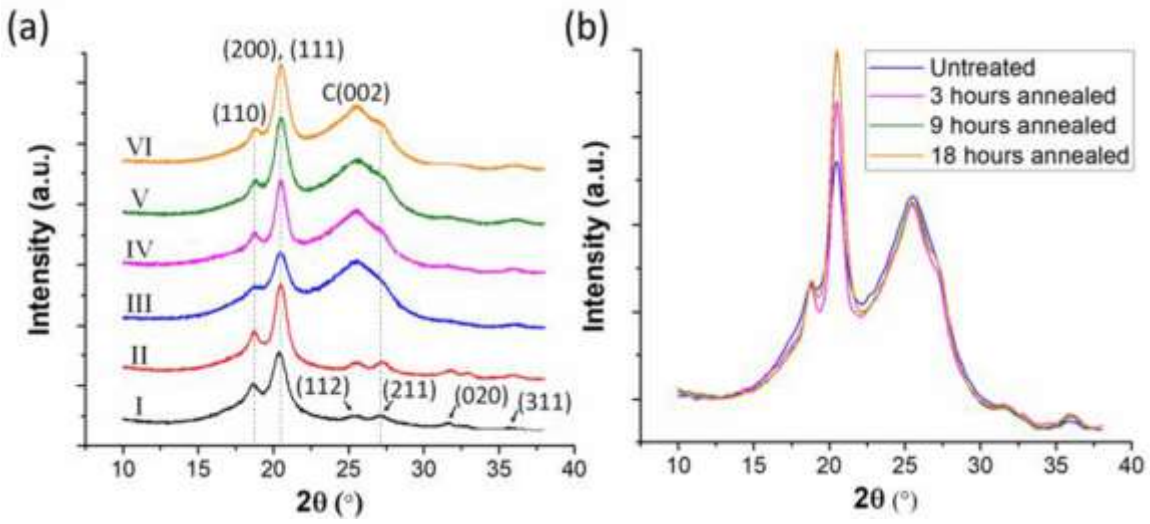

Figure 13: (a) WAXD patterns of neat PPS and carbon fiber reinforced PPS: I. injection molded neat PPS, no heat treatment; II. Injection molded neat PPS, annealed for 3 h at 250 ℃; III. AM PPS/CF (50 wt %), no heat treatment; IV. AM PPS/CF (50 wt %), annealed for 3 h at 250 ℃; V. AM PPS/CF (50 wt %), annealed for 9 h at 250 ℃; VI. AM PPS/CF (50 wt %), annealed for 18 h at 250 ℃; (b) WAXD patterns of AM PPS/CF (50 wt %) with different thermal histories. **[91]** Copyright 2018, Elsevier Sci. Ltd.

3 PPS processing

The melting point of PPS is relatively high (285 ℃), and PPS molding takes place at high temperature [92-101]. As a result, in order to avoid the degradation of the polymer, it is highly desirable to have a process for molding PPS during a minimum of molding time. The general process for producing PPS containing mixtures was disclosed in [102]. This process could be described as follows: PPS is first mixed with the selected filler and subsequently they were molded in a compressive way to form a part of a needed shape. This part is then freely sintered by being subjected to a gradually increasing temperature in an oven and cured for some time. After the curing process, the part is cooled and is ready for utilization. Other related processes to produce PPS-based materials (film, fibers) can be found in the patents of [103, 104]. Virgin PPS presents difficulties in injection molding. Its high fluidity in the molten state will require the usage of a shutter nozzle and to cure sealing of the mold. Moreover, the patent of [105] introduced a sheet formed by randomly dispersing and accumulating PPS filaments. The filaments drawn by a high-velocity air stream were formed directly into a sheet. This produced sheet could be used as industrial filters and heat insulating materials due to its outstanding chemical and thermal properties.

Additionally, the properties of injection molded PPS thermoplastics are shown in Table 4[70]:

Table 4: Properties of injection molded PPS [70]

Property	Units	PPS	PPS/glass fiber (60/40)
Specific gravity		1.35	1.65
Tensile strength			
21 ℃	MPa	64-77	150
204 ℃	MPa	33	33
Flexural modulus 21 ℃	MPa	4200	15500
Elongation at break	%	3	2-3
Dielectric constant ($10^{\wedge}3 – 10^{\wedge}6$ Hz)		3.1	3.8
Dissipation factor (1 kHz)		0.004	0.0037
Volume resistivity	Ω cm	$2.5*10^{\wedge}16$	
Water absorption	%	<0.02	<0.05

4 Blending

With the development of society and the economy, more polymers have increasingly been synthesized and applied in different domains. However, they are not sufficient to meet the requirements of the growing demand of polymers with different properties (e.g., miscible or immiscible [106-110], electrical [111-117], thermal [40, 117-121],

mechanical [40, 111, 122-126] and tribological properties [23, 28, 127-132]). Thus, blends and composites are compounded to improve the utilization of different polymers. In particular, in this section, we pay more prominent attention to the polymer blends, especially those with the compositions containing PPS [130, 131, 133-136].

As mentioned above, neat PPS is rather brittle and has low impact strength as well as difficulties in injection molding. Thus, many approaches have been proposed to overcome these disadvantages of PPS. To modify PPS by physical blending or alloying with other polymers or with other reinforcement materials is the most common and widespread method in industrial and academic domains currently [28, 137-145].

Thus, in this section, we introduce the modifications according to the following three aspects: 1) PPS blending with other polymers; 2) PPS mixing with nanotubes at the nanoscale range; and 3) other additives in blending.

4.1 PPS blending with other polymers

There is a wide range in the literature regarding discussions about blending PPS with other polymers. For example, Lim et al. [146] investigated the thermal behavior and phase morphology of binary blends of PPS with polycarbonate(PC), and they found the melt viscosity of PPS/PC blends was largely decreased when the PC was added to the PPS polymer. Moreover, the melting behavior of PPS and its blends with PSF (polysulfone) and PEK-C (polyetherketone with phthalidydene groups) was reported in Ref [141]. The results showed the melt temperature T_m and melt time t_m increased, and the intensities of the lower melting peaks of PPS increased. These phenomena could be attributed to the structure of

PPS which impedes the formation of upper melting crystals and the transformation of lower melting crystals into upper melting crystals.

In addition, Oyama et al. [147] studied the high-performance reactive blends containing PPS. They clarified that the reactive PPS blends showed good thermal stability up to 400 ℃.

Furthermore, the crystallization behaviors of polymers blending with PPS are a primary concern of many researchers. Shingankuli et al. [148] explored the thermal and crystallization behavior of engineering polyblends (glass reinforced PPS with polyethylene terephthalate). They revealed that the degree of crystallinity of PPS was reduced, whereas that of PET was increased due to blending. The crystalline morphologies of isothermally and nonisothermally crystallized PPS and their blends with PA66 were investigated [149]. The results exhibited that the presence of PA66 remarkably affected the crystallization process of PPS. Moreover, the nonisothermal crystallization behavior and kinetics of the PPS/polycarbonate blend were studied in the report of [150], and showed that the crystallization temperature of the PPS component in the blend decreased with the increasing of PC contents. In addition, some researchers [131] prepared the PPS/polyvinylidene fluoride(PVDF) polymer alloys by melt blending, and the results indicated that the addition of PVDF can accelerate the crystallization of PPS and improve the thermal stability of PPS/PVDF alloys. The multiple melting behaviors of PPS blends with Polyamide 6 were also studied [151], and the results suggested that PA 6 can accelerate the cold-crystallization of amorphous PPS. The researchers of [152] also investigated the through-thickness distribution of liquid crystalline polymer (LCP) in PPS/LCP blends. They concluded that a nonuniform distribution of LCP in the PPS-rich region occurred.

In addition, the mechanical properties of these blending polymers with PPS also attracted some attention from the investigators. The dynamic mechanical behavior of blending PPS with acetylene-terminated sulfone was studied by Zeng et al. [153]. They demonstrated that the flexural modulus and interlaminar shear strength of continuous unidirectional carbon fiber composites with a blended matrix of ESF/PPS=10/90 were obviously higher than those of composites with the pure PPS matrix. Similarly, the microdispersion of polyphenylene ether in PPS/PPE alloy can also affect the mechanical behaviors [143]. In this study, it showed that the weld strength of PPS/SG/PPE was found to be significantly decreased because of the increasing particle diameter.

In addition, styrene-b-ethylene/butylene-b-styrene triblock copolymer (SEBS) and maleic anhydride grafted SEBS (sebs-g-MA) for the blends of polyphenylene sulfide/nylon 66(PPS/PA 66) were prepared by Tang et al. [140]. They demonstrated that the addition of elastomers remarkably increased the toughness of PPS/PA66 blends. Wang et al. [154] explored the kinetic and thermodynamic behavior of water absorption in unidirectional fiber reinforced composites by blending PES and PPS. The results revealed that PPS reduced water absorption by weakening the polarity of benzene and forming a compact structure by crystallization.

4.2 PPS mixing with nanotubes at the nanoscale range

From the aspect of mixing with carbon nanotubes under nanoscale conditions, there are also considerable research reports. For example, Yu et al. [155] fabricated multiwall carbon nanotube reinforced PPS nanocomposites through melt compounding. The results showed that the incorporation of carbon nanotubes into PPS had a remarkable increase in

the aspect of thermal stability for this nanocomposite. Similarly, PPS/multiwall carbon nanotube composites through melting compounds were prepared and investigated by Yang et al. [156], and they concluded that the concentration of multiwall nanotubes can have some effects on the structure and chain mobility of the prepared composites. More intensively, they found a significant increase of T_g and the storage modulus when multinanotubes were added in PPS. Moreover, the research in this reference [157] studied PPS/multiwall nanotube composites from the perspective of physical aspects. The report revealed that the multiwall nanotube was fully dispersed in the PPS matrix, especially at low loading levels due to their good affinity. The presence of multiwall nanotubes can make a positive contribution to both the tensile properties and dynamic thermal mechanical properties. In addition, single-walled carbon nanotube (SWCNT) buckypaper (BP) reinforced-PPS composite laminates were manufactured by Pascual et al. [158] through hot-press processing. The TGA analysis demonstrated a remarkable improvement in the degradation temperature of the polymers by the incorporation of the BP. These authors also investigated the mechanical properties of carbon nanotube/PPS composites incorporating polyetherimide and inorganic fullerene-like nanoparticles, and the results revealed that mechanical properties were enhanced in aspects of stiffness and strength by the addition of both nanofillers. Moreover, multiwall carbon nanotube reinforced PPS nanocomposites were fabricated by Yu et al. [159] through melt compounding, and they found both thermal and mechanical properties showed an increase with the addition of CNT friction. As the results show in Figure 14, the spherical shape of the nanoparticles contributed to a lower contact hindrance with the polymer segments, and simultaneously, the SWCNTs with a larger interfacial contact area with the matrix showed a good advantage in hindering the diffusion of the PPS chains,

resulting in higher T_g. The performed tests confirmed that hybrids incorporating the optimized amounts of both nanofillers have enhanced dynamic mechanical performance when compared with composites reinforced only with SWCNTs wrapped in PEI. This phenomenon can be explained as follows: a single-walled carbon nanotube with a larger interfacial contact area is favorable to having a larger contact area with the matrix, which can positively contribute to the friction between the carbon nanotube and the matrix from the viewpoint of tribology. This larger contact area will restrict the mobility of PPS macromolecule chains and hinder the mobility of the PPS chains. Moreover, Han et al. [160] used the melt mixing method to fabricate PPS/multiwalled carbon nanotube composites, and they reported that the homogenous dispersion of multiwalled carbon nanotubes in the polymer matrix contributed to the increasing complex viscosity of the PPS/multiwall carbon nanotube. Similarly, Yang et al. [156] prepared PPS/multiwall carbon nanotube composites and observed an increased T_g and storage modulus of PPS via DMA.

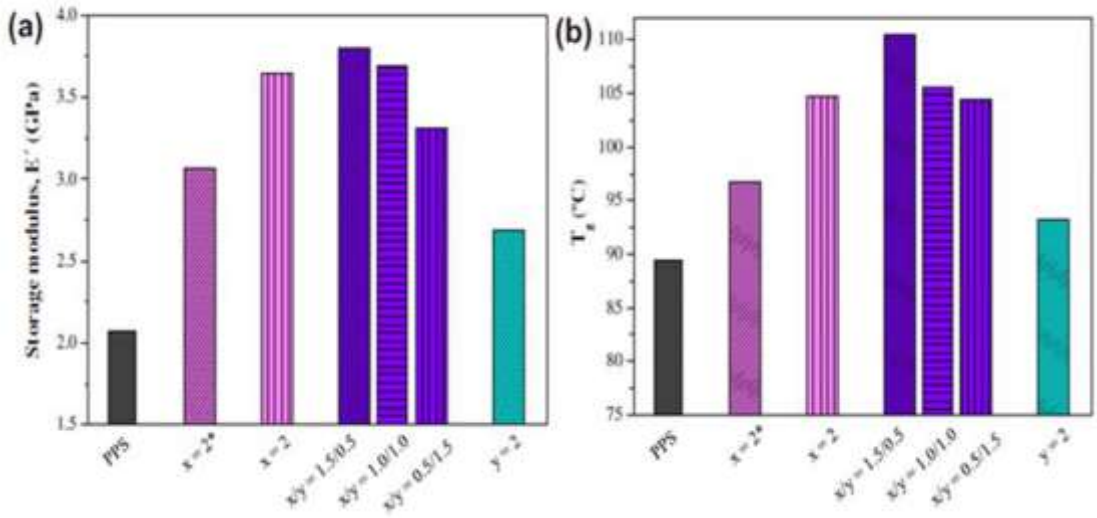

Figure 14: Comparison of the room temperature storage modulus E' (a) and glass transition temperature T_g (b) for the different PPS-based composites. To simplify the nomenclature, x and y denote the weight percentage of SWCNTS and IF-WS_2, respectively, and the composite incorporating nonwrapped SWCNTs is designated by (*).[158] Copyright 2012, Elsevier Sci. Ltd.

4.3 Other additives in blending

In addition to the fillers or particles (e.g., short/long fibers, particles and nanotubes), there are also some additives (e.g., antioxidants [161], heat stabilizers [162], UV stabilizers [163], carbon black [164], titanium dioxide [165], clay [166], mica [145], metal deactivators [167, 168], plasticizers [169], pigments [2], adhesives [170], nucleating agents [145] and flame retardants [171] compositions), which may be added in the industrial PPS materials to deionize and/or acidify the PPS, or to reach some particular purposes or to achieve better functions.

Some examples are as follows:

- Zou et al. [166] added a small amount of clay into PPS/polyamide 66 blends, and they found the morphology changed gradually from a sea-island structure into continuity and a lamellar supramolecular structure with the increase in clay content.
- The patent of US4418029A [162] provides some information about the stabilized PPS fiber. In this patent, the heat stability of PPS was improved by the addition of cure retarders consisting of Group VIIA or Group VIIB metal salts of fatty acids to reduce gel formation during melt extrusion.

Another patent (see US4535117A) [172] introduced the addition of cure retarders containing metal sorbates, an alkaline earth metal nitrite for the improvement of the heat stability of PPS.

- Moreover, Bo et al. [173] obtained a polymer blend consisting of linear PPS and hyperbranched PPS in the melt. They found the crystallization degree of the blends decreased with the increase in HPPS content. Both the storage modulus and loss modulus increased with the increase of HPPS content.
- Moreover, one can note in Figure 15 that the maximal tensile strength is obtained at the optimal content of 1% nano-SiO_2 and the elongation has the minimal value at the same content of 1% nano-SiO_2. Young's modulus increases with an enhanced content in nano-SiO_2. The main reason can be attributed to mobility restriction due to the nano-SiO_2 added in the matrix.

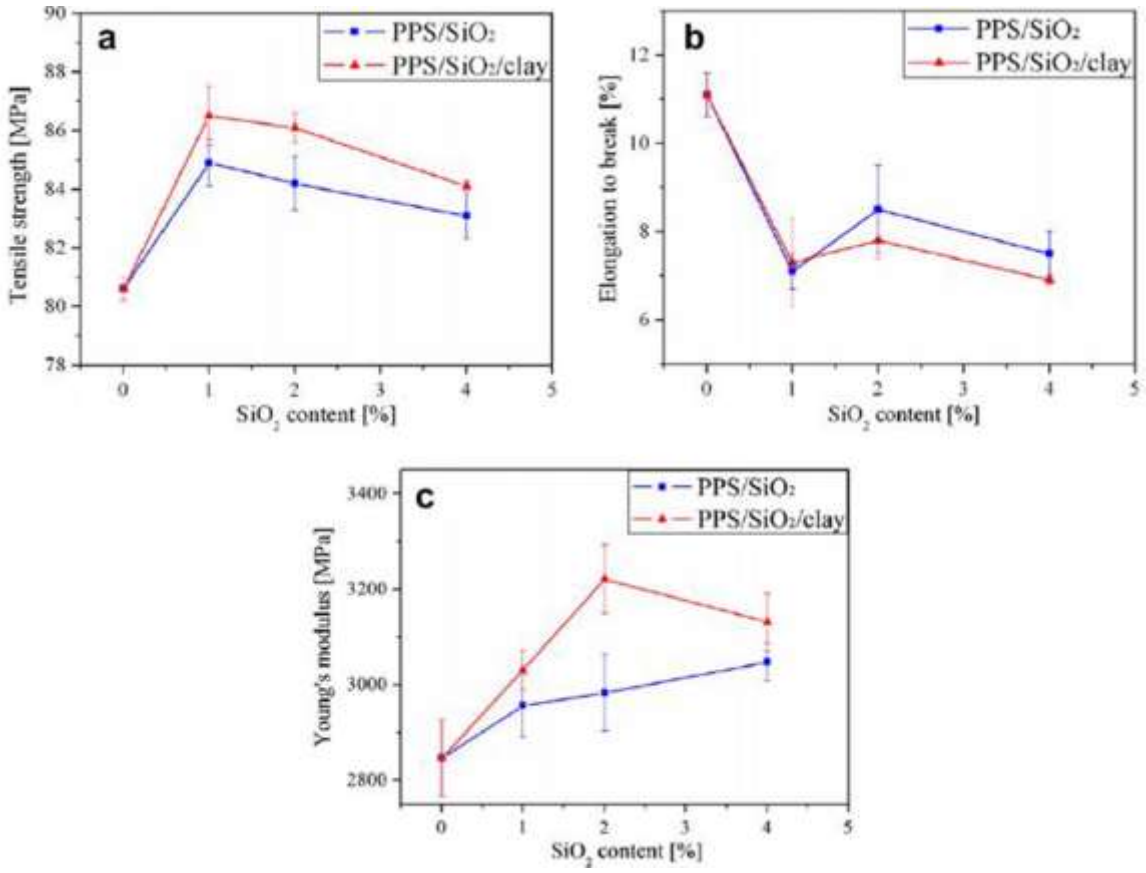

Figure 15: Tensile properties of PPS composites as a function of nano-SiO_2 weight fraction: (a) tensile strength, (b) elongation to break, and (c) Young's modulus. [13]

5 PPS – high-performance polymer/properties of PPS

5.1 Thermal behavior

PPS exhibits good dimensional stability and thermal stability. This is mainly due to its ordered alternating arrangement of phenylene and sulfide atoms. Several studies have discussed these aspects: 1) thermal expansion/shrinkage/conductivity; 2) thermal stability; 3) thermal aging and thermal stability [174, 175]; and 4) viscoelastic properties.

5.1.1 Thermal expansion/shrinkage/conductivity

The temperature-dependent coefficient of thermal expansion for PPS was reported in previous research by Bonnet et al. [176], as shown in a schematic figure of annealed PPS (see Figure 16). One can observe a shrinking above the glass-transition temperature (105 ℃) while a softening appears in the zone of 10-30 K, above T_a (T_a refers to the isothermal annealing temperature in this research).

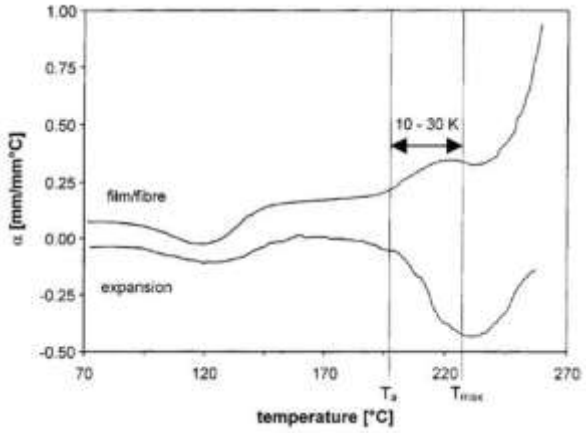

Figure 16: Temperature-dependent coefficient of thermal expansion for annealed PPS (expansion and film/fiber modus). [176] Copyright 1999, Springer.

In addition, Goyal et al. [177] explored the thermal properties of new high-performance PPS/aluminum nitride (AIN) composites prepared with hot pressing technology for usage in electronic packaging. As seen in Figure 17, the linear thermal strain (ΔL/L) for pure PPS and the 29.3 vol. % composite are exhibited. The expansion occurred because there was a movement of molecules or segments when they acquired energy with an increase in temperature. The thermal strain of the 29.1 vol. % was lower than that of pure PPS.

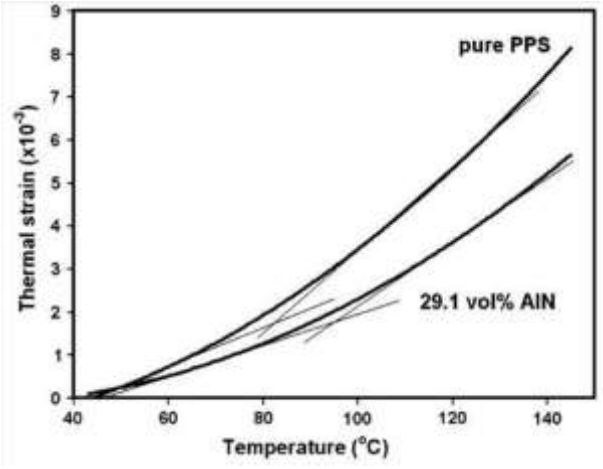

Figure 17: Thermal strain (ΔL/L) of composites as a function of temperature. [177]

The thermal conductivity of PPS is 0.3 W/mK at 25 ℃. In the research of Pak et al[178], they concluded that PPS is suitable for the application as a thermally conductive polymer. These authors investigated the thermal conductivity of composites with a PPS matrix and multiwall carbon nanotubes (MWCNT) as fillers. The results showed that the thermal conductivity of the composite was affected by the interaction and interfacial thermal resistance between the PPS matrix and the MWCNTs. Similarly, the thermal conductivity of single-walled carbon nanotube (SWCNT) buckypaper (BP) embedded in PPS was studied by Pascual et al. [179]. Furthermore, they also concluded that the thermal conductivity of PPS composites with SWCNTs could be well predicted by theoretical models. More interesting results can also be found in the reference of Khan et al.[180], in which the study demonstrated that various carbon-based fillers, including pitch-based carbon fibers (CFs), multiwalled carbon nanotubes (MWNTs), and graphene nanoplatelets (GNPs), can be dispersed in the polyphenylene sulfide (PPS) matrix to tailor the material's effective thermal conductivity. Gu et al. [181] also conducted some innovative work

concerning thermal conductivity of PPS-based materials. They found the thermal conductivities of the GNPs/PPS composites were improved with the increasing mass fraction of GNPs, and the thermally conductive coefficient of the fGNPs/PPS composite 30 with 40 wt% fGNPs is greatly improved to 4.414 W/mK, approximately 19 times higher than that of the original PPS (0.226 W/mK). Moreover, in their other related studies [182], they employed hybrid fillers of micrometer boron nitride/nanometer boron nitride (mBN/nBN) to fabricate the highly thermally conductive insulating mBN/nBN/polyphenylene sulfide ((mBN/nBN)/PPS) composites via mechanical ball milling followed by the hot-compression method. The thermally conductive coefficient (k), dielectric constant (e) and dielectric loss tangent values and thermal stabilities were all enhanced with the increasing addition of mBN/nBN hybrid fillers.

5.1.2 Thermal stability

Similarly, the kinetics of the thermal degradation of hyperbranched poly (phenylene sulfide) were studied [183], and the results showed that the degradation temperature (T_d) increased to a higher temperature with the increase in the heating rate. The change occurred from 476 ℃ for 5 ℃/min to 529 ℃ for 40 ℃/min. The change was from 28.2% for 5 ℃/min to 45.4% for 40 ℃/min, and the char yield at 850 ℃ increased significantly with the rise in the rate.

Additionally, there are some other studies reporting the thermal stability of PPS or their reinforced parts. For example, high-resolution thermal gravimetric properties of polyphenylene sulfide film under four atmospheres were investigated by Li et al. [184], and they found that there was a strong dependent relationship between thermal degradation

parameters (e.g., temperature, the maximal degradation rate), testing atmosphere and method. More intensively, the kinetics behavior on pyrolysis of PPS under different oxygen concentrations was examined by Teng et al. [185], and they concluded that only one stage occurred in inert atmosphere while two stages existed in oxidative atmosphere in the pyrolysis process of polyphenylene sulfide. The activation energy[186] of PPS blending can also be affected by the blending composition. In addition, an increased heating rate[187] and partial crosslinking [188] can enhance the initial thermal decomposition temperature of PPS blending materials. Moreover, Tanthapanichakoon et al. [189] examined the degradation behavior of semicrystalline PPS bag-filter materials by NO and O_2 at high temperature, and they summarized that the fabric strength depended on the crystallinity and the damages/defects in the amorphous region.

5.1.3 Thermal aging and thermal degradation

In this section, the aspects of thermal aging and degradation phenomena of PPS after aging are emphasized, and we try to investigate the degradation process of PPS according to classical studies [190]. As mentioned above, PPS has good stability against water and acid as well as many other chemicals due to the sulfur atoms which can endow the polymer with flexibility. These sulfur atoms, however, cause problems such as so-called crosslinking and coloration when the polymer is heated in the presence of oxygen. This significantly limits the utilization of the polymer. According to the previous studies, the change in PPS during thermal curing may result in the main chain scission or crosslinking reactions [191]. Ref [192] reported the isothermal kinetic behavior under the fluidized-bed condition of linear PPS and the branched PPS, which was formed by curing at 340 ℃. The authors concluded that the bond strength influenced the activation energies

required for cleavage and the formation of the two families of products (see Figure 18). When the pyrolysis temperature increased, more Ph-S bonds were cleaved; therefore, the pyro-products obtained were of low molecular weight (dimer and trimer), and the secondary reactions yielding dibenzothiophenes became dominant. Moreover, this pyrolysis method can provide a better understanding regarding the aspect of polymer structure via the examination of their thermal fragmentation products.

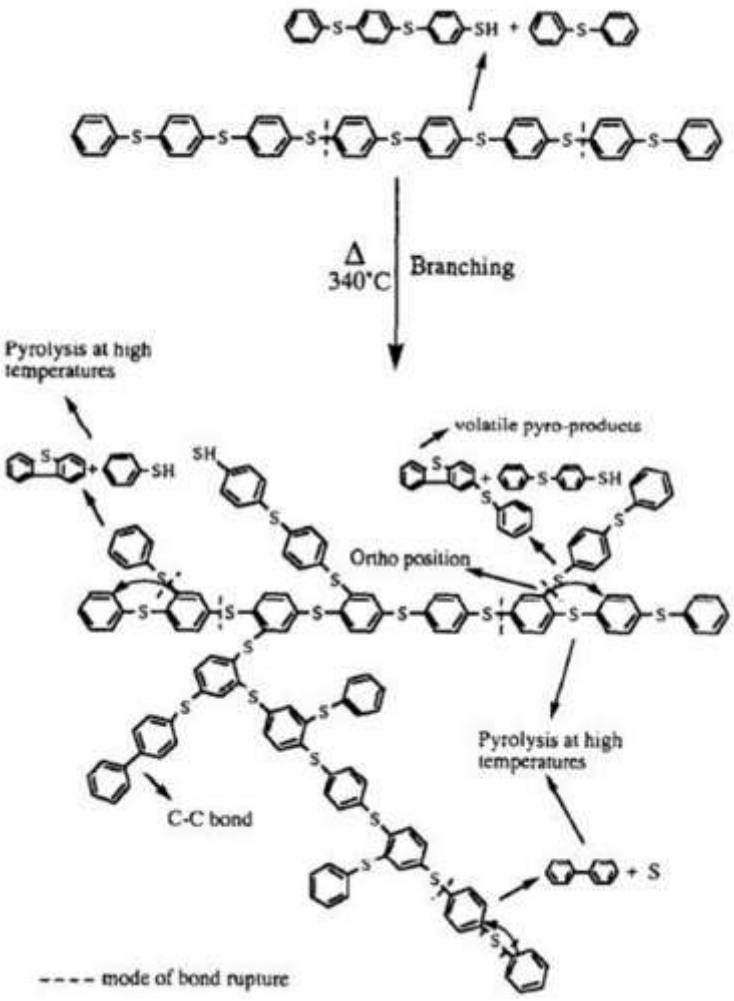

Figure 18: Scheme of curing of LPPS under nitrogen at 340 ℃. [192] Copyright 1993, Elsevier Sci. Ltd.

The exact aging process of PPS was clarified in depth by Ehlers et al. [7]. They concluded that cleavage of carbon-sulfur bonds and abstraction of hydrogen from some of the rings resulted in chain fragments with phenyl and phenylmercapto end groups. Cleavage of the C-SH bonds and abstraction of more hydrogen led to hydrogen sulfide. As shown in Table 5, hydrogen sulfide was the predominant volatile product at the lower temperature, and hydrogen at the two higher temperatures. Only very small amounts of other volatiles were present. Above 450 ℃, the reactions tended to be more complex with the formation of some water, carbon dioxide and carbon monoxide as well as sulfur dioxide.

Table 5: Analysis of the residues of Poly (1,4-phenylene sulfide) [7]

Analysis of volatiles from PPS								
Temperature (℃)	Volatile products, mole- %							
	H_2	H_2O	CH_4	CO	H_2S	CO_2	SO_2	C_6H_6
20-450	8.5	0.4	1.4	1.0	84.5	1.1	1.8	1.3
450-550	59.7	3.1	1.2	2.9	29.8	0.2	----	3.1
550-620	61.4	2.8	1.4	2.3	28.7	0.2	----	3.2

Thermal degradation of polyphenylene sulfide (PPS) film in four types of atmospheres including air, nitrogen and helium as well as argon were studied by Li et al. [184]. In this research, they pointed out that most polymers contain weak bonds that break with a higher probability than other stronger bonds. When the thermal energy began to surpass the bond energies of various bonds in the PPS chains, a random chain scission occurred and the rate of degradation enhanced rapidly. Similarly, thermal degradation of Poly (phenylene sulfide) was examined by Christopher et al. [6] through a weight loss method. They indicated that in a closed system, poly (phenylene sulfide) broke down by chain-scission and transferred reactions, yielding largely an involatile residue containing some low molecular weight chain fragments. Moreover, an understanding that the mechanism of PPS involved a combination of crosslinking, chain scission and aging reactions was concluded in the literature of [193].

Similarly, Deslauriers et al. [194] studied the aspects of PPS degradation and stabilization. They found that polymer end groups played an important role in the thermal-oxidative coloration of PPS. In semicrystalline samples PPS, the end groups or any other imperfection would be concentrated at spherulite boundaries in the amorphous phase. Moreover, an obvious degradation of the mechanical properties can be observed due to the serious degradation that was enhanced with the increase in treatment temperature and time [195].

5.1.4 Viscoelastic properties

Generally, the classical theory of elasticity is concerned with the mechanical properties of elastic solids in accordance with Hooke's law. In this case, stress is always

directly proportional to strain in a small deformation; however, the mechanical properties of elastic solids are definitely independent of the rate of strain. The classical theory of hydrodynamics addresses the properties of viscous liquids, and in this case, the viscous liquids follow Newton's law, where the stress is always directly proportional to rate of strain but independent of the strain itself. However, the materials with viscoelasticity exhibit both viscous and elastic characteristics when undergoing deformation. That is, viscoelastic materials have both elements of elastic and viscous materials. The viscoelastic response of PPS or PPS-based materials has been studied over the past several decades [136, 196-202]. In this section, the principle purpose is focused on overviewing viscoelastic properties of PPS polymer materials.

Dynamic mechanical analysis (DMA or DMTA) helps us to obtain the related values and parameters including the storage modulus and loss modulus as well as the parameters concerning the damping behavior of polymers. With the DMA method, Guo et al. [200] investigated the isothermal physical aging behavior of PPS film by creep and stress relaxation, and they indicated stress and strain remained in the linear viscoelastic regime. Annealing effects in PPS were also studied by dynamic mechanical analysis in the reference of [203]. Annealing of injection molded Izod bars was performed in a vacuum oven at temperatures of 160, 180, 200 and 220 ℃ with a constant annealing time at 4 h. The authors found an area of the increased endotherm with the increase in the annealing temperature. Similarly, thermal behaviors and viscoelastic properties of PPS/epoxy resin were studied [204], and the results showed that the epoxy resin can promote degradation and branching of PPS during melting mixing due to its poor thermal stability.

Moreover, the morphology and mechanical performance of carbon fiber reinforced PPS composites was reported [205], and the results showed the variation of the apparent storage modulus (E') and the loss factor (tan δ) as a function of temperature for different molding and loading conditions. Furthermore, the authors showed that the treatment temperature could have a remarkable effect on the viscoelastic properties although the crystallinity of the composite did not change with molding conditions.

The effects of annealing on the relaxation behavior and charge trapping in film-processed PPS was studied in reference [84]. In this study, DMA results showed a corresponding increase in the temperature location of the dissipation peak and a decrease in its amplitude when T_α increased above 100 ℃.

Some researchers also focus on the rheological properties of PPS or PPS related materials [206-208]. In detail, PPS and PPS/MWNTs (multiwall nanotubes) were prepared by Yang et al. [156] and as shown in Figure 19, they evaluated the change of viscosity before and after adding multiwall nanotubes and explained an obvious improvement on viscoelasticity of the nanocomposites due to the presence of the nanotube network interpenetrating into the PPS matrix.

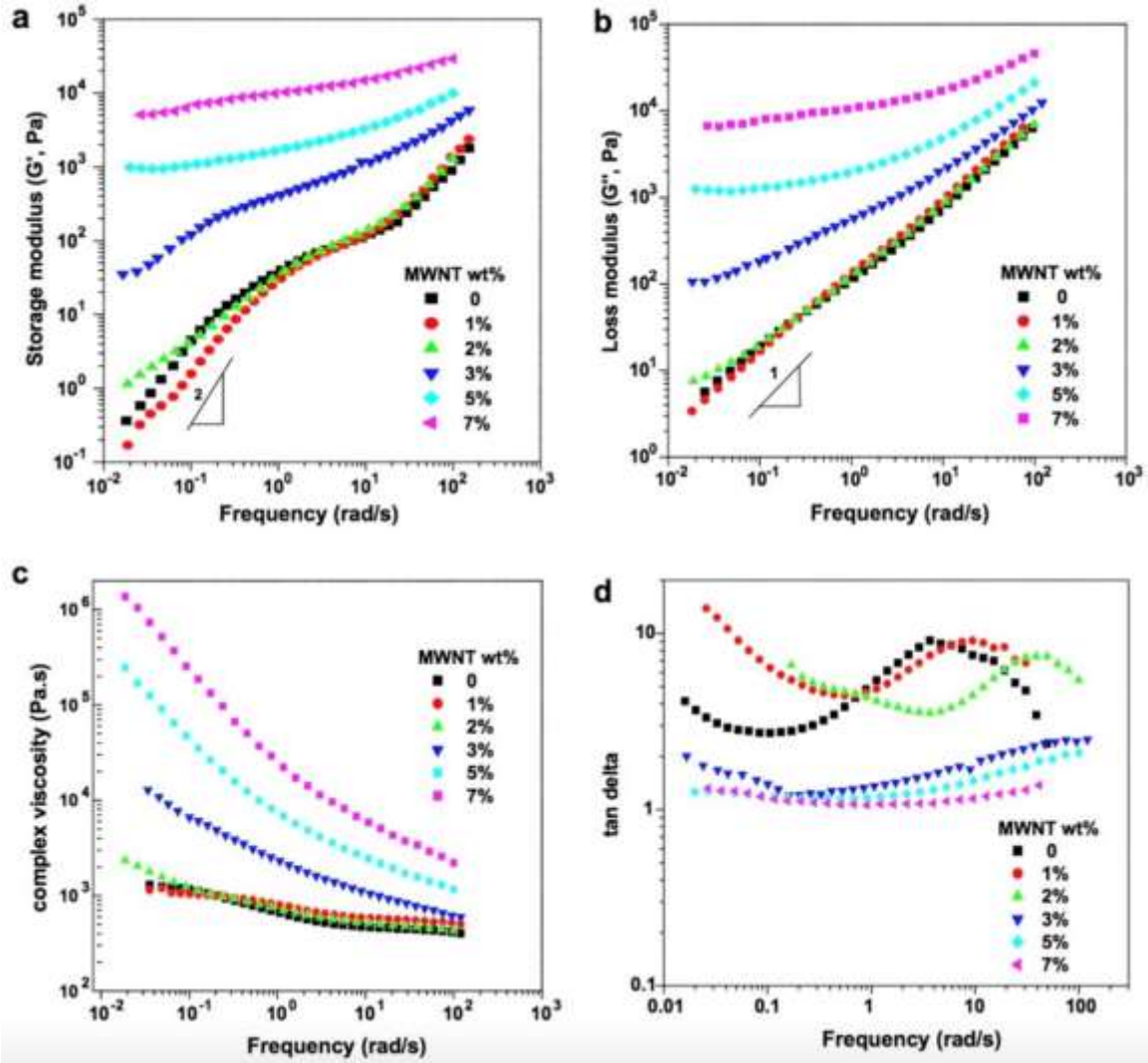

Figure 19: (a) Storage modulus; (b) loss modulus; (c) complex viscosity; (d) tan delta versus frequency for PPS and PPS/MWNTs composites with various MWNTs loading. Rheology testing performed at 320 ℃. [156] Copyright 2009, Elsevier Sci. Ltd.

In Ref [209], the research studied the rheological behavior of polyphenylene sulfide (Ryton-type PPS and Fortron PPS). The results showed that the apparent viscosity of the Ryton PPS decreased obviously with the increase in the shearing rate or shearing stress.

5.2 Mechanical properties and applications

5.2.1 Factors affecting the mechanical behaviors of fiber reinforced composites

- **Fiber selection**

Normally, fiber can be divided into three categories according to its origin: plant, animal or mineral. There are major structural components in all plant fibers while protein exists in animal fibers. In addition, high-performance plant fibers possess much higher strengths and stiffness than available animal fibers. Comparatively, mineral-based natural fibers are less frequently used due to health issues associated with carcinogenic substances acquired through ingestion. As a result, plant fibers are the most suitable and popular for utilization in composites that have high structural strength requirements.

- **Matrix selection**

In a fiber-reinforced composite, the matrix plays an important role to prevent consequences from harsh environments including thermal impact as well as chemical resistance. Moreover, it can transfer the load to the fibers. In commercial utilizations, polymeric materials are the most commonly applied matrix due to their light weight and good process ability at a relatively low temperature.

- **Fiber-matrix adhesion**

Fiber-reinforced polymer composites can transfer the applied force to the surrounding fibers. As a result, the bonding strength between the fiber and matrix plays an important role for the mechanical properties of composites. Some planted fibers may have some drawbacks due to the poor bonding from the hydrophilic nature of the fiber and the hydrophobic nature of the resin. Some solutions to overcome these drawbacks were

proposed by using mechanical interlocking, chemical bonding, electrostatic bonding and interdiffusion bonding as well as a coupling agent or chemical pretreatment [210, 211].

- **Fiber dispersion**

Fiber dispersion varies according to the fiber length (short or long) and processing factors such as pressure and temperature. Good dispersion of fibers favors a good bonding, which can improve the mechanical properties [212].

- **Fiber orientation**

Generally, the composites with the fibers aligned parallel to the direction of the applied load can have the best mechanical properties. By increasing the fiber orientation with respect to the fiber loading, one can reduce the strength and modulus. In addition, different strengths and moduli correspond to various physical phenomena including different self-heating properties and damage propagation.

- **Used technique in composite manufacturing**

Compression molding, injection molding and resin transfer molding [213, 214] are the three commonly used techniques to fabricate the reinforced polymer composites. It is necessary to point out that the final properties vary along with the evolution of the fabrication process by using different parameters, including processing, pressure and temperature as well as speed.

- **Porosity of composites**

Porosity can occur due to the inclusion of air bubbles while pouring resin over the fibers at the time of processing. The formation and the influence mechanism of composite porosity were studied by Li et al. [215]. They showed that the main reason that porosity was

formed was the poor wettability of fibers, the retention of vapor molecules and the molecular volatilization generated during the crosslinking reaction. Additionally, the increased cure pressure can decrease the porosity factor and porosity size remarkably.

- **Void content in composites**

There is a possibility that air or other volatiles will be trapped in the composites during the fabrication of composites. These air or other volatiles can form microvoids in the composites, which can affect the mechanical properties of composites. For example, the influence of voids on the flexural fatigue performance of unidirectional carbon fiber composites was investigated by Chambers et al. [216]. They concluded that a strong correlation existed between large voids (area > 0.03 mm^2), and these voids had a detrimental effect on the mechanical properties. Furthermore, they reported that this detrimental effect can be attributed to the voids on the crack propagation in the resin-rich interply regions.

5.2.2 General mechanical behaviors of PPS and PPS composites

In this section, we particularly focus on the mechanical properties of PPS and PPS composites [19, 135, 217-220]. There is a wide range of studies concerning PPS-based composites from the aspect of mechanical properties, including (1) tensile behavior and impact test behaviors; (2) bending or flexion behavior; (3) shear behavior; (4) compressive behavior; and (5) fatigue behavior.

5.2.2.1 Tensile behavior and impact test behaviors

Tensile behaviors are generally affected by environmental conditions [221, 222]. In the previous studies, environmental effects on glass reinforced PPS composites were studied by Lou et al. [223]. They revealed that this material possessed excellent mechanical properties at temperatures above the glass transition temperature, and this was due to high crystallinity and long glass reinforcement. They also clarified that the loss in properties was caused principally by the degradation of the fiber-matrix interface. Good strength property retentions were observed after exposure to both hot air and water.

Zhai et al. [224] also showed that the mechanical properties of glass fiber reinforced PPS composites were affected by thermal treatment. Moreover, the effect of temperature on the mechanical properties was studied [225], and the result showed maximum stress and elastic modulus increased obviously with the increase in glass fiber content below the glass transition temperature of the PPS matrix. In particular, the results showed the maximum stress and elastic modulus of PPS composites at various temperatures (see Figure 20).

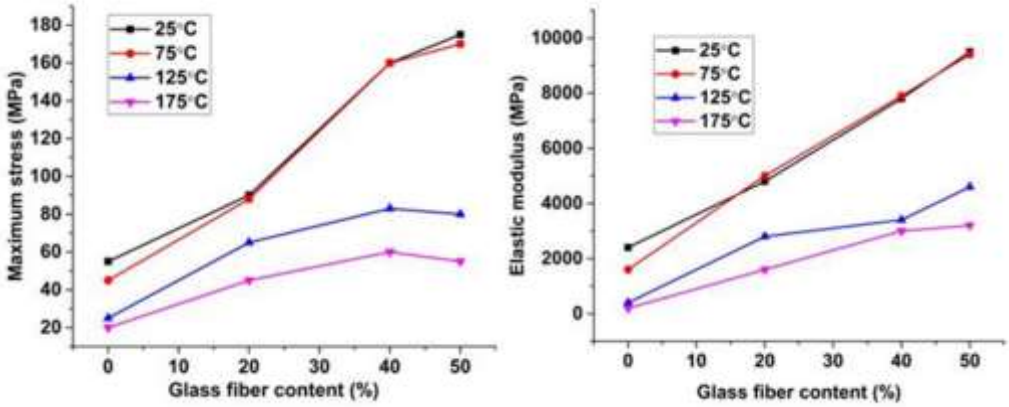

Figure 20: Maximum stress (Left) vs Elastic modulus (Right) as a function of glass fiber content for PPS/glass fiber composites at various testing temperatures. [225] Copyright 1996, Springer.

Moreover, PPS, as a high-performance polymer, is always used as a matrix of composites, and there is a wide range of reports to clarify this aspect. C/PPS laminates subjected to monotonic off-axis tensile loadings showed strongly matrix-dominated response results in an elastic-ductile behavior, while the PPS resin at 120 ℃ displayed a lower longitudinal stress with a long longitudinal strain.

Similarly, PPS, as a good blending composition, shows good mechanical properties when blended with other polymers. For example, in the research of [138], the authors reported the mechanical properties of PPS with other liquid crystalline polymers (LCPs), and the detailed results are shown in Table 6:

Table 6: Mechanical properties of the injection molded blends [138]

Materials	Tensile strength (MPa)	Elastic modulus (MPa)	Elongation (%)	Charpy impact strength (kJ/m^2)
PPS/0	82	3697	2.7	8.0
PPS/5	84	4035	2.9	12
PPS/10	87	4040	3.4	24
PPS/20	73	4512	2.2	15
PPS/30	69	4952	1.7	14
PPS/50	100	6447	2.1	13

The effect of thermal treatment on the tensile properties of PPS composites reinforced by carbon fibers was studied by Pantelakis et al. [195], and they exhibited an appreciable decrease in tensile strength when these specimens were subjected to thermal treatment. The report of [226] also studied the mechanical behaviors of PPS fiber materials after heat treatment, and they found that excess heat treatment, longer than two days, resulted in over-oxidative crosslinking and was detrimental to the thermal mechanical properties of the samples at high temperature. In addition, Garrell et al. [35] studied the mechanical properties of PPS bonded with Nd-Fe-B permanent magnets from -40 ℃ to 180 ℃, and they revealed the ultimate tensile strength of PPS bonded magnets decreased with the increase in temperature.

Moreover, the influence of temperature on the impact behavior of woven-ply carbon fiber reinforced PPS composites was studied by Wang et al. [227] et. Figure 21 is the experimental equipment used for the low velocity impact tests. As shown in the results in Figure 22, the temperature has a crucial effect on the limited propagation of delamination due to the geometry of the woven plate. The shape of the impact-induced damage of the specimens for 15 J and 25 J impacts transformed from nearly circular to oval or even cross-shaped with increasing temperature. In addition, the results showed that the damage propagation along the longitudinal direction was seriously confined at elevated temperatures.

Figure 21: Experimental equipment used for low velocity impact tests. [227] Copyright 2018, Elsevier Sci. Ltd.

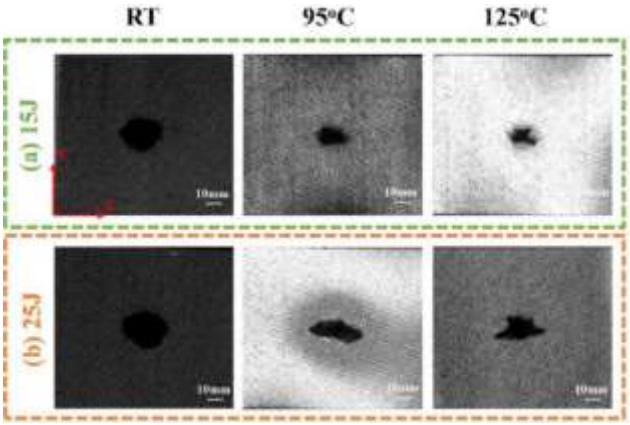

Figure 22: C-scan inspection of CF/PPS impacted specimens for 15 J and 25 J at different temperatures: (a) 15 J; (b) 25 J. [227] Copyright 2018, Elsevier Sci. Ltd.

In addition, Sinmacelik et al. [228] studied the nature weathering effects on the mechanical and surface properties of PPS composites. They showed that the percentage

decrease in the impact strength after natural weathering of fiber/particle-filled PPS composite was smaller when compared to short fiber-filled PPS composite.

The impact damage effect on the fatigue life of PPS composites reinforced using carbon fiber was evaluated by Kytyr et al. [229], and they revealed that the module of elasticity computed from three-point bending elasticity decreased without a significant influence of the impactor diameter. In addition, they concluded frequencies, ultrasound wave propagation and bending stiffness were suitable as measurement parameters for the evaluation of the material degradation process in C/PPS composite during its fatigue life.

5.2.2.2 Bending or flexion behavior

The load bearing performance of pin-connected carbon/PPS composites under static loading conditions was investigated by Yylmaz et al. [230], and they found the bearing strength of the pin connection highly depended on the joint and material parameters (for example the connection geometry, fiber orientation, layer orientation, and pressure distribution along the plate thickness). Furthermore, the effect of carbon fiber reinforcement on the mechanical properties of Polyamide 6/PPS composites was studied in [28], and the report revealed that with the addition of carbon fibers, the strength, and modulus improved while the breaking elongation rate and impact strength just decreased to a small degree. In this study, the authors revealed that bending strength and bending modulus increased apparently with the addition of carbon fiber. Luo et al. [130] prepared PPS/ polytetrafluoroethylene composite reinforced with short carbon fibers, and they revealed that the incorporation of carbon fibers apparently improved the tensile strength, flexural modulus and hardness of PPS/PTFE blends.

5.2.2.3 Shear behavior

The interlaminar shear strength (ILSS), translaminar and interplane shear strength as well as transverse stretch strength are the most commonly used measures to evaluate the quality of bonding in the structural pieces. In other application of PPS, the joint part from polymer composites is very significant for the aerospace industry since aircraft structures are large and complex and cannot be manufactured in a single step. PPS-based composites are popularly applied as a joint part in this domain. For example, welded glass fiber reinforced PPS joints were used and tested in a wide range of temperatures by Koutras et al. [231]. This research reported that the lap shear strength decreased with increase in temperature. The shear strength behaviors of PPS/glass fiber composites was also studied by Costa et al. [232], and they considered different environmental condition effects. One can see the fracture, observed by the interlaminar shear strength, in Figure 23. The results showed that fractures (submitted to (a) no conditioning, (b) hydrothermal conditioning and (c) seawater conditioning) followed the same multiple delaminating and interlaminar cracks at the horizontal and vertical positions; however, the fracture submitted to UV conditioning exhibited a compressive buckling or compressive yielding in some parts situated at the upper part of the beam.

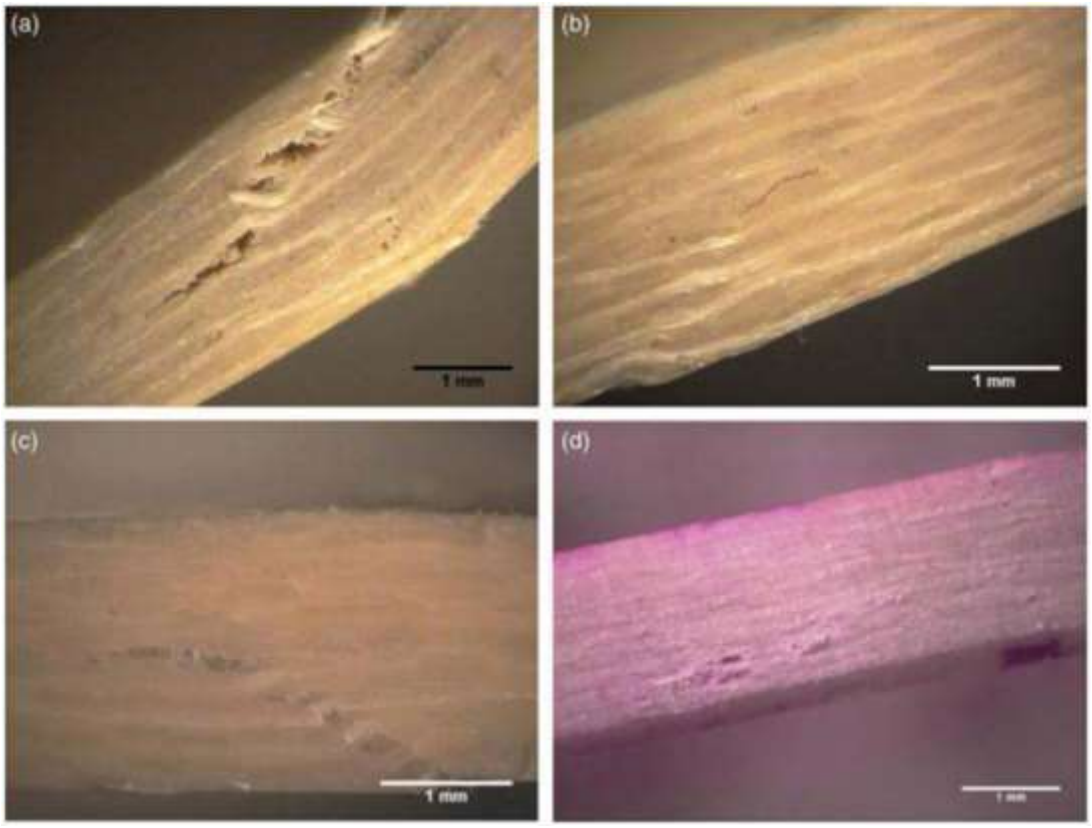

Figure 23: Representative fracture observed by the interlaminar shear strength test: (a) no conditioning, (b) hygrothermal conditioning, (c) seawater conditioning and (d) UV conditioning. [232] Copyright 2018, Elsevier Sci. Ltd.

5.2.2.4 Compressive behavior

The compressive behavior of notched and unnotched carbon woven-ply PPS thermoplastic laminates at different temperatures was studied by Wang et al. [233]. The results (see Figure 24) showed that the stress-strain curve of the unnotched specimen at RT had a similar linear trend as that of the notched one. Nonlinearity also existed for the notched specimen at elevated temperatures, which was associated with the softened matrix. Comparatively, as seen in Figure 25 and Figure 26, the matrix and interface cracks can be seen in notched specimens at RT and 95 ℃, which were similar to the unnotched

specimens. They concluded that a transition of failure modes existed from the wedge shear failure and an obvious delamination at RT, whereas in the other case, kink bands or even microbuckling occurred at elevated temperatures.

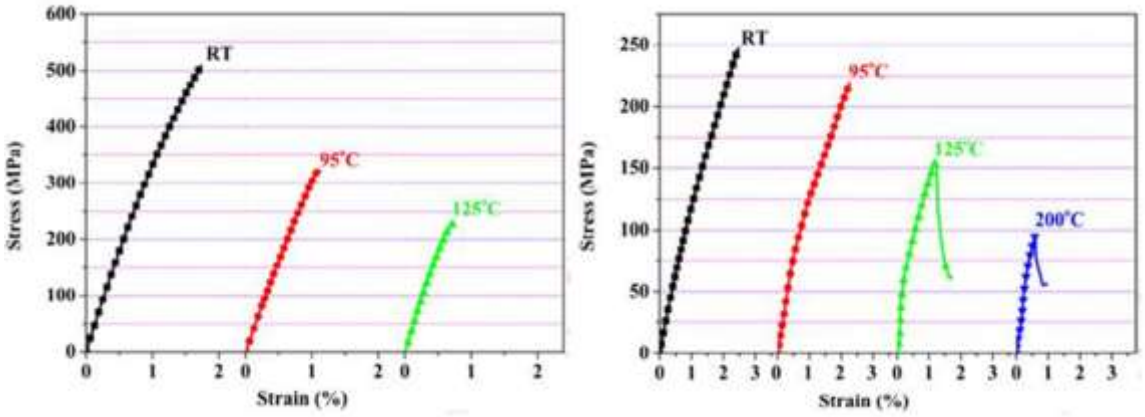

Figure 24: Compressive stress-strain curves of unnotched (left) and notched (right) specimens at different temperatures. [233] Copyright 2017, Elsevier Sci. Ltd.

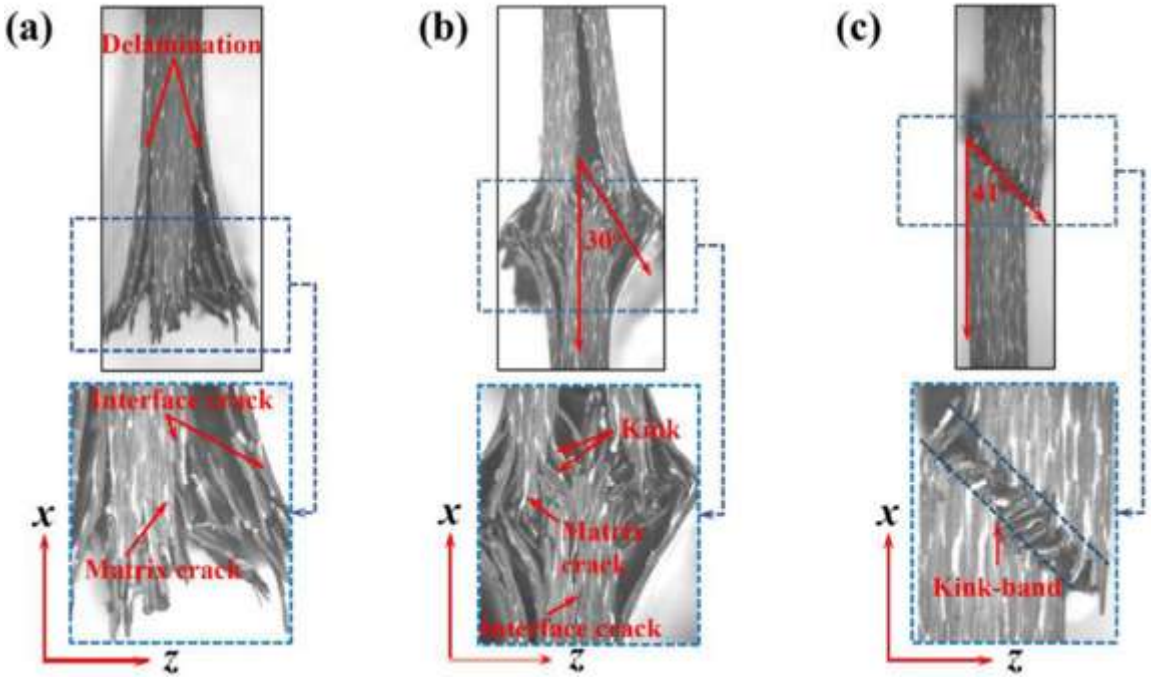

Figure 25: Failure modes of unnotched specimens at different temperatures: (a) RT; (b) 95 ℃; (c) 125 ℃. [233] Copyright 2017, Elsevier Sci. Ltd.

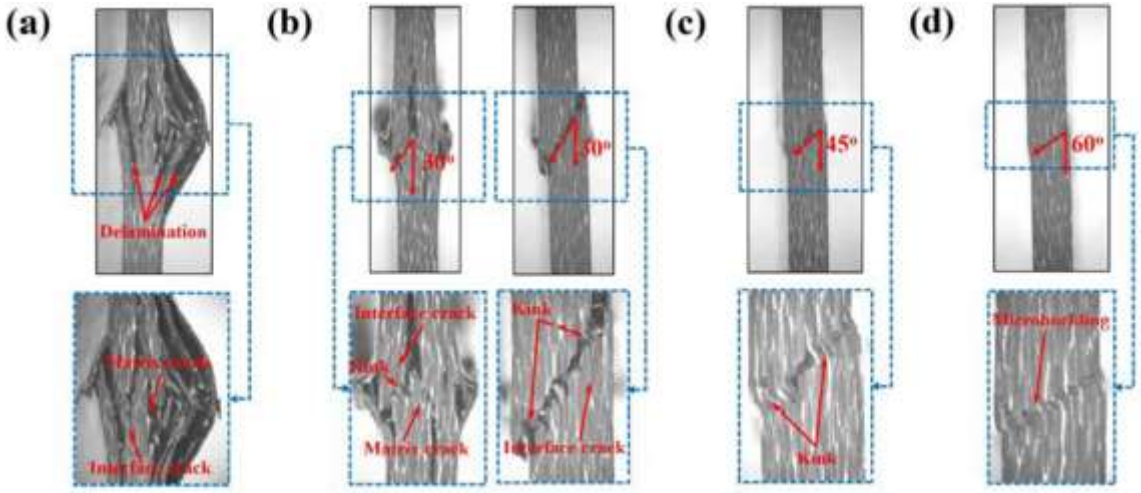

Figure 26: Failure modes of notched specimens at different temperatures: (a) RT; (b) 95 ℃; (c) 125 ℃; (d) 200 ℃. [233] Copyright 2017, Elsevier Sci. Ltd.

Postfire compressive behaviors of carbon fibers woven-ply PPS laminates were studied by Maaroufi et al. [234, 235], and Figure 27 shows the experimental setup and anti-bulking fixture. In addition, the different compressive responses were compared for all fire-testing conditions in Figure 28. In their similar works [234-236], the authors concluded that a compressive loading led to further delamination, which was explained by the mechanism in Figure 29. In particular, localized bending at the crimp was found to cause microbuckling in woven-ply misaligned structures. Furthermore, microbuckling occurred along with a plastic deformation of the matrix in highly ductile matrix systems, resulting in the formation of the deformed inclined kink bands also called plastic buckling.

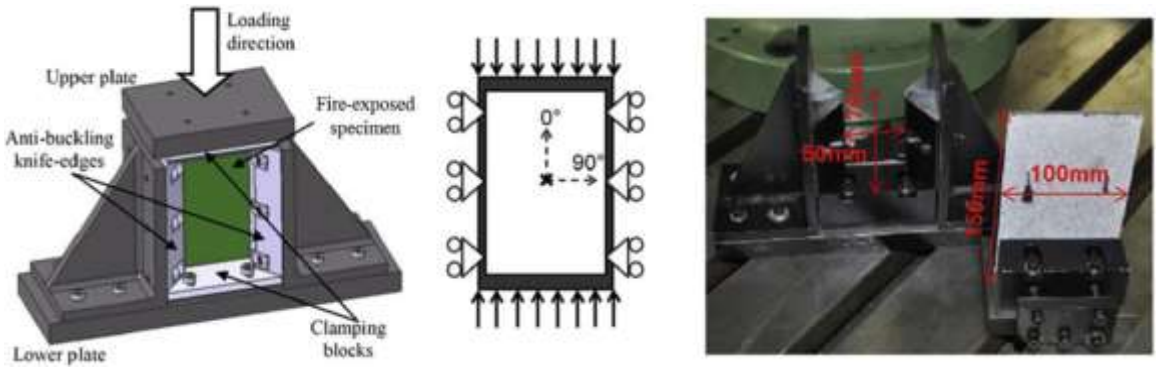

Figure 27: Compression test after fire exposure: experimental setup and anti-bulking fixture. [234] Copyright 2017, Elsevier Sci. Ltd.

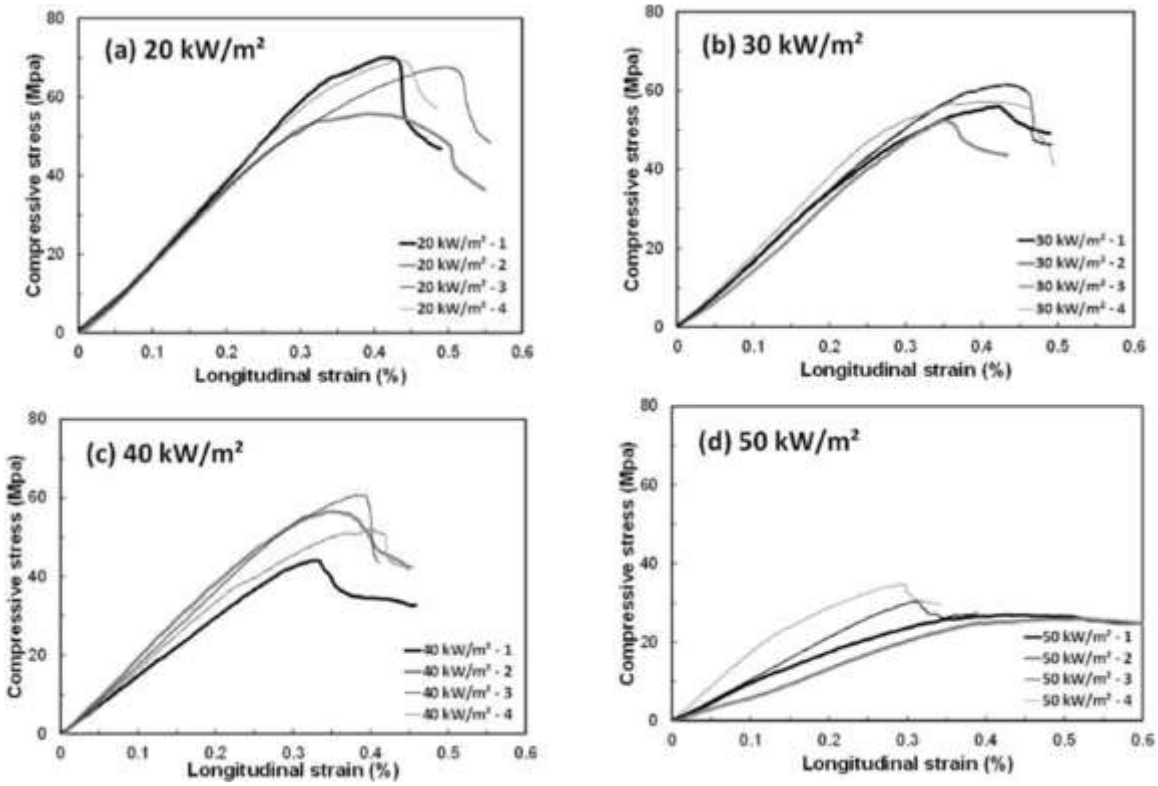

Figure 28: Thermomechanical responses of quasi-isotropic C/PPS laminates subjected to a compressive loading after different prior fire testing conditions. [234] Copyright 2017, Elsevier Sci. Ltd.

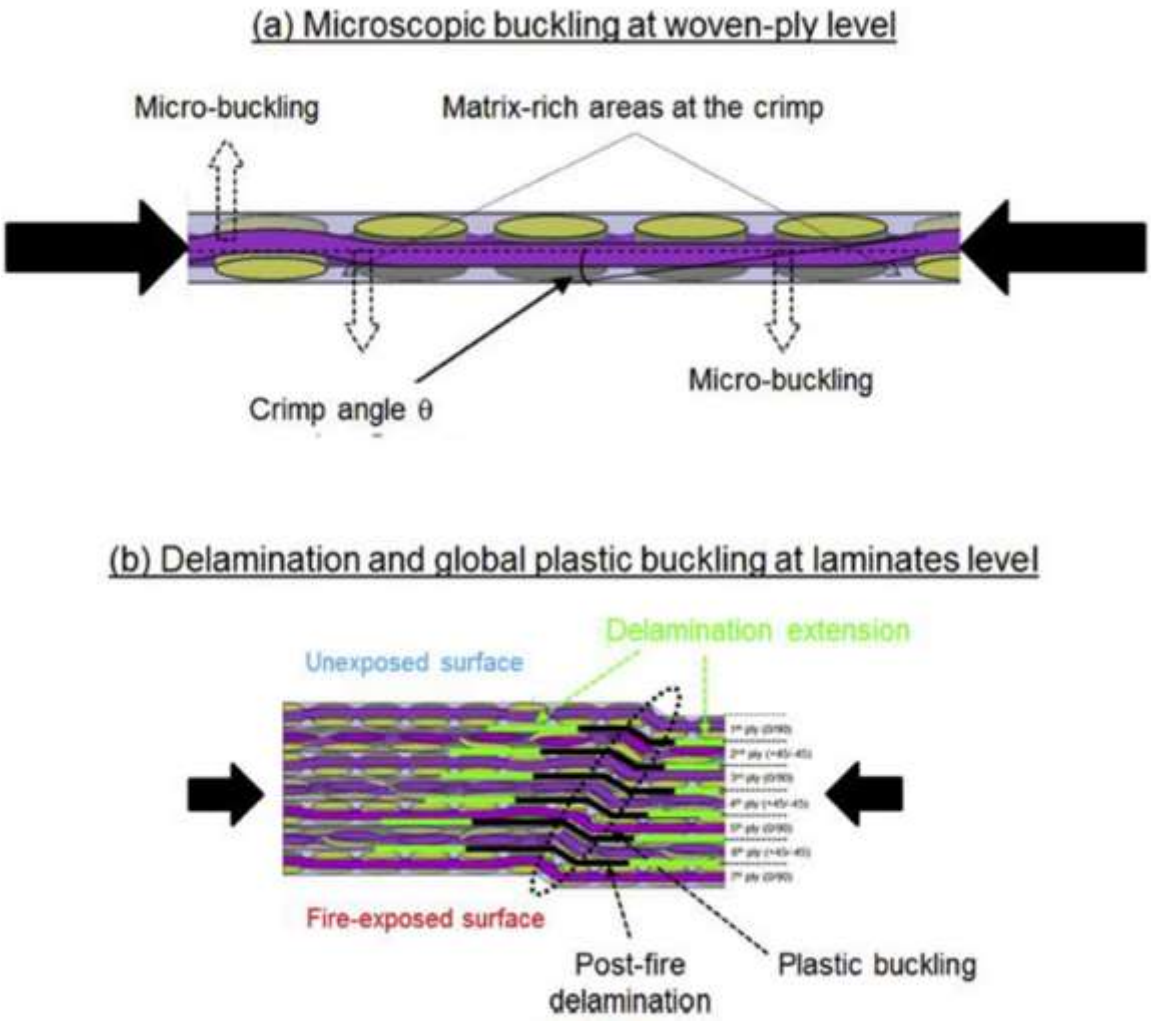

Figure 29: Damage mechanisms in woven-ply quasi-isotropic C/PPS laminates subjected to compression after fire exposure: (a) Local microbulking of fiber bundles at the crimp in a 5-harness satin weave; (b) Delamination and global plastic buckling induced by postfire delamination and the formation of plastic kink bands. [234] Copyright 2017, Elsevier Sci. Ltd.

In addition, the effect of microsized and nanosized carbon fillers on the thermal properties of PPS composites was studied by Khan et al. [237], and they found that various

carbon-based fillers, including pitch-based carbon fibers, multiwalled carbon nanotubes, and graphene nanoplatelets, can be dispersed in the PPS matrix to tailor the material's compressive modulus.

Furthermore, the effect of a carbon-based filler on the glass transition temperature (T_g) of the PPS composites was discussed. The hindrance of mobility of the polymer chains caused by the presence of microsized and nanosized filler particles could increase the T_g of the composites.

5.2.2.5 Fatigue behaviors

In the aspect of fatigue behaviors, there is a wide range of earlier published studies. The fatigue behavior of the material blended by using polyphenylene ether ketone and PPS was studied by Zhou et al. [238]. They found the constructed S-N curves shifted their trends dramatically at the maximum cyclic stress. In addition, Baere et al. [239] examined the interlaminar behavior of a 5-harness carbon fabric reinforced PPS by using lap experiments, they considered the quasi-static, hysteresis and fatigue loading conditions and they found that under quasi-static loading, both until failure and with continuously loading and unloading with an increasing maximum load, there was no crack growth. For fatigue loading, cracks growth can be seen clearly from the beginning of fatigue life. In other works of [240], they evaluated two types of welding procedures (extra sheets of PPS were added to the bond). It was found that one-sided welding yielded irreproducible results, not only between separate welding cycles with the same settings but also between the three specimens originating from one cycle. However, the two–sided welding showed reproducible results, both within one welding cycle and different welding cycles.

The ultrasonic fatigue behavior and microstructure of carbon fiber fabric reinforced PPS in the very high cycle fatigue regime were studied in the report [241], and the authors analyzed the very high cycle fatigue behavior of a carbon fiber twill 2/2 fabric reinforced PPS (CF-PPS) systematically up to 10^9 loading cycles. The different stress ratios between R=0.21 and 0.51 showed an exponential decrease of the bearable stress amplitude in the range between 10^6 and 10^9 cycles. One can observe the following in Figure 30: the results showed an exponential decrease of the bearable shear stress amplitude over the number of cycles until delamination. Furthermore, it was marked as a prevention interval in which the specimen failure of all further experiments would appear with a probability of 95%.

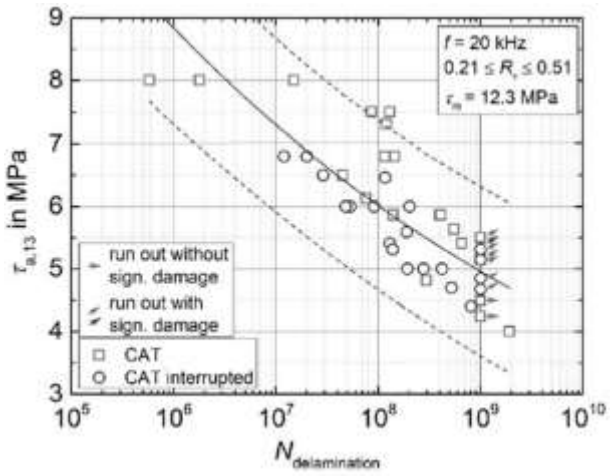

Figure 30: S-$N_{delamination}$ curve for CF-PPS in the very high cycle fatigue regime. [241]

Moreover, the environmental effects on glass reinforced PPS composites were studied by Lou et al. [223]. They revealed that this material had excellent mechanical properties at temperatures much higher than the glass transition temperature, and good

fatigue property retentions were observed after exposure to both hot air and water. Regarding the fatigue behavior of glass and carbon fiber reinforced engineering thermoplastics PPS, the S-N curve appeared linear with no evidence of a fatigue limit up to 10^6 cycles. The glass reinforced PPS composite degraded while the carbon reinforced materials with a brittle matrix degraded more slowly that that with the ductile matrix [242].

In this research, the authors also provided all S-N curves for several injection molded thermoplastics and their glass or carbon-filled composites. The measurements were made at room temperature in a uniaxial tension-tension mode with minimum stress/maximum stress equal to 0.1. There was no evidence of a fatigue limit for any of the thermoplastic matrix composites studied in the range up to 10^6. This study reported that PPS composites failed by a crack propagation mechanism. Similarly, the tensile fatigue resistance of 40% glass fiber/ PPS composites was measured by Oya et al. [243], and they reported that the fatigue strength decreased continuously with the number of loaded applications at 23 ℃.

Conclusion

This review cited a considerable number of publications on the synthesis, characterization, and different applications of PPS polymer or PPS-based composite materials. An overview on PPS has been presented in this paper. According to the literature report, it is of importance to combine physicochemical properties with mechanical properties and take these two aspects into consideration together because of their close relationship. In addition, PPS has been widely used in commercial applications, where high temperatures are required, so it is also crucial to conduct intensive and extensive research in this aspect. Furthermore, it is noteworthy that PPS has many interesting properties that reveal why PPS or PPS-based materials are used in a wide range of applications including automobile parts, coating, chip carriers, wear rings, ball valves, and as a thermoplastic matrix for composite materials, etc. However, it is self-evident that there are still numerous areas that need more study to obtain a better understanding and enlarge the application domains of PPS more extensively and intensively. In particular, there is a lack of knowledge about the long time thermal aging effect on PPS under fatigue conditions or in other harsh environments. In addition, more investigation on the fatigue properties of PPS-based composites materials is needed, which will contribute to the structural applications of PPS as a high-performance engineering material. Moreover, the mechanical degradation of PPS-based composites is also of significance to an in-depth investigation. Undoubtedly, more researchers can find interesting topics of PPS since much more remains to be learned about PPS materials, not only about the science but also about the engineering applications in practice.

Acknowledgements

The authors are grateful to Dr. R.C. Benevides and Dr. Manuel Henner (Valeo) for collaboration and fruitful discussions. The Valeo Company is also gratefully acknowledged for providing the material. Financial support from the CASCADE program (2015-2018) under project “FSN Calcul Intensif et Simulation Numérique” by DGE is gratefully acknowledged.

The authors also thank the China Scholarship Council (CSC) for their funding (2015-2018) of Peiyuan Zuo's thesis.

References

[1] H. A. Karimi-Varzaneh, P. Carbone, F. Müller-Plathe, *Macromolecules* **2008**, *41*, 7211.
[2] H. W. Hill, D. Brady, *Polym. Eng. Sci.* **1976**, *16*, 831.
[3] L. C. López, G. L. Wilkes, *Polymer* **1989**, *30*, 882.
[4] L. Caramaro, B. Chabert, J. Chauchard, T. Vu-Khanh, *Polym. Eng. Sci.* **1991**, *31*, 1279.
[5] M. Favaloro, "Properties and Processes of Linear Polyphenylene Sulfide (PPS) for Continuous Fiber Composites Aerospace Applications", in *SAE International*, 2009.
[6] N. Christopher, J. Cotter, G. Knight, W. Wright, *J. Appl. Polym. Sci.* **1968**, *12*, 863.
[7] G. Ehlers, K. Fisch, W. Powell, *J. Polym. Sci., Part A: Polym. Chem.* **1969**, *7*, 2955.
[8] L. Yu, S. Bahadur, Q. Xue, *Wear* **1998**, *214*, 54.
[9] L. A. Gyurova, K. Friedrich, *Tribo. Int.* **2011**, *44*, 603.
[10] Q. Zhao, S. Bahadur, *Wear* **1998**, *217*, 62.
[11] Z. Jiang, L. A. Gyurova, A. K. Schlarb, K. Friedrich, Z. Zhang, *Compos. Sci. Technol.* **2008**, *68*, 734.
[12] K. Stoeffler, S. Andjelic, N. Legros, J. Roberge, S. B. Schougaard, *Compos. Sci. Technol.* **2013**, *84*, 65.
[13] Y. Yang, H. Duan, S. Zhang, P. Niu, G. Zhang, S. Long, X. Wang, J. Yang, *Compos. Sci. Technol.* **2013**, *75*, 28.
[14] L. Lopez, G. Wilkes, *J. Macromol. Sci., Part C* **2012**, *29*, 83.
[15] B. G. Risch, *Syst. & Comput. in Japan* **1994**, *35*, 1.
[16] Y. Zhou, L. Jia, T. Wang, Y. Du, C. Wang, *Int. J. Hydrogen Energy* **2018**, *43*, 7356.
[17] T. Wang, Y. Jiang, Y. Zhou, Y. Du, C. Wang, *Appl. Surf. Sci.* **2018**, *442*, 1.
[18] Y. Shao, F. Xu, W. Li, K. Zhang, C. Zhang, R. Li, Y. Qiu, *Compos. Part A. Appl Sci Manuf.* **2016**, *88*, 98.
[19] M. Park, J. H. Park, B. J. Yang, J. Cho, S. Y. Kim, I. Jung, *Compos. Part A. Appl Sci Manuf.* **2018**, *109*, 124.
[20] X. Chen, Y. Zheng, Y. Zhang, *Catal. Commun.* **2018**, *105*, 16.
[21] M. Cho, *Wear* **2016**, *346-347*, 158.
[22] J. Gu, C. Xie, H. Li, J. Dang, W. Geng, Q. Zhang, *Polymer Composites* **2014**, *35*, 1087.
[23] H. Qi, L. Zhang, G. Zhang, T. Wang, Q. Wang, *J. Colloid Interface Sci.* **2018**, *514*, 615.
[24] D. Luo, M. Chen, J. Xu, X. Yin, J. Wu, S. Chen, L. Wang, H. Wang, *Compos. Sci. Technol.* **2018**, *157*, 119.
[25] J. Y. Kim, K. Ahn, S. Y. Jeong, E. D. Jeong, J. S. Jin, J. S. Bae, H. G. Kim, C. R. Cho, *Curr. Appl. Phys.* **2014**, *14*, 118.
[26] J. Huang, X. Zhang, L. Bai, S. Yuan, *J. Environ. Sci.* **2012**, *24*, 1433.
[27] D. Lian, J. Dai, R. Zhang, M. Niu, Y. Huang, *Polym. Degrad. Stab.* **2016**, *129*, 77.
[28] S. Zhou, Q. Zhang, C. Wu, J. Huang, *Mater. Des.* **2013**, *44*, 493.
[29] M. C. Lopes de Oliveira, I. J. Sayeg, G. Ett, R. A. Antunes, *Int. J. Hydrogen Energy* **2014**, *39*, 16405.
[30] K. Moran, P. Lake, J. Dole, *World Pumps* **2002**, *2002*, 27.
[31] B. Liu, Z. Liu, X. Wang, G. Zhang, S. Long, J. Yang, *Polym. Test.* **2013**, *32*, 724.
[32] B. Caglar, P. Fischer, P. Kauranen, M. Karttunen, P. Elsner, *J. Power Sources* **2014**, *256*, 88.
[33] L. Korugic-Karasz, J. Farugia, *Thin Solid Films* **2002**, *417*, 155.
[34] C.-M. Chen, T.-E. Hsieh, M. O. Liu, *React. Funct. Polym.* **2008**, *68*, 1307.
[35] M. G. Garrell, B.-M. Ma, A. J. Shih, E. Lara-Curzio, R. O. Scattergood, *Mater. Sci. Eng., A* **2003**, *359*, 375.

[36] L. Guo, H. Q. Zhu, Y. B. Sun, *Applied Mechanics and Materials* **2012**, 184, 872.
[37] Z. Hu, L. Li, B. Sun, S. Meng, L. Chen, M. Zhu, *Progress in Natural Science: Materials International* **2015**, *25*, 310.
[38] S.-S. Yao, F.-L. Jin, K. Y. Rhee, D. Hui, S.-J. Park, *Composites Part B* **2017**, *142*, 241.
[39] B. Lingesh, B. Rudresh, B. Ravikumar, *Procedia Materials Science* **2014**, *5*, 1231.
[40] D. G. Dikobe, A. S. Luyt, *Thermochim. Acta* **2017**, *654*, 40.
[41] M. Shirinbayan, J. Fitoussi, N. Abbasnezhad, F. Meraghni, B. Surowiec, A. Tcharkhtchi, *Compos. B. Eng.* **2017**, *131*, 8.
[42] A. E. Wiącek, K. Terpiłowski, M. Jurak, M. Worzakowska, *European Polymer Journal* **2016**, *78*, 1.
[43] K. Laux, A. Jean-Fulcrand, H. Sue, T. Bremner, J. Wong, *Polymer* **2016**, *103*, 397.
[44] D. J. Kim, C. H. Park, S. Y. Nam, *international journal of hydrogen energy* **2016**, *41*, 7641.
[45] J. da Silva Burgal, L. G. Peeva, S. Kumbharkar, A. Livingston, *Journal of membrane science* **2015**, *479*, 105.
[46] R. Shrestha, J. Simsiriwong, N. Shamsaei, *Polymer Testing* **2016**, *56*, 99.
[47] D. J. Kim, D. H. Choi, C. H. Park, S. Y. Nam, *International Journal of Hydrogen Energy* **2016**, *41*, 5793.
[48] D. J. Kim, B.-N. Lee, S. Y. Nam, *International Journal of Hydrogen Energy* **2017**, *42*, 23759.
[49] G. Skirbutis, A. Dzingutė, V. Masiliūnaitė, G. Šulcaitė, J. Žilinskas, *Stomatologija* **2017**, *19*, 19.
[50] S. Wu, R. B. Ladani, J. Zhang, E. Bafekrpour, K. Ghorbani, A. P. Mouritz, A. J. Kinloch, C. H. Wang, *Carbon* **2015**, *94*, 607.
[51] D. Quan, A. Ivankovic, *Polymer* **2015**, *66*, 16.
[52] D. Carolan, A. Ivankovic, A. Kinloch, S. Sprenger, A. Taylor, *Polymer* **2016**, *97*, 179.
[53] M. Chen, J. Yin, R. Jin, L. Yao, B. Su, Q. Lei, *Thin Solid Films* **2015**, *584*, 232.
[54] J. Liu, Y. Liu, W. Yang, Q. Ren, F. Li, Z. Huang, *Journal of Power Sources* **2018**, *396*, 265.
[55] T. Deplancke, O. Lame, S. Barrau, K. Ravi, F. Dalmas, *Polymer* **2017**, *111*, 204.
[56] L. Melk, N. Emami, *Composites Part B: Engineering* **2018**, *146*, 20.
[57] L. Dumas, L. Bonnaud, M. Olivier, M. Poorteman, P. Dubois, *European Polymer Journal* **2015**, *67*, 494.
[58] A. Bhattacharyya, D. Paul, P. Dutta, G. Bhattacharjee, *arXiv preprint arXiv:1509.01016* **2015**.
[59] C. Liu, H. Yan, Q. Lv, S. Li, S. Niu, *Carbon* **2016**, *102*, 145.
[60] W. Ciesińska, *Journal of Thermal Analysis and Calorimetry* **2017**, *130*, 187.
[61] X. Wang, Y. Deng, Y. Li, K. Kjoller, A. Roy, S. Wang, *RSC Advances* **2016**, *6*, 76318.
[62] Y. Cui, X. Hou, W. Wang, J. Chang, *Materials* **2017**, *10*, 668.
[63] L. Weng, Y. Zhang, X. Zhang, L. Liu, H. Zhang, *Journal of Materials Science: Materials in Electronics* **2018**, *29*, 2831.
[64] J. Jiao, L.-z. Zhao, Y. Xia, L. Wang, *High Performance Polymers* **2017**, *29*, 458.
[65] P. Li, T. Li, H. Yan, *Journal of Materials Science & Technology* **2017**, *33*, 1182.
[66] A. D. MACALLUM, *J. Org. Chem.* **1948**, *13*, 154.
[67] R. W. Lenz, W. K. Carrington, *J. Polym. Sci., Part A: Polym. Chem.* **1959**, *41*, 333.
[68] R. W. Lenz, C. E. Handlovits, H. A. Smith, *J. Polym. Sci., Part A: Polym. Chem.* **1962**, *58*, 351.
[69] R. W. Lenz, C. E. Handlovits, *J. Polym. Sci.* **1960**, *43*, 167.
[70] J. Brydson, "*Plastics Materials*", Elsevier, 2013.
[71] C. J. Stacy, *J. Appl. Polym. Sci.* **1986**, *32*, 3959.
[72] T. Housaki, K. Satoh, *Polym. J.* **1988**, *20*, 1163.
[73] C. C. M. Ma, L. T. Hsiue, W. G. Wu, W. L. Liu, *J. Appl. Polym. Sci.* **1990**, *39*, 1399.
[74] N. L. Batista, M. C. Rezende, E. C. Botelho, *Polym. Degrad. Stab.* **2018**, *153*, 255.
[75] C. Auer, G. Kalinka, T. Krause, G. Hinrichsen, *J. Appl. Polym. Sci.* **1994**, *51*, 407.

[76] L. B. Nohara, E. L. Nohara, A. Moura, J. M. Gonçalves, M. L. Costa, M. C. Rezende, *Polímeros: Ciência e Tecnologia* **2006**, *16*, 104.
[77] D. Lian, J. Dai, R. Zhang, M. Niu, *J. Therm. Anal. Calorim.* **2017**, *129*, 377.
[78] P. Huo, P. Cebe, *J. Polym. Sci., Part B: Polym. Phys* **1992**, *30*, 239.
[79] S. S. Song, J. L. White, M. Cakmak, *Polym. Eng. Sci.* **1990**, *30*, 944.
[80] J. Sheng‐Ling, G. Xiao‐Yu, Z. Zhi‐Yuan, *J. Appl. Polym. Sci.* **2013**, *127*, 224.
[81] M. Cho, S. Bahadur, *Tribo. Let.* **2007**, *25*, 237.
[82] S. Deng, L. Cao, Z. Lin, W. Qiu, K. Liang, W. Li, *Thermochim. Acta* **2014**, *584*, 51.
[83] S. Lee, D.-H. Kim, J.-H. Park, M. Park, H.-I. Joh, B.-C. Ku, *Advances in Chemical Engineering and Science* **2013**, *3*, 145.
[84] S. X. Lu, P. Cebe, *J. Appl. Polym. Sci.* **1996**, *61*, 473.
[85] D. Brady, *J. Appl. Polym. Sci.* **1976**, *20*, 2541.
[86] J. Chung, J. Bodziuch, P. Cebe, *J. Mater. Sci.* **1992**, *27*, 5609.
[87] G. P. Desio, L. Rebenfeld, *J. Appl. Polym. Sci.* **1992**, *44*, 1989.
[88] L. Ye, T. Scheuring, K. Friedrich, *J. Mater. Sci.* **1995**, *30*, 4761.
[89] D. Lu, Y. W. Mai, R. K. Li, L. Ye, *Macromol. Mater. Engi.* **2003**, *288*, 693.
[90] N. Nishihata, T. Koizumi, Y. Ichikawa, T. Katto, *Polym. Eng. Sci.* **1998**, *38*, 403.
[91] P. Liu, R. B. Dinwiddie, J. K. Keum, R. K. Vasudevan, S. Jesse, N. A. Nguyen, J. M. Lindahl, V. Kunc, *Composites Science and Technology* **2018**, *168*, 263.
[92] R. K. Goyal, K. R. Kambale, S. S. Nene, B. S. Selukar, S. Arbuj, U. P. Mulik, *Mater. Chem. Phys.* **2011**, *128*, 114.
[93] S. Pappadà, A. Salomi, J. Montanaro, A. Passaro, A. Caruso, A. Maffezzoli, *Aero. Sci. Technol.* **2015**, *43*, 314.
[94] R. T. Young, D. G. Baird, *Compos. B. Eng.* **2000**, *31*, 209.
[95] A. Miller, C. Wei, A. G. Gibson, *Compos. Part A. Appl Sci Manuf.* **1996**, *27*, 49.
[96] M. Hou, L. Ye, "Understanding the Thermoforming Issues of Carbon Fibre Reinforced Polyphenylene Sulphide [PPS] Composite", in *Composite Technologies for 2020*, L. Ye, Y.W. Mai, and Z. Su, Eds., Woodhead Publishing, 2004, p. 805.
[97] S. M. A. Durani, E. E. Khawaja, H. M. Masoudi, Z. Bastl, J. Šubrt, A. Galíková, J. Pola, *J. Anal. Appl. Pyrolysis* **2005**, *73*, 145.
[98] H. Wang, J. Zhao, Y. Zhu, Y. Meng, Y. Zhu, *J. Colloid Interface Sci.* **2013**, *402*, 253.
[99] S. Radhakrishnan, B. T. S. Ramanujam, A. Adhikari, S. Sivaram, *J. Power Sources* **2007**, *163*, 702.
[100] H. M. El-Dessouky, C. A. Lawrence, *Compos. B. Eng.* **2013**, *50*, 91.
[101] C. Lv, H. Wang, Z. Liu, W. Zhang, C. Wang, R. Tao, M. Li, Y. Zhu, *Appl. Surf. Sci.* **2018**, *435*, 903.
[102] H. D. Coale, "Poly (phenylene sulfide) containing mixtures and processes for producing free sintered parts therefrom", Google Patents, **1976**.
[103] M. Akatsu, E. Nakano, H. Endo, K. Sonoda, "Method of producing poly (phenylene sulfide) fibers", Google Patents, **1993**.
[104] H. N. Beck, R. D. Mahoney, H. S. Wan, C.-C. Chau, T. M. Finney, R. A. Wessling, J. Kawamoto, M. F. Sonnenschein, "Process of making microporous hollow fiber or film membrane of poly (phenylene sulfide)(PPS)", Google Patents, **1993**.
[105] S. Fukata, "Sheet of polyphenylene sulfide filaments and process for producing the same", Google Patents, **1984**.
[106] J. S. Reinaldo, L. M. Pereira, E. d. S. Silva, M. M. Ueki, E. N. Ito, *Polym. Test.* **2018**, *67*, 257.
[107] J. Yang, X. Qi, N. Zhang, T. Huang, Y. Wang, *Compos. Commun.* **2018**, *7*, 51.

[108] A. Sangroniz, A. Gonzalez, L. Martin, L. Irusta, M. Iriarte, A. Etxeberria, *Polym. Degrad. Stab.* **2018**, *151*, 25.
[109] E. Meaurio, E. Sanchez-Rexach, E. Zuza, A. Lejardi, A. d. P. Sanchez-Camargo, J.-R. Sarasua, *Polymer* **2017**, *113*, 295.
[110] H. Shinzawa, J. Mizukado, *Spectrochimica Acta Part A: Molecular and Biomolecular Spectroscopy* **2018**, *192*, 236.
[111] J. Chen, X. Cui, K. Sui, Y. Zhu, W. Jiang, *Compos. Sci. Technol.* **2017**, *140*, 99.
[112] P. Senthil Kumar, A. Sakunthala, M. V. Reddy, M. Prabu, *Solid State Ionics* **2018**, *319*, 256.
[113] S. A, S. R. Manohara, L. Gerward, *J. Mol. Liq.* **2017**, *247*, 328.
[114] N. Halawani, J. L. Augé, H. Morel, O. Gain, S. Pruvost, *Compos. B. Eng.* **2017**, *110*, 530.
[115] Q. Guo, Y. Chen, J. Zhang, Z. Yao, *Polym. Test.* **2017**, *63*, 587.
[116] J. Gao, H. Wang, X. Huang, M. Hu, H. Xue, R. K. Y. Li, *Compos. Sci. Technol.* **2018**.
[117] O. J. Botlhoko, J. Ramontja, S. S. Ray, *Polymer* **2018**, *139*, 188.
[118] N. Mehra, L. Mu, T. Ji, Y. Li, J. Zhu, *Compos. Sci. Technol.* **2017**, *151*, 115.
[119] Y.-l. Xu, A. Q. Dayo, M. Derradji, J. Wang, W.-b. Liu, S. Song, T. Tang, *React. Funct. Polym.* **2018**, *123*, 97.
[120] K. Lewandowska, A. Sionkowska, S. Grabska, B. Kaczmarek, *Int. J. Biol. Macromol.* **2016**, *92*, 371.
[121] A. R. Zanjanijam, S. Hakim, H. Azizi, *Polym. Test.* **2018**, *66*, 48.
[122] N. Z. Tomić, A. D. Marinković, Đ. Veljović, K. Trifković, S. Lević, V. Radojević, R. Jančić Heinemann, *Int. J. Adhes. Adhes.* **2018**, *81*, 11.
[123] H. Y. Ang, J. Chan, D. Toong, S. S. Venkatraman, S. J. Chia, Y. Y. Huang, *J. Mech. Behav. Biomed* **2018**, *79*, 64.
[124] N. Zheng, W. Sun, H.-Y. Liu, Y. Huang, J. Gao, Y.-W. Mai, *Compos. Sci. Technol.* **2018**, *159*, 180.
[125] X. He, Z. Qiu, *Polym. Test.* **2018**, *67*, 421.
[126] R. Malinowski, *Chem. Phys. Lett.* **2016**, *662*, 91.
[127] Y. Kanca, P. Milner, D. Dini, A. A. Amis, *J. Mech. Behav. Biomed* **2018**, *78*, 36.
[128] R. Araujo Borges, D. Choudhury, M. Zou, *Tribo. Int.* **2018**, *122*, 1.
[129] M. T. Mathew, J. Novo, L. A. Rocha, J. A. Covas, J. R. Gomes, *Tribo. Int.* **2010**, *43*, 1400.
[130] W. Luo, Q. Liu, Y. Li, S. Zhou, H. Zou, M. Liang, *Compos. B. Eng.* **2016**, *91*, 579.
[131] J. Xing, Q.-Q. Ni, B. Deng, Q. Liu, *Compos. Sci. Technol.* **2016**, *134*, 184.
[132] Z. Chen, T. Li, Y. Yang, X. Liu, R. Lv, *Wear* **2004**, *257*, 696.
[133] Z. Luo, Z. Zhang, W. Wang, W. Liu, *Surface and Coatings Technology* **2009**, *203*, 1516.
[134] R. Steffen, M. Meir, J. Rekstad, B. Röder, *Polymer* **2018**, *136*, 71.
[135] H.-h. Ren, D.-x. Xu, G.-m. Yan, G. Zhang, X.-j. Wang, S.-r. Long, J. Yang, *Compos. Sci. Technol.* **2017**, *146*, 65.
[136] K. Zhang, G. Zhang, B. Liu, X. Wang, S. Long, J. Yang, *Compos. Sci. Technol.* **2014**, *98*, 57.
[137] Y. Yang, B. Li, L. Dong, *J. Appl. Polym. Sci.* **1996**, *59*, 531.
[138] J. Seppälä, M. Heino, C. Kapanen, *J. Appl. Polym. Sci.* **1992**, *44*, 1051.
[139] M. T. Heino, J. V. Seppälä, *J. Appl. Polym. Sci.* **1992**, *44*, 2185.
[140] W. Tang, X. Hu, J. Tang, R. Jin, *J. Appl. Polym. Sci.* **2007**, *106*, 2648.
[141] K. Mai, M. Zhang, H. Zeng, S. Qi, *J. Appl. Polym. Sci.* **1994**, *51*, 57.
[142] R. T. Alvarez, "Polyalloy of polyphenylene sulfide and polyimide", Google Patents, **1977**.
[143] K. Kubo, J. Masamoto, *J. Appl. Polym. Sci.* **2002**, *86*, 3030.
[144] M. Ajbani, A. Auerbach, K. Feng, "Polyether ether ketone/polyphenylene sulfide blend", Google Patents, **2012**.

[145] S. Kadoi, H. Yabe, K. Kobayashi, "Polyphenylene sulfide resin composition", Google Patents, **1996**.
[146] S. Lim, J. Kim, M. Park, C. R. Choe, J. Lee, D. Kim, *Polym. Eng. Sci.* **1996**, *36*, 2502.
[147] H. T. Oyama, M. Matsushita, M. Furuta, *Polym. J.* **2011**, *43*, 991.
[148] V. Shingankuli, J. Jog, V. Nadkarni, *J. Appl. Polym. Sci.* **1988**, *36*, 335.
[149] R. Zhang, Y. Huang, M. Min, Y. Gao, A. Lu, Z. Lu, *J. Appl. Polym. Sci.* **2008**, *107*, 2600.
[150] D. Wu, Y. Zhang, M. Zhang, L. Wu, *J. Appl. Polym. Sci.* **2007**, *105*, 739.
[151] K. Mai, S. Zhang, Q. Gao, H. Zeng, *J. Appl. Polym. Sci.* **2000**, *78*, 1579.
[152] G. Shonaike, S. Yamaguchi, M. Ohta, H. Hamada, Z. Maekawa, M. Nakamichi, W. Kosaka, K. Toi, *Polym. Eng. Sci.* **1995**, *35*, 240.
[153] H. ZENG, M. KANCHENG, *Die Makromolekulare Chemie* **1986**, *187*, 1787.
[154] J. Wang, K.-X. Li, H.-W. He, J.-L. Wang, G.-H. Sun, *Colloids Surf., A* **2011**, *377*, 330.
[155] S. Yu, W. Wong, X. Hu, Y. Juay, *J. Appl. Polym. Sci.* **2009**, *113*, 3477.
[156] J. Yang, T. Xu, A. Lu, Q. Zhang, H. Tan, Q. Fu, *Compos. Sci. Technol.* **2009**, *69*, 147.
[157] D. Wu, L. Wu, W. Zhou, T. Yang, M. Zhang, *Polym. Eng. Sci.* **2009**, *49*, 1727.
[158] A. M. Díez-Pascual, M. Naffakh, C. Marco, G. Ellis, *Compos. Part A. Appl Sci Manuf.* **2012**, *43*, 603.
[159] S. Yu, W. M. Wong, X. Hu, Y. K. Juay, *J. Appl. Polym. Sci.* **2009**, *113*, 3477.
[160] M. S. Han, Y. K. Lee, H. S. Lee, C. H. Yun, W. N. Kim, *Chem. Eng. Sci.* **2009**, *22*, 4649.
[161] A. Kojima, T. Nishi, H. Iwamura, "Polyphenylene sulfide resin compositions", Google Patents, **2009**.
[162] J. O. Reed, R. D. Mathis, "Stabilized polyphenylene sulfide fiber", Google Patents, **1983**.
[163] J. C. Goossens, R. F. Sieloff, "Method of surface impregnating hot polycarbonate sheet with an ultraviolet radiation screener composition", Google Patents, **1990**.
[164] M. C. L. de Oliveira, I. J. Sayeg, G. Ett, R. A. Antunes, *Int. J. Hydrogen Energy* **2014**, *39*, 16405.
[165] H. Izutsu, T. Yamaguchi, "Polyphenylene sulfide resin composition containing mixture of silicon compounds", Google Patents, **1987**.
[166] H. Zou, N. Ning, R. Su, Q. Zhang, Q. Fu, *J. Appl. Polym. Sci.* **2007**, *106*, 2238.
[167] D. M. Dean, R. J. Arhart, "Polyphenylene sulfide alloy composition", Google Patents, **2003**.
[168] K. E. Mitchell, "Inferred water analysis in polyphenylene sulfide production", Google Patents, **2007**.
[169] K. Kodama, T. Sugata, T. Yamanaka, "Polyphenylene sulfide resin composition", Google Patents, **2010**.
[170] N. Anagreh, L. Dorn, C. Bilke-Krause, *Int. J. Adhes. Adhes.* **2008**, *28*, 16.
[171] T. Asano, "Non halogen, organic or inorganic flame retardants in thermoplastic polymer blends", Google Patents, **2003**.
[172] R. D. Mathis, J. O. Reed, "Stabilization of polyphenylene sulfide", Google Patents, **1985**.
[173] Y. Bo, C. Yanmo, Y. Hao, S. Bin, Z. Meifang, *J. Appl. Polym. Sci.* **2009**, *111*, 1900.
[174] P. Zuo, A. Tcharkhtchi, M. Shirinbayan, J. Fitoussi, F. Bakir, *Polym. Adv. Technol.* **2018**, *In press*.
[175] P. Zuo, J. Fitoussi, M. Shirinbayan, F. Bakir, A. Tcharkhtchi, *Polym. Eng. Sci.* **2018**, *In press*.
[176] M. Bonnet, K.-D. Rogausch, J. Petermann, *Colloid. Polym. Sci.* **1999**, *277*, 513.
[177] R. Goyal, P. Jadhav, A. Tiwari, *J. Electron. Mater.* **2011**, *40*.
[178] S. Y. Pak, H. M. Kim, S. Y. Kim, J. R. Youn, *Carbon* **2012**, *50*, 4830.
[179] A. M. Díez-Pascual, J. Guan, B. Simard, M. A. Gómez-Fatou, *Composites Part A: Applied Science and Manufacturing* **2012**, *43*, 1007.

[180] M. O. Khan, S. N. Leung, E. Chan, H. E. Naguib, F. Dawson, V. Adinkrah, *Polymer Engineering & Science* **2013**, *53*, 2398.
[181] J. Gu, J. Du, J. Dang, W. Geng, S. Hu, Q. Zhang, *RSC Advances* **2014**, *4*, 22101.
[182] J. Gu, Y. Guo, X. Yang, C. Liang, W. Geng, L. Tang, N. Li, Q. Zhang, *Composites Part A: Applied Science and Manufacturing* **2017**, *95*, 267.
[183] B. Yan, Y. Chen, H. You, B. Sun, M. Zhu, *J. Appl. Polym. Sci.* **2009**, *111*, 1900.
[184] X. G. Li, M. R. Huang, H. Bai, Y. L. Yang, *J. Appl. Polym. Sci.* **2002**, *83*, 2053.
[185] C. Teng, J. Liu, N. Mao, X. Tian, *International Conference on Chemical, Material and Food Engineering (CMFE-2015)* **2015**.
[186] I. Bhardwaj, V. Kumar, A. Das, *Thermochim. Acta* **1989**, *144*, 165.
[187] D. Q. Chang, J. X. Liu, N. Mao, B. Z. Chen, "Study on the Thermal Stability of Polyphenylene Sulfide Filter Media by Non-Isothermal Thermogravimetry", in *Adv. Mater. Res.*, Trans Tech Publ, 2013, p. 663/988.
[188] C.-C. M. Ma, H.-C. Hsia, W.-L. Liu, J.-T. Hu, *J. Thermoplast. Compos. Mater.* **1988**, *1*, 39.
[189] W. Tanthapanichakoon, M. Furuuchi, K.-h. Nitta, M. Hata, S. Endoh, Y. Otani, *Polym. Degrad. Stab.* **2006**, *91*, 1637.
[190] L. Perng, *Polym. Degrad. Stab.* **2000**, *69*, 323.
[191] T. Yamashita, T. Kudo, K. Horie, S. Maeda, K. Nagata, *Polym. Degrad. Stab.* **1993**, *39*, 279.
[192] Y. Cohen, Z. Aizenshtat, *J. Anal. Appl. Pyrolysis.* **1993**, *27*, 131.
[193] R. Black, C. List, R. Wells, *J. Appl. Chem.* **1967**, *17*, 269.
[194] P. Deslauriers, J. F. Geibel, P. Das, *Die Angewandte Makromolekulare Chemie* **1997**, *247*, 45.
[195] S. G. Pantelakis, C. V. Katsiropoulos, P. Lefebure, *J. Appl. Polym. Sci.* **2008**, *107*, 3190.
[196] L. N. Zhang, X. H. Zhang, H. M. Yang, Q. Zheng, *Chin. Chem. Lett.* **2012**, *23*, 478.
[197] B. Vieille, W. Albouy, L. Taleb, *Compos. B. Eng.* **2016**, *90*, 278.
[198] D. Wu, L. Wu, J. Wang, Y. Sun, M. Zhang, *Mater. Chem. Phys.* **2011**, *128*, 274.
[199] T. Hou, H. Chen, *Polymer* **2012**, *53*, 2509.
[200] Y. Guo, R. D. Bradshaw, *Polymer* **2009**, *50*, 4048.
[201] T. H. Lee, F. Y. C. Boey, N. L. Loh, *Compos. Sci. Technol.* **1993**, *49*, 217.
[202] A. M. Díez-Pascual, M. Naffakh, *Mater. Chem. Phys.* **2012**, *135*, 348.
[203] J. Scobbo, C. Hwang, *Polym. Eng. Sci.* **1994**, *34*, 1744.
[204] D. Wu, L. Wu, J. Wang, Y. Sun, M. Zhang, *Mater. Chem. Phys.* **2011**, *128*, 274.
[205] L. Caramaro, B. Chabert, J. Chauchard, T. Vu‐Khanh, *Polym. Eng. Sci.* **1991**, *31*, 1279.
[206] A. El-Hadi, R. Schnabel, E. Straube, G. Müller, S. Henning, *Polym. Test.* **2002**, *21*, 665.
[207] S. L. Bo, B. C. Chun, Y. C. Chung, *Fibers. Polym.* **2004**, *5*, 145.
[208] P. Gulgunje, *Mater. Sci. Eng., Publications & Other Works* **2010**.
[209] C. Hou, B. Zhao, J. Yang, Z. Yu, Q. Wu, *J. Appl. Polym. Sci.* **1995**, *56*, 581.
[210] N. Saba, M. T. Paridah, M. Jawaid, *Constr Build Mater* **2015**, *76*, 87.
[211] M. Abdelmouleh, S. Boufi, M. N. Belgacem, A. Dufresne, *Compos. Sci. Technol.* **2007**, *67*, 1627.
[212] K. L. Pickering, M. A. Efendy, T. M. Le, *Compos. Part A. Appl Sci Manuf.* **2016**, *83*, 98.
[213] Q. Hou, D. W. Grijpma, J. Feijen, *Biomaterials* **2003**, *24*, 1937.
[214] M. E. Sayer, "Injection moulding apparatus", Google Patents, **1988**.
[215] L. Shujian, Z. Lihua, C. Rong, Z. Liran, Z. Yuanqi, *Rare. Metal. Mat. Eng.* **2016**, *45*, 2282.
[216] A. Chambers, J. Earl, C. Squires, M. Suhot, *Int. J. Fatigue* **2006**, *28*, 1389.
[217] K. Zhang, G. Zhang, B. Liu, X. Wang, S. Long, J. Yang, *Composites Science and Technology* **2014**, *98*, 57.

[218] W. Luo, Q. Liu, Y. Li, S. Zhou, H. Zou, M. Liang, *Composites Part B: Engineering* **2016**, *91*, 579.
[219] D.-J. Zhou, L.-B. Dai, H. Ni, G.-L. Hui, S.-G. Yuan, *Chin. Chem. Lett.* **2014**, *25*, 221.
[220] P. Zuo, R. C. Benevides, M. A. Laribi, J. Fitoussi, M. Shirinbayan, F. Bakir, A. Tcharkhtchi, *Compos. B. Eng.* **2018**, *145*, 173.
[221] W. Albouy, B. Vieille, L. Taleb, *Compos. Part A. Appl Sci Manuf.* **2013**, *49*, 165.
[222] D. Blond, B. Vieille, M. Gomina, L. Taleb, *J. Reinf. Plast. Compos.* **2014**, *33*, 1656.
[223] A. Lou, T. Murtha, *Journal of materials engineering* **1988**, *10*, 109.
[224] H. Zhai, X. Zhou, L. Fang, A. Lu, *J. Appl. Polym. Sci.* **2010**, *115*, 2019.
[225] H.-J. Park, B. C. Chun, *Polym. Bull.* **1996**, *37*, 103.
[226] Y. Ma, P. Cong, X. Liu, R. Lv, T. Li, *J. Macromol. Sci., Part B* **2014**, *53*, 1786.
[227] Y. Wang, J. Zhang, G. Fang, J. Zhang, Z. Zhou, S. Wang, *Compos. Struct.* **2018**, *185*, 435.
[228] T. Sınmazçelik, *Mater. Des.* **2006**, *27*, 270.
[229] D. Kytýr, T. Fıla, J. Valach, M. Šperl, *U.P.B.Sci.Bull* **2013**, *75*, 157.
[230] T. Yýlmaz, T. Sýnmazçelik, *Mater. Des.* **2007**, *28*, 520.
[231] N. Koutras, I. F. Villegas, R. Benedictus, *Compos. Part A. Appl Sci Manuf.* **2018**, *105*, 57.
[232] A. Costa, E. C. Botelho, L. Pardini, *J. Appl. Polym. Sci.* **2010**, *118*, 180.
[233] Y. Wang, J. Zhang, J. Zhang, Z. Zhou, G. Fang, S. Wang, *Compos. B. Eng.* **2017**.
[234] M. Maaroufi, Y. Carpier, B. Vieille, L. Gilles, A. Coppalle, F. Barbe, *Compos. B. Eng.* **2017**, *119*, 101.
[235] B. Vieille, V. M. Casado, C. Bouvet, *Compos. Struct.* **2013**, *101*, 9.
[236] B. Vieille, V. M. Casado, C. Bouvet, *Compos. Struct.* **2014**, *110*, 207.
[237] M. O. Khan, S. N. Leung, E. Chan, H. E. Naguib, F. Dawson, V. Adinkrah, *Polym. Eng. Sci.* **2013**, *53*, 2398.
[238] J. Zhou, A. D'Amore, Y. Yang, T. He, B. Li, L. Nicolais, *Appl. Compos. Mater.* **1994**, *1*, 183.
[239] I. De Baere, W. Van Paepegem, J. Degrieck, *Polym. Test.* **2013**, *32*, 1273.
[240] I. De Baere, W. Van Paepegem, J. Degrieck, in *15th european conference on composite materials (ECCM15-2012)*, Ghent University, Department of Materials Science and Engineering, 2012.
[241] D. Backe, F. Balle, *Compos. Sci. Technol.* **2016**, *126*, 115.
[242] J. F. Mandell, D. Huang, F. McGarry, *Polym. Compos.* **1981**, *2*, 137.
[243] N. Oya, H. Hamada, *Compos. Part A. Appl Sci Manuf.* **1997**, *28*, 823.
[244] M. Rezakazemi, M. Sadrzadeh, T. Matsuura, *Prog. Energy Combust. Sci.* **2018**, *66*, 1.
[245] J. M. Chen, E. Woo, *J. Appl. Polym. Sci.* **1995**, *57*, 877.

Article N°2:

P. Zuo, R. C. Benevides, M. A. Laribi, J. Fitoussi, M. Shirinbayan, F. Bakir, A. Tcharkhtchi, "Multi-scale analysis of the effect of loading conditions on monotonic and fatigue behavior of a glass fiber reinforced polyphenylene sulfide (PPS) composite", Composites Part B: Engineering, 2018, 145: 173-181. **Published.**

Composites Part B 145 (2018) 173–181

Contents lists available at ScienceDirect

Composites Part B

journal homepage: www.elsevier.com/locate/compositesb

Multi-scale analysis of the effect of loading conditions on monotonic and fatigue behavior of a glass fiber reinforced polyphenylene sulfide (PPS) composite

P. Zuo[a,*], R.C. Benevides[b], M.A. Laribi[a,d], J. Fitoussi[a], M. Shirinbayan[a], F. Bakir[c], A. Tcharkhtchi[a]

[a] Arts et Métiers ParisTech, PIMM – UMR CNRS 8006, 151 Boulevard de l'Hôpital, 75013 Paris, France
[b] Valeo Thermique Habitacle, Valeo Powertrain Thermal Systems, 8 Rue Louis Lormand, 78321 La varrière, France
[c] Arts et Métiers ParisTech, Dynfluid – UMR CNRS 8006, 151 Boulevard de l'Hôpital, 75013 Paris, France
[d] Ecole Nationale d'Ingénieurs de Sousse, LMS, Pôle Technologique, Route de Ceinture, 4054 Sousse, Tunisia

ARTICLE INFO

Keywords:
Poly-phenylene sulfide (PPS)
Composite
Glass fiber
Fatigue behavior
Self-heating

ABSTRACT

In this paper, two kinds of PPS/GF composite samples (PPS-0°, PPS-90°) were prepared with two different fiber main orientations related to the injection direction. A wide range of their properties were discussed. Using DMTA analysis, it was shown that the PPS/GF composite under study obeyed the time-temperature equivalence principle. Moreover, Perez model was verified and gave a good estimation of the viscoelastic properties of the PPS/GF. Monotonic and fatigue behaviors and fatigue life of PPS/GF were investigated. Fiber's orientation, applied amplitude and loading frequency effects were emphasized. Self-heating effect on fatigue strength was also analyzed. SEM fracture surface observations allowed analyzing, at the local scale, the main deformation mechanisms occurring during mechanical loading. No evident damage development was observed for both monotonic and fatigue loading. PPS matrix plasticity appeared to be the predominant deformation mechanism until a semi-ductile or semi-brittle final failure depending on the loading conditions and local microstructure.

1. Introduction

Thermosetting resin-based composite materials have been extensively used over the past 40 years [1–4]. They provide us a wide range of useful mechanical properties, together with undeniable drawbacks, such as the need of low temperature storage, hand-made draping, irreversible defects of the manufacturing process and also difficult recycling. In the modern society, high-performance thermoplastic resins offer a promising alternative to thermosetting resins. Indeed, thermoplastic resins offer many advantages over conventional thermosetting resins and they also exhibit a high performance such as chemical resistance, as well as excellent damage and impact properties [5–8]. PolyPhenylene Sulfide (PPS) is a semi-crystalline polymer with an ordered alternating arrangement of phenylene and sulfide atoms. It is widely used as a high performance engineering polymer with a unique combination of excellent physical, thermal, and mechanical properties. It is applied in a wide range including electronics and electrical appliances, automotive parts, precision instruments, chemical sectors and aerospace fields [9–12]. Moreover, Poly-Phenylene Sulfide (PPS), as a high performance thermoplastic, is an attractive engineering thermoplastic which is widely used due to its good tribological properties, flame retardant and resistant to chemical and thermal abilities, as well as having good processing properties [13–19]. To improve the mechanical properties of pure PPS, composites formed using polymer blending, fiber reinforcing and/or fillers are usually used in industry [20–23]. It is well known that, the properties of fiber reinforced composites depend on several factors such as the characteristics of its matrix and fibers, form and volume fraction of fibers, chemical and physical interaction between fiber and polymer, and processing conditions. Especially the main factor is the compatibility between fibers and the matrix [24]. Good interfacial adhesion between fiber and matrix is necessary for obtaining composite with excellent mechanical properties. Recently, many researches were focused on fiber reinforced PPS composites. Ana et al. [25] studied novel carbon fiber (CF)-reinforced poly (phenylene sulfide) PPS laminates incorporating inorganic fullerene-like tungsten (IF-WS2) using melting-blending and hot-press processing. They found that those nanoparticles showed great potential to improve the mechanical and tribological properties of conventional thermoplastic/CF composites for structural applications. Liu et al. [26] explored the interfacial micromechanical performance of carbon fiber

* Corresponding author.
E-mail addresses: peiyuan.zuo@ensam.eu (P. Zuo), rodrigo.benevides@valeo.com (R.C. Benevides), mohamed-amine.laribi@ensam.eu (M.A. Laribi), joseph.fitoussi@ensam.eu (J. Fitoussi), mohammadali.shirinbayan@ensam.eu (M. Shirinbayan), farid.bakir@paris.ensam.fr (F. Bakir), abbas.tcharkhtchi@ensam.eu (A. Tcharkhtchi).

https://doi.org/10.1016/j.compositesb.2018.03.031
Received 31 October 2017; Received in revised form 26 February 2018; Accepted 16 March 2018
Available online 17 March 2018
1359-8368/

(CF) reinforced polyphenylene sulfide (PPS) composites by micro-bond test and concluded the interfacial shear strength increased with increasing fiber embedded length below 0.02 mm/s and above 0.04 mm/s. Vieille et al. [27] investigated the influence of temperature on mechanical properties and behaviors of carbon fiber fabric reinforced polyphenylene sulfide (PPS) laminates subjected to different loadings and they exhibited that a temperature up to the glass transition temperature (T_g) softens the matrix behavior and reduces mechanical properties (in-plane shear, compressive, flexural and interlaminar shear).

On the other hand, as a good composite candidate in mechanical properties, we pay much attention to the aspect of fatigue behavior of PPS. Especially it is very important to understand the damage mechanism and relative self-heating phenomenon of PPS under fatigue loading since these researches can give us a great help in industrial utilization. In this aspect, there are a wide range of published researches before. Lou et al. [28] studied environmental effects on glass reinforced PPS composites. They clarified that the loss in properties was caused mainly by the degradation of the fiber-matrix interface. Good fatigue property retentions were observed after the samples were exposed to both hot air and water. Mandell et al. [29] researched fatigue behavior of glass and carbon fiber reinforced engineering thermoplastics PPS. The tensile-tensile S-N fatigue curves showed that PPS reinforced with 40% glass fiber degraded more rapidly than that for PPS reinforced with 40% carbon fibers.

In this paper, two kinds of PPS/GF samples were prepared (PPS-0°, PPS-90°). Here, PPS-0° corresponds to fibers oriented in the mold flow direction while PPS-90° derives from the samples with fibers oriented perpendicularly to it. The main structure for this paper is as follows: firstly, microstructure is characterized by SEM. Therefore, a wide range of tests are applied to exhibit the physico-chemical properties of PPS/GF composite material. Finally, the most important attention is given to the discussion concerning some aspects of fatigue behavior of PPS/GF composite and the effects of some parameters (e.g. fiber orientation, frequency and amplitude).

2. Materials and characterization methods

2.1. Materials

PPS/GF composite materials with 30% (weight content) short glass fibers are kindly supplied by Valeo Company France in the form of injected plate. The material presents a density of 1.58 g/cm^3 and water absorption of about 0.02%.

2.2. Characterization methods

2.2.1. Microscopic observations

Microscopic observations and image analysis, using Scanning Electronic Microscope (HITACHI 4800 SEM), were used in the aim to investigate qualitatively the material microstructure and especially fibers orientation.

2.2.2. Differential scanning calorimetry (DSC)

The differential scanning calorimetry (DSC) measurements were carried out with the DSC Q 10 V 9.0 Build 275 (TA Instruments, Guyancourt, France). The samples of mass between 10 and 20 mg were placed in hermetic aluminum capsules. The sample was heated first up to 300 °C with a temperature rate of 5 °C/min in the atmosphere of Nitrogen (40 ml/min), in order to eliminate the effect of the thermal history of the material. It was cooled down to 0 °C in order to be reheated up to 300 °C with the same temperature rate. In this test, the melting point, T_m and the crystallization temperature, T_c of the sample have been measured.

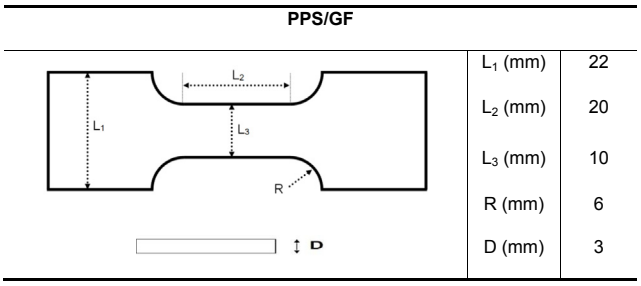

Fig. 1. Used specimen dimension of PPS/GF composite.

2.2.3. Dynamic thermo-mechanical analysis (DMTA)

Thermo-mechanical (DMTA) tests have been performed on PPS/GF composite samples using DMA Q 800 instrument, from TA Company, in order to measure the main transitions temperatures and to characterize the viscoelastic behavior of the polymer. The tests have been realized at following condition: alternating bending configuration; temperature range 25 °C–250 °C; frequency from 0.1 Hz to 50 Hz; temperature rate 2 °C/min. The sample has a rectangular shape with 35 × 12 × 3 mm^3 dimensions.

2.2.4. Thermal gravimetric analysis (TGA)

Thermal mass change of PPS/GF samples was followed using TGA Q500, the temperature program is from room temperature to 800 °C with 10 °C/min in the nitrogen atmosphere (40 ml/min). The original sample mass is 12.32 mg, which is put in the Al_2O_3 crucible (85 µL). This test may give an idea about the thermal stability of the polymer.

2.3. Tensile and fatigue devices

Tensile properties were measured with an INSTRON 5966 machine at room temperature. Dog bone shape samples (see Fig. 1) were used. The displacement rate was 0.5 mm/min. The load cell capacity was of 10 kN.

Tension-tension fatigue tests were performed at different applied maximum stresses on MTS 830 hydraulic fatigue machine. The minimum applied stress is always chosen to be equal to 10% of the maximum applied stress (R = 0.1). In this paper, the results of experiments performed at two frequencies 10 Hz and 50 Hz are presented. In order to measure precisely the stiffness reduction due to the first loading stage (initial damage), each fatigue test is preceded by a quasi-static tensile loading-unloading-reloading stage.

During cyclic loading, the rising temperature (due to self-heating) has been measured on the surface of the specimens using an infrared camera (Raynger-MX4). The damage effect has been evaluated through the measurement of the Young's modulus evolution. In this work, the experimental fatigue tests have been performed on the sample with the geometry as shown in Fig. 1. Fatigue experiments have been achieved at different load directions, amplitudes and frequencies.

3. Results and discussion

3.1. Characterization of microstructure

Fig. 2(a) is an optical microscopy photo after composite pyrolysis. Image analysis reveals short glass fibers with a diameter of about 15 µm and the length ranging from 70 to 360 µm with an average length of about 200 µm. This important dispersion of the length of the fibers can be explained by the fact that a large number of the fibers are broken during extrusion and injection by the metal screws. Fig. 2(b) show a typical microstructure of the PPS/GF composite obtained by SEM observation. One can notice that a large number of fibers are oriented in the mold flow direction.

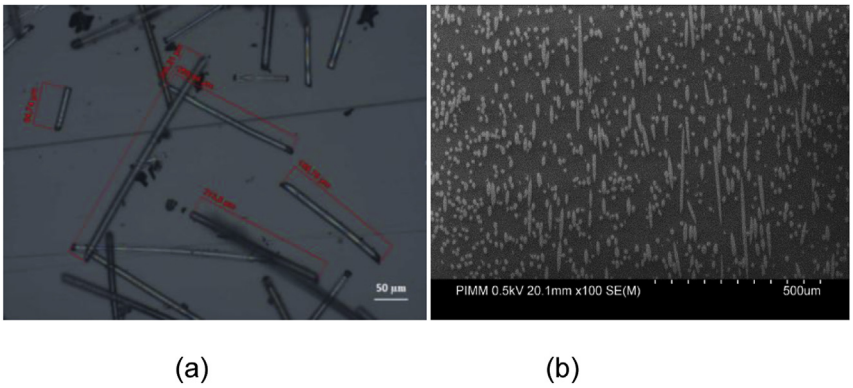

Fig. 2. (a) Optical microscopy photo after pyrolysis and (b) typical SEM PPS/GF microstructure.

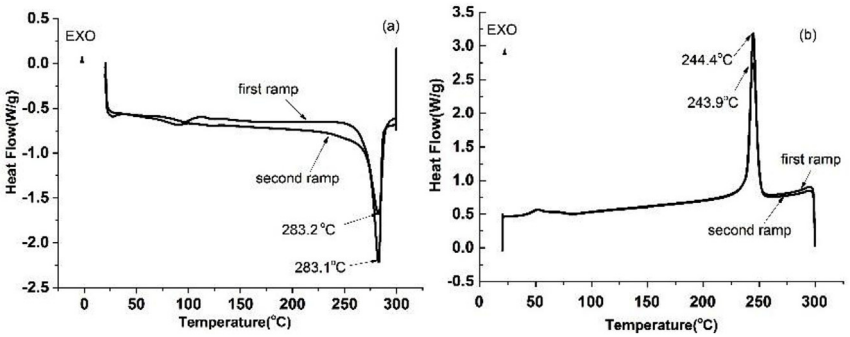

Fig. 3. DSC results performed on PPS/GF with two heating (a) and cooling (b) cycles.

3.2. Physicochemical characterization

3.2.1. DSC analysis

Fig. 3 shows the heat-cooling curves of PPS/GF after two cycles. According to the results, it is notable that the second heat-cooling cycle follows the first one in the same way and two cycles show almost the same melting point (T_m) and crystallization temperature (T_c). This reversible effect means that PPS/GF composite material is thermally stable and even heating up to 300 °C, its characteristics don't change. The results show that for PPS/GF composite material, T_m is about 283 °C and T_c is about 244 °C.

3.2.2. TGA characterization

The TGA curve of PPS/GF is shown in Fig. 4. The results show that the PPS/GF has no obvious weight loss before 370 °C. From this temperature until to 500 °C, the sample losses almost 10% of its initial weight. Then, the kinetic of weight loss changes indicates another mechanism. At the end of TGA test, all matrixes will be pyrolized and only the mineral glass fibers will remain in the system (almost 60%). In view of these TGA results, one can conclude that PPS/GF owns good thermal stability.

3.3. Thermo-mechanical properties

3.3.1. DMTA measurement

DMTA test is especially performed to study the thermomechanical behavior of the polymer and to determine the diverse transitions and change of physical state of polymers. In this work, DMTA tests have been performed according to alternating bending configuration, with the frequency of 1 Hz. The result of DMTA test is shown in Fig. 5. All three curves (E′, E″ and tanδ) show three physical state regions: glassy state, glass transition zone (called also α-transition) and rubbery state. From this result, it can be seen that PPS/GF exhibits a glassy state up to 80 °C. In this region the change of E′, E″ and tanδ is not significant. In glassy state, E′ is relatively high (> 3700 MPa). The second zone (between 80 °C and 160 °C) is α-transition zone. It corresponds to glass

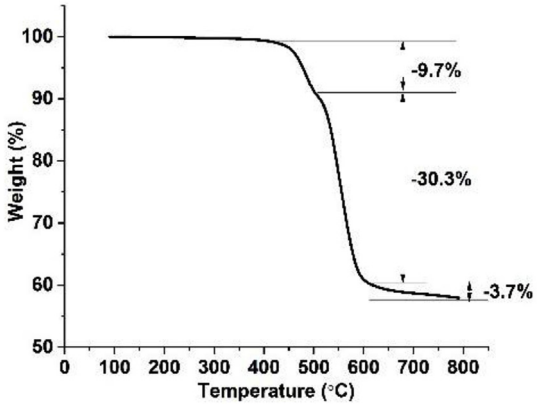

Fig. 4. TGA curve of PPS/GF.

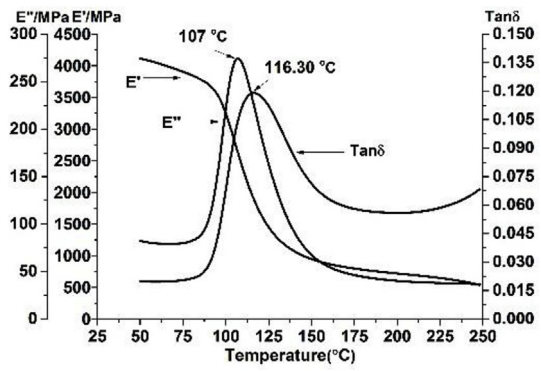

Fig. 5. DMTA test performed on PPS/GF.

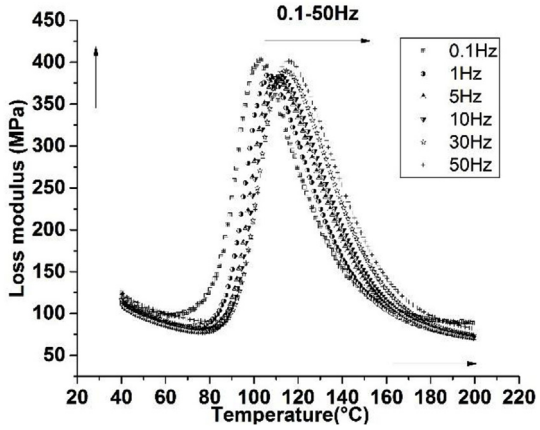

Fig. 6. Effect of frequency on loss modulus spectrum of PPS/GF compositein the range of 0.1 Hz–50 Hz.

transition phenomenon. In this zone, E′ decreases drastically from 3700 MPa to a value lower than 800 MPa. E″ increases first and then decreases; showing a pic at 107 °C (α-transition temperature). This value may be considered as glass transition temperature of the polymer. tanδ (E''/E′) shows the same tendency as E''. The rubbery state of PPS/GF, is then in the zone of temperature higher than 160 °C. As it can be seen the value of E′ in this state is low (< 800 MPa) and the sample is relatively soft.

3.3.2. WLF equation

To explore the effect of temperature on viscoelastic properties of PPS/GF, multi-frequencies DMA test was conducted on PPS-90° specimens in flexural bending mode and the results are shown in Fig. 6. One can note that when increasing frequency, the α-transition temperature, Tα (related to Tg) has an increasing trend to high temperatures. This evolution may be followed by WLF equation [30]:

$$\log \frac{f}{fr} = \frac{-C1(Ta - Tar)}{C2 + (Ta - Tar)} \quad (1)$$

where f is the frequency; T is the temperature; $T_{\alpha r}$ (1 Hz) is the reference temperature at reference frequency, f_r. C1 = B/(2.303 f_g) and C2 = $f_g/\Delta\alpha$ are WLF constants with f_g, free volume fraction, Δα heat expansion coefficient and B, a constant near to 1.

By linear regression method, WLF equation has been transformed to the following linear equation:

$$\frac{1}{\log \frac{f}{fr}} = \frac{-C2}{C1}\frac{1}{T - Tar} + \frac{1}{C1} \quad (2)$$

Then, $\frac{1}{\log \frac{f}{fr}}$ was plotted against $\frac{1}{T-Tar}$. A fitted curve to a linear function

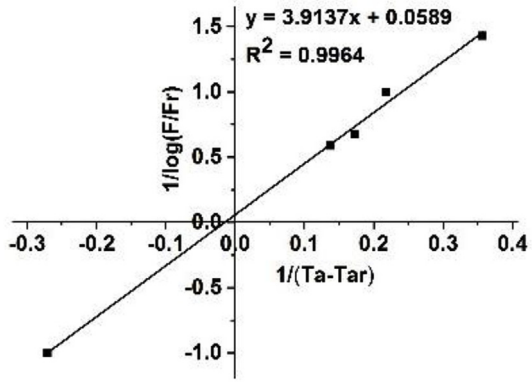

Fig. 7. Linear regression of WLF equation.

Table 1
The values of WLF constants.

Composite	C1	C2	fg	Δα
PP/GF - 90°	17.0	66.4	2.56×10^{-2}	3.85×10^{-4}

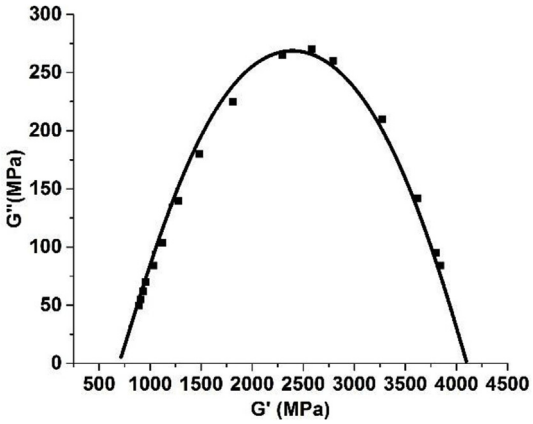

Fig. 8. Cole-Cole experimental diagram (the points) and Perez model (continuous curve).

with a correction coefficient (R^2 = 0.9964) is shown in Fig. 7. The value of C1, C2, fg and Δα are shown in Table 1. This means that PPS/GF composite under this study obeys the time-temperature equivalence principle.

3.3.3. Cole-Cole diagram

The viscoelastic behavior of PPS/GF composite may be shown by Perez model [31,32] using Cole-Cole method. The Cole-Cole diagram presents the variation of G'' (loss modulus) versus G' (storage modulus), obtained from the DMTA test on PPS-90° samples of PPS/GF (Fig. 8).

The Perez model gives an expression of the complex Young modulus G* as a function of frequency and relaxation time:

$$G^* = G' + i\,G'' = G_0 + \frac{G_\infty - G_0}{1 + Q(i\,\omega\,\tau)^k + (i\,\omega\,\tau)^{k'}} \quad (3)$$

where ω, the angular frequency, is equal to 2πf, G and G are respectively the relaxed (rubbery state) and unrelaxed modulus (glassy state) and τ is the relaxation time. k, k' and Q are the parameters of the model. Experimental (the points) and Perez model (continuous curve) Cole-Cole diagrams are shown in Fig. 8. This figure shows that with the identified values of the Perez model parameters shown in Table 2, the experimental Cole-Cole diagram is highly consistent with the chosen model. So, Perez model predict accurately the thermo-mechanical properties of PPS/GF.

3.4. Mechanical properties

3.4.1. Tensile behavior

The results of the stress-strain tensile tests on PPS-0° and PPS-90° specimens at the room temperature are shown in Fig. 9 and the main characteristics are registered in Table 3. As it can be seen, the value of Young's modulus of PPS-0° is about 6000 MPa, which is higher than that for PPS-90° (4300 MPa). Moreover, because of the fibers orientation, PPS-0° specimens have higher failure stress (104 MPa) than that of PPS-

Table 2
The value of the Perez model constants.

G_0 (MPa)	G_∞(MPa)	k	k'	Q	τ (s)
700	4130	0.22	0.16	0.5	0.6

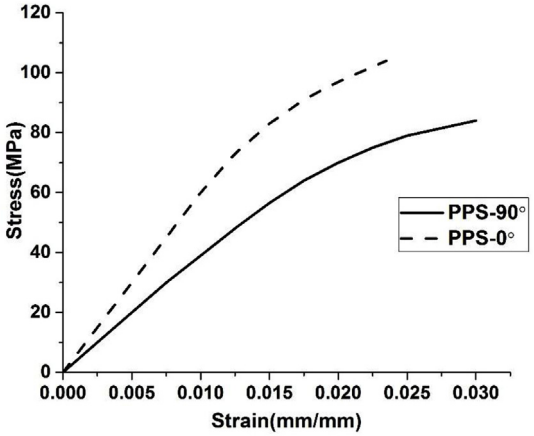

Fig. 9. PPS/GF typical tensile curves.

Table 3
Results of pure PPS, PPS-90° and PPS-0° samples obtained from tensile tests Standard deviation given by 5 repeated tests in each case.

	E(MPa)	σ_r(MPa)	ε_r(%)
Pure PPS [33]	3697	82	2.7
PPS-90°	4300 ± 41	84 ± 4.3	3 ± 0.14
PPS-0°	6000 ± 45	104 ± 4.4	2.85 ± 0.24

90° (84 MPa).

The results of tensile tests indicate that the reinforcement effect of the fibers remains relatively limited. This may be attributed to the small length of the fibers as shown before.

Moreover, the fracture surfaces after tensile failure, observed by SEM (see Fig. 10) allow the following comments:

- The fibers with a diameter 10–15 μm, mostly oriented in the mold flow direction during injection, are pulled out during the last stage of the failure (see Fig. 10 (a; c)).
- It is obvious to conclude a very good adhesion between matrix and fibers, probably due to the presence of a coupling agent. Indeed, fiber pull-out is not consecutive to fiber-matrix interface failure but rather to micro-cracking of the matrix surrounding the interfaces. Hence, all the fibers remain coated by a thin layer of PPS matrix after pull-out.
- Two kinds of broken zones can be distinguished: The first one corresponds to brittle failure of the matrix which mostly occurs locally between longitudinal fibers (see the dotted circles in Fig. 10(a)). The second one shows local semi-ductile failure of the matrix around and between the fibers (see Fig. 10(b) and (c)). This phenomenon seems to be favored when the fibers are miss-oriented versus tensile axis.

In order to quantify the possibility of plastic deformation and damage development, loading-unloading tensile test with progressive increase of the maximum stress have been performed (to be shown in a further publication). It was shown that the non-linear behavior of the PPS/GF composite is essentially due to plasticity (no significant loss of stiffness was observed). Therefore, together with the above SEM observations, one can conclude that, under monotonic loading, the predominant non-linear deformation mechanism is the local plasticity of PPS matrix. Indeed, because of an excellent adhesion between fiber and matrix, no progressive damage due to fiber-matrix interface de-bonding occurs as it is classically observed in reinforced thermoplastics [34,35]. Moreover, at room temperature, PPS is far from the transitions α and β, which implies semi-brittle or semi-ductile behavior depending on the local state of stress. This local plasticity is also limited because of the presence of fibers. Finally, stress concentrations around the fibers lead to matrix cracking near the interfaces and to semi-ductile failure or semi-brittle failure between fibers depending on the local microstructure configuration. The final failure occurs after the coalescence of micro-cracks and pull-out of matrix-coated fibers.

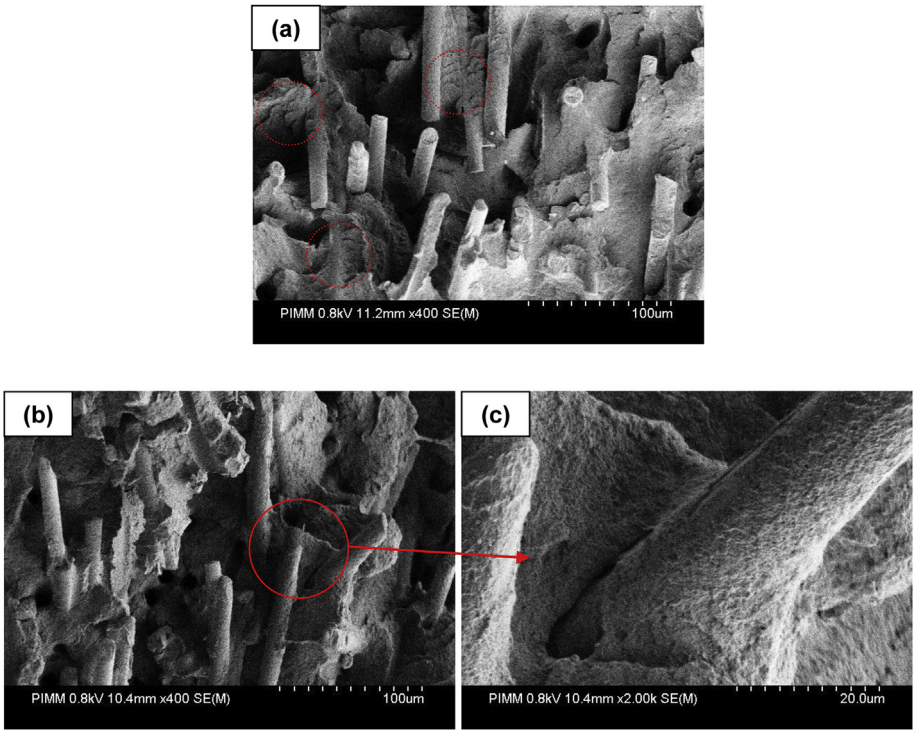

Fig. 10. SEM micrograph of PPS/GF composite fracture surface after tensile test. (a) Local brittle failure of the matrix between longitudinal fibers (PPS-0°); (b) and (c) local semi-ductile failure around the fiber (PPS-90°).

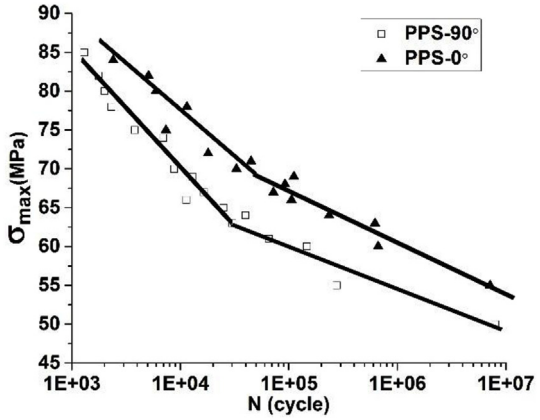

Fig. 11. Wöhler curves of PPS/GF composite performed on PPS-90° and PPS-0° specimens under tensile-tensile fatigue loading at the frequency of 10 Hz and room temperature, R = 0.1.

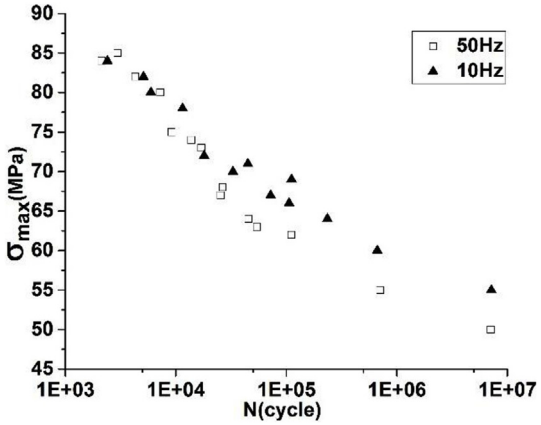

Fig. 12. The effect of frequency on the fatigue test results performed on PPS-0° samples, R = 0.1.

3.4.2. Fatigue behavior

3.4.2.1. Wöhler curves. Fig. 11 shows the Wöhler curves obtained in tension-tension tests at a frequency of 10 Hz for PPS-0° and PPS-90° specimens at room temperature.

From this figure one can have the following comments:

- For PPS-0°, and PPS-90° samples, the Wöhler curves don't show a clear asymptotic value representative of an endurance limit, σ_{end}. In contrast to metal materials, this is often observed in the case of thermoplastic composites [36].
- It is obvious that, for PPS-0°, their fibers' orientation shows more resistance against fatigue loading than that for PPS-90°. For example, under 60 MPa stress amplitude, PPS-90° is broken after 1×10^5 fatigue cycles. While for the same amplitude, PPS-0°, failure is observed after more than 1×10^6.
- For both two configurations, the Wöhler curves show two different domains; high and low stress amplitude. In each domain, SN curve can be modeled by a logarithmic linear expression:

$$\sigma_{max} = A.\ Log\ N + B$$

In this equation, A and B are the material parameters corresponding to the slope of the curve and the Y intercept, respectively. The slope A means the sensitivity of the fatigue resistance and the intercept B represents the apparent tensile strength.

Table 4 shows the value of A and B for PPS-0° and PPS-90° related to high and low stress domains.

3.4.2.2. Effect of frequency. 10 Hz and 50 Hz Wöhler curves obtained from fatigue test on PPS-0° specimens are shown in Fig. 12. As it can be seen, there is no evident difference between the two curves for the higher applied stresses (above 70 MPa). However, when the applied loading decreases, one can see obviously that samples submitted to higher frequency tends to have lower cycles to failure. As generally observed, with the improvement of frequency, the fatigue curve tends to shift to lower fatigue life. But in the case of PPS/GF it concerns only the lower range of amplitude. This will be further discussed.

Table 4
The values of A and B for PPS-0° and PPS-90° in each domain.

Samples	A (MPa)		B (MPa)	
	High stress domain	Low stress domain	High stress domain	Low stress domain
PPS-0°	−12.0	- 6.7	125.7	108
PPS-90°	−15.2	- 5.5	131	87.5

3.4.2.3. Self-heating phenomenon. In order to emphasize the effect of amplitude and frequency, it is generally appropriate to study the self-heating phenomenon under various fatigue conditions. Indeed, during the tensile-tensile fatigue test, the temperature of specimens increases. The intensity of self-heating is generally dependent on the applied stress amplitude and frequency. Figures (13 and 14) show the effect of these two parameters respectively. As shown in Fig. 13 (a), the temperature growth for PPS-90° samples is plotted versus the increasing cycle number. As expected, one can observe that self-heating is more pronounced for high values of the applied stress amplitudes. However, the maximum temperature reaches above 32 °C when applying high amplitude (85 MPa) while this value does not exceed 27 °C for amplitude of 65 MPa. Comparatively, for PPS-0° specimens (Fig. 13 (b)), the temperature increases at the beginning while after 4000 cycles, the temperature tends to decrease due to heat exchange with the external atmosphere. However, one can notice that the maximum temperature of self-heating also corresponds to the maximum applied amplitude (about 28.5 °C for PPS-0° at 85 MPa). Thus, one can conclude that self-heating under fatigue test is sensitive to the applied stress amplitude. While PPS-90° specimens develops more obvious self-heating phenomenon than PPS-0° specimens, one can also conclude to the influence of fiber orientation. Indeed, self-heating is due to local deformation of the matrix which is favored when the fibers are miss-oriented.

Fig. 14 shows the influence of frequency (10 Hz and 50 Hz) on self-heating. One can notice that applying a higher frequency (50 Hz) leads to a very fast temperature increases. The maximum temperature reached by a PPS-90° sample at 75 MPa is about 37.5 °C at breaking point where it does not exceed 27 °C for an applied frequency of 10 Hz. The same tendency is observed for PPS-0.

Therefore, one can conclude that:

- The amplitudes and frequencies affect obviously the self-heating phenomenon of PPS/GF composite [37].
- However, contrary to most of thermoplastic matrix based composite materials, the effect of self-heating observed in the condition of the performed experiments of this research work remains relatively limited. Indeed, the maximum temperature rise does not exceed 38 °C. At this temperature the matrix (presenting the α-transition temperature of 107 °C related to glass transition temperature) always remains at glassy state and its mechanical properties are not significantly influenced by temperature (see Fig. 5).
- Moreover, even if at room temperature, the composite is far from the ductile to brittle transition temperature, the fracture of the matrix remains almost brittle, especially because of the effect of the

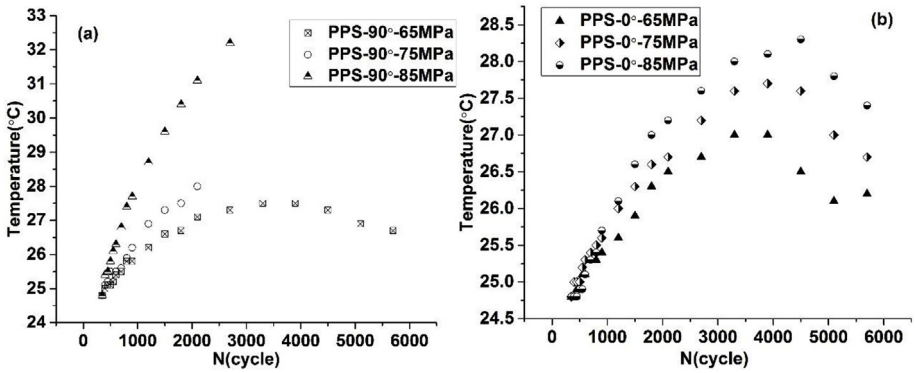

Fig. 13. Self-heating during fatigue tests (at 10 Hz), on PPS-90° (a) and PPS-0° (b) samples loaded under different amplitudes.

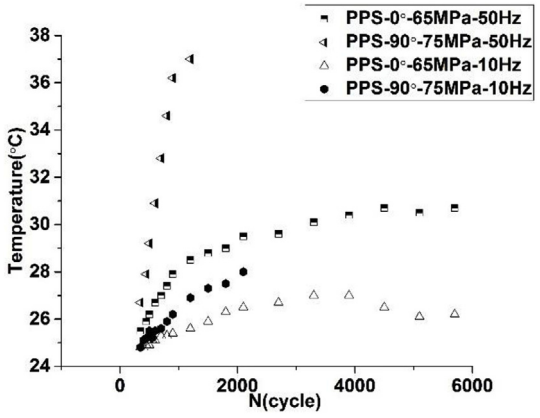

Fig. 14. Self-heating during fatigue tests with different frequencies, on PPS-90° and PPS-0° samples.

crystalline zones and the presence of the fibers.

3.4.2.4. Relative Young's modulus. The relative Young's modulus is generally identified to be an efficient parameter to detect the presence and evolution of damage during cyclic loading. It can also be used in a stiffness-based fatigue failure criterion [38]. The relative modulus is defined as the modulus E at each stage of fatigue test divided by the virgin material Young's modulus (i.e. without prior loading and damaging history), E_0. Fig. 15 shows the evolution of the relative modulus under different amplitudes at 10 Hz and 50 Hz. Fig. 15 (a) gives a global view of the Young's modulus evolution for an applied frequency of 10 Hz while Fig. 15(b) shows the same result for 50 Hz. For both frequencies, one can note the relative stability of Young's modulus which appears as a long plateau until failure, independently on the applied amplitudes. No significant loss of stiffness is observed: less than 1% at 10 Hz and less than 2% at 50 Hz. In regard to Figs. 5, 13 and 14, this very smooth evolution can be attributed to self-heating. This result is consistent with the conclusions drawn in paragraph concerning the local mechanisms observed in the case of monotonic loading (i.e. no damage development, local plasticity and semi-ductile failure).

3.4.2.5. Fracture surface analysis. In order to understand the influence of fiber orientation, amplitude and frequency on the fatigue life (Figs. 11 and 12), fracture surfaces have been investigated and the SEM observation are shown in Fig. 16.

Several observations can be drawn:

- Fracture surface of specimens submitted to high amplitude ((a) and (b)) show more rugged topography than those submitted to low level of stresses. Indeed, a high level of local stresses may result in sudden rupture and brittle failure of matrix around fiber clusters, especially when fibers are normally oriented to the principal stress ((b)).
- Under low applied stress amplitude, one can observe a semi-ductile failure due to the progressive accumulation of local plastic strain during cycling ((c) and (d)). Here again, normal orientation may amplify this effect ((d)).
- The application of higher frequency leads to more flat and homogeneous topography, indicating a more generalized plasticity of the continuous matrix leading to premature failure.

Here again, one can conclude semi-ductile or semi-brittle behavior driven by the local plasticity of the PPS matrix. No progressive damage is detected due to a very high strength of the fiber-matrix interface. Indeed, similarly to the monotonic loading case, the fibers are pulled out after local failure of the surrounding matrix without visible fiber-matrix interface debonding.

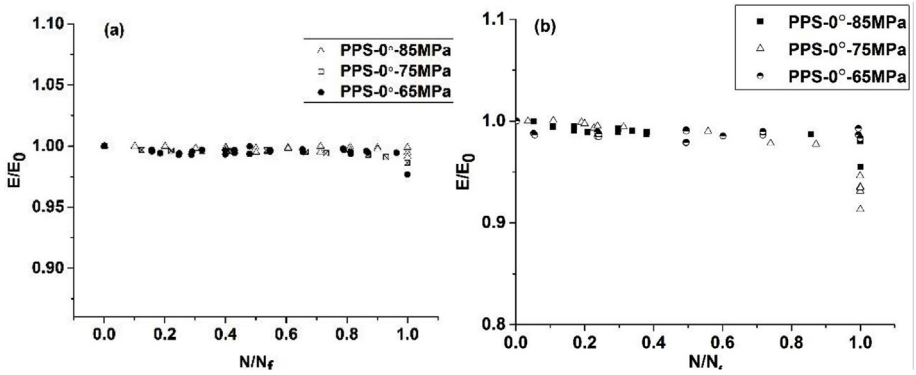

Fig. 15. Relative Young's modulus evolution of PPS-0° samples under different frequencies (a) 10 Hz, (b) 50 Hz.

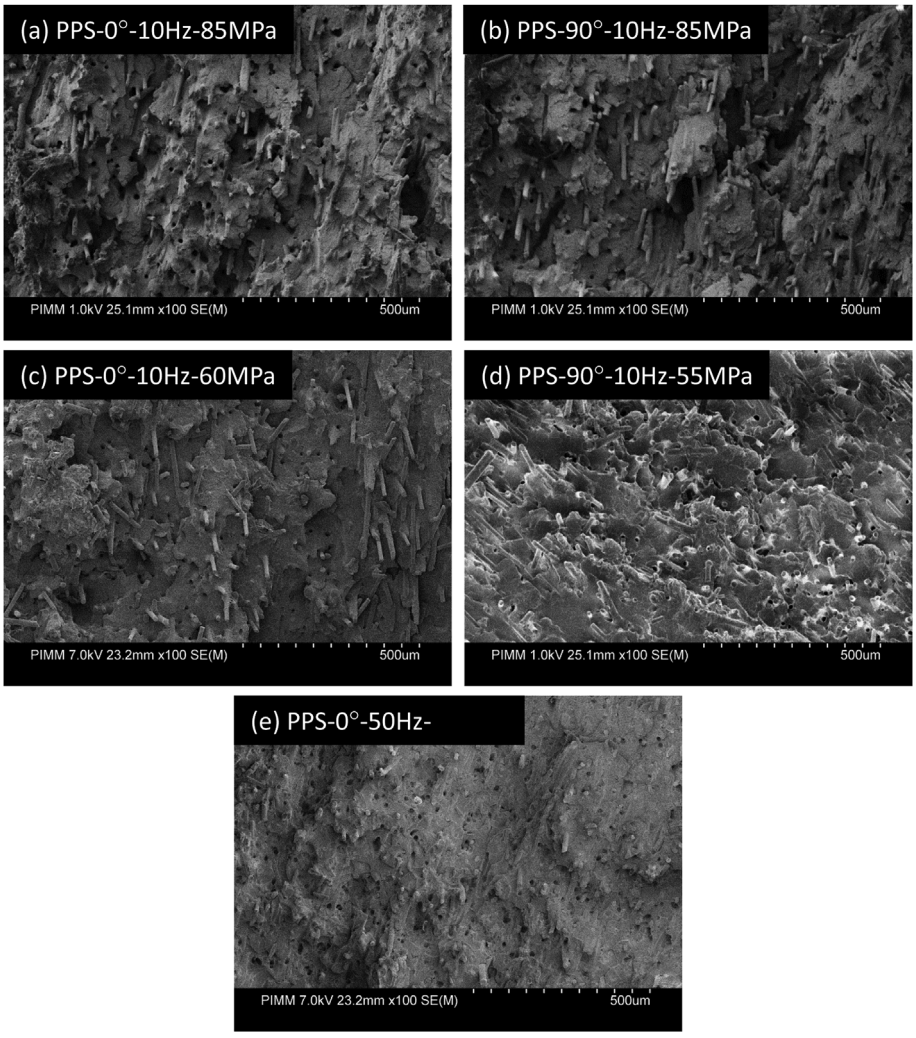

Fig. 16. SEM fracture surface observations for different fiber orientation, amplitude and frequency conditions.

4. Conclusion

In this paper, two kinds of PPS/GF samples (PPS-0°, PPS-90°) were prepared by injection molding. A complete characterization has been performed using several experimental methods. Microstructure, physico-chemical and mechanical properties have been explored including fatigue behavior and the different parameters affecting fatigue life. Finally, SEM fracture surface analysis provided a multi-scale interpretation of the origin of deformation and failure.

The main results can be summarized as follows:

- PPS/GF composites obey the time-temperature equivalence principle.
- Cole-Cole diagram has been successfully modeled by Perez model. It was shown that this model gives a good estimation of the viscoelastic properties of PPS/GF composites.
- Due to an excellent fiber-matrix adhesion, no progressive damage is developed, independently on the applied loading type (monotonic or fatigue).
- Even at high applied stress amplitude and high frequency, self-heating phenomenon observed during fatigue is not sufficiently pronounced to impact fatigue life of PPS/GF composite.
- Both monotonic and cyclic behaviors are essentially driven by the PPS matrix plastic deformation. However, at room temperature, the ability of the PPS matrix to develop plastic deformation remains limited.
- Consequently, final failure and fatigue life is highly dependent on the loading conditions (amplitude and frequency) and local microstructure.
- Bi-linear Whöler curves emphasized the influence of the loading amplitude. More brittle failure was observed at high amplitude and low frequency.
- Increasing frequency leads to lower fatigue life and more generalized plasticity.
- Fiber orientation in the loading direction improves both monotonic and fatigue strength.

Acknowledgement

The authors would like to thank China Scholarship Council (CSC) and the Valeo Company for the financial and technical support of this work.

References

[1] Pascault J, Williams R. Glass transition temperature versus conversion relationships for thermosetting polymers. J Polym Sci B Polym Phys 1990;28(1):85–95.
[2] Bogetti TA, Gillespie JW. Two-dimensional cure simulation of thick thermosetting composites. J Compos Mater 1991;25(3):239–73.
[3] Hayes BS, Seferis JC. Modification of thermosetting resins and composites through preformed polymer particles: a review. Polym Compos 2001;22(4):451–67.
[4] Gibson RF. A review of recent research on mechanics of multifunctional composite materials and structures. Compos Struct 2010;92(12):2793–810.
[5] Gabrion X, et al. About the thermomechanical behaviour of a carbon fibre

reinforced high-temperature thermoplastic composite. Compos Part B: Eng 2016;95:386–94.
[6] Eftekhari M, Fatemi A. Creep behavior and modeling of neat, talc-filled, and short glass fiber reinforced thermoplastics. Compos Part B: Eng 2016;97:68–83.
[7] Lu D, et al. Impact strength and crystallization behavior of nano-SiOx/poly (phenylene sulfide)(PPS) composites with heat-treated PPS. Macromol Mater Eng 2003;288(9):693–8.
[8] Del Saz-Orozco B, et al. Lignin particle- and wood flour-reinforced phenolic foams: friability, thermal stability and effect of hygrothermal aging on mechanical properties and morphology. Compos Part B: Eng 2015;80(Supplement C):154–61.
[9] Hill HW, Brady D. Properties, environmental stability, and molding characteristics of polyphenylene sulfide. Polym Eng Sci 1976;16(12):831–5.
[10] López LC, Wilkes GL. Non-isothermal crystallization kinetics of poly (p-phenylene sulphide). Polymer 1989;30(5):882–7.
[11] Caramaro L, et al. Morphology and mechanical performance of poly-phenylenesulfide carbon fiber composite. Polym Eng Sci 1991;31(17):1279–85.
[12] Favaloro M. Properties and processes of linear polyphenylene sulfide (PPS) for continuous fiber composites aerospace applications. SAE International; 2009.
[13] Christopher N, et al. Thermal degradation of poly (phenylene sulfide) and perfluoropoly (phenylene sulfide). J Appl Polym Sci 1968;12(4):863–70.
[14] Ehlers G, Fisch K, Powell W. Thermal degradation of polymers with phenylene units in the chain. II. Sulfur-containing polyarylenes. J Polym Sci 1 Polym Chem 1969;7(10):2955–67.
[15] Yu L, Bahadur S, Xue Q. An investigation of the friction and wear behaviors of ceramic particle filled polyphenylene sulfide composites. Wear 1998;214(1):54–63.
[16] Gyurova LA, Friedrich K. Artificial neural networks for predicting sliding friction and wear properties of polyphenylene sulfide composites. Tribol Int 2011;44(5):603–9.
[17] Zhao Q, Bahadur S. A study of the modification of the friction and wear behavior of polyphenylene sulfide by particulate Ag 2 S and PbTe fillers. Wear 1998;217(1):62–72.
[18] Jiang Z, et al. Study on friction and wear behavior of polyphenylene sulfide composites reinforced by short carbon fibers and sub-micro TiO 2 particles. Compos Sci Technol 2008;68(3):734–42.
[19] Yang Y, et al. Morphology control of nanofillers in poly (phenylene sulfide): a novel method to realize the exfoliation of nanoclay by SiO2 via melt shear flow. Compos Sci Technol 2013;75:28–34.
[20] De Baere I, et al. On the tension–tension fatigue behaviour of a carbon reinforced thermoplastic part II: evaluation of a dumbbell-shaped specimen. Polym Test 2011;30(6):663–72.
[21] Zhou S, et al. Effect of carbon fiber reinforcement on the mechanical and tribological properties of polyamide6/polyphenylene sulfide composites. Mater Des 2013;44:493–9.
[22] Yýlmaz T, Sýnmazçelik T. Investigation of load bearing performances of pin connected carbon/polyphenylene sulphide composites under static loading conditions. Mater Des 2007;28(2):520–7.
[23] Liang J-Z. Crystallization of glass fiber-reinforced poly(p-phenylene sulfide) nanocomposites. Polym Int 2012;61(4):511–5.
[24] Sliwa F, et al. Mechanical and interfacial properties of wood and bio-based thermoplastic composite. Compos Sci Technol 2012;72(14):1733–40.
[25] Díez-Pascual AM, Naffakh M. Tuning the properties of carbon fiber-reinforced poly (phenylene sulphide) laminates via incorporation of inorganic nanoparticles. Polymer 2012;53(12):2369–78.
[26] Liu B, et al. Interfacial shear strength of carbon fiber reinforced polyphenylene sulfide measured by the microbond test. Polym Test 2013;32(4):724–30.
[27] Vieille B, Aucher J, Taleb L. Carbon fiber fabric reinforced PPS laminates: influence of temperature on mechanical properties and behavior. Adv Polym Technol 2011;30(2):80–95.
[28] Lou A, Murtha T. Environmental effects on glass fiber reinforced PPS stampable composites. J Compos Mater 1987;21(10):910–24.
[29] Mandell JF, Huang D, McGarry F. Fatigue of glass and carbon fiber reinforced engineering thermoplastics. Polym Compos 1981;2(3):137–44.
[30] Williams ML, Landel RF, Ferry JD. The temperature dependence of relaxation mechanisms in amorphous polymers and other glass-forming liquids. J Am Chem Soc 1955;77(14):3701–7.
[31] Alberola N, Bergeret A. Physical modeling of the interphase in amorphous thermoplastic/glass bead composites. Polym Compos 1994;15(6):442–52.
[32] Cavaille J, Perez J, Johari G. Molecular theory for the rheology of glasses and polymers. Phys Rev B 1989;39(4):2411.
[33] Seppälä J, Heino M, Kapanen C. Injection-moulded blends of a thermotropic liquid crystalline polymer with polyethylene terephthalate, polypropylene, and polyphenylene sulfide. J Appl Polym Sci 1992;44(6):1051–60.
[34] Fitoussi J, Bocquet M, Meraghni F. Effect of the matrix behavior on the damage of ethylene–propylene glass fiber reinforced composite subjected to high strain rate tension. Compos Part B: Eng 2013;45(1):1181–91.
[35] Arif MF, et al. Multiscale fatigue damage characterization in short glass fiber reinforced polyamide-66. Compos Part B: Eng 2014;61:55–65.
[36] Fatemi A, Socie DF. A critical plane approach to multiaxial fatigue damage including out-of-phase loading. Fatig Fract Eng Mater Struct 1988;11(3):149–65.
[37] Bellenger V, Tcharkhtchi A, Castaing P. Thermal and mechanical fatigue of a PA66/glass fibers composite material. Int J Fatig 2006;28(10):1348–52.
[38] Degrieck J, Van Paepegem W. Fatigue damage modeling of fibre-reinforced composite materials. Appl Mech Rev 2001;54(4):279–300.

Article N°3:

P. Zuo, A. Tcharkhtchi, M. Shirinbayan, J. Fitoussi, F. Bakir, "Multi-scale physicochemical characterization of a short glass fiber reinforced Polyphenylene Sulfide composite under aging and its thermo-oxidative mechanism", Polymers for advanced technologies, 2018. In press.

Received: 30 August 2018 | Revised: 25 September 2018 | Accepted: 21 October 2018

DOI: 10.1002/pat.4495

RESEARCH ARTICLE

WILEY polymers advanced technologies

Multiscale physicochemical characterization of a short glass fiber–reinforced polyphenylene sulfide composite under aging and its thermo-oxidative mechanism

Peiyuan Zuo[1] | Abbas Tcharkhtchi[1] | Mohammadali Shirinbayan[1] | Joseph Fitoussi[1] | Farid Bakir[2]

[1] PIMM–UMR CNRS 8006, Arts et Métiers ParisTech, 75013 Paris, France

[2] Dynfluid, Arts et Métiers ParisTech, 75013 Paris, France

Correspondence
Peiyuan Zuo, Arts et Métiers ParisTech, PIMM–UMR CNRS 8006, 151 Boulevard de l'Hôpital, 75013 Paris, France.
Email: 2015-1027@ensam.eu

In this paper, the thermo-oxidation for a short glass fiber–reinforced polyphenylene sulfide (PPS/GF) composite was experimentally and theoretically studied by a wide range of physicochemical and mechanical techniques. The accelerated thermal aging temperatures were fixed at 100°C, 140°C, 160°C, 180°C, and 200°C. Firstly, the results of weight loss under aging indicate the formation of volatile products because of chain scission of end groups. Also, Fourier-transform infrared spectroscopy (FTIR) results suggest that the formation and accumulation of carbonyl group arising from the formation of hydroperoxides in oxidative propagation process. In all cases of different thermal oxidation temperatures, it is hard to observe some significant change about the concentration of carbonyl group during the induction time. This induction time depends inversely on the oxidation temperature. Moreover, the cross-linking and chain scissions exist together according to the results of rheological results and it is easier to see the cross-linking phenomenon at the beginning of oxidation while the chain scissions are more pronounced, with the oxidation process developing further. In aspect of mechanical properties, σ_{max} increases at the beginning of oxidation because of cross-linking, and subsequently, the σ_{max} always decreases because of thermo-oxidation of the PPS matrix. In addition, the detailed thermo-oxidation processes are fully discussed in the end of this study. A mechanistic schema has been proposed to present different oxidation reactions of PPS polymer and then a kinetic model has been extracted from this mechanism. Afterwards, the model has been verified by experimental results at different temperatures.

KEYWORDS

aging, mechanical properties, polyphenylene sulfide (PPS), rheology, thermo-oxidation mechanism modeling

1 | INTRODUCTION

Polyphenylene sulfide (PPS) is a thermoplastic polymer consisting of aromatic rings linked by sulfur atoms. It is widely used as a high performance engineering plastic with a unique combination of excellent mechanical and thermal properties. In detail, it is applied in a wide range, including automobile pieces, precision instruments, and aerospace products.[1-4]

As an engineering composite, PPS composite possesses high-temperature resistance combined with good mechanical properties. In our previous research,[5] we have comprehensively characterized this PPS composite and also fully discussed their fatigue behaviors. Moreover, since thermal treatment can have an important effect on mechanical properties of PPS materials, there are various researches focusing on this aspect. For example, Ma et al[6] studied the mechanical behaviors of PPS materials after heat treatment and they found

excessive heat treatment, longer than 2 days, resulted in over oxidative cross-linking and was detrimental to the thermal mechanical properties of the samples at high temperature. Zhai et al[7] also found the mechanical properties of glass fiber–reinforced PPS (PPS/GF) composites were negatively affected by thermal treatment. Moreover, in some study,[8] the authors verified the effect of thermal treatment on the tensile and in-plane shear behavior of carbon fiber-reinforced PPS composite specimens and the results suggested that there was a significant degradation of mechanical properties, and this degradation can be enhanced by increasing treatment temperature and time.

On the other hand, exploring the thermal degradation details about PPS materials can give us some more useful guidance in practice. Many researchers had focused their attention on aspect of thermal degradation of sulfur-containing aromatic polymers, PPS polymers, and their reinforced composites. For example, Yamashita et al[9] studied the photodegradation of sulfur-containing aromatic polymers: polyethersulfone (PESF) and polysulfone (PSF). It was found that the main chain scission and cross-linking occurred simultaneously during the photodegradation process of these two polymers. Moreover, Ehlers et al[10] clarified in-depth about the cross-linking phenomenon during the PPS aging process. They concluded that cleavage of carbon-sulfur bonds and abstraction of hydrogen from some of the rings resulted in chain fragments with phenyl- and phenylmercapto end groups. Also, cleavage of the C—SH bonds and abstraction of more hydrogen favored to produce hydrogen sulfide. Moreover, Li et al[11] studied thermal degradation process of PPS films in different atmospheres with the temperature ranging from 25°C to 790°C. In that research, they pointed out that most polymers contained weak bonds that were expected to break with a higher probability than other stronger bonds. When the thermal energy began to surpass the bond energies of various bonds in the PPS chains, a random chain scission took place and the rate of degradation would be enhanced rapidly. Also, Black et al[12] concluded the degradation mechanism of PPS involved a combination of cross-linking and chain scission reactions. In addition, some researchers[13] also studied the different aspects of PPS degradation and stabilization. They found that chemical end groups of polymer played an important role in the thermal oxidation of PPS and the coloration reasons of PPS were mainly derived from the accumulation of specific, colored products (eg, phenyl-phenyl moieties) and some intermolecular products. In other aspect, there are also some reports using different ways to investigate the degradation of PPS. For example, Perng et al[14] researched thermal decomposition characteristics of PPS by stepwise pyrolysis/gas chromatography/mass spectrometry (Py-GC/MS) and thermogravimetric analysis/mass spectrometry (TG/MS) techniques, they clarified the mechanism and kinetic model for thermal decomposition of PPS in-depth. Similarly, Christopher et al[15] studied thermal degradation of Poly (phenylene sulfide) by following the weight loss during the time of aging. All of these applied techniques are very powerful and favorable to explore extensive thermal oxidation mechanism of PPS materials.

However, there is no report talking about the exact thermo-oxidation process of PPS under air or oxygen and there is no research details concerning quantitative calculation of oxidation products from PPS materials during accelerated thermal aging process. Especially, there is no study talking about modeling of thermo-oxidation of PPS, but this modeling is very important to predict the lifetime of PPS materials.

So, in this paper, the main work is to follow the evolution of physicochemical and mechanical properties of PPS during accelerated aging at different temperatures. Afterwards, a mechanism has been proposed to describe the thermo-oxidation process of PPS materials. This mechanism can give us an access to obtain a kinetic model and also it can not only remarkably contribute to quantitative calculation of thermal oxidation products, but also leads to efficient prediction of thermos-oxidative lifetime for PPS materials.

2 | MATERIALS AND CHARACTERIZATION METHODS

2.1 | Materials and sample preparation

PPS composite materials reinforced with short glass fibers (30% weight fraction) were kindly supplied by Valeo Company in France. According to our previous research results,[5] image analysis of optical microscopy (OM) reveals short glass fibers with a diameter of about 15 μm and the length from 70 to 360 μm with an average length of about 200 μm after pyrolysis.

Moreover, the original plate with a thickness of 3 mm was used for preparing the films. First of all, one part of an original plate was cut and pasted on a base support. Then this complete specimen with a base support was fixed on a LEICA microtome. The LEICA RM2255 is a fully automatic, motorized rotary microtome with a separate control panel for creating thin sections of specimens of varying hardness for various domains, including industry, medicine and biology, etc. The apparatus can set up different moving forward speeds and obtain the variously needed cutting thickness by controlling accurate location distance automatically. For this study, the thickness of film is 20 μm and every film is put into one separate bag to stock and use in thermal aging research. Also, other basic parameters can be referred in Table 1.

Also, it should be emphasized that two kinds of specimen were used in this study. One kind is a film with a thickness of 20 μm, which was obtained by microtome. The other samples have a standard dimension (see Figure 1). In fact, the received PPS plates were cut by the Lokicoup Company with the desired sample dimension we have designed. All samples for the mechanical tests have the same standard dimensions.

The films with a thickness of 20 μm (obtained from PPS plate) and dog-bone shape samples were put into the ovens and the aging temperatures were fixed at 100°C, 140°C, 160°C, 180°C, and 200°C. It is necessary to describe that the accurate thermal test conditions are as follows:

1. For weight change test, four aging temperatures (100°C, 140°C, 180°C, and 200°C) were recorded from 0 hours to a maximum of 5256 hours.
2. For the Fourier-transform infrared spectroscopy (FTIR) test, the samples were taken at the aging time ranging from 0 hours to a

TABLE 1 Basic parameters of polyphenylene sulfide (PPS) composite materials

PPS	Fiber type	Density (g/cm^3)	T_g (°C)	T_m(°C)	T_c(°C)
Parameters	Short glass fiber	1.58	109	283	241

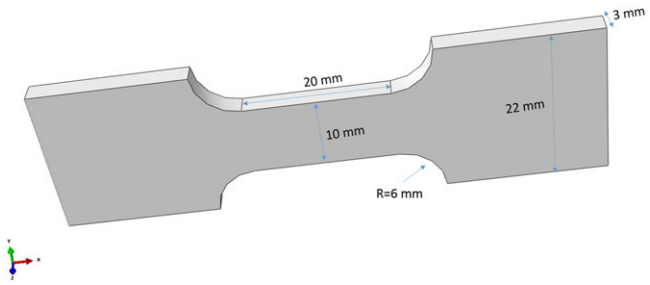

FIGURE 1 The detailed dimension of glass fiber–reinforced polyphenylene sulfide (PPS/GF) sample for tensile tests [Colour figure can be viewed at wileyonlinelibrary.com]

maximum of 5256 hour at four aging temperatures (140°C, 160°C, 180°C, and 200°C).

3. For the dynamic mechanical analysis (DMTA) test, four aging temperatures (100°C, 140°C, 180°C, and 200°C) were recorded from 0 hours to a maximum of 5688 hours.
4. For the ultraviolet (UV) test, a virgin film sample was used.
5. For rheological tests, virgin samples and aged samples at 180°C and 200°C were used. The aging time was chosen from 0 hours to a maximum of 606 hours.
6. For OM analysis, virgin sample and aged samples at 180°C and 200°C were used. The aging time was chosen from 0 hours to a maximum of 5256 hours.
7. For tensile test, four aging temperatures (100°C, 140°C, 180°C, and 200°C) were chosen, and the aging time was from 0 hours to a maximum of 5256 hours.

2.2 | Characterization methods

2.2.1 | Weight loss characterization

The dog-bone–shaped samples (in Figure 1) were prepared before the test, and afterwards, the samples were suspended in ovens, which can keep them in full contact with air at different temperatures. The weight of the sample was measured in different interval time points to observe the residual weight percent W%, and the calculation equation is as follows:

$$W\% = \frac{W_t}{W_0} * 100\% \quad (1)$$

Where W_t, is the weight in the time of t and W_0 is the weight of virgin sample.

2.2.2 | Tensile tests

Tensile properties were measured with an INSTRON 5966 machine at room temperature. The test velocity was 0.5 mm/min. Dog-bone–shaped samples (see Figure 1) were employed. The received PPS plates were cut by the Lokicoup Company with the desired sample dimension we needed. All samples for the mechanical tests have the same standard dimensions.

2.2.3 | Infrared analysis (FTIR)

FTIR spectrometry was used to characterize the extent of polymer oxidation, using a Nicolet impact 410 spectrophotometer in transmission mode. Measurements were made on spectra resulting from the accumulation of 32 runs, the resolution being 4 cm^{-1}. The film with a thickness of 20 μm (preparation by microtome) was used. The absorbance of carbonyl was converted to the concentration using a molar absorptivity of 300 L mol^{-1} cm^{-1} at the peak maximum (1780 cm^{-1}).[16] Also the concentration of [C═O] or other degradation products can be calculated according to the Beer–Lambert law, which is as follows:

$$C = \frac{A}{\varepsilon . \ e}. \quad (2)$$

Where A is the absorbance or optical density for the FTIR spectrum, e is the thickness of samples (20 μm) and ε is the extinction coefficient. Similarly, the concentration of [C—S] and [C—H] are calculated using the same way and the extinction coefficients for [C—S][17] and [C—H][18] are 114 and 42 L mol^{-1} cm^{-1}, respectively.

It should be emphasized that different film thickness will change the final values of concentration. In this manuscript, a standard thickness of 20 μm was chosen for all samples under study.

2.2.4 | Rheological characterization

Viscosity measurements were conducted by the Rheometer MCR 502 from Anton Paar. The tests were performed on film samples at different temperatures under nitrogen, as well as in a plate-plate configuration with a gap of 1 mm.

There are three main rheological tests in this study:

1. To see the viscosity evolution as a function of aging condition at 180°C, virgin and aged specimens were used and the experimental temperature was fixed at 290°C (strain = 0.2%, angular frequency = 1 rad s^{-1}).
2. To see the viscosity evolution as a function a time at a fixed temperature, one virgin specimen was used and the isothermal temperature was fixed at 290°C (strain = 0.2%, angular frequency = 1 rad s^{-1}).

3. To compare different rheological properties, virgin and aged samples from 180°C and 200°C were used and the experimental temperature was fixed at 300°C (strain = 0.2%, angular frequency ranging from 0.1 to 100 rad s^{-1}).

2.2.5 | Optical microscopy analysis (OM)

The oxidation layer thickness for PPS sample is measured by the OM technique and the plate samples are observed via Zeiss Axio Imager 2. The detailed operation can be briefly described as follows: virgin or aged samples from ovens were cut from crossing section and the prepared samples with a crossing section surface were observed by OM apparatus. The objective lens was chosen x 5 and the corresponding scale label was put on lower right corner of images. Finally, every three thickness points were measured to obtain the average thickness of oxidation layer.

2.2.6 | Dynamical mechanical analysis (DMTA)

DMTA tests have been performed on PPS/GF samples using DMTA Q800 instrument in order to measure the main transition temperatures and the characterization of viscoelastic behavior. The tests have been realized under the following condition: alternating bending configuration was necessary and test temperatures were chosen from 25°C to 200°C with a frequency ranging from 0.1 to 50 Hz as well as temperature rate at 0.5°C min^{-1}. The sample had a rectangular shape with a dimension of 35 × 12 × 3 mm^3.

2.2.7 | Ultraviolet (UV) spectrometry analysis

The UV spectrometry analysis does not only check the absence or presence of stabilizers in the materials, but can also be used to quantitatively calculate the amount of absent or present products. This spectra under study is obtained using PERKINELMER UV–visible spectrophotometer (model Lambda 5), equipped with an integrated sphere. They are recorded in absorbance mode 66 over a spectral range extending from 200 to 400 nm. The analysis of the data is done by applying the same method of IR spectrometry using the Beer–Lambert law.

3 | RESULTS

3.1 | Weight loss characterization

Thermo-gravimetric method is commonly used to follow the oxidation process, but it is important to emphasize that this method can only give information about the weight loss related to the volatile oxidation products, which means the small molecules are formed due to the scission at the end of molecular chains. Also, it should be noted that this technique cannot give more information when the chain scission is not at the end of chain and when the oxidative products are not volatile.

Figure 2 records the residual weight percent of PPS/GF samples as a function of aging time in the ovens fixed at different temperatures (100°C, 140°C, 180°C, and 200°C, respectively). For all of these tests, the weight loss ratio remains small (below 1%) until approximately 5000 hours, while the degradation trend is different under different oxidation temperatures. The result suggests that the weight loss contains several steps and also depends on oxidation temperatures. At the beginning, the samples loss some weight because of the evaporation of humidity or moisture in matrix. After long time aging (more than 2000 h), the sample aged under 100°C, 140°C stay stable without obvious weight loss while the weights of samples under 180°C and 200°C decrease obviously. This indicates that weight loss is highly dependent on applied thermal aging temperature.

3.2 | Evolution of chemical groups in PPS/GF composite

Figure 3 records the FTIR spectrum comparison of PPS from virgin sample and aged sample at 200°C–504 hours. Several remarkable changes can be noticed from the spectrum. First of all, the densities of C—H bonds corresponding to the wavenumber position of 2856 and 2923 cm^{-1} decrease sharply during aging process at 200°C. Also, it should be emphasized that after 504 hours, the C—H bond can hardly be detected, which suggests that a large amount of C—H bonds break during aging. Moreover, one can observe that C═O chemical groups increase in some relative extent after 504 hours. For C—S chemical bonds, it is difficult to distinguish some change from this whole spectrum. So, to get more information of the FTIR spectrum, more details about different chemical group concentrations are calculated from enlarged wavenumber positions corresponding to different chemical groups, which are shown in the following text.

In detail, the evolution of [C—S] concentration is shown in Figure 4. It is interesting to notice that the [C—S] concentration has a sudden decrease at the beginning of aging and subsequently it stays stable for a long time. But it should be emphasized that after

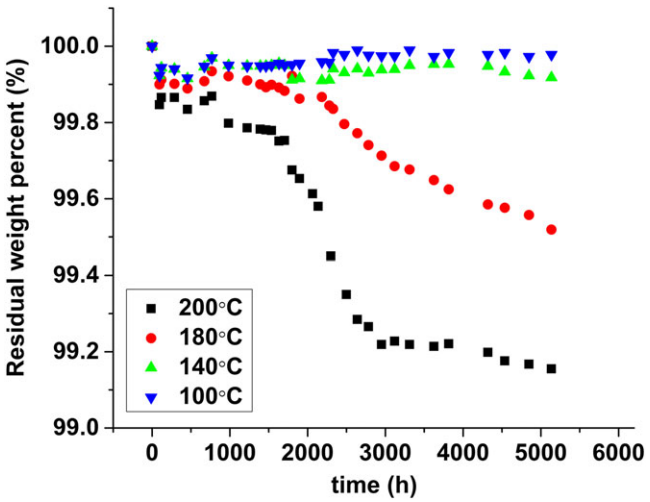

FIGURE 2 Residual weight percent versus different thermal aging temperatures and aging time [Colour figure can be viewed at wileyonlinelibrary.com]

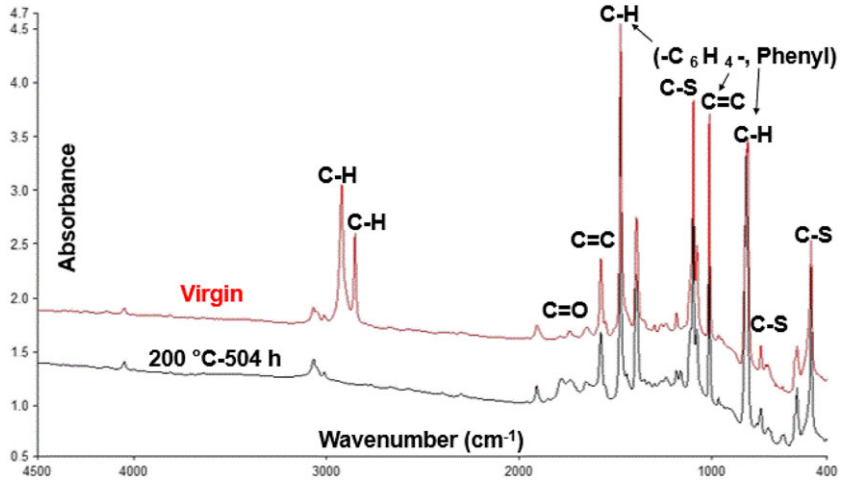

FIGURE 3 Fourier-transform infrared spectroscopy (FTIR) results for different polyphenylene sulfide (PPS) samples (virgin sample and aged sample at 200°C-504 h) [Colour figure can be viewed at wileyonlinelibrary.com]

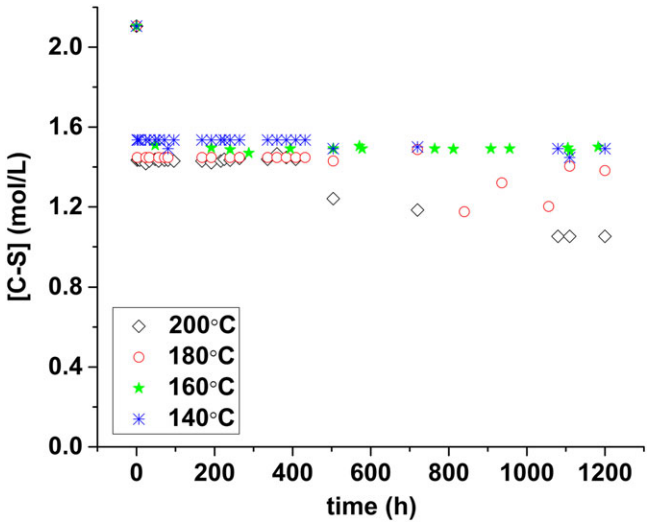

FIGURE 4 C—S concentration (1075 cm^{-1}) evolution as a function of oxidation time under different temperatures [Colour figure can be viewed at wileyonlinelibrary.com]

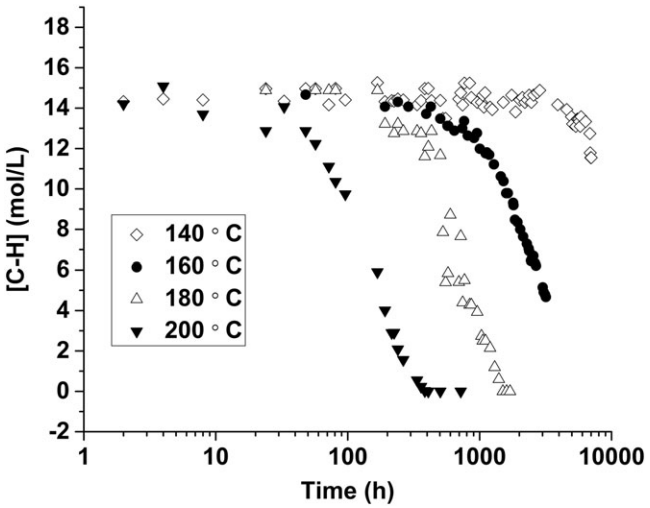

FIGURE 5 C—H concentration (2923 cm^{-1}) evolution versus oxidation time under different temperatures

500 hours, the [C—S] concentration starts to decrease in higher thermal oxidation temperatures (eg, 180°C, 200°C). How can we explain this phenomenon? The answer is as follows: according to the literature,[19,20] C—S (276 kJ mol^{-1}) is weaker than C—H (414 kJ mol^{-1}) bond and C═C (477 kJ mol^{-1}) from the view of bond energy theory. It suggests obviously that the [C—S] concentration slightly decreases because the weakest bond energy of C—S bond leads to breakage in the position of C—S bond. However, it should also be emphasized that PPS is one kind of polymer with sulfur atoms, which can easily have numerous cross-linking reactions, in return, leading to formation of other more stable cross-linking products containing C—S bonds.

The evolution of [C—H] concentration is shown in Figure 5, which is calculated according to the results of wavenumber position of 2923 cm^{-1}.[21] It is obvious to see that [C—H] concentration evolution highly depends on oxidation temperatures. In general, higher temperature corresponds to shorter induction time. For example, it can be seen that at 200°C, the [C—H] concentration decreases sharply starting from 33 hours while induction time at 180°C is about 192 hours. This indicates that decreasing oxidation temperature leads to significant delay of induction time. Comparatively, the propagation process tends to be finished after 400 hours at 200°C, while this time point for 180°C is by 2000 hours. Besides, at 160°C, the induction time and termination time of C—H bond rupture tend to be longer than the case in 180°C and 200°C. On the contrary, at 140°C, the corresponding oxidation phenomenon is too weak to detect until 5000 hours exposition according to the concentration of [C—H]. Until this time point of 5000 hours, [C—H] concentration does not appear an obvious decreasing trend.

Figure 6 shows the experimental results of C═O (1780 cm^{-1}) concentration evolution versus oxidation temperature and time.[21] In all cases, the curves have three different periods: In the first period, there is no change of C═O concentration and it remains nearly constant. It is interesting to note that at 200°C, the induction time of oxidation is less than 30 hours, while this value at 180°C is about 300 hours. In addition, it is noteworthy that the oxidation phenomenon at 160°C has a moderate oxidation trend before 1000 hours of oxidation. Comparatively, in the case of oxidation temperature at 140°C, there is no obvious increase of [C═O] until 1200 hours.

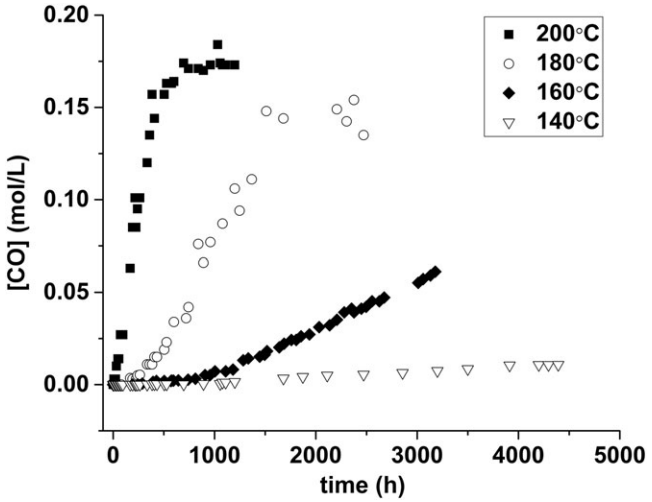

FIGURE 6 C=O concentration (1780 cm^{-1}) evolution as a function of oxidation time under different temperatures

The second step corresponds to the period of auto-acceleration of C=O formation. This auto-acceleration depends on oxidation temperature and it is more remarkable when the temperature is higher. In the third period, the amount of C=O from the formation is almost the same as that of disappearing. As a result, its concentration remains relatively constant. In the case of this study, after 1000 hours of oxidation at 200°C, the C=O concentration tends to be stable.

3.3 | Evolution of molecular weight

In order to follow the effect of aging on molecular weight of PPS, the viscosity of virgin and aged samples at molten state has been measured.

In this study, to characterize the thermal aging effects on different properties, five different aging temperatures ranging from 100°C to 200°C were chosen. It is reasonable to choose 180°C than 200°C for rheological study. This main reason is that the induction time of oxidation. According to the FTIR results, the induction time at 180°C is more than 300 hours while the value at 200°C is less than 30 hours. In other words, the aging temperature of 200°C leads to more rapid and serious degradation than 180°C. However, for the purpose of this research, the main goal is to see how the degradation happens at the beginning of oxidation. As a result, it is more logical to see the aging temperature with relatively longer and remarkable induction time since it is more reasonable to characterize the evolution of starting oxidation process rather than the period of serious oxidation at 200°C.

Table 2 gives the evolution of viscosity obtained from samples with different aging conditions. One can note that the viscosity has some increasing trend from 9700 to 9750 Pa s^{-1} at the beginning of oxidation from 0 to 30 hours. After that, the viscosity decreases with the oxidation time increasing, which means that thermo-oxidation favors to the diminution of molecular chain length during the aging time from 30 to 606 hours at 180°C. Also, one can see that the thickness of oxidation layer increases from 0 to 113 μm during this oxidation period.

TABLE 2 Values of complex viscosity η (pa s) as a function of time at the shear rate of 1 s^{-1} as well as the other parameters (viscosity measurement thickness of plate, D (mm) = 1, in the atmosphere of nitrogen at 290°C)

Time (h)	η (pa s)	Thickness of oxidation layer, d (μm)
Virgin	9700	0
180°C-30 h	9750	37 ± 8.4
180°C-48 h	3650	43 ± 6.2
180°C-240 h	3050	66 ± 2.3
180°C-571 h	3000	100 ± 3.8
180°C-606 h	1800	113 ± 12.9

4 | DISCUSSION

4.1 | Non-Arrhenius nature of induction time

As discussed, induction time (τ_{ind}) of oxidation phenomenon depends strongly on oxidation temperature. The induction time significantly decreases by increasing the temperature. Table 3 shows the induction time of oxidation at different temperatures. In order to study the nature of this phenomenon, $\ln\tau_{ind}$ is plotted versus 1/T.

The result of the relationship of ln (τ_{ind}) versus 1/T is shown in Figure 7. One can see clearly that the curve in this figure is not a linear curve; this may indicate that the Arrhenius Law cannot explain the temperature dependence of the oxidation induction period of PPS/GF.

TABLE 3 Induction time versus oxidation temperature

T (°C)	Induction time (h)
140	1200
160	890
180	260
200	25

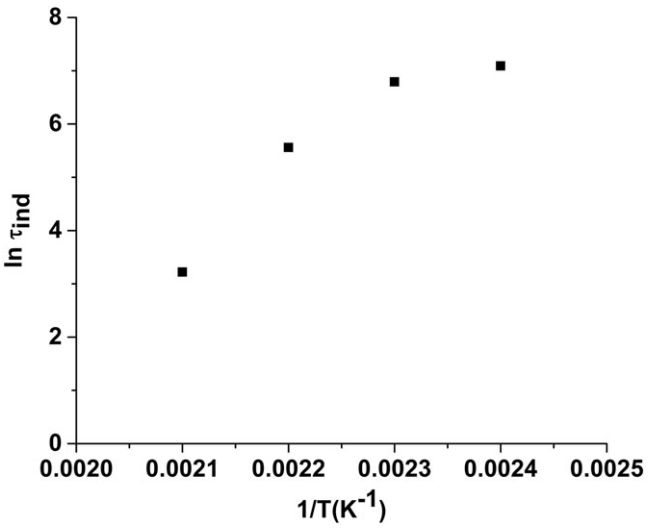

FIGURE 7 The relationship of ln (τ_{ind}) versus 1/T

In order to explain intensively and extensively, several tests have been performed.

4.2 | Rheological properties at molten state during oxidation

The viscosity at molten state gives information about molecular weight of polymers via the Mark–Houwink equation ($[\eta] = \eta_0 \times M^a$). That means higher viscosity corresponds to bigger macromolecules.[22,23]

Viscosity measurement was carried out on the sample of PPS/GF in the atmosphere of nitrogen with an isothermal condition of 290°C. The results are shown in Figure 8. The viscosity increases obviously with the time increasing. This improvement of viscosity is mainly because of the evolution of molecular weight by postpolycondensation. It should be emphasized that the molecular chain tends to be extended, not shortened with this high temperature.

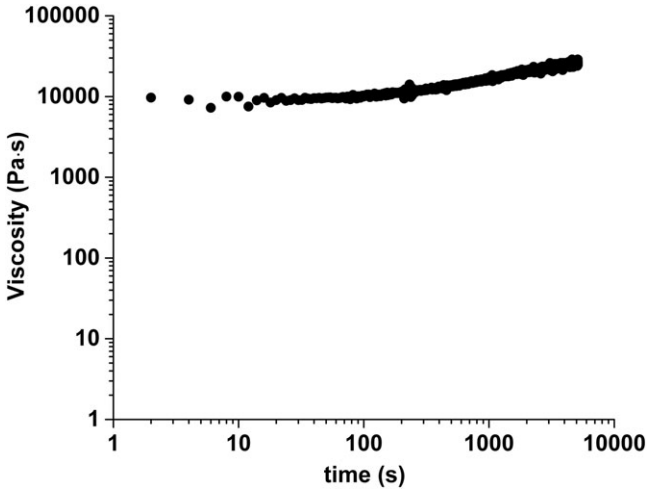

FIGURE 8 Viscosity evolution as a function of time for glass fiber–reinforced polyphenylene sulfide (PPS/GF) composite, in the atmosphere of nitrogen at 290°C

Other rheological tests were performed on virgin and aged (at 180°C and 200°C) samples of PPS/GF in the atmosphere of nitrogen at 300°C. Table 4 and 5 exhibits the evolution of storage modulus and viscosity of PPS/GF aged at different temperatures and times as a function of shear rate. In general, one can note evidently after oxidation, the rheology behavior of PPS/GF at molten state changes significantly.

i. Firstly, for all samples, storage modulus (G') favors to an increasing trend while viscosity (η) has a decreasing trend with the shear rate increasing.
ii. Moreover, η and G' firstly increase and subsequently decrease for aged samples. This process can be accelerated by aging temperature. In detail, for the samples aged at 180°C during 100 hours and 390 hours, η and G' increase, when compared with the virgin sample. This increase of viscosity and storage modulus can be attributed to the cross-linking phenomenon.
iii. Also it is interesting to notice when the oxidation time increases to 503 hours, η and G' are lower when compared with the aged sample after 390 hours at 180°C. The decrease of η and G' after a certain time of aging is attributed to the decrease of molecular weight arising from chains' scission.
iv. Also, in the case of 200°C, one can see also an obvious increase for the storage modulus and viscosity decrease with the increasing of shear rate.
v. In aspect of thermo-oxidation, the viscosity becomes higher after 100 hours of oxidation. This is also because of the cross-linking in PPS materials. However, after 339 hours of oxidation, the viscosity is very low, even lower than the case of virgin sample because of important chains' scission and obvious drop of molecular weight.
vi. The results also suggest that cross-linking takes place essentially during the induction period of PPS/GF thermo-oxidation. However, this phenomenon may continue even after this period when oxidation reaches to its auto-accelerated step.

TABLE 4 Values of storage modulus (G') of different samples at different shear rates

	PPS/GF	Shear rate (s^{-1})									
		0.1	0.25	0.4	1	2.5	4	10	25	40	100
G' (pa)	Virgin	898	1430	1680	2280	3050	3540	4940	7290	9040	14400
	180°C-100 h	3090	4000	4390	5100	6030	6630	8320	11000	13000	18800
	180°C-390 h	3000	6480	7450	7920	9820	11100	14600	19700	23400	34800
	180°C-503 h	2710	4930	5650	7010	8640	9740	12700	17300	20500	29300
	200°C-100 h	4460	6400	7170	8640	10400	11600	14800	20100	23900	36200
	200°C-339 h	132	105	107	119	137	148	163	155	159	-

TABLE 5 Values of viscosity of different samples at different shear rates

	PPS/GF	Shear rate (s^{-1})									
		0.1	0.25	0.4	1	2.5	4	10	25	40	100
η (pa s)	Virgin	12800	7810	5800	3170	1750	1320	791	505	410	276
	180°C-100 h	33700	17200	11900	5610	2750	1970	1060	610	473	292
	180°C-390 h	41200	30900	22100	9340	4780	3480	1920	1090	841	518
	180°C-503 h	34900	22900	16300	8090	4090	2950	1600	899	683	399
	200°C-100 h	52300	28600	20100	9810	4920	3550	1950	1150	899	570
	200°C-339 h	2670	883	575	257	114	76.1	34.8	16	10.6	4.17

vii. Also, it is worth noting that during the oxidation process of PPS/GF, the cross-linking and chain scissions exist together. At the beginning of oxidation (essentially in induction period), cross-linking is the predominant phenomenon, while the serious chain scissions are more pronounced with the oxidation developing further.

4.3 | Glass transition temperature evolution and mechanical properties

4.3.1 | Evolution of glass transition temperature

Figure 9 shows the T_g evolution as a function of aging time under different temperatures from 100°C to 200°C. The value of T_g is derived from the peak position of loss modulus via the DMA technique at 1 Hz. At all temperatures, with the increase of thermo-oxidation time, T_g tends to increase because of cross-linking of the PPS.[24] While with the temperature increasing, the T_g also has an improvement. This mainly means that for PPS/GF composites, the T_g value is sensitive to the aging time and temperature,[24,25] and thermal aging leads to the embrittlement phenomenon of PPS/GF composite.

4.3.2 | Evolution of maximum stress and Young's modulus

The mechanical properties as a function of aging time under different temperatures are recorded in Figure 10. Firstly, for all temperatures, σ_{max} increases very slightly at the beginning of oxidation because of the cross-linking phenomenon. After then, it drops progressively with the oxidation time increasing. For example, after approximately 3000 hours at 200°C, the σ_{max} reduces sharply from 84 to 40 MPa, while these values at 180°C and 100°C are 54 and 88 MPa, respectively. Also, it should be emphasized that intensive distributions of tensile test values sufficiently reflect the serious mechanical degradation evolution as a function of long time aging. This is also consistent with the DMTA analysis results. According to the DMTA results, one

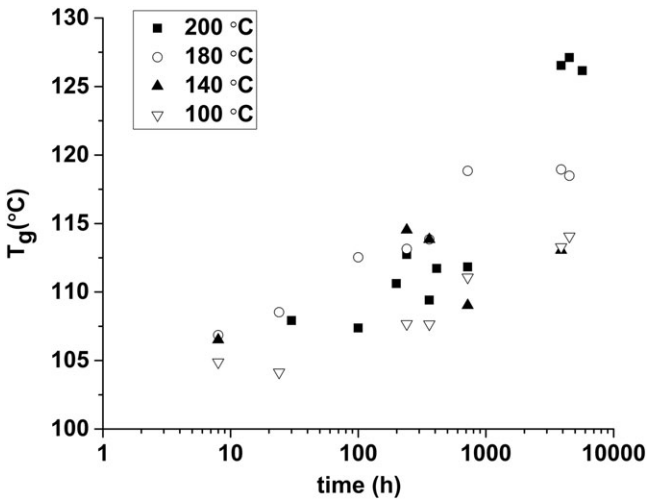

FIGURE 9 T_g evolution as a function of aging time under different temperatures, obtained from the DMA results at 1 Hz

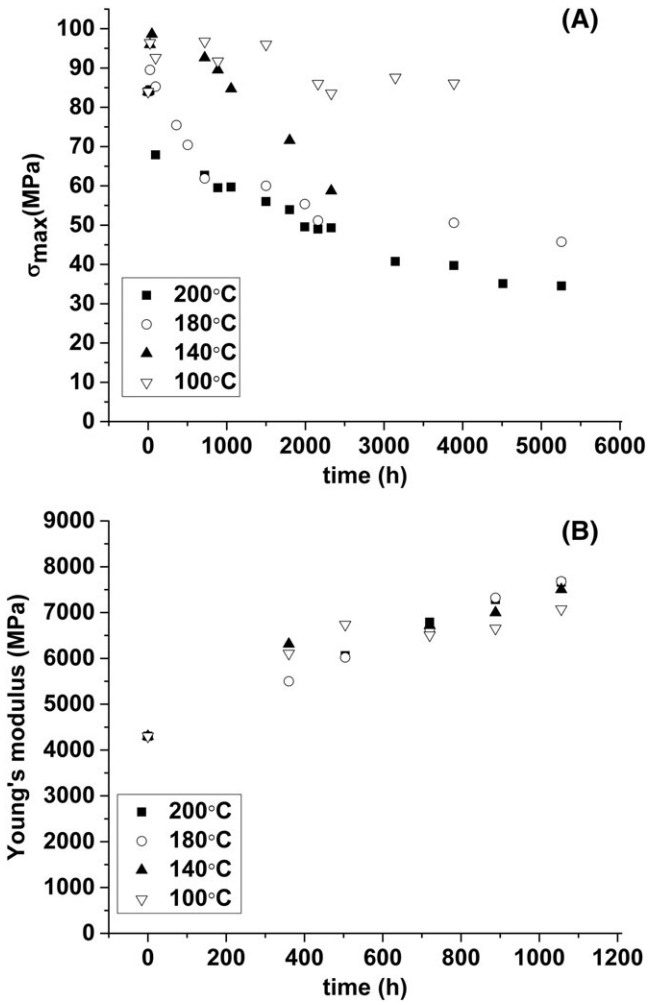

FIGURE 10 (a) Evolution of σ_{max} for glass fiber–reinforced polyphenylene sulfide (PPS/GF), as a function of oxidation time at different temperatures (100°C, 140°C, 180°C, and 200°C), and (b) evolution of E for PPS/GF, as a function of oxidation time at different temperatures (100°C, 140°C, 180°C, and 200°C)

can note the thermal aging temperature and time can affect sensitively T_g, and T_g increases dramatically with the higher aging temperature and longer aging time. This indicates thermal aging process triggers the molecular interaction or reaction and limits the mobility of molecules, making the material become brittle, which finally undermines the mechanical properties.[26]

Concerning Young's Modulus, as it can be seen, the virgin sample has a value of 4300 MPa. After aging, all of Yong's modulus values increase and this trend becomes more obvious with the aging temperature enhancing. Some researchers also reported that the thermal aging could enhance the Young's modulus.[26] This is in some extent because of the cross-linking reactions, which restrict the molecular mobility,[27] and this phenomenon is favored to higher Young's modulus.

4.4 | Thermo-oxidation mechanism

4.4.1 | UV measurement

In the absence of the supplier's information regarding antioxidant in the PPS/GF under study, UV spectrometry analysis is shown in

Figure 11 to detect the existing possibility of antioxidants in PPS material. One can see in the range of given spectrum, there is no obvious peak (283 nm) corresponding to the antioxidants (eg, benzophenolic group, Ar-OH).[28,29] This may indicate it is not easy to detect the antioxidants. In other words, this may imply that it is not necessary to take the effect of antioxidants into account under this research.

4.4.2 | Thermo-oxidation mechanism and corresponding kinetic equations

The standard thermo-oxidation mechanism of polymers under air or oxygen condition, which considers simultaneous process, is reported in several research works[30-32]:

On the basis of this standard mechanism, several researchers explained the degradation mechanism of PPS polymer or PPS composites.[9,20,33-36]

In order to propose an acceptable oxidation mechanism of PPS/GF, the first question is about the energy of different bonds. According to the literature,[19,20] C—S (276 kJ mol^{-1}) and C—H (414 kJ mol^{-1}) bond are weaker than the C═C (477 kJ mol^{-1}) from the view of bond energy theory. So, the first main scission happens in the position of C—S bond or C—H bond. In this case, the possible detailed reactions can be shown as follows[37]:

According to this schema, one can note clearly that the oxidative degradation process contains main routes which can start from the bond position of C—S or C—H. It is noteworthy that, as the past research,[30,38] the classic oxidative degradation mechanism of PPS can be displayed by the differential equations. With the use of these differential equations, it is possible to calculate quantitatively the C═O evolution as a function of time under different oxidative aging temperatures and the detailed equations are as follows:

$$\frac{d\left[P^{\circ}\right]}{dt} = 2{*}k_{1u}{*}[POOH] + k_{1b}{*}[POOH]^2 - k_2{*}\left[P^{\circ}\right]{*}[O] + k_3{*}\left[POO^{\circ}\right]{*}[PH] - 2{*}k_4{*}\left[P^{\circ}\right]^2 - k_5{*}\left[P^{\circ}\right]{*}\left[POO^{\circ}\right] + k_{h1}{*}[PH], \quad (3)$$

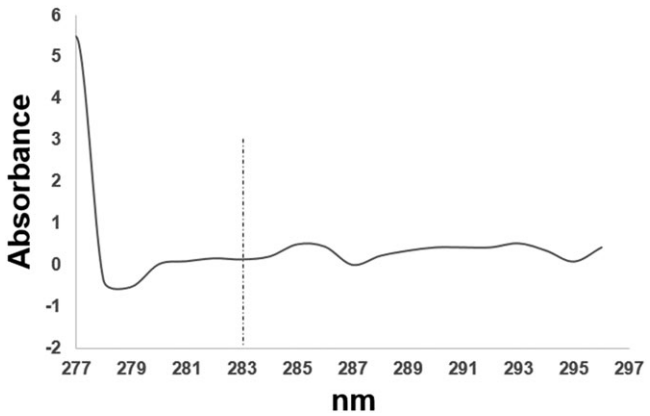

FIGURE 11 Ultraviolet (UV) spectrum of glass fiber–reinforced polyphenylene sulfide (PPS/GF) composites

$$\frac{d\left[POO^{\circ}\right]}{dt} = k_{1b}{*}[POOH]^2 + k_2{*}\left[P^{\circ}\right]{*}[O] - k_3{*}\left[POO^{\circ}\right]^2{*}[PH] - k_5{*}\left[P^{\circ}\right]{*}\left[POO^{\circ}\right] - 2{*}k_6{*}\left[POO^{\circ}\right]^2, \quad (4)$$

$$\frac{d[POOH]}{dt} = -k_{1u}{*}[POOH] - 2{*}k_{1b}{*}[POOH]^2 + k_3{*}\left[POO^{\circ}\right]{*}[PH], \quad (5)$$

$$\frac{d[PH]}{dt} = -k_3{*}\left[POO^{\circ}\right]{*}[PH] - k_{s1}{*}[PH], \quad (6)$$

$$\frac{d[CO]}{dt} = k_{1u}{*}[POOH] + k_{1b}{*}[POOH]^2, \quad (7)$$

$$\frac{d\left[P_1^{\circ}\right]}{dt} = k_{s1}{*}[PH] - k_{s2}{*}\left[P_1^{\circ}\right]\left[P_2^{\circ}\right]{*}[O], \quad (8)$$

$$\frac{d\left[P_2^{\circ}\right]}{dt} = k_{s1}{*}[PH] - k_{s2}{*}\left[P_1^{\circ}\right]\left[P_2^{\circ}\right]{*}[O], \quad (9)$$

Here, $[P^{\circ}]$, $[POO^{\circ}]$, [POOH], [PH] stand for the concentration of alkyls radicals, peroxy radicals, hydroperoxides, and substrate, respectively. Also, two other possible radicals are marked as: $\left[P_1^{\circ}\right]$, $\left[P_2^{\circ}\right]$, respectively. The *k* series represent the kinetic constants of every equation.

4.5 | Modeling results

It should be emphasized that the concentration of [C—S] changes slightly according to the FTIR results. So, it may imply that this Step (1) in Schema 1 is a minor reaction. So, here, some simplification is taken and it is considered that $\left[P_1^{\circ}\right]$, $\left[P_2^{\circ}\right]$ concentrations are very small (approximately 0). Also the classical mechanistic oxidation mechanism (closed loop) mainly takes k_{1u} to k_6 into consideration.

On the basis of the analysis in mind, to prove the correctness of our proposed differential equations of oxidative degradation process, the experimental results are verified by the modeling curve from differential equations and we choose the data of 160°C, 180°C, and 200°C as an example.

With the tool of MATLAB software, the simulative verification process can be drawn that it is practical to give a group of random values for k_{1u} to k_6 from related literatures and the differential equations are also input into the MATLAB program. Subsequently, these values can be adjusted progressively to obtain a good modeling result. That is to say, this simulative verification process can be converted by solving differential equations and compared with the experimental results (the MATLAB program created by ourselves can realize this process automatically). The modeling results are shown in Figure 12 and in Table 6.

One can see the experimental results are highly superposed with the modeling. This definitely implies that our proposed oxidative degradation mechanism is correct. According to the analysis, one can conclude that with this modeling, we can precise the oxidative degradation process in a quantitative way and predict the lifetime of PPS/GF composites under the service of thermal condition in practice.

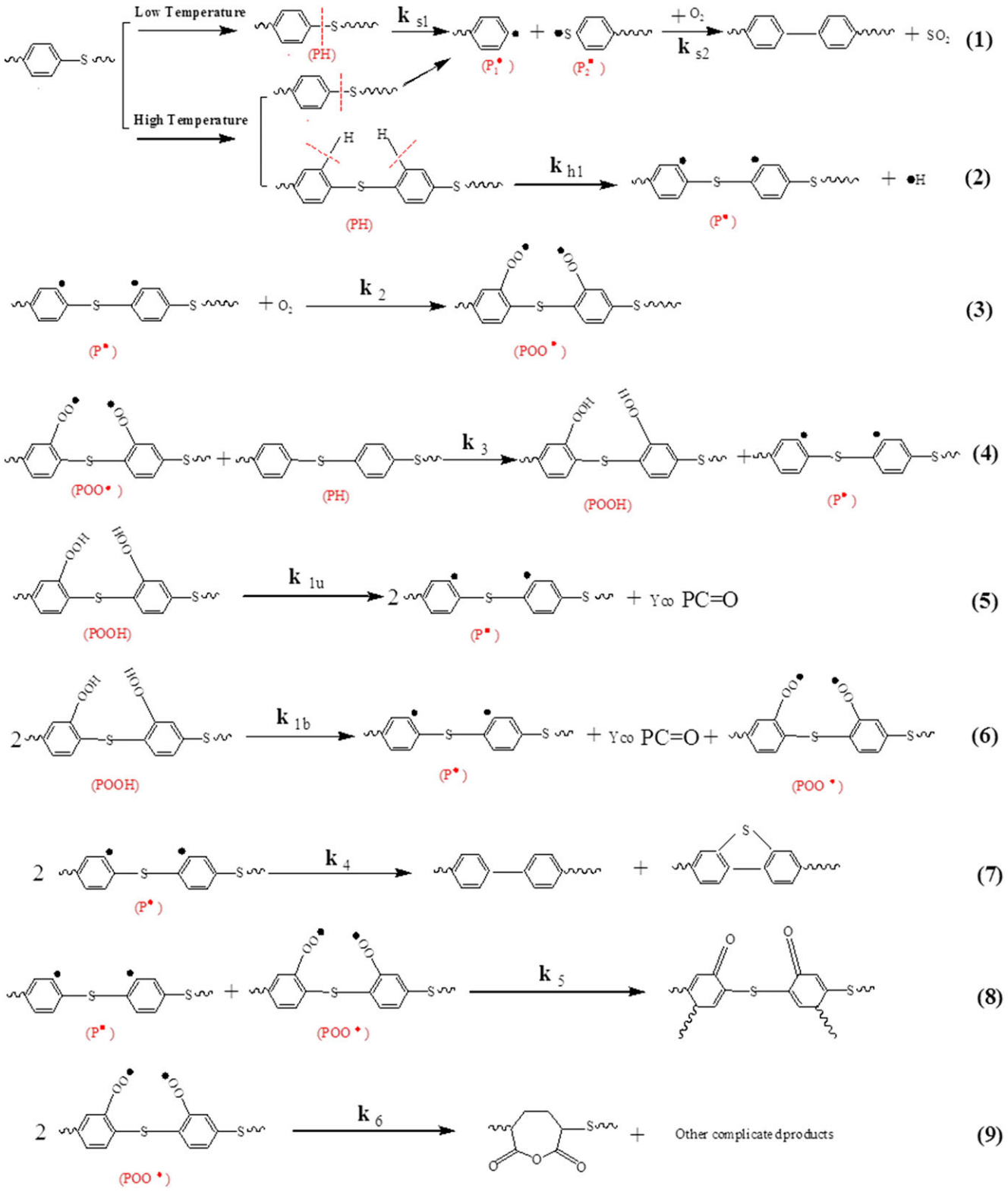

SCHEMA 1 Possible schematic diagram for the degradation of PPS/GF composite in air. [Colour figure can be viewed at wileyonlinelibrary.com]

With the help of the Arrhenius equation:

$$\ln k = -\frac{E_a}{RT} + \ln A \tag{10}$$

We can also calculate the corresponding activation energy values according to the rate constants (see Figure 13 and Table 7).

One can have the following comments:

- For k_{1u}, it corresponds to activation energy of 33.4 kJ mol^{-1} and it is highest among all values. This means that the reaction related to k_{1u} is highly dependent on the aging temperature and increasing temperature can favor higher unimolecular hydroperoxide. In a wide range researches using classic polymer oxidation mechanism,[39-41] the activation energy is always the maximum. Why is always this case? Because this step (hydroperoxide build-up) is

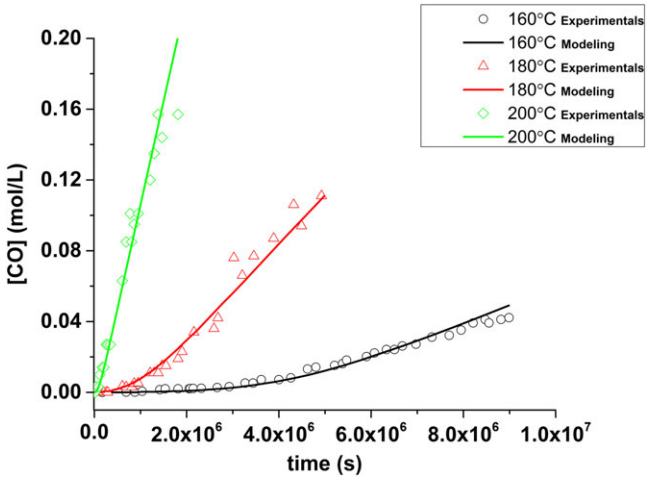

FIGURE 12 Modeling results of the thermo-oxidative equations at the peak of 1780 cm^{-1} under different aging temperatures: 160°C, 180°C, and 200°C [Colour figure can be viewed at wileyonlinelibrary.com]

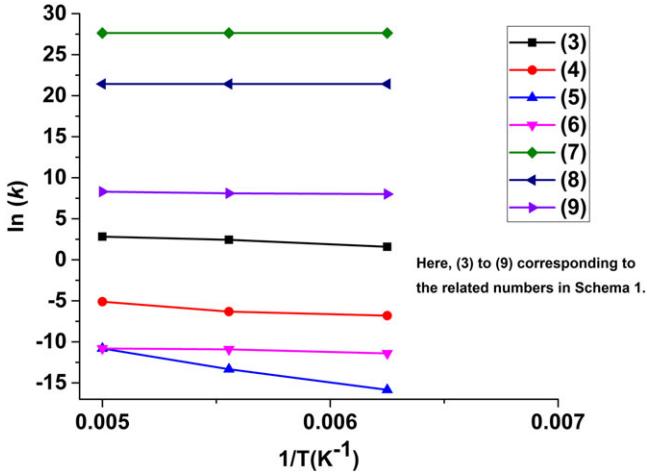

FIGURE 13 Relationship of ln (*k*) versus 1/T [Colour figure can be viewed at wileyonlinelibrary.com]

the controlling–speeding step for the oxidation, and it decides the fastness or slowness of the oxidation process.

- For k_{1b}, one can note that the corresponding activation energy is 4 kJ mol^{-1}, which is obviously lower than the value of k_{1u}. This implies that bimolecular hydroperoxide build-up is less sensitive to the aging temperature when compared with unimolecular hydroperoxide build-up. In addition, one can see that with the aging temperature increasing, k_{1u} and k_{1b} are more and more approaching the same values.
- For k_2, the activation energy is 8.4 kJ mol^{-1} and the constant of k_2 can be affected by aging temperature. It is interesting to note that "k_2 >> k_1." This is the step of propagation, which indicates the propagation process is highly quick and will finish once the initiation process starts.
- For k_3, the activation energy is 11.1 kJ mol^{-1} and it is interesting to note that "k_2 >> k_3 >> k_1." This is also the step of propagation. In addition, it should be noted that radical POO° is less stable than radical P°. If there is enough oxygen, POO° will react very faster than P°.
- For k_4, k_5, and k_6, the activation energies are very small (near 0 kJ mol^{-1}). This mainly indicates that the termination process is insensitive to the aging temperature.
- Moreover, the constants have the following order: k_4 > k_5 > k_6, k_2 >> k_3 >> k_1, which are in high agreement with other wide ranges of researches.[39-42]

4.6 | Influence of thermo-oxidative temperatures

It is worthy noticing that the slope of the propagation step (see Figure 14 and Table 8) obtained from the concentration [C═O] curve, is a good parameter to characterize the kinetic process of PPS oxidation.

Moreover, with the combination of the Arrhenius equation, one can calculate the activation energy, which is 20.7 kJ mol^{-1} and the R^2 is 0.99 (see Figure 15). These two methods give us a good guidance to calculate the thermal oxidation activation energy of PPS/GF composites.

According to the results, one can clearly conclude that the thermo-oxidation of PPS is highly sensitive to the applied temperature. Once the oxidation temperature increases, the induction time will shorten and the lifetime has an inverse trend.

As one can see, Figure 16 shows the comparison of the OM photos before and after degradation. The samples come from the dog-bone–shaped specimen with a crossing section surface before and after degradation. One can see the crossing section surface of virgin sample has a continuous and consistent gray color without any obvious difference while for the sample aged 5256 hours at 200°C, one can see the edge of crossing section surface has an obvious dark color and the degree of darkness tends to be light from exterior to interior. This change of color can mainly prove that the serious degradation happens in PPS/GF composite. In addition, because of the limitation of oxygen diffusion, the degradation trend of interior parts is less serious than that of exterior parts.

TABLE 6 Rate constants determined by inverse method

	k_{1u} (s^{-1})	k_{1b} (l Mol^{-1} s^{-1})	k_2 (l Mol^{-1} s^{-1})	k_3 (l Mol^{-1} s^{-1})	k_4 (l Mol^{-1} s^{-1})	k_5 (l Mol^{-1} s^{-1})	k_6 (l Mol^{-1} s^{-1})
T = 160°C	$1.3 \times 10^{(-7)}$	$1.1 \times 10^{(-5)}$	1.3×10^{6}	$1.1 \times 10^{(-3)}$	1.0×10^{12}	2.0×10^{9}	3.0×10^{3}
T = 180°C	$1.6 \times 10^{(-6)}$	$1.8 \times 10^{(-5)}$	1.5×10^{6}	$1.8 \times 10^{(-3)}$	1.0×10^{12}	2.0×10^{9}	3.4×10^{3}
T = 200°C	$2.0 \times 10^{(-5)}$	$2.0 \times 10^{(-5)}$	1.6×10^{6}	$6.0 \times 10^{(-3)}$	1.0×10^{12}	2.0×10^{9}	4.0×10^{3}

TABLE 7 Activation energy determined by inverse method

Number in Schema 1	(3)	(4)	(5)	(6)	(7)	(8)	(9)
Activation energy (kJ mol^{-1})	8.4	11.1	33.4	4.0	0	0	1.8
R^2	0.98	0.91	0.99	0.91	1	1	0.94

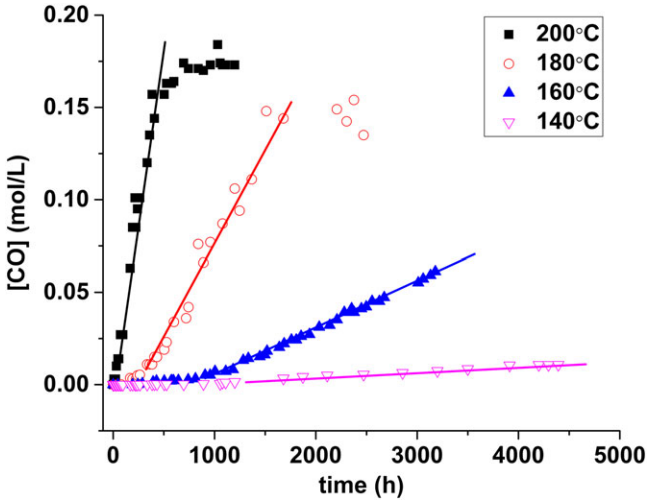

FIGURE 14 The slope of the concentration [C═O] in different oxidation temperatures, in step of propagation [Colour figure can be viewed at wileyonlinelibrary.com]

TABLE 8 Rate constants determined by inverse method in step of propagation

T (°C)	Slope
140	1.8*10^(−6)
160	2.3*10^(−5)
180	1.2*10^(−4)
200	3.6*10^(−4)

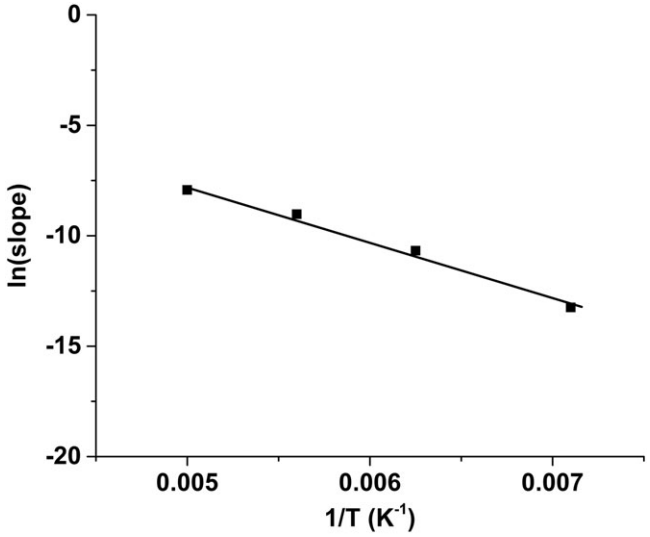

FIGURE 15 The relationship of ln (slope) versus 1/T

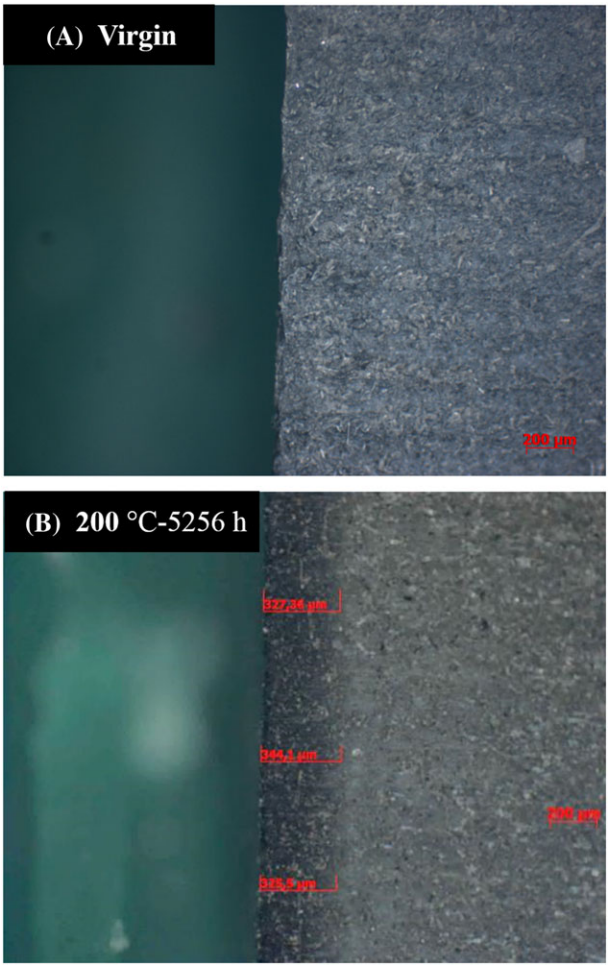

FIGURE 16 (a) Optical microscopy observation on crossing section surface of virgin sample, and (b) optical microscopy observation on crossing section surface of sample aged at 200°C-5256 hours [Colour figure can be viewed at wileyonlinelibrary.com]

5 | CONCLUSIONS

In this paper, the mechanism and modeling of thermo-oxidation for PPS/GF composites were studied. The main results are as follows:

According to the rheological results, during the oxidation process of PPS materials, the cross-linking and chain scissions exist together. At the beginning of oxidation, it is easier to see the cross-linking phenomenon, while the chain scissions are more pronounced with the oxidation developing further. In addition, to PPS/GF composites, the T_g value is sensitive to the aging time and temperature. Also, the mechanical strength first increases and subsequently decreases with the aging time and aging temperature increasing because of the predominance of embrittlement arising from thermal aging. In the end,

the possible schematic diagram for the degradation of PPS/GF composites was confirmed by the combination of experimental results and modeling of the differential equations from our proposed thermo-oxidative degradation mechanism. In general, higher temperature and longer oxidation time lead this PPS/GF material into more obvious degradation.

ACKNOWLEDGEMENTS

The authors are grateful to Dr. R.C. Benevides and Dr. Manuel Henner (Valeo) for collaboration and fruitful discussions. Valeo Company is also gratefully acknowledged for providing the material. Financial support from the CASCADE program under project "FSN Calcul Intensif et Simulation Numérique" by DGE is gratefully acknowledged.

The authors also thank China Scholarship Council (CSC) for their funding of Peiyuan Zuo's thesis.

ORCID

Peiyuan Zuo http://orcid.org/0000-0003-3140-8650

REFERENCES

1. Hill HW, Brady D. Properties, environmental stability, and molding characteristics of polyphenylene sulfide. *Polym Eng Sci*. 1976;16(12):831-835.
2. López LC, Wilkes GL. Non-isothermal crystallization kinetics of poly (p-phenylene sulphide). *Polymer*. 1989;30(5):882-887.
3. Caramaro L, Chabert B, Chauchard J, Vu-Khanh T. Morphology and mechanical performance of polyphenylenesulfide carbon fiber composite. *Polym Eng Sci*. 1991;31(17):1279-1285.
4. Favaloro M. Properties and processes of linear polyphenylene sulfide (PPS) for continuous fiber composites aerospace applications. SAE International2009.
5. Zuo P, Benevides RC, Laribi MA, et al. Multi-scale analysis of the effect of loading conditions on monotonic and fatigue behavior of a glass fiber reinforced polyphenylene sulfide (PPS) composite. *Composites Part B*. 2018;145:173-181.
6. Ma Y, Cong P, Liu X, Lv R, Li T. Effect of heat treatment on the mechanical and tribological properties of polyphenylene sulfide fiber materials. *J Macromol Sci, Part B*. 2014;53(12):1786-1799.
7. Zhai H, Zhou X, Fang L, Lu A. Study on mechanical properties of powder impregnated glass fiber reinforced poly (phenylene sulphide) by injection molding at various temperatures. *J Appl Polym Sci*. 2010;115(4):2019-2027.
8. Pantelakis SG, Katsiropoulos CV, Lefebure P. Effect of thermal treatment on the tensile and in-plane shear behavior of carbon fiber-reinforced poly (phenylene sulfide) composite specimens. *J Appl Polym Sci*. 2008;107(5):3190-3199.
9. Yamashita T, Tomitaka H, Kudo T, Horie K, Mita I. Degradation of sulfur-containing aromatic polymers: Photodegradation of polyethersulfone and polysulfone. *Polym Degrad Stab*. 1993;39(1):47-54.
10. Ehlers G, Fisch K, Powell W. Thermal degradation of polymers with phenylene units in the chain. II. Sulfur-containing polyarylenes. *J Polym Sci, Part A: Polym Chem*. 1969;7:2955-2967.
11. Li XG, Huang MR, Bai H, Yang YL. High-resolution thermogravimetry of polyphenylene sulfide film under four atmospheres. *J Appl Polym Sci*. 2002;83(10):2053-2059.
12. Black R, List C, Wells R. Thermal stability of p-phenylene sulphide polymers. *J Appl Chem*. 1967;17:269-275.
13. Deslauriers P, Geibel JF, Das P. Aspects of poly (p-phenylene sulfide) degradation and stabilization. Part 1. Influence of polymer end groups on exposure induced coloration. *Die Angewandte Makromolekulare Chemie*. 1997;247(1):45-59.
14. Perng L. Thermal decomposition characteristics of poly (phenylene sulfide) by stepwise Py-GC/MS and TG/MS techniques. *Polym Degrad Stab*. 2000;69(3):323-332.
15. Christopher N, Cotter J, Knight G, Wright W. Thermal degradation of poly (phenylene sulfide) and perfluoropoly (phenylene sulfide). *J Appl Polym Sci*. 1968;12(4):863-870.
16. Lisa G, Hamciuc C, Hamciuc E, Tudorachi N. Thermal and thermo-oxidative stability and probable degradation mechanism of some polyetherimides. *J Anal Appl Pyrolysis*. 2016;118:144-154.
17. Jing C, Lei Y, Jieping Z, Sidong L, Yongjun C, Kui X. Drying kinetics and cross-linking of sulfur prevulcanized thick natural rubber latex film. *Rubber Chem Technol*. 2013;86(1):57-67.
18. Matyshak V, Krylov O. Problems of quantitative spectroscopic measurements in heterogeneous catalysis: molar absorption coefficients of vibrations in adsorbed substances. *Kinet Catal*. 2002;43(3):391-407.
19. Li XG, Huang MR, Bai H. High-resolution thermogravimetry of poly (phenylene sulfide) film under four atmospheres. *J Appl Polym Sci*. 2002;83(9):1940-1946.
20. George K, Komalan C, Kumar P, Varughese K, Thomas S. Dynamic mechanical analysis of binary and ternary polymer blends based on nylon copolymer/EPDM rubber and EPM grafted maleic anhydride compatibilizer. 2007.
21. Zuo P, Fitoussi J, Shirinbayan M, Bakir F, Tcharkhtchi A. Thermal aging effects on overall mechanical behavior of short glass fiber reinforced polyphenylene sulfide composites. *Polym Eng Sci*. 2018. In press
22. Stacy CJ. Molecular weight distribution of polyphenylene sulfide by high temperature gel permeation chromatography. *J Appl Polym Sci*. 1986;32(3):3959-3969.
23. Housaki T, Satoh K. Molecular weight distribution of polyphenylene sulfide by high temperature gel permeation chromatography. *Polym J*. 1988;20(12):1163-1166.
24. Bandyopadhyay A, Valavala PK, Clancy TC, Wise KE, Odegard GM. Molecular modeling of crosslinked epoxy polymers: the effect of crosslink density on thermomechanical properties. *Polymer*. 2011;52(11):2445-2452.
25. Yang J, Xu T, Lu A, Zhang Q, Tan H, Fu Q. Preparation and properties of poly (p-phenylene sulfide)/multiwall carbon nanotube composites obtained by melt compounding. *Compos Sci Technol*. 2009;69(2):147-153.
26. Shafee EE. Effect of aging on the mechanical properties of cold-crystallized poly (trimethylene terephthalate). *Polymer*. 2003;44(13):3727-3732.
27. Kim SY, Lee TH, Park YI, et al. Influence of material properties on scratch-healing performance of polyacrylate-graft-polyurethane network that undergo thermally reversible crosslinking. *Polymer*. 2017;128:135-146.
28. Richaud E. Kinetic modelling of phenols consumption during polyethylene thermal oxidation. *Eur Polym J*. 2013;49(8):2223-2232.
29. Richaud E. Durabilité des géotextiles en polypropylène: Arts et Métiers ParisTech; 2006.
30. Richaud E, Farcas F, Fayolle B, Audouin L, Verdu J. Hydroperoxide build-up in the thermal oxidation of polypropylene–a kinetic study. *Polym Degrad Stab*. 2007;92(1):118-124.
31. Rychly J, Matisova-Rychla L, Csmorova K, et al. Kinetics of mass changes in oxidation of polypropylene. *Polym Degrad Stab*. 1997;58(3):269-274.
32. Tcharkhtchi A, Farzaneh S, Abdallah-Elhirtsi S, Esmaeillou B, Nony F, Baron A. Thermal aging effect on mechanical properties of polyurethane. *Int J Polym Anal Charact*. 2014;19(7):571-584.
33. Landel RF, Nielsen LE. *Mechanical Properties of Polymers and Composites*. 2nd Edition. CRC Press; 1993. ISBN 9780824789640.
34. Kim K, Lee C, Kim P, Ryu B. Dielectric properties on the radiation and thermal aged PEEK. Solid Dielectrics, 2004 ICSD 2004 Proceedings of the 2004 IEEE International Conference on: IEEE; 2004. p. 332–335.

35. Kang PH, Lee C, Kim KY. Radiation and thermal effects on the dielectric relaxation properties of PEEK. *J Ind Eng Chem* -Seoul-. 2007;13:250.
36. Ibarra L, Macias A, Palma E. Viscoelastic properties of short carbon fiber thermoplastic (SBS) elastomer composites. *J Appl Polym Sci*. 1995;57(7):831-842.
37. Ernault E, Richaud E, Fayolle B. Thermal-oxidation of epoxy/amine followed by glass transition temperature changes. *Polym Degrad Stab*. 2017;138:82-90.
38. Tobolsky AV, Metz DJ, Mesrobian RB. Low temperature autoxidation of hydrocarbons: the phenomenon of maximum Rates1, 2. *J Am Chem Soc*. 1950;72(5):1942-1952.
39. Richaud E, Fayolle B, Verdu J. Polypropylene stabilization by hindered phenols–kinetic aspects. *Polym Degrad Stab*. 2011;96(1):1-11.
40. Richaud E, Monchy-Leroy C, Colin X, Audouin L, Verdu J. Kinetic modelling of stabilization coupled with stabilizer loss by evaporation. Case of dithioester stabilized polyethylene. *Polym Degrad Stab*. 2009;94(11):2004-2014.
41. El-Mazry C, Hassine MB, Correc O, Colin X. Thermal oxidation kinetics of additive free polyamide 6-6. *Polym Degrad Stab*. 2013;98(1):22-36.
42. Mikdam A, Colin X, Minard G, Billon N, Maurin R. A kinetic model for predicting the oxidative degradation of additive free polyethylene in bleach desinfected water. *Polym Degrad Stab*. 2017;146:78-94.

How to cite this article: Zuo P, Tcharkhtchi A, Shirinbayan M, Fitoussi J, Bakir F. Multiscale physicochemical characterization of a short glass fiber–reinforced polyphenylene sulfide composite under aging and its thermo-oxidative mechanism. *Polym Adv Technol*. 2018;1–14. https://doi.org/10.1002/pat.4495

Article N°4:

P. Zuo, J. Fitoussi, M. Shirinbayan, F. Bakir, A. Tcharkhtchi, "Thermal aging effects on overall mechanical behavior of short glass fiber reinforced PolyPhenylene Sulfide composites ", Polymer Engineering & Science, 2018. In press.

Thermal Aging Effects on Overall Mechanical Behavior of Short Glass Fiber-Reinforced Polyphenylene Sulfide Composites

Peiyuan Zuo,[1] Joseph Fitoussi,[1] Mohammadali Shirinbayan,[1] Farid Bakir,[2] Abbas Tcharkhtchi[1]
[1]*Arts et Métiers ParisTech, PIMM – UMR CNRS 8006, 151 Boulevard de l'Hôpital, 75013, Paris, France*
[2]*Arts et Métiers ParisTech, Dynfluid, 151 Boulevard de l'Hôpital, 75013, Paris, France*

In this article, the overall mechanical properties of a short glass fiber-reinforced polyphenylene sulfide (PPS) composite were tested after oxidation at different temperatures (140, 160, 180, and 200°C), with a maximum oxidation time of approximately 5,300 h. In aspect of thermal aging process, the oxidation rates in 200 and 180°C are considerably harsher and faster than the case in 160 and 140°C, according to the concentration evolution of [C=O]. In aspect of mechanical properties, for virgin samples, due to an excellent fiber–matrix adhesion, no progressive damage is developed. Moreover, the fatigue results of aged samples show that the fatigue lifetime of PPS composites decreases more and more obviously with the oxidation time increasing while no significant loss of stiffness is observed. In addition, both monotonic and cyclic loadings are basically driven by the PPS matrix deformation. In the end, the relationship between fatigue lifetime and concentration of [CO] is built and discussed. POLYM. ENG. SCI., 9999:1–8, 2018.

INTRODUCTION

In the past several decades, glass fiber-reinforced polyphenylene sulfide (PPS) composites are widely used to lighten automotive parts and other application sections [1–15]. The main reason to use this thermoplastic composite is that the sulfur atom is attached to the contraposition of benzene ring, which makes it rigid and displays some special features. For example, PPS has a short-term heat distortion temperature of 260°C. Furthermore, PPS has high stiffness and strength, as well as good stability against water, acid and many other chemicals [1–4,16–18]. The composite under study is a short glass fiber composite with a PPS matrix which is a high performance thermoplastic. One of the applications of PPS composite is to use as an inlet tank which is exposed to hot air. In this case both of thermal and mechanical properties are very important. Due to PPS matrix properties, this composite has many advantages to other equivalent composites such as high thermal stability, excellent humidity-proof ability and good mechanical properties.

In aspect of thermal oxidation of PPS, there are a wide range of reports published in the past several decades. Ehlers et al. [6] clarified in depth about the crosslinking and oxidation process of PPS. They gave extensive research about cleavage of carbon–sulfur bonds and abstraction of hydrogen process from the other rings. Similarly, some research concluded also the thermal oxidation mechanism of PPS involving a combination of crosslinking, chain scission and oxidation reactions [19]. During the same earlier period, Christopher et al. [5] studied thermal degradation of PPS by a weight loss method. They indicated that in a closed system, PPS broke down by chain-scission and transferred reactions. In another research domain, it was reported that thermal treating or annealing can affect the mechanical properties of PPS. For example, Scobbo and Hwang [20] studied the annealing effects on PPS by dynamic mechanical analysis. Annealing was performed in a vacuum oven at temperatures of 160–220°C. Annealing time was constant at 4 h. They found an increased modulus accompanied by an increase in the glass transition temperature. Other reports studied the effect of thermal treatment on the tensile and in-plane shear behavior of carbon fiber-reinforced PPS composite specimens. They found the mechanical properties have shown an appreciable degradation and the observed degradation enhanced with increasing treatment temperature and time [21]. Also some investigations utilized different methodologies to study thermal degradation of PPS. For example, Perng [22] studied thermal decomposition of PPS by stepwise (pyrolysis/gas chromatography/mass spectrometry) and (thermogravity/mass spectroscopy) methods; they clarified the mechanism and kinetic model for thermal decomposition of PPS. Cao and Chen [23] used calorimetry to record the coefficient of thermal expansion and tensile modulus of PPS composites under thermal cycling. They indicated that thermal cycling at high temperatures can increase the degree of crystallinity of PPS. These literatures give us a good reference about the degradation of PPS polymer and its reinforced parts.

As a good engineering thermoplastic material, PPS/GF composites show excellent mechanical properties and fatigue performance. In fact, there are a wide range of reports concerning this issue [24–33]. Some researchers pay attention to PPS composites with different types of reinforcements. For example, some authors studied the fatigue behavior of a carbon fabric-reinforced PPS. They concluded that PPS composite with the fiber orientations of 0 and 90° did not show significant stiffness reduction and the materials showed a very brittle failure [27]. These authors moved further to examine the inter-laminar behavior of a carbon fabric reinforced PPS by using lap experiments and they considered several loading conditions. The results showed that no crack growth was observed [25,26], both under quasi-static loading until failure and successive loading-unloading stages with increasing maximum load. Kytýr et al. [34] also evaluated impact damage effect on residual fatigue life of PPS composites reinforced by carbon fibers. They revealed that elasticity modulus decreased according to the result of three-point bending test. Moreover, frequencies, ultrasound wave propagation and bending stiffness were shown to be suitable indicators to evaluate material degradation process in carbon fiber-reinforced PPS composite during fatigue. In addition, S-N curves were studied in PPS composite systems to explore the fatigue behavior and lifetime. For example, Zhou et al. [24]

*Correspondence to: p. Zuo; e-mail: peiyuan.zuo@ensam.eu
Contract grant sponsor: China Scholarship Council.
DOI 10.1002/pen.25003
Published online in Wiley Online Library (wileyonlinelibrary.com).

investigated the fatigue behavior of PPS- polyphenylene ether ketone blends. They found the S-N curves shifted their trends obviously for maximum cyclic stress. Mandell et al. [30] compared fatigue behavior of glass and carbon fiber reinforced PPS and both S-N curves appeared linear trends.

To assess the reliability of composite structures, Weibull distribution function has been widely used by different researchers [35–37]. For example, the statistical analysis of fatigue life using two-parameter Weibull distribution function was carried out by Bedi and Chandra [38] and they characterized fatigue life by probability density and cumulative distribution functions. Similarly, S-N curves at specific reliability levels were studied by statistical analysis in the reference of [39]. The authors showed that the stiffness-based degradation and S-N curves were correlated and can be studied by statistical analysis.

Literature review provides a lot of information about general properties of PPS and PPS/GF composites. However, PPS/GF fatigue response under thermal aging condition is lacking. Indeed, in practice, PPS/GF composites materials are used for long time service under a harsh temperature or environment. As a result, it is meaningful to propose some innovative works to get a better understanding of thermal aging effects on microstructure and mechanical properties, especially on fatigue behavior. This kind of investigation is very important to industrial applications. Therefore, this study pays attention to analyze the mechanical properties of PPS/GF composites after thermal aging.

More specifically, the first part of the present paper concerns thermal aging effect analysis. After that, quasi-static loading responses of virgin and aged samples are analyzed. In the next part, tensile tests until failure and loading-unloading with progressive increase of the maximum stress are performed on a PPS/GF composite. Thermal aging effect on fatigue properties of PPS/GF is also followed. Finally, an important issue of this work is to propose a clear relationship between thermal oxidation (e.g., [C=O]) and the principal mechanical properties (e.g., tensile strength, relative Young's modulus, fatigue lifetime) of PPS/GF composites.

MATERIAL AND METHODS

Sample Preparation

The material used for this study is a PPS composite based on short glass fibers. Its matrix is a semi-crystalline high performance thermoplastic with high thermal stability, low water absorption (<0.02%) and high mechanical resistance and stiffness. For this study, the material was kindly supplied by Valeo Company in the form of injected plates.

This sampling method provides geometrically clean samples without negative edge effects. Experiments showed a very low dispersion of mechanical test results with this sampling method. It is important to note that, with this method there is no any effect of water on the properties of the composite for different reasons: the water absorption of PPS is very low and the time of this method is very short (<30 s). Besides, the temperature of aging is high (between 140 and 200°C) and at these temperatures all residual water will go out of the samples just at the beginning of aging tests.

The samples with a standard dog-bone dimension (see the reference 40) were put into ovens under different thermal aging temperatures (140, 160, 180, and 200°C, respectively). Total aging time was up to about 53:00 h. Samples were progressively taken out from ovens at different applied aging time for physicochemical and mechanical characterizations.

Characterization Methods

Microscopic Observations. A scanning electronic microscope (HITACHI 4800 SEM) has been used to investigate qualitatively the PPS composite microstructure and especially the fiber-matrix interface evolution.

Infrared Analysis. Fourier transform infrared (FTIR) spectrometry was used to characterize the extent of polymer oxidation, using a Nicolet impact 410 spectrophotometer in transmission mode. Measurements were made on spectra resulting from the accumulation of 32 runs, the resolution being 4 cm^{-1}. The absorbance of C=O group was converted to the concentration using a molar absorptivity of 300 L. mol^{-1}. cm^{-1} at the peak position (1,780 cm^{-1}) [41] and a molar absorptivity of 42 L.mol^{-1}. cm^{-1} at the peak position (2,923 cm^{-1}). Also the concentration of [C=O] or other degradation products can be calculated according to the Beer–Lambert law and the equation is as follows:

$$C = \frac{A}{e.\varepsilon} \tag{1}$$

where, A is the absorbance for FTIR spectrum, e is the thickness of samples (20 μm) and ε is the molar attenuation coefficients (ε = 300 L. mol^{-1}. cm^{-1}).

Differential Scanning Calorimetry. The differential scanning calorimetry (DSC) measurements have been carried out with the DSC Q10 V9.0 Build 275TA Instruments (Guyancourt, France). The different samples were placed in hermetic aluminum capsules. The sample was heated up to 300°C with a temperature rate of 10°C/min in the atmosphere of Nitrogen (40 mL/min). To accumulate the degree of crystallinity of PPS/GF composite [42,43], the equation below was used:

$$X_C = \frac{\Delta H\mathrm{f}}{\Delta H_f^0 * \varphi} * 100\% \tag{2}$$

where X_c is the crystallinity, ΔH_f is the sample enthalpy with unknown crystallinity and ΔH_f^0 is the pure reference PPS enthalpy (80 J/g), and φ is the percentage of PPS/GF in our material, with φ of 0.7 in this study.

Quasi-Static and Fatigue Test. Tensile properties and loading-unloading-reloading tests have been performed at room temperature using a MTS 830 hydraulic machine (capacity 10KN). The applied displacement rate was always 2 mm/min. Moreover, tension-tension fatigue tests also have been performed at different applied maximum stresses on the same machine. The minimum applied stress is always chosen to be equal to 10% of the maximum applied stress (R = 0.1) [44–47]. In this article, results of experiments performed at frequency of 10 Hz are presented. During cyclic loading, the plastic deformation and loss of stiffness evolution have been systematically evaluated. A previous paper [40] showed that under this frequency, the effect of

self-heating can be reasonably neglected in regard to the high values of transition temperatures for PPS.

RESULTS AND DISCUSSIONS

Thermal Aging Analysis

As mentioned earlier, the evolution of [C=O] concentration provides a very clear description of the oxidation process and the degree of degradation in the matrix. Figure 1a shows the FTIR results of C=O peaks after several exposition times at 200°C. One can note the location of the peaks at the wavenumber of 1,780, 1,735, and 1,710 cm^{-1}. Specifically, it can be classified into three different types of C=O group. One can note that there is an obvious increasing trend for the absorbance of C=O chemical group, which indicates that the PPS/GF composites are seriously oxidized at 200°C.

Another analysis shows that C-H peaks can be a second relevant indicator for thermal aging analysis of PPS composites. Figure 1b shows FTIR results of C-H peaks, corresponding to the wavenumber of 2,923 and 2,852 cm^{-1}, respectively. One can note clearly that these peaks decrease sharply during oxidation due to the rupture of C-H chemical group. It can be also noticed that after an exposition of 504 h at 200°C, the C-H peaks tend to completely disappear. At this stage, the materials should be considered to be extremely degraded.

The [C=O] concentration evolution of PPS/GF composite under different oxidation temperatures at the peak positions of 1,780 cm^{-1} is shown in Fig. 2a. Classically, the oxidation process can be divided into three periods, induction, propagation, and termination. It can be seen that the induction time is very short (about 24 h) for the specimens aged at 200°C while this value significantly increases for the temperatures of 180 and 160°C (240 and above 1,100 h, respectively), and for 140 °C, the induction time is very long (>2,000 h). Indeed, one can note that the induction time at temperatures of 180 and 160°C is about 10 and 45 times higher than the case in 200°C, respectively. Besides, the rate of propagation is very sharp for the oxidation temperature in 200 and 180°C. After less 1,000 h of oxidation in 200°C, the propagation tends to be saturated when the amount of oxidation products reaches a maximum. At 180°C, the saturation seems to

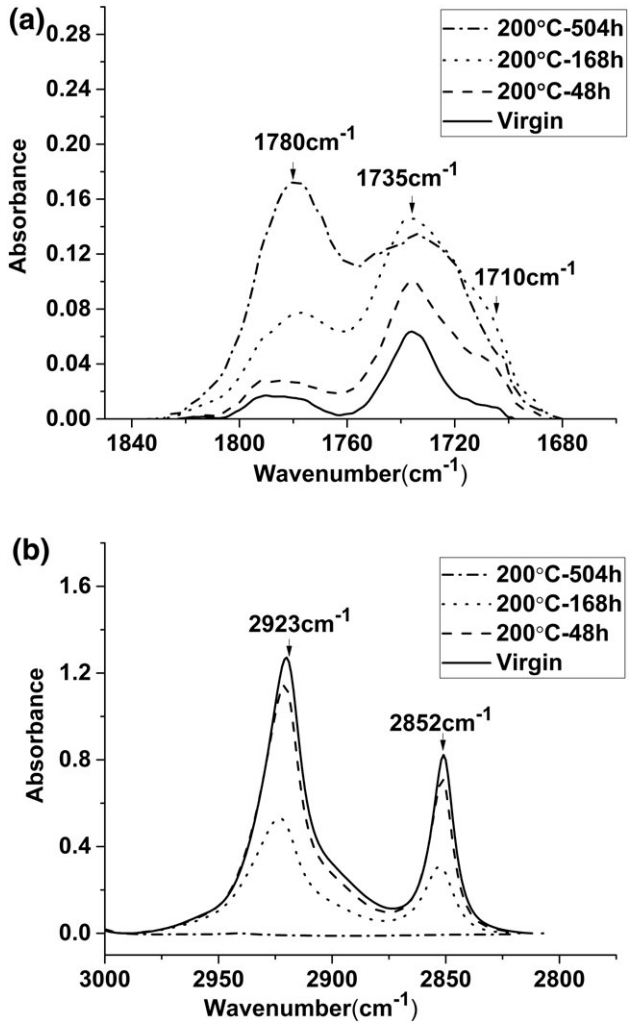

FIG. 1. (a) FTIR results of C=O peaks situated at 1,780, 1,735, and 1,710 cm^{-1}; specimens aged at 200°C. (b) FTIR results of C-H peaks situated at 2,923 and 2,852 cm^{-1}; specimens aged at 200°C.

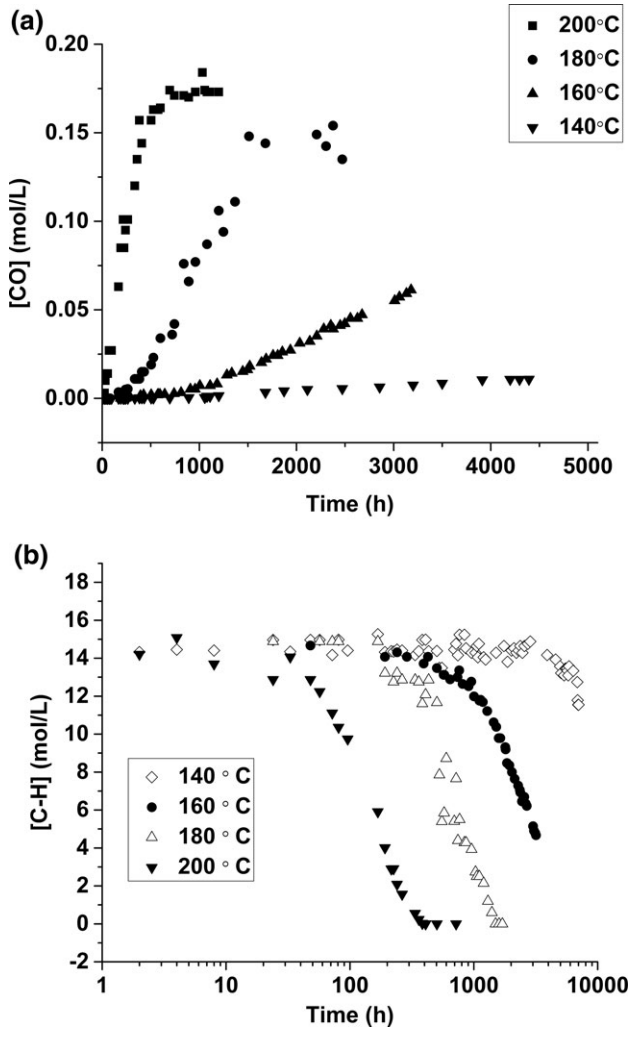

FIG. 2. (a) Concentration evolution of [C=O] at 1,780 cm^{-1}, as a function of oxidation time under different oxidation temperatures (140, 160, 180, and 200°C). (b) Concentration evolution of [C-H] at the peak of 2,923 cm^{-1}, as a function of oxidation time under different oxidation temperatures (140, 160, 180, and 200°C).

be reached until 2,000 h of exposition. Comparatively, there is no comparable evolution and no stable plateau tendency observed for 140°C oxidation even after above 4,000 h of exposition. So, it can be concluded that, to the PPS/GF composite, the oxidation rate at 200 and 180°C are considerably harsher and faster than the cases of oxidation conditions of the temperature of 160 and 140°C. [C=O] concentration evolution analysis shows that induction time, oxidation kinetic, and saturation are obviously affected by temperature in the range from 140 to 200°C.

To complete the analysis, the evolution of [C-H] concentration obtained from the peak at 2,923 cm^{-1} is shown in Fig. 2b. According to this figure, one can note that at 200°C, the [C-H] concentration decreases sharply starting from 33 h. This analysis implies the induction time of [C-H] is slightly higher than that for [C=O] concentration. This delay indicates that these two mechanisms may occur simultaneous and are probably coupled. Moreover, one can note that after 360 h, the [C-H] bonds tend to completely disappear at 200°C. One can consider that, at this point, oxidation is over. Comparatively, the induction and termination points of oxidation at 180°C, are about 192 and 1500 h, respectively. This indicates that decreased oxidation temperature leads to significant delay of the induction and termination times. At 160°C, the induction time and termination time of C-H bond rupture tends to be longer than the case in 180 and 200°C. At 140°C, the corresponding oxidation phenomenon is too weak to detect until 5,000 h exposition according to the concentration of [C-H]. Until this time, [C-H] concentration still seems stable.

According to the analysis, one can note that the oxidation temperature can obviously affect the induction, propagation and termination time of the C-H bond rupture. Higher oxidation temperatures (e.g., 200°C) are more pronounced to the tendency of C-H bond rupture.

A complete discussion about the mechanism of thermal aging for PPS composite will be presented in future publication. However, the above information allows studying the effects of thermal aging on the mechanical behavior of PPS composite under four aging temperatures (140, 160, 180, and 200°C). Different aging times have been considered. One should be noticed in mind that the so called virgin sample corresponds to the virgin sample (23°C–0 h).

Evolution of Morphology

The effect of aging on morphology of polymer has been followed by measuring its degree of crystallinity during the time. Table 1 shows the evolution of the degree of crystallinity of the samples aged at 180 and 200°C. The result shows that the degree of crystallinity of polymer increases at the beginning of the aging period for 180 and 200°C. Then it decreases during second step before stabilizing during relatively long time.

TABLE 1. The evolution of the degree of crystallinity of the samples aged at 180 and 200°C.

Time of aging (h)	Degree of crystallinity (%)	
	Aging temperature = 180°C	Aging temperature = 200°C
0	44.2	44.2
20	47.1	45.0
96	51.5	55.8
144	46.0	52.9
720	43.9	54.6
1,080	48.9	36.6

This increase of degree of crystallinity has yet been observed during the aging of certain thermoplastic polymers [48,49]. This increase is due to the chain scission and the rearrangement of the morphology of the polymer. This increase in the degree of crystallinity will lead to the increase of strength and rigidity of the polymer.

Effects of Thermal Aging on Overall Mechanical Behavior

Hereafter, three types of tests have been considered:

- Tensile test [50,51]: The effects of aging on the stress–strain curves obtained by tensile tests are presented. The evolution of Young's modulus, failure stress and failure strain are plotted for different aging conditions: Tensile response is analyzed for an oxidation temperature of 200°C after various aging times of 0, 30, 50, 100, and 199 h.
- Loading-unloading test [52–54]: It is necessary to analyze the loss of stiffness and the plastic deformation evolution to understand the effect of aging conditions on the damage and deformation mechanisms. Loading-unloading tensile tests are performed at aging temperature of 200°C after various oxidation times of 0, 30, 50, 100, and 199 h.
- Fatigue loading [45,55–58]: Tension–tension fatigue tests have been performed at 10 Hz to compare the fatigue life time of PPS composite at various aging temperatures and times. Moreover, analysis of stiffness reduction and fractography during and after cyclic loading are presented. Fatigue behaviors on four kinds of oxidized samples at 140, 160, 180, and 200°C at different aging times have been analyzed. One can note that two loading amplitudes have been selected from the analysis of the Wöhler curve obtained on virgin sample [40].

Tensile Tests Analysis. Tensile tests results clarify the influence of aging on the mechanical properties of PPS composite (see Fig. 3a–c). It was shown an improvement of elastic modulus and failure stress during the first stage of exposition. Several authors have attributed this improvement to the crosslinking and crystallinity, depending on the temperature and the time of exposure [59,60]. To be clear, during aging process, molecular chain scission, post-crosslinking and increase of crystallinity can occur simultaneously in our PPS polymer material. Also, it should be noted that at the beginning of thermal oxidation, the post-crosslinking and increase of crystallinity are pronounced while extensively long time thermal oxidation mainly corresponds to chain scission and serious degradation of PPS polymer.

Table 2 gives more details about the relative values and standard deviation of tensile test results of PPS composite at different stage of aging at 200°C, which is obtained from the MTS machine.

As a result, after the first stage of exposition, a second stage of aging during which the effect of chain scission becomes predominant at the surface of the specimen, finally leading to loss of properties of the PPS composite especially in terms of loss of

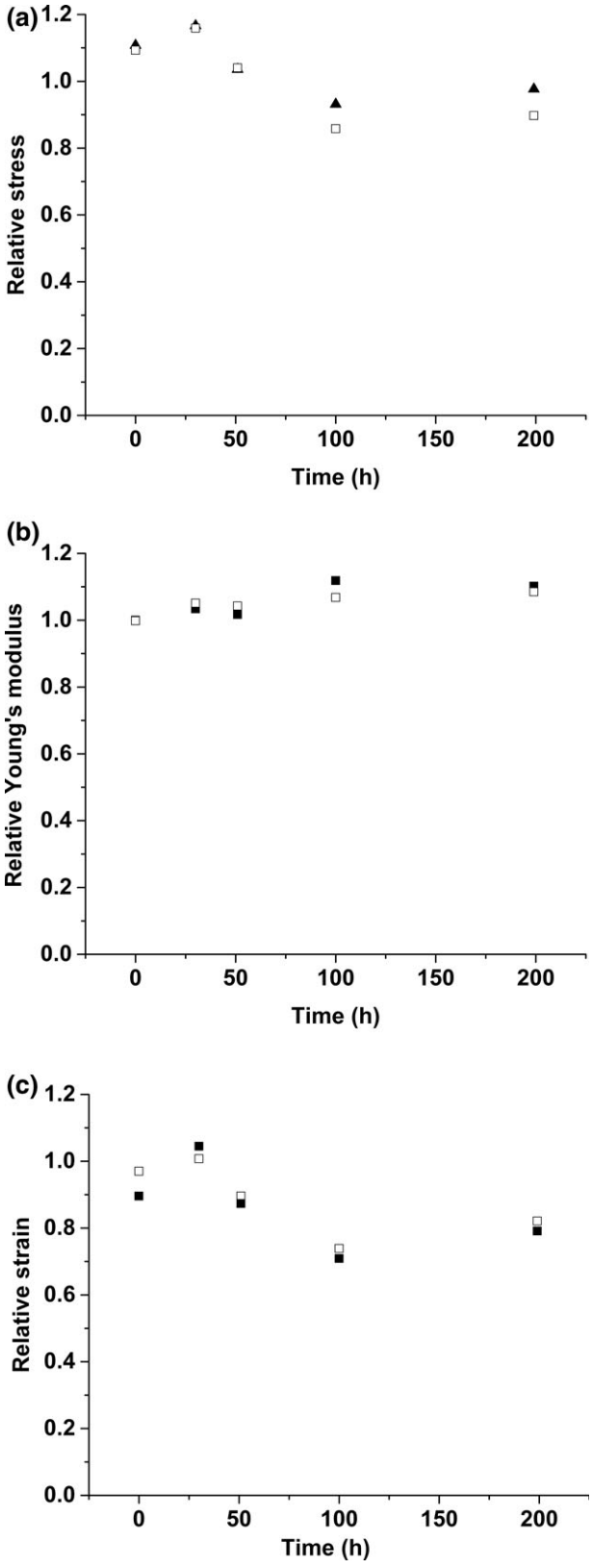

FIG. 3. (a) Evolution of relative failure stress during aging at 200°C: (Relative stress (resp. strain) = stress (resp. strain)/ultimate stress (resp. strain) obtained in virgin sample). (b) Evolution of relative Young's modulus during aging at 200°C: (Relative stress [resp. strain] = stress [resp. strain]/ultimate stress [resp. strain] obtained in virgin sample). (b) Evolution of relative failure strain during aging at 200°C: (Relative stress [resp. strain] = stress [resp. strain]/ultimate stress [resp. strain] obtained in virgin sample).

TABLE 2. Relative tensile results of PPS composites aged at 200°C.

Aging conditions	Time (h)	Relative failure stress σ/σ_0	Relative failure strain $\varepsilon/\varepsilon_0$	Relative Young's Modulus E/E_0
Virgin	0	1.13 ± 0.06	0.96 ± 0.07	1 ± 0.005
200°–30 h	30	1.17 ± 0.01	1.02 ± 0.02	1.01 ± 0.01
200°–51 h	51	1.04 ± 0.01	0.88 ± 0.01	1.05 ± 0.03
200°–100 h	100	0.92 ± 0.06	0.74 ± 0.05	1.09 ± 0.03
200°–199 h	199	0.94 ± 0.04	0.8 ± 0.01	1.1 ± 0.01

ductility. This issue can be explained by the fact that thermoplastics have linear or branched molecular structure and easily become more brittle because of chain scission or crosslinking and increase of crystallinity happening in aspect of chemical structure of PPS polymer.

From fracture surface analysis of virgin sample submitted to tensile loading until failure in Fig. 4a, it is obvious to indicate that fiber–matrix adhesion seems to be of very high quality, probably due to the presence of a coupling agent. Indeed, fibers have been pulled out in such a brittle way but still remain coated by a thin layer of PPS matrix.

Comparatively, in the case of aged sample at 200°C for 199 h, Fig. 4b, one can note that the residual matrix on the exposed surface of fibers and almost fibers surfaces are smooth. This indicates that the matrix degrades very seriously. Thermal aging has destroyed the matrix and leads to the separation of matrix and fibers, which in return reduces the mechanical retention of PPS original material.

Loading–Unloading Analysis. One can observe that, under monotonic loading, the predominant non-linear deformation mechanism seems to be the local plasticity of PPS matrix [40]. In order to quantify the possibility of plastic deformation and damage development, loading–unloading tensile test with progressive increase of the maximum stress have been performed in two cases: virgin samples and aged specimens at 200°C for 199 h (Fig. 5) shows the plastic deformation (ε_p) and loss of stiffness parameter (E/E_0) evolutions as a function of maximum stress for aged specimen. As it was shown above, the failure stress and strain decrease by aging. One can notice the relative stability of the Young's modulus which indicates no significant damage occurs during quasi-static loading (<1% decrease). Also, the plasticity increases about 5%.

Fatigue Behavior Analysis. *Effect of loading amplitude.* Figure 6 shows the Wöhler curves obtained in tension-tension fatigue tests at a frequency of 10 Hz for PPS-90° specimens at room temperature [40]. According to previous work, final failure and fatigue life of PPS/GF composite is highly dependent on the loading conditions (amplitude and frequency) and local microstructure. Bilinear Wöhler curves emphasized the influence of the loading amplitude. More brittle failure was observed at high amplitude.

For studying the effect of oxidation on fatigue behavior of the composite, iso-stress fatigue tests have been performed on the aged samples during the time. For these tests the choice of stress amplitude is very important. In order to have enough results during a reasonable time, for high aging temperatures, we must choose a low σ_r while for low aging temperatures; we must

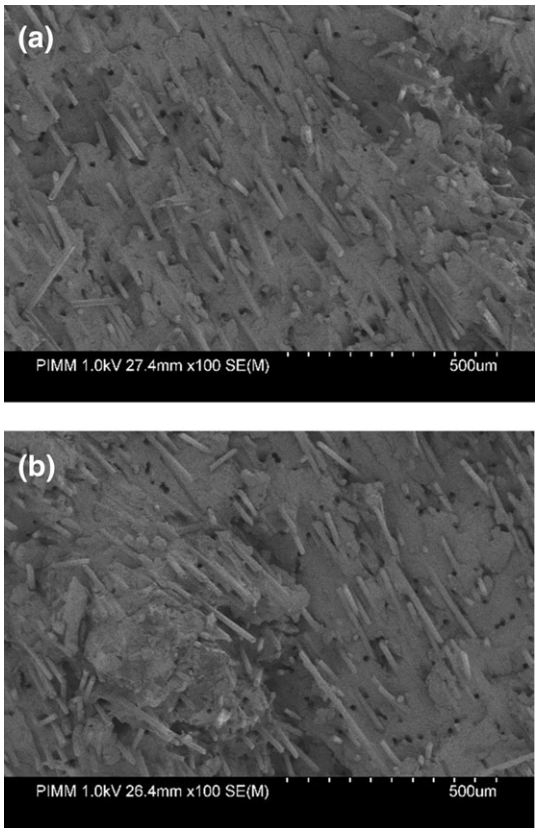

FIG. 4. (a) SEM micrograph of PPS/GF composite; fracture surface after tensile test of virgin sample. (b) SEM micrograph of PPS/GF composite; fracture surface after tensile test of aged sample at 200°C–199 h.

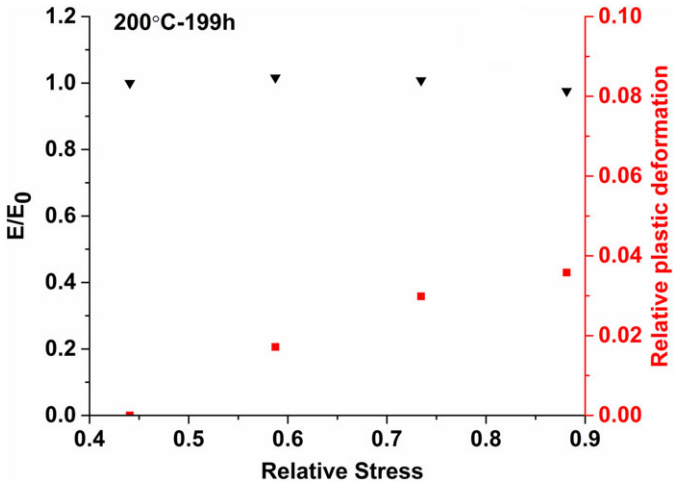

FIG. 5. The plastic deformation (ε_p) and loss of stiffness parameter (E/E_0) evolutions as a function of maximum stress: (Relative stress [resp. strain] = stress [resp. strain]/ultimate stress [resp. strain] obtained in virgin sample). [Color figure can be viewed at wileyonlinelibrary.com]

choose a high σ_r. So in the basis of the Wöhler curves for the study of fatigue behavior during aging at high temperatures (180 and 200°C) and also at low temperatures (140 and 160°C) for comparison, we have chosen $\sigma_r = 0.6\ \sigma_{ultimate\text{-}virgin}$.

In order to study the fatigue lifetime of aged PPS composite at 180°C at different aging times tension-tension fatigue tests have been performed at different loading amplitudes of 0.6 $\sigma_{ultimate\text{-}virgin}$ and $\sigma_{ultimate\text{-}virgin}$ (see Fig. 7). One can notice that the cycle number decreases with the loaded amplitudes increasing. In particular, the applied amplitude of 0.6 $\sigma_{ultimate\text{-}virgin}$ favors to a higher cycle (maximum to about 10^7 cycle) while one can also notice that the considerable reduction of cycle number with the amplitude of $\sigma_{ultimate\text{-}virgin}$, from 1.4×10^4 to 1.2×10^3 with an oxidation time of approximately 250 h. From Fig. 7, one can also note that the lifetime reduction rate is increased from the tests with loading amplitude from 0.6 $\sigma_{ultimate\text{-}virgin}$ to $\sigma_{ultimate\text{-}virgin}$. Results show the fatigue lifetime sharply decreases by aging time increasing in the case of loading amplitude of 0.6 $\sigma_{ultimate\text{-}virgin}$. Also the temperature of 180 °C favors an obvious diminution of fatigue cycle number with the increasing oxidation time.

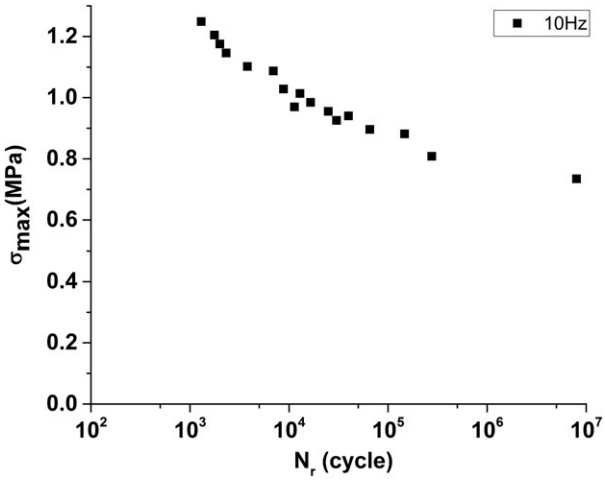

FIG. 6. Relative Wöhler curves of PPS/GF composite performed on PPS-90° specimens under tensile-tensile fatigue loading at the frequency of 10 Hz and room temperature, $R = 0.1$ (Relative stress = stress /ultimate stress obtained in virgin sample after tensile test [$\sigma_{ultimate\text{-}virgin}$]).

Effect of Thermal Aging Temperature. Figure 8 shows the fatigue lifetime evolution as a function of oxidation time under different oxidation temperatures of 140, 180, and 200°C. One can note that fatigue lifetime reduction rate increases with thermal aging temperature. Indeed, at 200°C the fatigue lifetime is submitted to a very sharp decrease. This indicates the 200°C is very harsh to destroy the mechanical properties of PPS materials. This is to say, the fatigue lifetime is very sensitive to the oxidation temperature and decided by the thermal aging conditions.

Fatigue Behavior Coupled With Oxidation Phenomenon. Figure 9 shows the relation between N_r and [CO] in different oxidation temperatures. One can note that generally it can be divided into two zones, high oxidation temperatures (e.g., 200 and 180°C) and moderate temperatures (140 and 160°C). For the same rupture cycle number (N_r), one can see the moderate temperatures produce less [CO] amount while the high temperatures correspond to more [CO]. However, it needs to be noted that the large amount of [CO] in high temperatures is produced in a short time since the induction time for high oxidation temperature is very short and quick, which can be referred to the relative section above in this article.

Considering our PPS polymer material subjected to dynamic loading, the samples aged at high temperature will consume a short time to reach degradation while the low temperature will take more time to appear the same degree of degradation. Comparatively, the

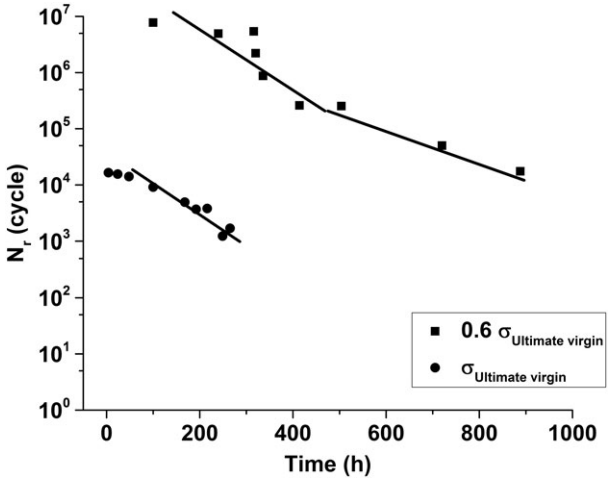

FIG. 7. Effect of aging and loading amplitude on fatigue lifetime of samples aged at 180°C (f = 10 Hz).

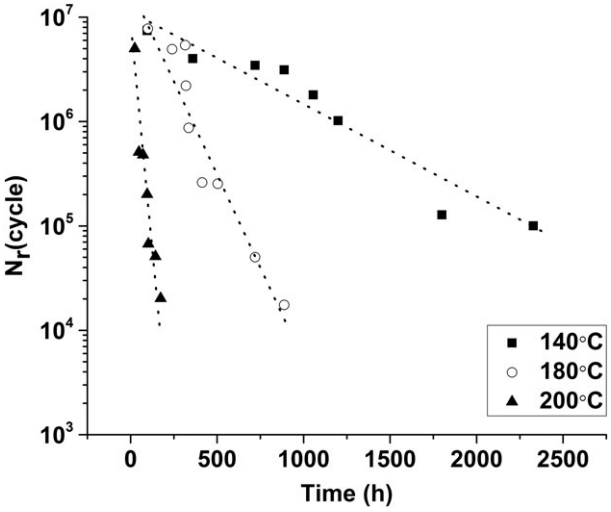

FIG. 8. Effect of aging temperature on fatigue lifetime; fatigue tests at 10 Hz and loading amplitudes of 0.6 $\sigma_{ultimate\text{-}virgin}$.

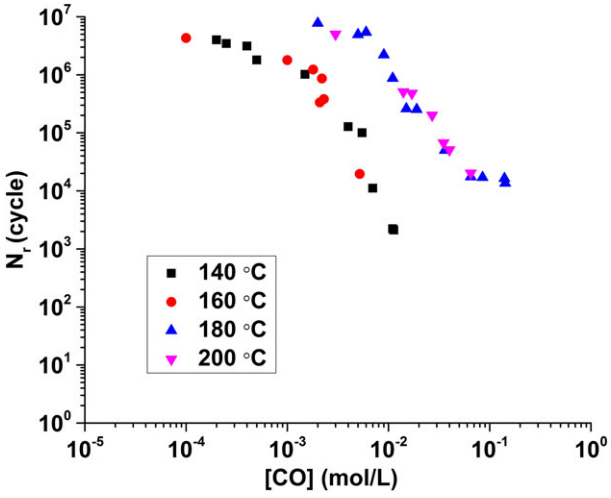

FIG. 9. Relation between N_r and [CO] in different oxidation temperatures. [Color figure can be viewed at wileyonlinelibrary.com]

[CO] can stand for the degradation degree. When the same cycle number was applied until rupture, the high temperature leads to more degradation, which is equivalent to high [CO] while the value for low temperature is small. Moreover, one can see that Nr decreases sharply with the increase of [CO], not only in the case of high temperatures (180 and 200°C), but also in the case of low temperatures (140 and 160°C).

CONCLUSION

PPS/GF composite was tested after oxidation at different temperatures (140, 160, 180, and 200°C) until approximately 5,300 h under tensile, loading–unloading and cyclic loading. The main results are as follows:

The oxidation rate increases by increasing the temperature. At 200°C it is considerably harsher and faster than at 140°C and this difference is related to the exothermic nature of global apparent activation energy of oxidation reactions.

Tensile behavior of sample aged at 200°C exhibited that at the beginning of oxidation from 0 to 30 h, the tensile behavior stays its mostly original retention. This is mainly due to the post-crosslinking and also to the increase of the degree of crystallinity of PPS. After then, the tensile strength decreases sharply almost of its 25% strength during 200 h. One can note that the relative Young's modulus slowly increases at the beginning of oxidation and this trend tends to be constant with the thermal oxidation time increasing. This also proves the crosslinking and increase of crystallinity exist during the oxidation process. Moreover, the strain has a consistent decrease. This indicates the material tends to be brittle during oxidation, showing a decreasing elongation.

Loading–unloading tests presented that the PPS/GF composite has an evident nonlinear elasticity-limited plasticity, not only for virgin sample, but also for aged samples.

Fatigue analysis of aged samples showed that the fatigue lifetime decreases with the loaded amplitudes increasing. The cycle number for aged samples has an obvious decreasing trending due to oxidation, and this trend tends to be more excessive with the oxidation temperature and oxidation time increasing. PPS/GF composite will lose its fatigue performance obviously at the beginning of oxidation and the fatigue performance will tend to be worse with the oxidation process going further.

ACKNOWLEDGMENTS

The authors are grateful to Dr R.C. Benevides and Dr Manuel Henner (Valeo) for collaboration and fruitful discussions. Valeo Company is also gratefully acknowledged for providing the material. Financial support from the CASCADE program under project "FSN Calcul Intensif et Simulation Numérique" by DGE is gratefully acknowledged. The authors also thank China Scholarship Council (CSC) for their funding of Peiyuan Zuo's thesis.

REFERENCES

1. H.W. Hill and D. Brady, *Polym. Eng. Sci.*, **16**, 831 (1976).
2. L.C. López and G.L. Wilkes, *Polymer*, **30**, 882 (1989).
3. L. Caramaro, B. Chabert, J. Chauchard, and T. Vu-Khanh, *Polym. Eng. Sci.*, **31**, 1279 (1991).
4. M. Favaloro, "Properties and Processes of Linear Polyphenylene Sulfide (PPS) for Continuous Fiber Composites Aerospace Applications," *SAE Aerotech Conf.*, Seattle, WA, Paper Number 2009-01-3242 (2009).

5. N. Christopher, J. Cotter, G. Knight, and W. Wright, *J. Appl. Polym. Sci.*, **12**, 863 (1968).
6. G. Ehlers, K. Fisch, and W. Powell, *J. Polym. Sci., Part A: Polym. Chem.*, **7**, 2955 (1969).
7. L. Yu, S. Bahadur, and Q. Xue, *Wear*, **214**, 54 (1998).
8. L.A. Gyurova and K. Friedrich, *Tribo. Int.*, **44**, 603 (2011).
9. Q. Zhao and S. Bahadur, *Wear*, **217**, 62 (1998).
10. Z. Jiang, L.A. Gyurova, A.K. Schlarb, K. Friedrich, and Z. Zhang, *Compos. Sci. Technol.*, **68**, 734 (2008).
11. K. Stoeffler, S. Andjelic, N. Legros, J. Roberge, and S. B. Schougaard, *Compos. Sci. Technol.*, **84**, 65 (2013).
12. Y. Yang, H. Duan, S. Zhang, P. Niu, G. Zhang, S. Long, X. Wang, and J. Yang, *Compos. Sci. Technol.*, **75**, 28 (2013).
13. L. Lopez and G. Wilkes, *J. Macromol. Sci., Part C*, **29**, 83 (2012).
14. B.G. Risch, *Syst. Comput. Japan*, **35**, 1 (1994).
15. M.Ö. Bora, O. Çoban, T. Kutluk, S. Fİdan, and T. Sinmazçelİk, *Polym. Compos.*, **39**(**5**), 1604 (2016).
16. J. Edmonds Jr and H. Hill Jr, US Patent 3354129, 1967, in *Chem. Abstr*, pp. 13598 (1968).
17. R.T. Young and D.G. Baird, *Compos. B. Eng.*, **31**, 209 (2000).
18. X. Han, H. Ding, L. Wang, and C. Xiao, *J. Appl. Polym. Sci.*, **107**(**4**), 2475 (2008).
19. R. Black, C. List, and R. Wells, *J. Appl. Chem.*, **17**, 269 (1967).
20. J. Scobbo and C. Hwang, *Polym. Eng. Sci.*, **34**, 1744 (1994).
21. S.G. Pantelakis, C.V. Katsiropoulos, and P. Lefebure, *J. Appl. Polym. Sci.*, **107**, 3190 (2008).
22. L. Perng, *Polym. Degrad. Stab.*, **69**, 323 (2000).
23. J.Y. Cao and L.S. Chen, *Polym. Compos.*, **26**, 713 (2005).
24. J. Zhou, A. D'Amore, Y. Yang, T. He, B. Li, and L. Nicolais, *Appl. Compos. Mater.*, **1**, 183 (1994).
25. I. De Baere, W. Van Paepegem, and J. Degrieck, *Polym. Test.*, **32**, 1273 (2013).
26. I. De Baere, W. Van Paepegem and J. Degrieck, in *15th European Conference on Composite Materials (ECCM15-*2012*).* Ghent University, Department of Materials Science and Engineering (2012).
27. I. De Baere, W. Van Paepegem, C. Hochard, and J. Degrieck, *Polym. Test.*, **30**, 663 (2011).
28. K. Tanaka, K. Oharada, D. Yamada, and K. Shimizu, *Int. J. Fatigue*, **92**, 415 (2016).
29. D. Backe and F. Balle, *Compos. Sci. Technol.*, **126**, 115 (2016).
30. J.F. Mandell, D. Huang, and F. McGarry, *Polym. Compos.*, **2**, 137 (1981).
31. R. Růžek, M. Kadlec, and L. Petrusová, *Int. J. Fatigue*, **113**, 253 (2018).
32. B. Vieille and W. Albouy, *Int. J. Fatigue*, **80**, 1 (2015).
33. W. Albouy, B. Vieille, and L. Taleb, *Int. J. Fatigue*, **63**, 85 (2014).
34. D. Kytýr, T. Fıla, J. Valach, and M. Šperl, *U.P.B. Sci. Bull.*, **75**, 157 (2013).
35. R. Sakin and I. Ay, *Mater. Des.*, **29**, 1170 (2008).
36. M. Alqam, R.M. Bennett, and A.-H. Zureick, *Compos. Struct.*, **58**, 497 (2002).
37. H. Rinne, The Weibull Distribution: A Handbook, Chapman and Hall/CRC, Boca Raton (2008).
38. R. Bedi and R. Chandra, *Compos. Sci. Technol.*, **69**, 1381 (2009).
39. T. Philippidis and A. Vassilopoulos, *Compos. Sci. Technol.*, **60**, 2819 (2000).
40. P. Zuo, R. Benevides, M. Laribi, J. Fitoussi, M. Shirinbayan, F. Bakir, and A. Tcharkhtchi, *Compos. B. Eng.*, **145**, 173 (2018).
41. G. Lisa, C. Hamciuc, E. Hamciuc, and N. Tudorachi, *J. Anal. Appl. Pyrolysis*, **118**, 144 (2016).
42. D. Brady, *J. Appl. Polym. Sci.*, **20**, 2541 (1976).
43. J.E. Spruiell, A review of the measurement and development of crystallinity and its relation to properties in neat poly (phenylene sulfide) and its fiber reinforced composites[R]. *ORNL* (2005).
44. M. Shirinbayan, J. Fitoussi, N. Abbasnezhad, F. Meraghni, B. Surowiec, and A. Tcharkhtchi, *Compos. B. Eng.*, **131**, 8 (2017).
45. V. Bellenger, A. Tcharkhtchi, and P. Castaing, *Int. J. Fatigue*, **28**, 1348 (2006).
46. E.A. Toubia and A. Elmushyakhi, *Mater. Des.*, **131**, 102 (2017).
47. W. Zhang, Z. Zhou, B. Zhang, and S. Zhao, *Mater. Des.*, **66**, 77 (2015).
48. L. Boukezzi, S. Rondot, O. Jbara, and A. Boubakeur, *Radiat. Phys. Chem.*, **149**, 110 (2018).
49. C. Han, E. Sahle-Demessie, A.Q. Zhao, T.I. Richardson, and J. Wang, *Carbon*, **129**, 137 (2018).
50. B. Yang, L. Lu, X. Liu, Y. Xie, J. Li, and Y. Tang, *Mater. Des.*, **131**, 470 (2017).
51. N. Abbasnezhad, A. Khavandi, J. Fitoussi, H. Arabi, M. Shirinbayan, and A. Tcharkhtchi, *Int. J. Fatigue*, **109**, 83 (2018).
52. S.M. Daghash and O.E. Ozbulut, *Mater. Des.*, **111**, 504 (2016).
53. A. Gosar and M. Nagode, *Int. J. Fatigue*, **43**, 160 (2012).
54. R.P. Skelton, *Int. J. Fatigue*, **26**, 253 (2004).
55. N.H. Mostafa, Z.N. Ismarrubie, S.M. Sapuan, and M.T.H. Sultan, *Mater. Des.*, **92**, 579 (2016).
56. M. Berer, D. Tscharnuter, and G. Pinter, *Int. J. Fatigue*, **80**, 397 (2015).
57. Y. Hu, H. Li, J. Tao, L. Pan, and J. Xu, *Polym. Compos.*, **39**, 1447 (2018).
58. L. Chen and B. Gu, *Polym. Compos.*, **39**(**5**), 1455 (2018).
59. S. Lee, D.-H. Kim, J.-H. Park, M. Park, H.-I. Joh and B.-C. Ku, *Advances in Chemical Engineering and Science*, **3**, 145 (2013).
60. R.T. Hawkins, *Macromolecules*, **9**, 189 (1976).

Etude de l'effet du vieillissement thermique sur le comportement en fatigue du composite de poly (sulfure de phénylène) renforcé par des fibres de verre (PPS/FV)

RESUME : Dans ce travail, l'effet du vieillissement thermique sur le comportement en fatigue du composite de poly (sulfure de phénylène) renforcé par fibres de verre (PPS/FV) a été étudié. Ce matériau est d'abord étudié par différentes méthodes d'analyse afin de déterminer ses caractéristiques physico-chimiques et mécaniques. Ensuite, le matériau subit un vieillissement thermo-oxydatif accéléré à différentes températures comprises entre 100 °C et 200 °C. Certaines caractéristiques du matériau sont d'ailleurs suivies au cours du vieillissement. A partir des résultats obtenus, un mécanisme d'oxydation est proposé et un modèle cinétique est développé. La validité de ce modèle est vérifiée par les résultats expérimentaux, essentiellement obtenus par la spectrométrie infrarouge. L'effet du vieillissement sur le comportement mécanique est étudié par les deux axes suivants : D'abord d'une manière indirecte en étudiant l'évolution de la morphologie de la phase cristalline au cours du temps et ensuite par la méthode directe. Dans cette méthode directe, premièrement, le comportement en fatigue et en traction-traction du PPS/FV a été étudié en faisant varier la fréquence et l'amplitude de la sollicitation. La courbe de Wöhler est tracée en fonction du nombre de cycles à la rupture. Il a été constaté que le vieillissement modifie le positionnement et l'allure de la courbe de Wöhler. Ensuite les éprouvettes vieillies à différentes températures sont testées en fatigue (traction-traction) avec une amplitude maximale (σ_{max}=40 MPa) et un rapport de chargement (R=0,1) afin de suivre l'influence de la dégradation thermo-oxydative au cours du vieillissement. Il a été constaté que l'oxydation a un effet néfaste sur le comportement en fatigue du PPS/FV. Ce matériau perd significativement de ses performances même au début du vieillissement et surtout à haute température de vieillissement. La perte de la performance en fatigue du matériau s'accentue au fur et à mesure que le processus d'oxydation se poursuit.

Mots clés : Composite de poly (sulfure de phénylène) (PPS) ; fibre de verre; oxydation thermique; comportements de fatigue; modélisation cinétique; cristallisation ; propriétés mécaniques.

Study of thermal aging effect on fatigue behaviors of a short glass fiber reinforced Polyphenylene Sulfide (PPS/GF) composite

ABSTRACT: In this work, the effect of thermal aging on the fatigue behavior of a glass fiber reinforced poly (phenylene sulfide) composite (PPS/GF) was studied. This material is first characterized by different methods of analysis to determine its physicochemical and mechanical characteristics. Subsequently, the material undergoes accelerated thermo-oxidative aging at different temperatures between 100 °C and 200 °C. Some characteristics of this material are followed during thermal aging. From the results obtained, an oxidation mechanism is proposed and a kinetic model is developed. The validity of this model is verified by the experimental results, essentially obtained by infrared spectrometry. The effect of thermal aging on mechanical behavior is studied in two ways: Firstly, indirect manner by studying the evolution of the morphology of the crystalline phase over time and subsequently by the direct method. In this direct method, firstly the tension-tension fatigue behavior of PPS/GF was studied by varying the frequency and amplitude of stress. The Wöhler curve is plotted on the basis of the number of cycles at break. Thermal aging has been found to alter the position and shape of the Wöhler curve. Then the samples aged at different temperatures were tested by tension-tension fatigue with a maximum amplitude (σ_{max} = 40 MPa) and a loading ratio (R = 0.1) to follow the influence of thermo-oxidative degradation during aging. It has been found that thermal aging has a detrimental effect on the fatigue behavior of PPS/GF. This material loses its performance significantly even at the beginning of aging, especially in high aging temperature. The loss of fatigue performance grows in the oven as the oxidation process continues.

Keywords : Polyphenylene Sulfide (PPS) composite; short glass fiber; thermal oxidation; fatigue behaviors; kinetic modeling; crystallization; mechanical properties.

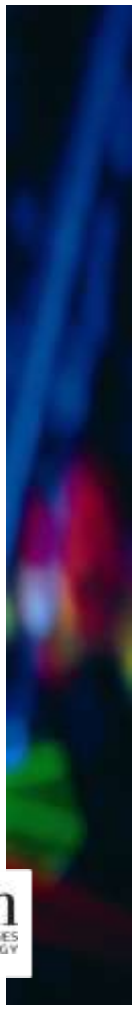

ARTS ET MÉTIERS ParisTech

ParisTech INSTITUT DES SCIENCES ET TECHNOLOGIES PARIS INSTITUTE OF TECHNOLOGY